The Chemistry of Warm Cores in Low-Mass Star Forming Regions

Zainab Mohamed Abdel-Hamed Awad

Thesis submitted for the Degree of Doctor of Philosophy
of University College London

Department of Physics & Astronomy
UNIVERSITY COLLEGE LONDON

September 2010

I, Zainab M. A. Awad, confirm that the work presented in this thesis is my own. Where information has been derived from other sources, I confirm that this has been indicated in the thesis.

To my father, my mother, and my sister
for their constant support over the years despite the distance,
and to all those who get past this page.

“It is the theory that decides what can be observed.”

- Albert Einstein

ACKNOWLEDGEMENTS

When it comes to writing acknowledgements, it becomes even more difficult than writing the whole thesis as the list is too long. No doubt, I was so worried and stressed when I started in London, the city of magic; different place, culture, people and language; '*Oh my God, what I had done to myself? Am I gonna make it and one day I'll be Dr.!* (**;)'. All of my worries were relieved the moment I joined the astrophysics group, Group A, and was surrounded by the friendly members especially my colleagues in room G16. Many thanks to you all.

First and above all, I praise God, the almighty for providing me this opportunity to be a postgraduate student of the honoured University College London, UCL, and granting me the capability to proceed successfully. I still cannot believe that I made it, but I finally have. This thesis appears in its current form due to the assistance and guidance of several people. I would therefore like to offer my sincere thanks to all of them.

I want to express my gratitude to my esteemed supervisor **Dr. Serena Viti**. Thanks first of all for accepting me as a PhD student, for taking care of all the details when I started at UCL while she was abroad. Thank you for your warm encouragement, thoughtful guidance, critical comments, for being very patient teaching me several issues about coding and observations (my nightmare). In addition, many thanks for all of the time you granted me discussing my progress or writing reference letters for my job application.

I am indebted to **Prof. David A. Williams**, the person who I dreamt of meeting one day. It was/is always a privilege for me to talk to you and learn from your flood of knowledge. Many thanks to you for your fruitful discussions during the meetings we had, for listening carefully to my ideas and thoughts while explaining the results even if those ideas were wrong. I will never forget your support during my first year interview and the special way you have in breaking my fears and making me feel more self confident with the kindest smile one would ever see. I am

grateful for your efforts proofreading and correcting this thesis.

It is a pleasure for me to thank my office mates, the G16 people for making these three years unforgettable. Thanks to **Estelle Bayet** for her fruitful discussions about Chapter 3, for teaching me few things about extragalactic environments when we collaborated in the project she led, and for making me laugh every time she says in anger 'merde'. Thanks to **Mark Westmoquette** who 'NEVER' says 'NO' even once to any of my questions even those silly ones "*What's the past tense of ...*" and for proofreading this acknowledgement. Thanks to **Roger Wesson** for helping me with the Linux system when I started and for supplying me daily with an amazing dash of his strong coffee!! Thanks to **Mikako Matsuura** for explaining some issues related to observations and a special thanks goes to the former G16 star **Julia Roberts** for providing her deuterium reaction file which I updated and used in Chapter 3. I am also thankful to **Mark Collings** for giving me his chemical kinetic code I used to determine the desorption temperature in Chapter 2. A huge thank you goes to the warmest heart I ever met, to my loving friend **Magda Vasta**, thanks for all of your support scientifically and personally, for keeping our friendship alive even through skype despite the distance. Thanks to all of you in G16 for the regular 2:30 p.m. coffee breaks that usually comes just on time.

I would like to show my deepest gratitude to my parents for raising me the way I am, for giving me freedom deciding what to do and where to go, for their prayers and courage when I was fed up, for giving me my sister, Amina. Thanks to all of you for being there all the time over the years, despite the distance.

Thanks to **Dr. Helen Fraser** who first opened the door to Europe for me when she advised me to apply to Greenberg Fellowship in Leiden. I am indebted to **Prof. Osama Shalabiea** for opening the window to the new world of astrochemistry, years ago, and for his constant support "come on you can make it young lady", and for his following up of my progress. Many thanks to **Prof. Mohamed Fathi** for keeping in touch and for his support since I left home.
Thanks to all of those who should be acknowledged.

Zainab Awad

September 2010,

London, the United Kingdom

ABSTRACT

My thesis deals with the investigation of the chemical and physical properties of the gas and dust involved in the formation of low mass stars. As the stars form, warm cores (or 'hot corinos') are detected in molecular emission. The study of such emissions allows us to get an insight on the physical conditions of low-mass star formation, and trace its various evolutionary stages.

Through out this thesis I make use of a chemical model originally developed for the study of high mass star forming regions. I have adapted this model for the study of low mass stars and first applied it to explore the sensitivity of the chemistry of hot corinos to the changes in the physical conditions of the surrounding environment. It is found that the chemical trends of these cores does not qualitatively differ much from that of hot cores (remnant of high mass star formation) leading us to conclude that, at least in some cases, the formation of low-mass stars may be a scaled-down version of that of massive stars. One of the most studied hot corinos is that surrounding IRAS 16293-2422: in order to validate my model, I compare the predicted chemical abundances to the molecular emission from this object and find a relatively good match.

Observations of warm cores also revealed that they are rich in deuterium content. I enlarge our chemical network to include all the possible mono-deuterated species, as well as D_2CO. In this study, I look into the chemical evolution of the deuterated species, and aim to identify a set of deuterated molecules as evolutionary indicators for the protostellar stage of the core.

A very debated issue when validating chemical models is that of whether the initial chemical conditions of the gas affect the chemical evolution of the star forming cores. I investigate this issue by running a large grid of dark and dense cloud models where the initial conditions are varied, in particular I investigate whether a pre-processed gas (e.g. 'left over' from a pre-

vious star formation event) may affect subsequent star formation processes and find that in general the initial chemical composition of the gas is in fact irrelevant.

Finally, I took part of a study, led by Dr Bayet, where the chemistry of deuterated species in extragalactic environments is investigated and in this thesis I highlight my contribution to this work.

Hubble Space Telescope Image of the **N90** Star Forming Region.

CONTENTS

LIST OF FIGURES

LIST OF TABLES

CHAPTER 1

INTRODUCTION

1.1 The Interstellar Medium: An Overview

The interstellar medium (ISM) is the material filling the space between stars in a galaxy. The ISM is an important component in the evolution of galaxies as it is the reservoir of mass from which new stars form, and into which ashes of old stars are ejected. The material in the ISM is therefore being continually consumed by star formation, and enriched by elements, molecules, and dust by stellar evolution processes. The discovery of molecules and the rich chemistry in ISM led to intense research in gas-phase ion-molecule and neutral-neutral reactions. When the role of dust particles in the formation of other molecules (in particular H_2) became clear, studies on gas-grain interactions started, both theoretically and experimentally (e.g. Williams 2003a, and references therein).

The ISM contains only 10 - 15% of the total mass of the Galaxy and is organised into large structures, 1 - 100 pc in size, known as interstellar clouds. Observations show that the ISM has a complex and inhomogeneous structure in which different types of astronomical regions exist, varying in their physical conditions (van Dishoeck 1998). Field *et al.* (1969) presented a model of the interstellar medium based on detailed calculations of low-energy cosmic rays, CR. Their model predicted the ISM to be divided into two phases; the intercloud phase of temperature 10^4 K and the cloud phase at temperatures < 300 K. Including the effect of supernovae, McKee & Ostriker (1977) classified the ISM into three phases: the Cold Neutral Medium (CNM), often referred to as "clouds"; the Warm Ionised Medium or Warm Neutral Medium (WIM or WNM), which is sometimes considered the boundary layers of the CNM;

and the Hot Ionised Medium (HIM), which is sometimes referred to as the intercloud medium or the coronal gas. More recently, Wooden *et al.* (2004) in their review, divided the ISM into five components: (1) the hot ionised medium which is also known as coronal gas, (2) the warm ionised medium containing ionised hydrogen (H^+), (3) the warm neutral medium containing the neutral hydrogen, (4) the atomic cold neutral medium, also known as diffuse clouds which is dominated by atomic hydrogen, H, with some in molecular form, H_2, and (5) the molecular cold neutral medium which is dominated by H_2 and also known as molecular clouds (Wooden *et al.* 2004). Table (1.1) summarises the ISM components and their physical parameters.

Table 1.1: The components of the ISM and their physical properties, taken from (Wooden *et al.* 2004; Williams 2003a).

ISM component	T(K)	Density (cm^{-3})	State of H	Diagnostics
Hot ionised medium (coronal gas)	10^6	$<10^{-2}$	H^+ UV absorption	X-ray emission,
Warm ionised medium (HII regions)	10^4	>10	H^+	Optical, UV, IR, H_α
Warm neutral medium (Intercloud HI)	10^3-10^4	>0.1	H	21-cm emission
Atomic cold neutral medium (diffuse clouds)	100	$\sim$100	H & H_2	21-cm emission, 3.4-μm absorption, UV absorption
Molecular cold neutral medium (dense clouds)	10 - 50	10^3-10^5	H_2	FIR, Radio
Molecular hot cores	100 - 300	$>10^6$	H_2	Rovibrational emission

† This parameter varies only during the collapsing phase (Phase I).

About half of the mass of the ISM is in interstellar clouds (Wooden *et al.* 2004) that are made of gas and tiny dust grains, made of silicate or carbon and of an average radius of $\sim$ 0.1μm. Dust particles contain 1% of the ISM mass in our Galaxy (Herbst 1995). Interstellar clouds can be divided into two main categories; diffuse and dense clouds. Diffuse clouds are normally detected along low visual extinction ($A_v < 1$ mag) lines-of-sight toward nearby bright stars. Their density and temperature range between $n_H \sim 10-10^3$ cm^{-3} and 50 - 100 K, respectively, where n_H is the total hydrogen nucleon number density given by '$n_H = n(H) +$

$2n(H_2)$' (Duley & Williams 1984). The interstellar UV radiation dissociates molecules, ionises species, apart from H, and heats the gas (van Dishoeck & Blake 1998). Both ζ-Per and ζ-Oph are two famous examples of typical diffuse clouds.

Dense (dark) clouds have low temperature ($<$ 50 K) with high gas density ($n_H \sim 10^4 - 10^6$ cm^{-3}) and hence high dust concentrations ($n_g \sim 10^{-12} n_H$, where n_g is the dust grain number density) causing the interstellar radiation field to be heavily extinguished ($A_v \geq 10$ mag). Therefore, CRs provide the major source of ionisation in these clouds (Dyson & Williams 1997; van Dishoeck & Blake 1998). Since the discovery of molecules such as H_2 in dark clouds, the terms molecular clouds and dark clouds are often used interchangeably as they refer to two main characteristics of the clouds; their molecular composition, and their opaque optical appearance (Bergin & Tafalla 2007). Translucent clouds form the bridge between these two limiting cases with $1 < A_v < 5$ mag. Some dense clouds are inhomogeneous, they contain some denser clumps of material surrounded by lower-density envelopes . Some of these clouds show little evidence of star formation; such regions are referred to as quiescent clouds (Herbst 1995). Giant molecular clouds are those with masses $> 10^5$ M$\odot$ where star-forming regions and newly formed stars can exist. The radiation from new stars heats up the surrounding regions of the cloud. If the temperature becomes high enough, the cloud will be detectable by their bright ionised hydrogen, and hence they are called HII regions (Herbst 1995). Farther from the new star are warm, mainly neutral regions dominated by photons known as photo-dominated regions (PDR) (Herbst 1995; Morrison *et al.* 1996).

Interstellar dust has been known or suspected for almost 80 years, its existence was first convincingly shown by Trumpler (1930) based on the discovery of colour excess (see; Li & Greenberg 2003). Historically, dust was regarded by astronomers as interstellar 'fog' which prevented an accurate measurement of the distances to stars. This view totally underestimated the role of interstellar grains. The development of UV, infrared (IR), and radio observations, the advances in laboratory astrophysics, and theoretical modelling have had a tremendous impact on our understanding of the physical and chemical nature, origin and evolution of grains and their role in the evolution of different interstellar regions (e.g Salpeter 1977; Li & Greenberg 2003 and references therein). Now, it is well-established that dust grains play a vital role not only by providing 30% of the Galactic luminosity via their IR emission, or by tracing the physical conditions of the environment they are observed in, but grain surfaces are also factories of many interstellar molecules which can not be reproduced via gas-phase reactions only, such as H_2 , H_2CO, CH_3OH, and even more complex species like $HCOOCH_3$, CH_3OCH_3

(e.g. Tielens & Hagen 1982; Watanabe *et al.* 2003; Horn *et al.* 2004; Garrod & Herbst 2006; Bennett & Kaiser 2007a,b; Pirronello *et al.* 2007; Watanabe & Kouchi 2008, and references therein).

1.2 Star Formation and Star Forming Regions

Molecular clouds are the sites where stars are born. These sites are more complex in physical terms than quiescent interstellar clouds. In star-forming regions, clumps of the interstellar gas are compressed when the force of gravity overcomes the resistance provided by gas pressure, magnetohydrodynamic (MHD) turbulence, magnetic pressure, and rotation. The chemistry is not in steady state during this collapse, and can therefore be used as a tracer of the evolution of the collapse. In addition, the chemistry modifies and controls the collapse through the provision of molecular coolants of the gas, and by determining the fractional ionisation in the gas (van Dishoeck *et al.* 1995). The chemical evolution of star-forming regions starts with the dark and dense cloud cores out of which new stars are born. Cold dark cores are nearby members of the densest and coldest phase in the Galactic interstellar medium, and represent the sites where low-mass stars are currently being born.

1.2.1 Early stages of star formation

Attempts to study the nature of the early stages of star formation sequence were started by Lada & Wilking (1984) in their photometric study of the IR broadband (1 - 20 μm) of a number of embedded sources in the core of the Ophiuchus dark cloud. The authors plotted the observed flux density (λF_λ) of their embedded sources as a function of the observed wavelength (λ), in a logarithmic scale, so that they constructed the so-called spectral energy distribution (SED) of all their sample. The shapes of these plots are used to distinguish between the different embedded sources in a molecular cloud. The authors found that their classification is more quantitative by calculating the slope of their SED, α_{IR}, as defined in Eq. (1.1).

$$\alpha_{IR} = dlog(\lambda F_\lambda)/dlog(\lambda) \tag{1.1}$$

Their analysis revealed that there are three categories of IR embedded sources

Class I sources : $0 < \alpha_{IR} \lesssim 3$.

Their SEDs are broader than that of a black body, and rise for wavelengths greater than

$\sim$2μm. They are very deeply embedded and invisible in the optical. The SEDs fit models of objects accreting mass from circumstellar matter. They often have molecular outflows.

Class II sources : -2 $\lesssim \alpha_{IR} \lesssim$ 0.

Their SEDs are also broader than that of a black body, but they are flat or decreasing for wavelengths greater than $\sim$ 2μm. They are visible in the optical and are mostly associated with T-Tauri stars with optically thick discs which are still accreting onto the young stellar object (YSO). This phase is also known as the classical T-Tauri phase (CTT). Their SEDs are well fitted by models of photospheres surrounded by a circumstellar disk and they often have molecular outflows.

Class III sources : -3 $< \alpha_{IR} \lesssim$ -2.

Their SEDs can be modelled by reddened black bodies. They have little or no excess near infrared emission, but slight excess in the mid infrared caused by the cool dust grains which are responsible for the extinction. Their SEDs resemble model SEDs for reddened photospheres of stars very near to or on the zero age main sequence, with an optically thin disc and the envelope already dispersed. This phase is known as weak-line T-Tauri (WTT).

The SED of these classes is shown in Fig. (1.1) which is taken from Lada (1987).

More recently, submillimetre (submm) observations of dust continuum revealed another category of embedded cores known as Class 0 sources (André *et al.* 1993). They are less evolved than Class I sources and have the following observational properties:

(a) Indirect evidence for a central YSO, as indicated by, for instance, the detection of a compact centimetre-wave radio continuum source, a collimated CO outflow, or an internal heating source. This property distinguishes Class 0 objects from the prestellar cores (cores without central objects; see below) and condensations.

(b) Centrally peaked but extended submm continuum emission tracing the presence of a spheroidal circumstellar dust envelope (as opposed to just a disc).

(c) High ratio of submm to bolometric luminosity suggesting the envelope mass exceeds the central stellar mass.

The last two properties distinguish Class 0 objects from more evolved stages, Class I and Class II. Combining the IR and submm data, it is possible to define a complete empirical evolutionary

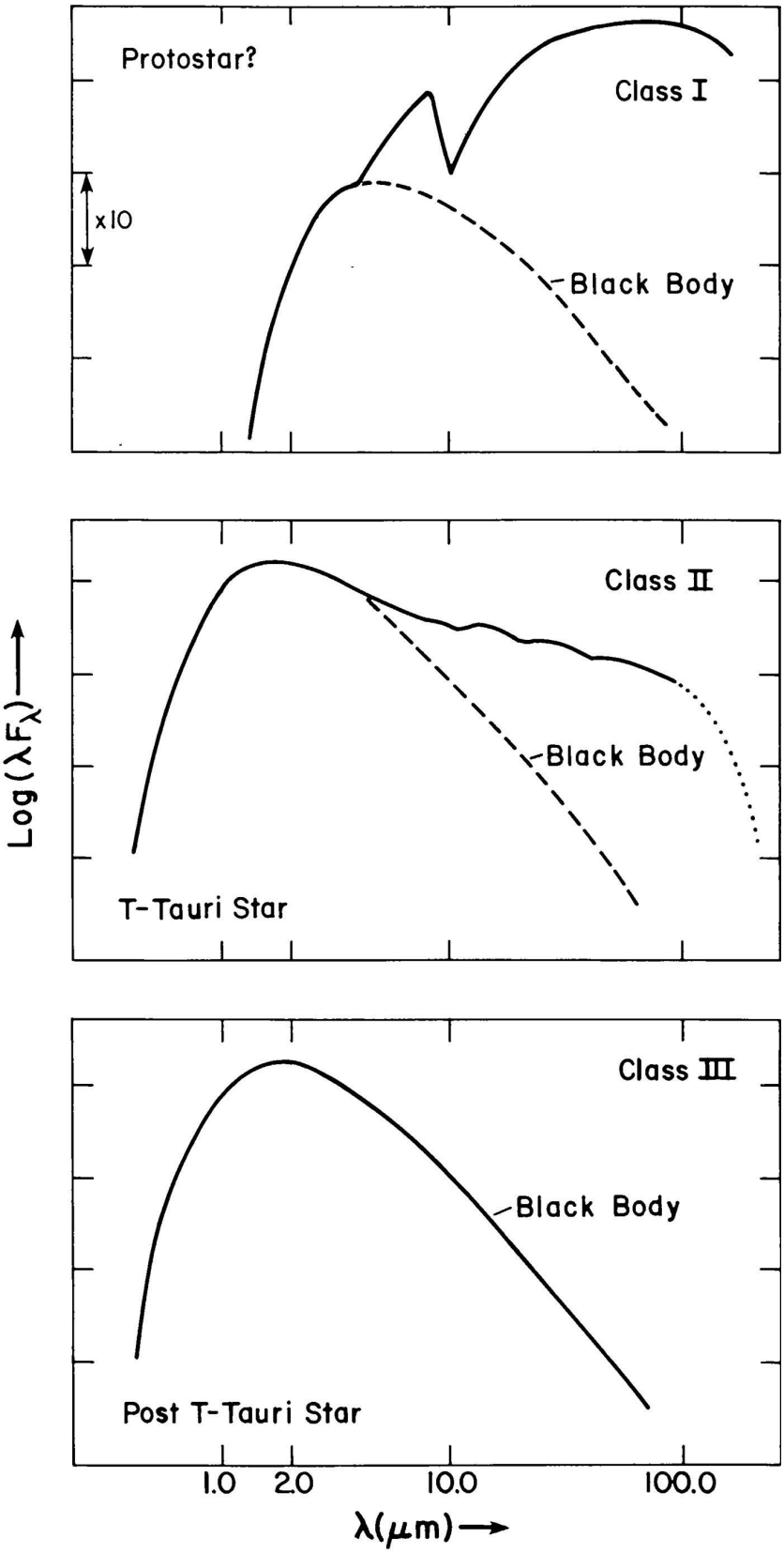

Figure 1.1: The spectral energy distribution (SED) of the three categories of IR embedded cores: Class I, II, and III. Figure is taken from Lada (1987).

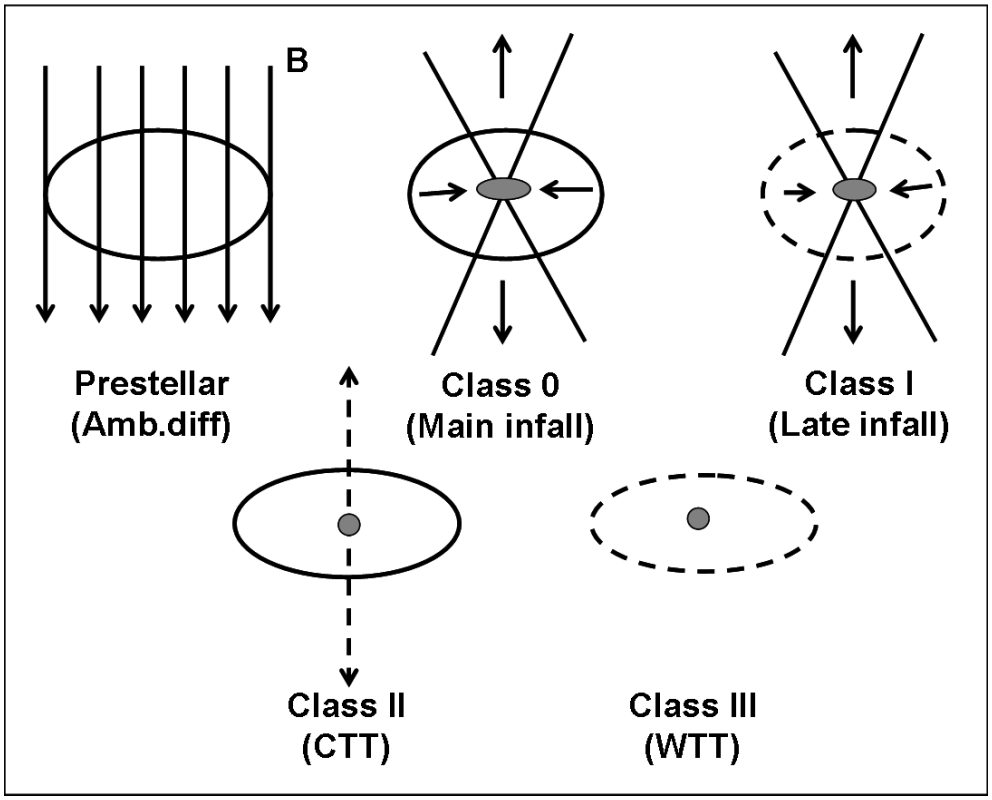

Figure 1.2: Cartoon summarising the five stages of low-mass YSO evolution from a prestellar core to the most evolved Class III protostellar core. Figure is taken from Ward-Thompson (1996).

sequence for low-mass YSO (Class 0 $\longrightarrow$ Class I $\longrightarrow$ Class II $\longrightarrow$ Class III) which corresponds to different stages of evolution: (main accretion phase $\longrightarrow$ late accretion phase $\longrightarrow$ PMS[1] stars with protoplanetary discs $\longrightarrow$ PMS stars with debris discs). A summary of this empirical evolutionary sequence is given in Fig. (1.2), taken from Ward-Thompson (1996).

Embedded cores in a molecular cloud can be categorised as: starless cores, prestellar cores, and Class 0 protostellar cores (see André *et al.* (2009); di Francesco *et al.* (2007) and references therein). *Starless cores* are transient concentrations of molecular gas and dust ($\sim 10^4$ cm^{-3}) without embedded young stellar object (YSO), typically observed in tracers of $C^{18}O$, NH_3, and do not show evidence of infall. *Prestellar cores* are also starless cores, but they are denser (10^5 - 10^6 cm^{-3}) than the previous category, show a centrally-concentrated population of cores that are self-gravitating, hence unlikely to be transient. They are typically detected in submm wavelengths due to the dust continuum emission and dense (10^4 - 10^5 cm^{-3}) molecular gas

[1]PMS stands for pre-main sequence

tracers such as NH_3 or N_2H^+ (e.g. Ward-Thompson *et al.* 1994; Caselli *et al.* 2002b), often seen in absorption at mid- and far-IR wavelengths (e.g Bacmann *et al.* 2000). These cores exhibit evidence of infall motions (André *et al.* 2009 and references therein). The evolutionary stage of the material is, therefore, known as the *prestellar stage*, in which a gravitationally bound core has formed in a molecular cloud, but no central object exists yet within the core. Subsequently, a prestellar core evolves towards progressively higher degrees of central condensation, eventually leading to collapse and causing the formation of a central hydrostatic *protostar*. A protostar is a stellar object that is in the process of assembling the bulk of material it will contain when it ultimately reaches the main sequence.

The last category is the *Class 0* sources; the young accreting protostars. They represent the stage where a new born star is deeply embedded in a thick circumstellar envelope. In this stage, the mass of the star is much smaller than that of the envelope. SED observations of these sources are dominated by the continuum emission of the cold dust in the outer layers of their envelopes at mm and submm wavelengths (for more details see: André *et al.* 1993; Ward-Thompson 1996; di Francesco *et al.* 2007; André *et al.* 2009, and references therein).

1.2.2 Formation of low-mass stars

It is now well established that the formation of low-mass stars involves a series of conceptually different stages. The first stage corresponds to the fragmentation of a clumpy molecular cloud into a number of gravitationally-bound dense cores which are initially supported against gravity by a combination of thermal, magnetic, and turbulent pressures. Dense cores have been observed and mapped in ammonia emission, for example. These cores typically have average $n(H_2)$ = 10^4 - 10^5 cm^{-3}, T $\sim$10 - 30 K, and masses of one to several tens of Solar masses. Some dense cores have densities up to 10^7 cm^{-3} and for some of them masses up to 100 $M_\odot$ are found, in particular in regions of massive star formation (e.g. Hartquist *et al.* 1998; André *et al.* 2000). These fragments form and evolve as a result of poorly understood mechanisms, involving ambipolar diffusion, the dissipation of turbulence, and/or an outside impulse (see; André *et al.* 2000, and references therein). Once they become gravitationally unstable, due to disturbances in one or more of these supporting mechanisms, cores collapse. Gravitationally induced collapse of a core is an important step in star formation, but once a YSO has formed in the region, its stellar winds may affect the collapse of other neighbouring cores. Hartquist *et al.* (1998) amongst others, showed that in some cases the ablation of a core by the YSO supersonic wind forms a flow of material which moves with supersonic speeds until it collides

with another flow from another nearby star. This collision mixes the two flows and the mixture passes through a shock as it is decelerated. This leads to the formation of an inter-core medium of regions of supersonic wind-ablated material mixtures and shells of decelerated mixtures. The shells might fragment leading to the formation of many new cores. In some cases, the ablation of cores is inefficient and nearly all cores collapse to form stars and the remnant of these cores may be blown by the strong stellar winds to larger distances, enough to consider it not associated with the region.

During a brief initial phase (10^4 - 10^5 yrs), after the gravitationally induced collapse, the gravitational energy is freely released away and the collapsing fragment stays roughly isothermal. The isothermal collapse tends to produce a strong central concentration of matter, with a radial density gradient proportional to either r^{-2}, for the inside-out collapse, or to $r^{-3/2}$, in the case of free-fall collapse, independent of initial conditions (Shu & Adams 1987). The collapse ends with the formation of an opaque, hydrostatic central protostar. The central object builds up its mass ($M_\star$) from a surrounding infalling envelope of mass (M_{env}) and accretion disk, while progressively warming up. The youngest accreting protostar has $M_{env} \gg M_\star$ and its luminosity is mainly due to the accretion luminosity, L_{acc}, given by

$$L_{acc} = GM_\star \dot{M}_{acc} \; / \; R_\star \tag{1.2}$$

where G is the gravitational constant, $R_\star$ is the stellar radius and $\dot{M}_{acc}$ is the accretion rate of the material on to the protostar which is considered to be constant in time ($\simeq a^3/G$, a is the effective isothermal sound speed) for isolated star formation (Shu & Adams 1987; André *et al.* 2000).

As a low-mass protostar accretes matter, it naturally evolves towards a state with a stellar wind. In this evolutionary phase, central objects are known as bipolar outflow sources (e.g. Snell *et al.* 1980; Lada & Harvey 1981; Lada 1985; Snell 1987). This picture is supported by observations that have shown that there is always a powerful ejection of a fraction of the accreted material in the form of bipolar jets/outflows which usually takes a well collimated form. These outflows are believed to carry away the excess of angular momentum of the infalling material (e.g. Bachiller 1996; Konigl & Pudritz 2000).

Stars are often part of a multiple system or members of an association. The majority of these stars are born in environments that are considerably more complex than the simple picture outlined in Fig. (1.3), taken from van Dishoeck & Blake (1998). This figure illustrates a summary for the evolutionary stages during the formation of an isolated low-mass star: from

the clumpy molecular clouds up to the formation of planetary discs and stellar systems. The process of star formation starts with dark molecular cores, roughly 1 pc in size, contracts until the magnetic support is overcome and the collapse starts at zero-time; Fig. (1.3 - a, b). In this stage, the IR spectrum is that of the collapsing core which is rich in ices such as H_2O, and CO. After 10^{4-5} yrs, a phase of both high accretion and supersonic outflow occurs in deeply embedded protostars (YSO). Evaporation of ices drives a hot core chemistry rich in organic molecules, whereas shocks propagating through the dense envelope release both refractory and volatile grain material, resulting in prominent SiO, OH, and H_2O emission; see Fig. (1.3-c). On time-scales of 10^{6-7} yrs, outflows will gradually clean the material surrounding the YSO, leaving the T Tauri star and a residual protoplanetary accretion disk which leads, at the end, to the formation of a mature planetary system at times $> 10^7$ yrs; Fig. (1.3 - d, e).

1.3 Modelling Star Forming Regions

In order to describe and understand the processes in star forming regions, physical and/or chemical modelling is needed. Since the 1940s, models have been developed ranging from pure gas-phase chemical networks (e.g. Herbst & Klemperer 1973; Ali *et al.* 2001) to pure grain-surface models (e.g. Pickles & Williams 1977; Tielens & Hagen 1982). Although pure gas-phase models were successful in explaining and reproducing many of the observed data in both diffuse, translucent as well as dark clouds, they could not reproduce the observed abundances of saturated molecules such as NH_3, large organic species such as CH_3OH, and they could not explain the existence of solidified species (e.g. van Dishoeck 1998 and references therein). For this reason, it has become clear that the interaction between gas-phase and grain-surface chemistry is important for astrochemical modelling. This interaction leads to the well-known gas-grain chemical models which are now more commonly used in astrochemical studies (e.g. Hasegawa *et al.* 1992; Shalabiea & Greenberg 1995a,b; Viti & Williams 1999; Ruffle & Herbst 2001; Viti *et al.* 2004; Garrod & Herbst 2006; Garrod *et al.* 2007*b*).

Since molecules are so important for the properties of interstellar clouds, we shall consider their formation reactions. If we consider two atoms A and B approaching each other, their energy of interaction can be described by the so-called potential energy curve as given in Fig. (1.4) which is attractive. If the two atoms are close enough (i.e. at the bottom of the potential well), they will collide and interact to form a new molecule, if some energy is removed from the colliding pair. If no energy is released, the atoms will merely bounce apart and no interaction

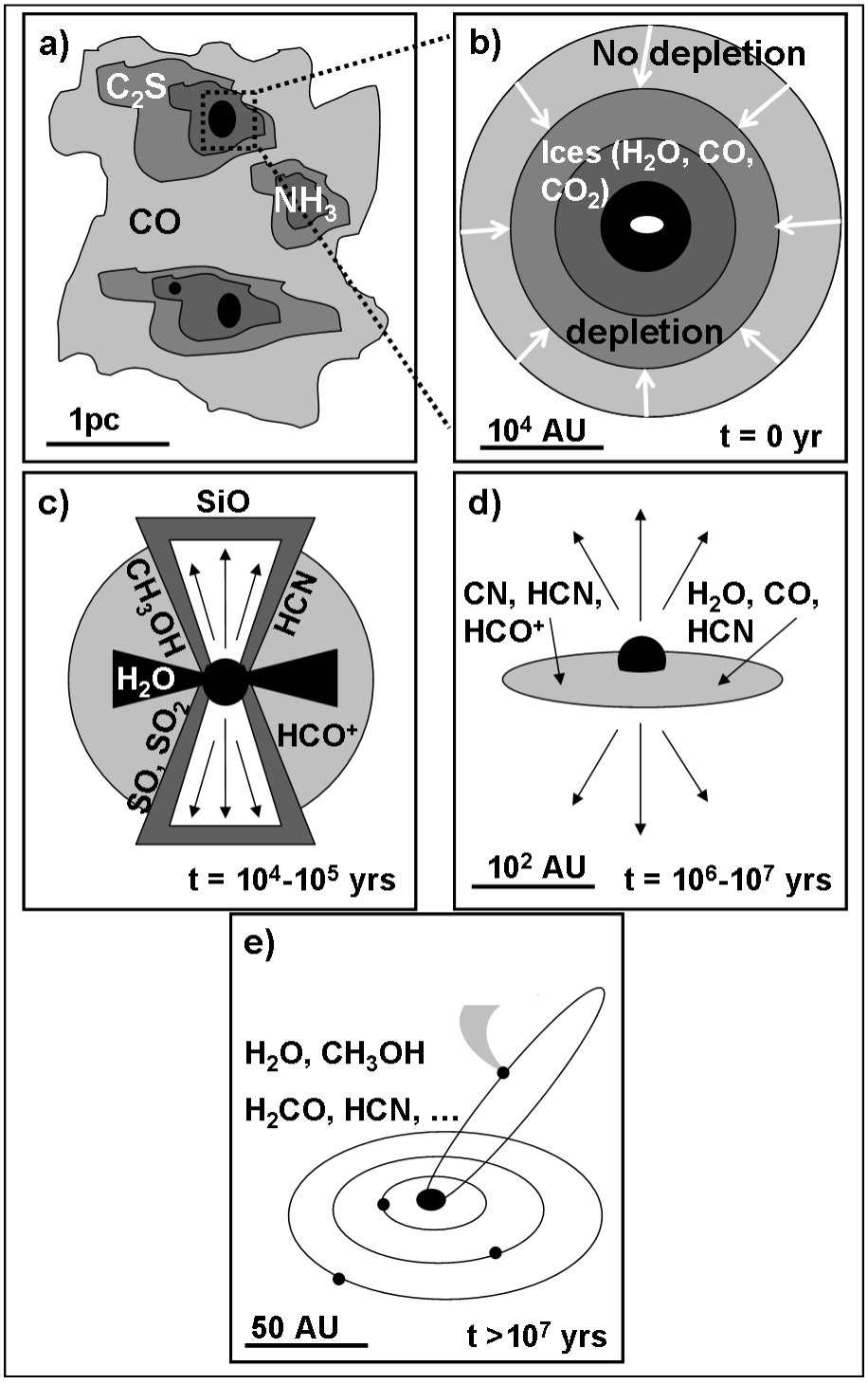

Figure 1.3: A schematic view of the process of an isolated, low-mass star formation. Characteristic molecules at each of these stages as well as the lifetime of each stage are indicated; see text for description. Sketch is taken from van Dishoeck & Blake (1998).

will occur (Dyson & Williams 1997). The complex does not easily radiate energy away on timescales as short as that of the period of a vibrational oscillation of a molecule ($\simeq 10^{-13}$ s^{-1}). This process is called the radiative association and it is very slow under the ISM conditions.

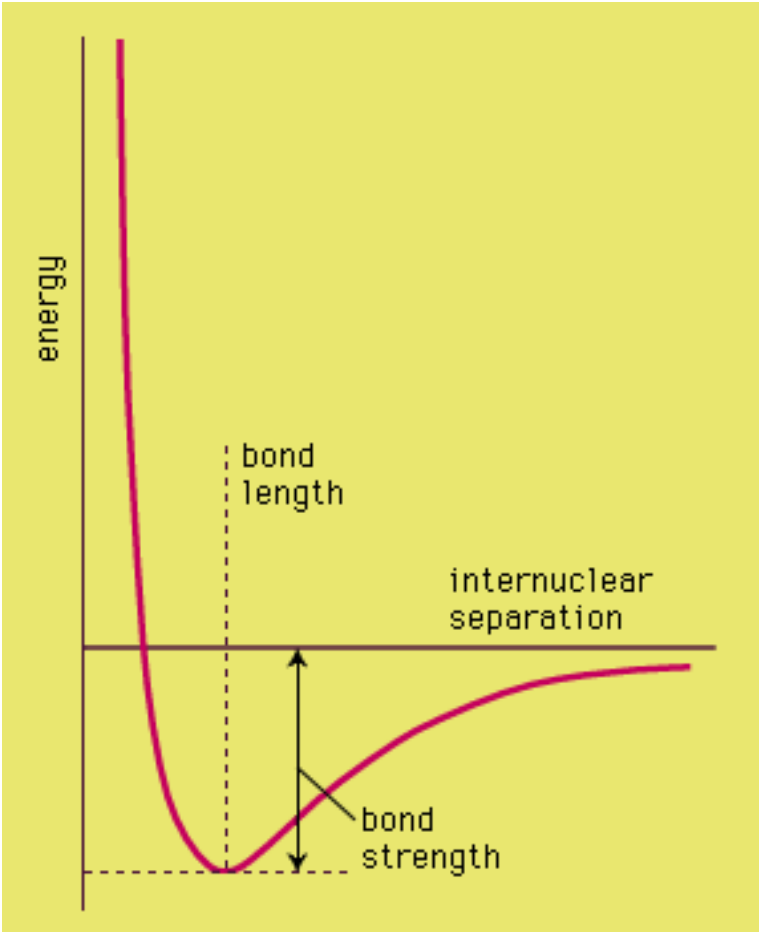

Figure 1.4: A schematic representation of the potential energy interaction curve of two atoms.

The removal of the energy from the complex (A+B) may happen and a new species AB be formed if another atom C collides with the system to keep the two atoms A and B at the bottom of the potential well. This process which involves three body reaction does not occur under the ISM circumstances because of the extremely low density.

From the above one can easily see how difficult is the formation of molecules in the ISM. In the next section I will briefly explain how molecules can form initially in the ISM.

1.3.1 Gas-phase chemical processes

The onset of the chemistry in the ISM is due to the formation of H_2 which is believed to result from the interaction of atomic hydrogen gas with dust grains; see §(1.3.2.1) below. Inside molecular/dark clouds, the penetration of external photons is not easy because of the high visual extinction caused by dust due to the high density of material. Therefore, the effect of external radiation is negligible due to their absorption and scattering by dust grains, and hence they have no influence on the chemistry of these regions. The interstellar medium is swept by cosmic rays which are mainly fast protons and electrons. Therefore, in such regions, CRs are the most important source of ionisation and hence drive the chemical reaction networks. H_3^+ is the most important ion in the interstellar regions because it initiates their chemistry. Helium ions (He^+) are also important in driving the ion-molecule chemistry in interstellar regions. CRs ionise H_2, the ion is then quickly converted into H_3^+ as shown in reactions (1.3).

$$H_2 \xrightarrow{CR} H_2^+ \xrightarrow{H_2} H_3^+ + H \tag{1.3}$$

H_3^+ initiates a chain of chemical reactions involving elements such as oxygen, O, and carbon, C, giving rise to the rich observed chemistry. In dark clouds, the reaction of H_3^+ with HD, the reservoir of deuterium (D) in interstellar medium, leads to the formation of H_2D^+ which leads the deuterium chemistry in interstellar clouds. Our detailed study on deuterium chemistry in low-mass star forming regions, in Chapter 3, covers this issue.

Below is a brief summary with examples of some types of fundamental gas-phase reactions that take place in molecular and dark clouds:

Cosmic ray ionisation: e.g. $H_2 + CR \rightarrow H_2^+ + e^- + CR$

As mentioned above, cosmic rays drive the chemistry inside dark clouds by creating H_3^+, and also by ionising other species such as He, C, N, O and CO. From the observed abundances of molecular ions inside molecular dark clouds, the ionisation rate of H_2 by cosmic rays has been estimated to be between 1-30$\times$ 10^{-17} s^{-1} (Dalgarno 2006).

Photoionisation and photodissociation: e.g. $C + h\nu \rightarrow C^+ + e^-$; $HCN + h\nu \rightarrow CN + H$

The UV component of the interstellar radiation field is capable of ionising species such as C, N, O and H. The photoionisation rates are proportional to $e^{-\gamma A_v}$, where γ is discussed in §(1.6), and A_v is the visual extinction caused by dust grains. For dark clouds, with $A_v \gtrsim 5$, the photoionisation rates are therefore highly suppressed. However, Prasad & Tarafdar (1983) showed that small but significant UV field can be maintained in the

interiors of dark clouds by cosmic rays, and hence some degree of ionisation can be retained in dark cores. In this mechanism, the authors showed that in dark clouds the UV radiation is produced by the decay of the Lyman and Werner states of molecular hydrogen[2], which has been excited by the energetic electrons emitted by cosmic ray ionisation of H_2.

Exchange reactions: These can either be ion-molecule (e.g. $H_3^+ + CO_2 \rightarrow HCO_2^+ + H_2$), neutral-neutral (e.g. $C + OH \rightarrow CO + H$), carbon insertion (e.g. $C + CH_2 \rightarrow C_2H + H$), or charge exchange (e.g. $N^+ + CO \rightarrow N + CO^+$).

Neutral-neutral reactions are often slow because the forces between the reactants are weak, so they therefore have a much smaller cross-section than that of ion-molecule reactions. Many neutral-neutral reactions also have an activation energy barrier, although they are difficult to predict theoretically and are often determined experimentally.

Radiative association: e.g. $C + O \rightarrow CO + h\nu$.

These reactions are slow, thus they do not contribute significantly to the chemistry in molecular clouds.

Recombination: The initial product of recombination reactions is generally in an unstable, excited state, so it either has to dissociate or emit a photon. Dissociative recombination is generally an efficient process because of the strong attraction between the reactants, and the excess energy is carried off in the form of kinetic energy of the products. An example of such reactions is the formation of water as follows: $H_3O^+ + e^- \rightarrow H_2O + H$. Radiative recombination, which occurs when atoms react with electrons, is less efficient because the resulting neutral atom is more likely to lose its newly acquired electron rather than emit a photon for stabilisation such as $O^+ + e^- \rightarrow O + h\nu$.

The full list of reactions includes two-body reactions (including ion-molecule, neutral-neutral and carbon insertion exchange reactions, charge exchange reactions and radiative association), direct cosmic ray ionisation, cosmic ray induced photoreactions (from the UV field generated by cosmic rays) and recombination reactions (both dissociative and radiative).

[2]Lyman series is the series of transitions resulting ultraviolet emission (absorption) lines of the hydrogen atom corresponding to transitions from n$\geqslant$2 to n=1 (n=1 to n$\geqslant$2) where n is the principal quantum number referring to the energy level of the electron. The Werner band is an absorption series with its first band at $\lambda < 1008\mathring{A}$. These bands comprise nearly 400 absorption lines between 912 and $1120\mathring{A}$.

Table 1.2: List of the different gas-phase reactions involved in chemical models.

Two body reactions	
Neutral-Neutral	$A + B \longrightarrow C + D$
Ion-Neutral	$A^+ + B \longrightarrow C^+ + D$
Insertion Reactions	$AX + B \longrightarrow CX + D$
Charge Transfer	$A^+ + B \longrightarrow A + B^+$
Recombination reactions	
Radiative Recombination	$A^+ + e^- \longrightarrow A + h\nu$
Dissociative Recombination	$AB^+ + e^- \longrightarrow A + B$
Photo-reactions	
Cosmic-ray ionisation	$A + CR \longrightarrow A^+ + e^- + CR$
Photoionisation	$A + h\nu \longrightarrow A^+ + e^-$
Photodissociation	$AB + h\nu \longrightarrow A + B$
Radiative Association	$A + B \longrightarrow C + h\nu$

1.3.2 Grain surface chemistry

Gas-phase reactions successfully reproduced the observed abundances of many molecules, however some are not efficiently formed via those schemes (for instance; H_2, and H_2O) and here comes the need of introducing interstellar grains to play the role of catalyst (e.g. Pirronello *et al.* 2007). Grains act as a catalytic surface for H_2 formation, they also accrete gas-phase material to form icy mantles in a process known as freeze-out. The latter has a large effect on the overall chemistry of interstellar regions where some species are now confirmed to be mantle species i.e. formed on grain surfaces via surface reactions, such as H_2, CH_3OH, and more complex species such as $HCOOCH_3$ (e.g. Tielens & Hagen 1982; Hasegawa *et al.* 1992; Watanabe *et al.* 2003; Horn *et al.* 2004; Garrod & Herbst 2006; Pirronello *et al.* 2007, and references therein).

1.3.2.1 H_2 Formation

Molecular hydrogen, H_2, is an essential ingredient in the interstellar chemistry. It is the parent molecule of H_3^+, the motor of interstellar chemistry, see reaction (1.3). In gas-phase, H_2 could be formed via radiative association reaction '$H + H \rightarrow H_2 + h\nu$'. The fact that the H_2 molecule

does not possess a permanent dipole moment makes it difficult for the molecule to stabilise by radiating a photon. In addition, the very low density of the ISM makes it difficult for a third species to collide with the molecule and take away this excess energy (Flower 2007). Hence, this reaction is strongly forbidden and is not significant even over long astronomical time scales (Williams 2003b). Other gas-phase routes to form H_2 are available such as

$$\begin{aligned} &H + e^- \rightarrow H^- + h\nu \\ &H^- + H \rightarrow H_2 + e^- \end{aligned} \tag{1.4}$$

and also

$$\begin{aligned} &H + H^+ \rightarrow H_2^+ + h\nu \\ &H_2^+ + H \rightarrow H_2 + H^+ \end{aligned} \tag{1.5}$$

however, these reactions are inadequate to form the observed amount of the species in the ISM of the Galaxy because the photodissociation of H_2 by stellar radiation is rather rapid (Stecher & Williams 1967).

H_2 was the first species that was accepted to be produced by surface reactions on grains, when conditions in clouds allowed only the presence of neutral H atoms. van de Hulst (1948) was the first to propose the formation of molecular hydrogen on grain surfaces, where grains act as catalyst. In the following years, the problem, however, had been studied almost exclusively on a theoretical ground (e.g. Gould & Salpeter 1963; Duley & Williams 1986; Duley 1996) because of the intrinsic difficulties of performing the needed experiments at that time (as reviewed by Pirronello *et al.* 2007). The development in experimental technologies allowed the study of H_2 formation and confirmed its efficiency on grain surfaces. More details on the experimental history regarding this issue is reviewed by Pirronello *et al.* (2007). There are three major mechanisms for surface reactions: the diffusive, or Langmuir-Hinshelwood; the Eley-Rideal; and the hot atom, all of which are depicted in Figure (1.5), which shows a regular surface with a periodic potential. Accretion, with a sticking efficiency S, occurs onto the potential minima, known as binding sites, which here represent physisorption sites. Desorption is also possible, with a minimum energy E_D, either by thermal evaporation (sublimation) for very light species or by non-thermal mechanisms. A more general sublimation occurs for all species on the ice as the surface temperature increases to 100 - 300 K in YSOs, see § (1.3.2.2). Below is a brief description of the three major mechanisms for surface reactions.

Langmuir-Hinshelwood (L-H) mechanism: H atoms adsorb to the dust grain surface where

they are thermalised. They then diffuse, by either tunnelling or thermal hopping over the barrier E_b between binding sites, over the surface, and can react when two H atoms meet. The newly formed H_2 molecule can then desorb from the surface of the dust grain back into the gas-phase due to the energy released when the two atoms react.

Eley-Rideal (E-R) mechanism: When an H atom collides with the dust grain, it reacts instantly with another H atom already adsorbed to the surface to form H_2. This mechanism is more likely when the coverage of hydrogen atoms on the grain surface is high; i.e. in dense regions.

Hot atom mechanism: This mechanism is an intermediate between the L-H and E-R mechanisms. In this case, one hydrogen atom is adsorbed and in thermal equilibrium with the grain, whereas the other H atom is not yet thermalised and therefore at a higher temperature. The non-thermalised hot atom can diffuse towards the thermalised H atom.

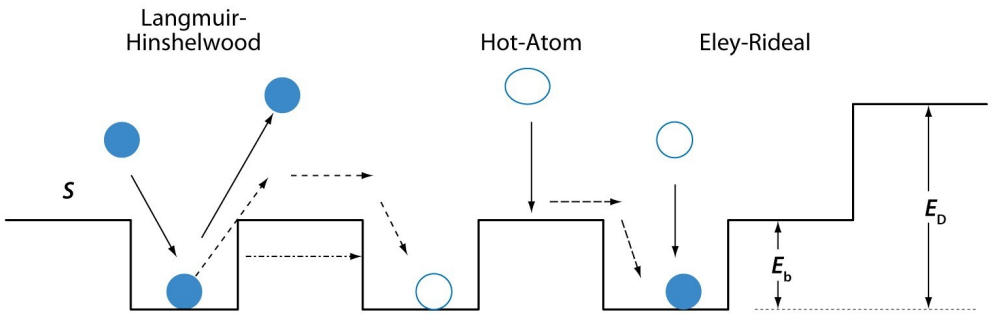

Figure 1.5: Three mechanisms for surface reactions on a regular grain surface. S is the sticking efficiency of a gas-phase species, E_D is the binding, or desorption, energy of the adsorbate to the surface, and E_b is the barrier from one site to an adjacent one. Figure is taken from (Herbst & van Dishoeck 2009).

It is now well-known that grain surfaces are sites for the formation of many types of interstellar molecules. The most significant are H_2 and H_2O, but there are many others, such as methanol, which is recently proved to be formed via the successive hydrogenation of CO molecules on grain surfaces (e.g. Watanabe *et al.* 2003; Watanabe & Kouchi 2008), and more complex species observed in the Universe such as $HCOOCH_3$ (Horn *et al.* 2004; Garrod & Herbst 2006). In addition, grain surfaces are factories of deuterated species such as HDCO, D_2CO, $DCOOCH_3$ (e.g. Tielens 1983; Demyk *et al.* 2010, and Chapter 3 in this work). The species formed on grains are returned to the gas-phase via desorption mechanisms which could be either thermal or non-thermal.

1.3.2.2 Desorption mechanisms

Observations of gas-phase heavy species along lines of sight everywhere in space indicates that the freeze-out of molecules onto grain surfaces is not an unlimited process. Observations of molecules such as CO in dark clouds (e.g. L134N Wakelam *et al.* 2006) imply that desorption processes must be operating for mantle growth to be limited. Many possible mechanisms have been proposed, most of which require impulsive heating of grains which can be caused by (i) direct impact of cosmic rays (e.g. Leger *et al.* 1985; Hartquist & Williams 1990; Hasegawa & Herbst 1993), (ii) X-rays (Leger *et al.* 1985), (iii) UV photons induced by cosmic rays (cosmic ray photodesorption) (e.g. Hartquist & Williams 1990), or (iv) exothermic reactions occurring on the grain surface, in particular the formation of molecular hydrogen (e.g. Duley & Williams 1993; Garrod *et al.* 2007*a*). Molecules can be desorbed either by classical evaporation (Leger *et al.* 1985; Tielens & Hagen 1982) or by chemical explosions (Leger *et al.* 1985; Shalabiea & Greenberg 1994). Chemical explosions can only occur by stored radicals in the icy mantles and they can be induced by (i) grain-grain collisions, and (ii) CR iron nuclei (Schutte & Greenberg 1991; Shalabiea & Greenberg 1994). In order to form radicals in icy mantles, they had to be previously irradiated by UV photons, therefore this mechanism is not likely to be in dense cores with $A_v > 5$ (Roberts *et al.* 2007).

Generally, desorption mechanisms can be then divided into two categorise; **thermal desorption** which requires a heating source such as a nearby protostar; **non-thermal desorption** which requires an external trigger, mainly CRs, to induce the mantle species to evaporate back to gas-phase. The latter includes photodesorption mechanisms. In dense clouds and in outer discs and disc mid-planes, desorption must occur non-thermally since the grain temperature is low enough, around 10 K, that thermal desorption is negligible (e.g. Roberts & Millar 2007; Öberg *et al.* 2009a,b). Shocks can also be counted as another desorption mechanism by sputtering.

Recently, McCoustra and his team carried out experimental studies aimed to investigate the thermal desorption characteristics of several astrophysical relevant molecules from laboratory analogues of the icy mantles on interstellar dust grains (Collings *et al.* 2003a,b, 2004). The authors showed that molecular ices can be divided into five categories: (i) CO-like; (ii) H_2O-like; (iii) intermediate; (iv) reactive; (v) refractory. For each category one can estimate the fraction of a particular molecular species that is desorbed in various temperature bands; see Table (2.2) in Chapter 2 which is taken from Viti *et al.* (2004). These bands can be summarised as (i) the

pure species; (ii) a monomolecular layer on H_2O 'solid desorption'; (iii) the volcano desorption mechanism which occurs during H_2O ice phase change; (iv) co-desorption regime when H_2O ice desorbs; and (v) desorption from the bare grain surfaces (more details about these bands are given in Chapter 2 in this thesis and the detailed description about the experiments can be found in Collings *et al.* (2003a,b, 2004)). Brown *et al.* (2006) studied the sensitivity of chemical models of high mass star forming regions to different types of dust grains and to different thicknesses of icy mantles to understand whether the nature and composition of the grain surface is important in dictating the chemistry that occur in star forming regions. Experimental results showed that reactions on different surfaces and for different thicknesses of mixed ices may lead to different desorption temperatures and also different species classification from that previously obtained by Collings *et al.* (2004); Viti *et al.* (2004). These differences led to an earlier evaporation of methanol and earlier formation of $HCOOCH_3$. For more details the reader is referred to Brown *et al.* (2006).

More recently, Roberts *et al.* (2007) modelled three different non-thermal desorption mechanisms in dark clouds; desorption resulting from H_2 formation on grains, direct cosmic ray heating and cosmic ray-induced photodesorption. The authors concluded that regardless of the qualitative differences between the studied mechanisms, they all are found to be potentially very significant in dark cloud conditions. Roberts et al. insist that those processes are therefore important and should be considered in studies of molecular clouds where freeze-out and desorption are believed to be important. More recently, Öberg *et al.* (2009a,b) carried out a series of experimental works under astrochemically relevant conditions to study the photodesorption mechanism via UV photons of key species such as CO, N_2, H_2O, and D_2O. Photodesorption is a non-thermal desorption mechanism, which may explain the small amounts of observed cold gas in cloud cores and disc mid-planes. In their study, the authors found both the UV photodesorption yield per incident photon and the photodesorption mechanism are highly molecule specific (Öberg *et al.* 2009a). They found that the CO photodesorption yield is temperature dependent between 15 and 27 K, N_2 co-desorbs with CO at 16 K in mixed or layered ices. The photodesorption of CO_2 starts by its photodissociation on ices into CO and O which either desorb or recombine to form CO_2 and CO_3 before desorbing. They also found that CO_2 desorption is a thickness dependent process. For the case of water and deuterated water, Öberg *et al.* (2009b) were unable to distinguish between the yield of both species, due to experimental uncertainties. However, the authors were able to conclude that the desorption yield depends on both the ice thickness as well as the temperature, but not, in the case of D_2O, on the ice nature

(amorphous or crystalline).

From the above discussion it is now clear how important the inclusion of desorption mechanisms in chemical models is, because they give us an understanding of the nature of the grain mantle in the interstellar environment under study.

1.4 Chemical Models: An Overview

In the last decades, chemical models have become powerful tools to investigate the properties of a wide range of astronomical regions. The calculation of chemical abundances in dense clouds and YSOs requires a specification of the physical parameters such as the temperature, density, radiation field, etc. In their simplest form, two different classes of models are considered according to their dependence on time:

Steady-state: here the abundances of the molecules do not change with time.

They also can be a function of depth, and then called steady-state, depth-dependent models such as those of translucent outer envelopes, and dense UV photon- or X-ray dominated regions near YSOs (e.g. Hollenbach & Tielens 1997). Models in this category are, generally, not used to study star-forming regions. If the abundances are not a function of depth, then the models are known as steady-state, depth-independent. In these models, physical conditions of the region under study are fixed (e.g. Hasegawa & Herbst 1993).

Time-dependent: here the abundances are computed as functions of time.

In time-dependent, depth-independent models, abundances are functions of time at a single point deep inside the region. Some models of starless/prestellar clouds, collapsing envelopes, and some hot cores near massive young stars fall in this category. Modelling these regions could also be time-dependent and depth-dependent (e.g. Nejad & Wagenblast 1999; Viti & Williams 1999). The time scale for reaching chemical equilibrium ranges from 10^5 to 10^7 years, depending on the degree of ionisation, temperature, density, and the species involved (van Dishoeck & Blake 1998).

For all chemical models, there are several input parameters in common: the initial elemental abundances and their nature (atomic, neutral, ionised, etc.), CR ionisation rate, ζ, the density and temperature profiles as a function of time and/or depth, the incident radiation field, the visual extinction. In addition, the geometry of the region (e.g. plane-parallel, spherical, etc.), and

the grain parameters, i.e. the extinction curve[3], albedo[4], and scattering function[5]. The temperature profiles of the gas and dust can be obtained either from the constraints of observations, or self-consistently from the balance of heating and cooling processes. Some chemical models proceed at fixed temperature. For more details of chemical models; see van Dishoeck & Blake (1998) and references therein.

Time dependent models can be classified as either real-time-dependent, in which the density changes as a function of time, or pseudo-time-dependent, in which the density is constant in time. Dynamical models are those in which both temperature and density vary with time. An additional category to the above is the chemical-dynamical models which couple the chemistry and the dynamics such as those treating collapsing clouds. These models are best for the study of the chemical evolution of the cloud during the collapse (e.g. Rawlings *et al.* 1992).

From the chemistry point of view, chemical models can be classified according to the chemical reaction networks used: pure gas-phase in which reactions take place only in gas-phase; and gas-grain chemical models where reactions occur in the gas-phase and on grain surfaces. There are two different approaches to model surface chemistry: the 'deterministic' and 'stochastic' methods. The first was introduced by Pickles & Williams (1977) and consists of rate equations governing the time evolution of surface species, in analogy with gas-phase models. Surface rate coefficients are given by the sum of the diffusion rates of reaction partners multiplied by the reaction probability, if an activation energy barrier exists. This method has been adopted in many models such as Hasegawa *et al.* (1992); Hasegawa & Herbst (1993); Shalabiea & Greenberg (1994); Viti & Williams (1999); Viti *et al.* (2004); Awad *et al.* (2010) and many others.

The second approach, the stochastic methods, takes into account the discrete nature of dust grains. Grain surface chemistry is normally limited by the rate at which reactive gases are transported to the surface (accretion limit) and not by surface reaction rates (reaction limit) once the species are adsorbed (Caselli *et al.* 1999). This is because the diffusion rates of reactive species are much faster than accretion rates. This method is used in Monte Carlo simulations

[3]Extinction is a term used in astronomy to describe the absorption and scattering of electromagnetic radiation emitted by astronomical objects by matter (dust and gas) between the emitting object and the observer. The extinction curve is the extinction as a function of wavelength.

[4]The albedo of an object is a measure of how strongly it reflects light from light sources. It is the ratio of total-reflected to incident radiation.

[5]The scattering function in physics is generally a function which describes the intensity of scattered radiation in any given direction

(e.g. Tielens & Hagen 1982; Tielens & Charnley 1997; Cuppen & Herbst 2007; Cuppen *et al.* 2009).

1.5 Chemistry in Low-Mass Star Forming Regions

One of the main goals of astrochemistry is to use certain molecules as temporal indicators of the evolutionary state of an object. The presence of several species in different astrophysical environments helps in achieving this goal. Chemistry controls important physical parameters such as the level of ionisation and the cooling of the gas. In addition, molecular abundances give constraints on the internal and external radiation fields because the fraction of a particular species that freezes onto grain surfaces contains important information on the temperature and irradiation history of the region (van Dishoeck & Blake 1998). Thus, detailed understanding of the chemistry of star forming regions is essential to fully understand their physics. As we described briefly in §(1.2.2) and shown in Fig. (1.3), during each phase of the formation sequence of stars, there are some species that could be used as evolutionary indicators. The presence of these species implies that there is rich chemistry going on in these regions. In the following context we briefly summarise the chemistry in both pre- and proto-stellar stages.

1.5.1 Chemistry in prestellar cores

Dark clouds are mainly studied via mm emission lines. Molecular lines, in particular CO, CS, NH_3, etc., can be used to constrain the density and temperature of these clouds (van Dishoeck & Blake 1998; Bergin & Tafalla 2007). Chemical reactions in cold clouds (10 K) are triggered by CR ionisation and proceed mainly via gas-phase ion-molecule reactions. While neutral-neutral reactions play an important role in forming molecules such as N_2. In addition, grain surface reactions play a role in the formation of organic and complex species (more details are in §(1.3)). Recent observations and modelling of low-mass starless (prestellar) cores show that many molecules in these cores show evidences of depletion (e.g. Caselli *et al.* 1999; Bacmann *et al.* 2002; Tafalla *et al.* 2002). Molecular depletion increases with both time and gas density of the core and hence it can provide a reliable clock to time the contraction history of the dense core (Tafalla *et al.* 2006). By comparing dust continuum and molecular line intensity, Tafalla *et al.* (2002) investigated the radial distribution of molecular abundances of N_2H^+ and C_2S in the prestellar core L1544. They found that in a depleted dense gas, N-bearing species survive much longer than C-bearing ones. As a result, a core gradually develops a differenti-

ated interior, characterised by a centre rich in depletion-resistant species surrounded by layers richer in depletion-sensitive molecules. Tafalla *et al.* (2006) emphasised that understanding this abundance pattern is critical to interpret molecular line observations of cores because different species will systematically trace different layers depending both on their response to depletion and their level excitation. Theoretical modelling of such cores support this view and show that species like CS and C_2S are destroyed by gas-phase reactions at early-times when CO is frozen on to grains. On the other hand, the N-bearing species such as N_2H^+ and NH_3 survive for longer times in the gas-phase due to the depletion of CO on to grain surfaces and to the low binding energy of their parent molecule, N_2, to grain surfaces (Tafalla *et al.* 2002; Aikawa *et al.* 2005; Maret *et al.* 2006). N_2H^+ is observed to be depleted in some prestellar cores such as B68 and L183 (Bergin *et al.* 2002; Pagani *et al.* 2005).

The species above are not the only observed ones in dark/prestellar cores; many other species are observed such as HCO^+, H_2CO, H_2S, HNC, CH_3OH, in addition to their deuterated species (e.g. Caselli *et al.* 2002a; Vastel *et al.* 2003; van der Tak *et al.* 2002). Theoretical and observational studies of dark/prestellar cores (e.g. Brown & Rice 1981; Turner 1990; Brown & Millar 1989a,b; Roberts & Millar 2000a,b; Ceccarelli 2002; Bacmann *et al.* 2002; Vastel *et al.* 2006; Roberts & Millar 2007; Sakai *et al.* 2009) showed that they are the origin of the deuterium fractionation in the interstellar clouds. Deuterium enrichment originates in some exothermic D-H exchange reactions. The deuterium enrichment in H_3^+ (as H_2D^+, HD_2^+, and/or D_3^+) propagates to other species, because H_3^+ is the key reactant in ion-molecule reaction network. Reaction (1.6) presents the general gas-phase pathway of deuteration.

$$\begin{aligned} H_3^+ + HD &\longrightarrow H_2D^+ + H_2 \\ H_2D^+ + X &\longrightarrow XD^+ + HD \end{aligned} \tag{1.6}$$

Deuterium fractionation occurs also on grain surfaces (Tielens 1983). The removal of heavy species from the gas-phase, in particular CO, enhances the deuterium fractionation in gas-phase because such species work on destroying H_3^+, and hence their depletion increases the life time of H_3^+ thus allowing more deuteration in gas-phase (Bacmann *et al.* 2003). More details about deuterium chemistry are given in §(3.1) in Chapter 3 in this thesis.

Many studies of various prestellar cores such as L1544, L1689N, Barnard 1 'B1', TMC-1 and L134N (= L183), either theoretical, observational or both are now available. The last two cores are used as template objects because of their rich chemistry and because they are unassociated with star-formation activity (Bergin & Tafalla 2007). Details about these studies

can be found in Ward-Thompson (1996); van Dishoeck (1998); van Dishoeck & Blake (1998); Caselli *et al.* (1999); Roueff *et al.* (2000); André *et al.* (2000); Loinard *et al.* (2001); Tafalla *et al.* (2002); Lis *et al.* (2002); Caselli *et al.* (2003); Flower *et al.* (2004); Aikawa *et al.* (2005); Roberts & Millar (2007); Aikawa (2008); André *et al.* (2009).

1.5.2 Chemistry in protostellar cores

As mentioned in §(1.2.2), the gravitationally bound prestellar cores will collapse once they became gravitationally unstable. The collapse leads to the formation of a dense central object that builds up its mass by accreting the surrounding material. At this stage, the opaque central object is known as a protostar (Stahler *et al.* 1980a,b; Hartquist *et al.* 1998; André *et al.* 2000).

It has been shown that very likely all low-mass protostars have inner regions warm enough to make the grain mantle evaporate (e.g. Ceccarelli *et al.* 2000b; Ceccarelli 2004). Sublimation of these mantles has a great impact on the gas-phase. Nowadays, many astronomers call these warm regions "hot corinos" because they show chemistry similar to that find in hot cores, sites of massive star formation. Therefore, **chemically**, hot corinos have been considered as the analogues of hot cores, but for low-mass stars (e.g. Ceccarelli 2004; Ceccarelli *et al.* 2007). In the context hereafter, we may use the term "warm core" interchangeably with "hot corino" because the former reflects physical information about the region. In fact, from a chemical point of view the envelope of Class 0 sources is formed by two zones: the zone where ices sublimate (dust temperature ≥ 100 K), the warm core region, and the outer cold envelope (dust temperature ≤ 100 K). The chemistry in the outer envelope is similar to that in prestellar cores, cold (~ 10 K) and dense ($\geq 1 \times 10^5$ cm^{-3}) condensations believed to be precursors of the Class 0 sources. Many molecules are frozen onto the grain mantles, so that their abundance is often lower than that in molecular clouds.

The deeply embedded low mass protostar IRAS 16293-2422 has been the subject of numerous far-infrared, millimetre and centimetre wavelength observations, which have revealed a complex structure within this source. In the next few lines we summarise our current knowledge about this source.

IRAS 16293-2422

IRAS 16293-2422 is a prototype Class 0 source in the ρ Oph complex at 120 pc from the Sun and has played the role of a prototypical solar-type protostar for astrochemical studies, just as Orion KL has done for high mass protostars because of its rich chemistry with exceptional high

deuterium fractionation (e.g. Ceccarelli 2007, for a review).

The first model of the thermal structure of a low-mass protostellar envelope was developed by Ceccarelli *et al.* (1996). In this model, the authors considered the chemistry and resulting line emission within the inside-out collapse model but down to much smaller scales of ~ 10 AU. In their model, the gas temperature in the innermost regions of the envelope reaches ~ 100 K, resulting in a sublimation of H_2O from grain mantles.

Mid-IR (MIR) observations, with the low wavelength spectrometer (LWS) on board of the Infrared Space Observatory (ISO) satellite, toward IRAS 16293-2422 over the 45μm - 197μm range showed a rich molecular spectrum dominated by OI (63μm) line and the CO, H_2O and OH rotational lines. These observations also revealed the presence of weak, diffuse and uniform CII (157μm) emission, which is a result of the illumination of the cloud by a faint UV-field (Ceccarelli *et al.* 1998a). The authors also observed a narrow profile of the CI (609μm) line that is probing the quiescent material around the source. The intensity and narrow profile of the CI (609μm) line together with a map of CII (157μm) line revealed that the region is relatively uncontaminated by PDR like emission. The authors also show that combining the high CO J_{up} = 14 to 25 observed emissions with the CO J_{up} = 6 measurements, stringent limits on the density, temperature and column density of the emitting gas are derived to be 3×10^4 cm^{-3}, ~ 1500 K, and 1.5×10^{16} cm^{-2}, respectively. The relatively low H_2O observed abundance ($\sim 2 \times 10^{-5} H_2$) reflects either that most of O is locked into grains, or that the time scale required to convert gaseous O to H_2O is larger than the outflow dynamical scale, or both (Ceccarelli *et al.* 1998a).

The detection of CO^+ rotational lines observed with LWS was also reported by Ceccarelli *et al.* (1998b). Those lines were not predicted by models. Using the Local Thermal Equilibrium (LTE) and optically thin approximations, the authors derived upper limits for the emitting gas temperature of $\geq$ 300 K and the predicted CO^+ column density was $\geq 7 \times 10^{10}$ cm^{-2}. The authors discussed the possibility that the observed CO^+ emission originates in the very dense PDR regions created in the accretion shock which is formed by the infalling material, and concluded that this is an improbable explanation because their model calculations showed a huge disagreement with observations among which is that the emitted OI (63μm) line should be at least 20 times brighter than its observed intensity. The authors concluded that the plausible origin of these emissions is a strong, dissociative J-shock at $\sim$ 500 AU from the central object.

Ceccarelli *et al.* (1999) detected FIR rotational H_2O emission lines in 5 low-mass YSOs using LWS. The emission fluxes seem to be related to the 1.3 mm continuum flux of the observed

sources, implying that these emissions are originated in the circumstellar envelopes rather than in the outflow. Although simple modelling for these emission lines shows that they originate in a compact, dense ($\sim 10^7$ cm^{-3}) and warm gas (~ 100 K) with H_2O column densities $\sim 10^{16}$ cm^{-2}, other lines are found to originate in a shock very close to the central object. A successful modelling for the H_2O, O, SiO emission lines show that they are originating in an envelope collapsing towards a protostar of mass 0.8 $M_\odot$ at rate of 3.5×10^{-5} $M_\odot$yr^{-1} (Ceccarelli *et al.* 2000a). The authors found that these emissions were likely to originate in the envelope rather than in the outflow shocks.

The H_2CO and $H_2^{13}CO$ line emissions have been observed toward IRAS 16293-2422 by Ceccarelli *et al.* (2000b). In this work, the authors developed a model in which H_2CO lines were found to be emitted by two components: a cold H_2CO-poor outer envelope and a warm H_2CO-rich core. Their model calculations show a dramatic increase in the abundances of H_2CO, H_2O, and SiO in the inner, warmer, and denser region of the envelope. This abrupt change occur when the dust temperature exceeds 100 K and grain mantles evaporate, injecting their mantle species in gas-phase.

Theoretically, no complex molecules are expected to be formed in gas-phase chemistry after ice mantle evaporation because the gas in the warm core region will accrete on to the central object in few hundred years, and would not have the time to evolve chemically (Ceccarelli 2004). Recent observations of low-mass star-forming regions show the presence of abundant complex organic molecules, COMs (e.g. Cazaux *et al.* 2003; Bottinelli *et al.* 2004). The sublimation of grain mantles seem to be a key process leading to the appearance of the large quantities of COMs in warm core regions. The jumps in the abundances of H_2O observed lines and the analysis of both H_2CO and CH_3OH multi frequency line ground-based observations are evidence of the presence of the evaporation of grain mantles in the warm core regions. In practice, when compared to massive hot cores, warm cores seem to possess larger quantities of COMs, by about a factor of 10. A list of the detected COMs in the studied warm core sources, so far, is given in Table 1 in Ceccarelli (2007) while a complete up-to-date list of all observed COMs in the Universe is given in Table 1 in Herbst & van Dishoeck (2009).

Recent research indicates that gas-phase reactions are not efficient enough to produce the large observed abundances of COMs (Horn *et al.* 2004). Garrod & Herbst (2006) demonstrated gas-grain formation mechanism for COMs as $HCOOCH_3$, CH_3OCH_3 and HCOOH in which formation takes place via the addition of simple radicals (OH, HCO,CH_3, CH_3O). The warming-up stage of warm core allows the strongly bound radicals to become more mobile, re-

sulting in the formation of larger molecules before evaporation takes place. Recently and based on this approach, the chemical network of gas-grain chemical models was extended to include the full set of reactions involving the radicals OH, HCO, NH, NH_2, CH_3, CH_3O, and CH_2OH, and their products, including appropriate destruction mechanisms (Garrod *et al.* 2007*a*). Their new model is capable of reproducing abundances of a number of complex molecules observed in star-forming regions, and can predict many that may be plausible candidates.

Observations revealed that warm cores around low-mass protostars are rich in their chemistry and they show high abundances of deuterated species with fractionation ratios larger than 10%, such as the case of IRAS 16293-2422 (van Dishoeck *et al.* 1995; Ceccarelli *et al.* 1998c). Observations confirmed the existence of mono-, doubly-, and even triply-deuterated species in warm cores. van Dishoeck *et al.* (1995) detected several lines for deuterated species toward IRAS 16293-2422 such as HDO, DCO^+, C_2D, HDCO, CH_3OD. After that, the first doubly deuterated species, D_2CO, was detected in the vicinity of IRAS 16293-2422 (Ceccarelli *et al.* 1998c). Following that, many surveys carried out led to the discovery of a forest of deuterated species lines and many species (e.g. Ceccarelli *et al.* 2001; Parise *et al.* 2002, 2004; Caux *et al.* 2005; Parise *et al.* 2006; Butner *et al.* 2007). Most recently, Demyk *et al.* (2010) revealed the detection of several lines of the mono-deuterated methyl-formate, $DCOOCH_3$, blinded with those of its main isotope $HCOOCH_3$, previously detected by Bottinelli *et al.* (2004).

1.6 The UCL Chemical Model: UCL_CHEM

This section describes in detail the chemical model that I use throughout this thesis, the UCL[6] chemical model (hereafter; UCL_CHEM). In recent years, at UCL, this chemical model has been developed by Dr. Serena Viti. The model was first published in Viti & Williams (1999). Since then, the model has been applied to a variety of astrophysical regions: Herbig-Haro objects (Viti & Williams 1999), hot cores (Viti *et al.* 2004), low-mass star forming regions (Viti *et al.* 2002), planetary nebulae (Redman *et al.* 2003), extragalactic environments (Bayet *et al.* 2008), and here in hot corinos 'warm cores' (Awad *et al.* 2010).

UCL_CHEM is a time-dependent gas-grain chemical model which considers the geometry of the studied region as a uniform slab. The chemistry, density, and temperature are calculated self-consistently at each time-step and/or depth point, producing chemical abundances as a function of time and/or depth. The code has the option for the user to run either a multi-

[6]University College London

point or a single point depth calculations. Generally, the chemistry is computed in a two-phase calculation step model. Phase I looks into the collapsing phase while Phase II explores the chemical evolution of the region when a source of radiation exists.

In Phase I, the collapsing phase, the material collapses, under fixed temperature from an initial density (an input parameter) until it reaches a final number density and/or time. The model applies the so-called modified collapse (Spitzer 1978; Nejad *et al.* 1990) which is described in detail by Rawlings *et al.* (1992) and is given by

$$\frac{dn}{dt} = B\,(\frac{n^4}{n_0})^{\frac{1}{3}} \left\{ 24\pi G m_H n_0 \left[\left(\frac{n}{n_0} \right)^{\frac{1}{3}} - 1 \right] \right\}^{\frac{1}{2}} \quad , n\ >\ n_0 \tag{1.7}$$

where t, G, and m_H are the time, gravitational constant, and the mass of a hydrogen atom. n_0, n are the initial and final number density of H atoms, and B is the factor that determines the collapsing mode. In the code, the collapse can proceed in a free-fall mode with B=1 or retarded if $B < 1$.

In this Phase, I, gas-phase chemistry occurs and atoms and molecules are depleted onto grain surfaces and hydrogenate when possible. The initial elemental abundances of the main species; H, He, C, O, N, and metals such as Si, Mg are the main input for the chemistry. In modelling chemical networks and in order to obtain accurate results, we have to know all the possible formation and destruction routes for each species. Consider the gas-phase reaction 'A + B $\longrightarrow$ C + D', the rate of this reaction (which estimates the amount of species produced per volume per second) can be expressed as

$$\frac{d[C]}{dt} = \frac{d[D]}{dt} = k_p[A][B] \tag{1.8}$$

where [X] stands for the concentration of the species X (cm^{-3}), and k_p is the production rate coefficient of X. The value of the rate coefficient is often temperature-dependent and hence can normally be expressed by the Arrhenius equation:

$$k(T) = A(T)\ exp\left(\frac{-E_a}{k_B T}\right) \tag{1.9}$$

where $A(T)$ is the Arrhenius constant which is temperature dependent, E_a is the activation energy[7], and k_B is Boltzmann constant. For endothermic reactions, E_a must be at least the energy required to form the products. At low temperatures $E_a \gg k_B$T, thus the exponential factor in expression (1.9) reduces $k(T)$ to nearly zero.

[7] Activation energy: the minimum energy needed for a reaction to occur

In reality, a species can be formed and destroyed via several pathways, and hence when calculating the net product, one should take into account all of these routes. In general, the production rate of any species can be written as

$$\frac{dn}{dt} = \sum \ (F - D) \tag{1.10}$$

where F and D are all the formation and destruction pathways, respectively. The gas-phase chemical network, in the code, is based on the UMIST database[8] where the rate coefficient for each reaction is calculated by a previous knowledge of the constants α, β, γ provided in the database. In UCL_CHEM, these constants are included in the chemical network input file. The code's rate coefficient calculator feeds these coefficients into the rate equations solver subroutine, O.D.E[9] solver. For a two-body reaction, a modified version of the Arrhenius equation, Eq. (1.9), is used to calculate the rate coefficient in that the constant γ is the activation energy

$$k = \alpha(T/300)^{\beta} exp(-\gamma/T) \tag{1.11}$$

Table (1.3) lists the formulae used in the code and based on the UMIST database rate files to calculate the rate coefficients for the different types of gas-phase reactions in the chemical network as given in Table (1.2).

Table 1.3: Calculation of the rate coefficients for reactions in the UMIST RATE99 and RATE06 databases, as we used in our models. T is the kinetic temperature, ω is the dust grain albedo and A_v is the visual extinction.

Reaction Type	**Rate constant (k)**	**Unit**
Two body reactions	$\alpha(T/300)^{\beta} exp(-\gamma/T)$	$\mathrm{cm^3 s^{-1}}$
Direct cosmic ray ionisation	α	$\mathrm{s^{-1}}$
Cosmic ray induced photoreactions	$\alpha\ (T/300)^{\beta}\gamma\ /\ (1-\omega)$	$\mathrm{s^{-1}}$
Photoreactions	$\alpha\ exp(-\gamma A_v)$	$\mathrm{s^{-1}}$

T, ω, and A_v are given in our code as input parameters either as an individual values or a profile. Each reaction has its specific α and γ value.

In addition to the gas-phase reaction network, some reactions occur on dust grain surfaces such as the H_2 formation, see §(1.3.2.1). The depletion efficiency of accreted species onto grain

[8]During the course of this thesis a new kinetic databased for astrochemistry KIDA was released by Wakelam (2009).

[9]O.D.E. refers to the ordinary differential equations. The rate equations are O.D.E

surfaces is determined by the fraction of material that is removed from the gas-phase. This fraction is arranged by adjusting the grain surface area per unit volume, and assumes a sticking probability of unity for all species. The fraction of material on grains is thus dependent on the product of the sticking probability and the amount of cross-section provided per unit volume by the adopted grain size distribution as

$$k_{ads} = S\sigma v \tag{1.12}$$

where S is the sticking probability ($\sim$ unity at low temperatures), σ is the grain cross-section, and v is the thermal velocity of the species.

Since the chemistry in UCL_CHEM is time-dependent, different species form at different times, and as a consequence the material frozen out on the grains at anytime is representative not of the whole gas but of selected species. It is important to bear in mind that the surface reaction network in UCL_CHEM is very simple. It includes direct hydrogenation of all species including the formation of CH_3OH and H_2CO from CO (Tielens & Hagen 1982; Watanabe *et al.* 2003) and that of CH_3CN from the reaction of methane, CH_4, with HCN (Garrod *et al.* 2008). In other words, the code is not using rate equations in computing the abundances of these mantle species.

The advantage of having Phase I as a separate step calculation is that the initial molecular fractional abundances used in Phase II calculations are computed by a real time-dependence of the chemical evolution of gas-dust interaction processes, i.e. not assumed.

In Phase II, the warming-up phase, we follow the chemistry of the region for some time, assuming either a uniform or fixed density, another input parameter. In this stage, a source of heat is warming up the region allowing the sublimation of mantle species. The treatment of the evaporation of the code is either time-dependent in which mantle species desorb in various temperature bands according to the experimental results by Collings *et al.* (2003a, 2004) or instantaneous in that all species will desorb off grain surfaces in the first time-step. For both cases, a temperature profile will be another input parameter for the code.

The above description of the UCL_CHEM code is summarised in Fig. (1.6). In this figure, the main code is fed by the output results of a collection of subroutines, in the red box, including: the temperature profile, the density profile, the rate coefficient calculator, the chemical network. The desorption subroutine is also an input but it is called in the warming up phase. The physical parameters are used in all of these subroutines and by the ODE solver. All of these input files are fed into the main code to calculate the chemistry and produce the chemical

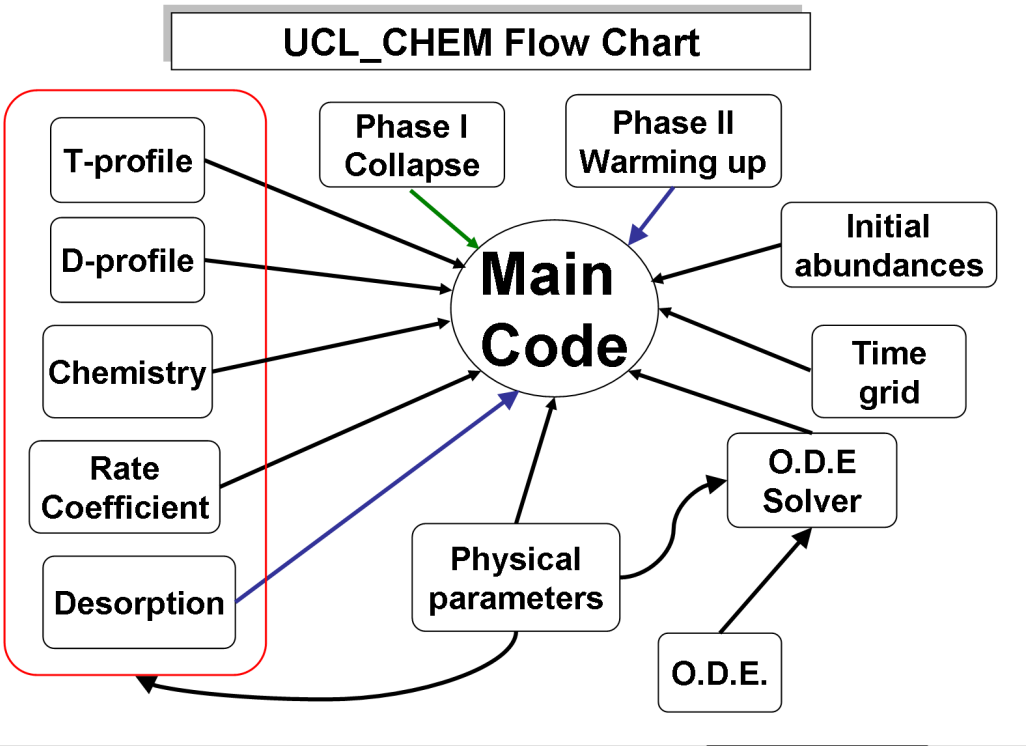

Figure 1.6: The UCL_CHEM flow chart. Note that the green arrow indicates the input data used only in Phase I while the blue arrows indicate the additional input of the warming up phase.The red box includes all the subroutines that are called by the main code. D- and T-profiles are the density and the temperature profiles, respectively. Black arrows are the parameters in common in the two phase calculations.

fractional abundances with respect to the total number of H nuclei.

1.7 Thesis Outlines

Star formation is one of the most studied topics in modern astronomy and is fast developing due to improvements in: observational techniques, theoretical modelling, and/or experiments. Recent observations revealed that cores around low-mass star forming regions are rich in chemistry. It is clear that there is still much to learn about the chemistry of these cores.

This thesis focuses on the chemistry of these cores and it is organised as follows:

Chapter 2: in this chapter we model the chemistry of cores around low-mass star forming regions and identify a set of species to be evolutionary indicators. We also compare the chemistry of these warm cores with that of hot cores for better understanding of the process of star formation. Finally, we compare our model results to the observations of

IRAS 16293-2422.

Chapter 3: in this chapter we extend the work in **Chapter 2** to include mono-deuterated species in order to explore the deuterium chemistry in warm cores, in particular at the protostellar stage; i.e. when the new star is formed. We also establish a set of deuterated molecules as evolutionary indicators for warm cores.

Chapter 4: in this chapter I highlight my contribution to the study of deuterium chemistry in extragalactic environment led by Dr. Estelle Bayet and summarise our main results and conclusions.

Chapter 5: in this chapter we study the role of grain surfaces in the formation of deuterated species. In this short study, we focus on the formation of large species, D_2CO, and complex organic molecules, $HCOOCH_3$ and $DCOOCH_3$.

Chapter 6: in this chapter we turn our attention to the origin of interstellar clouds, and present an attempt to understand whether we can use our present knowledge of interstellar chemistry to trace back its origin and nature.

We give our conclusions and suggestion for future work in **Chapter 7**.

CHAPTER 2

WARM CORES AROUND REGIONS OF LOW-MASS STAR FORMATION

Warm cores (hot corinos) around low-mass protostellar objects show a rich chemistry with strong spatial variations. This chemistry is generally attributed to the sublimation of icy mantles on dust grains initiated by the warming effect of the stellar radiation. In this chapter[1], we use a model of warm core chemistry in which the sublimation process is based on extensive laboratory data to investigate the chemistry of these objects. We briefly compare our model with observations of the well-studied source IRAS 16293-2422.

2.1 Introduction

The early stages of low-mass star formation are observed at millimetre and submillimetre wavelengths, where both the dust continuum as well as molecular emission from the outer regions of the envelope can be detected. The dynamical aspect of low-mass star formation, with low mass stars forming from dense and cold condensations called prestellar cores, and evolving into Class 0 and I sources, is relatively well defined. What is less well understood is how prestellar cores evolve chemically into protostellar cores which then, eventually, develop protoplanetary disks. Nevertheless, it is now clear that, as in the case of massive star formation, towards the end of the collapse phase the gas and dust are dense and cold enough that (other than H_2 and He) some material has frozen onto the dust and that surface chemistry has taken place, leading

[1]The work presented in this chapter is based on the paper by Awad *et al.* (2010)

to a rich gas phase chemistry once the star heats the surrounding dust so that icy mantles returned to the gas phase. The warm cores where the icy mantles sublime are often called 'hot corinos' (e.g. Ceccarelli 2004, 2007) due to their chemical resemblance with hot cores. Recent observations toward several warm cores around low-mass solar-like protostars have shown that they are rich in large, complex organic molecules (COMs) including methanol CH_3OH, methyl formate $HCOOCH_3$, methyl cyanide CH_3CN, and more complex species such as ethylene glycol $(CH_2OH)_2$ (e.g. Cazaux *et al.* 2003; Bottinelli *et al.* 2004; Hollis *et al.* 2004; Bisschop *et al.* 2008). In addition, they show some interesting deuterated species (e.g. Ceccarelli *et al.* 1998c; Caux *et al.* 2005). In fact, the envelope of Class 0 sources can be divided chemically into two zones: the zone where all the ices sublime (dust temperature $\geq$ 100 K), i.e. the warm core region, and the outer cold envelope (dust temperature $\leq$ 100 K) (e.g. Ceccarelli 2005). The chemistry in the outer envelope is similar to that in pre-stellar cores while in the inner regions, sublimation is clearly important. The first hot corino discovered is the one observed towards the low-mass Class 0 source IRAS 16293-2422. For a detailed description of this source, we refer the reader to §(1.5.2) in Chapter 1.

Evidently, in situations where a cool outer envelope and a warmer core exist, sublimation - and the subsequent gas-phase chemistry that this causes - will be important. Also, the sublimation will be a time- and space-dependent event as the central protostar warms up. Given the role of sublimation, it is important to take account of recent laboratory studies of the sublimation of ices (Collings *et al.* 2003a, 2004) which show that different species enter the gas phase at different temperatures, and that the sublimation occurs not continuously through a gradual warm-up but in several well-defined and narrow temperature bands. Such a process may give rise to a rather different gas-phase chemistry than a process in which instantaneous sublimation of all species in a mantle occurs; such a difference was earlier found to be the case for hot cores (Viti *et al.* 2004).

Our purpose in this chapter is, therefore, to model the sublimation process, taking account of the laboratory data, in the context of warm cores in low-mass star-forming regions. We wish to assess whether the more complex sublimation mechanisms indicated by the laboratory studies significantly affect the detectable chemistry in these objects, as compared to models in which the desorption is instantaneous for all species. The model we use is developed from a similar model used for the study of hot cores in regions of massive star formation (Viti *et al.* 2004). Further, if the two similar models can successfully describe cores in both types of star-forming region, then this may be taken as support for the view that star formation is carried out

by essentially the same process, regardless of stellar mass. We describe our model in §(2.2), the results are given in §(2.3), and we draw some conclusions in §(2.4).

2.2 The Model

In order to investigate the chemical evolution of low-mass star forming regions we have used the UCL_CHEM, described elsewhere §(1.6) in Chapter 1. It is important to clarify that throughout this thesis we are not aiming at modelling a specific source. We model the inner most component of warm cores, in general, where sublimation of mantle species occurs. In this study, we adapted the chemical model from the Viti *et al.* (2004) hot core model. Our model follows the chemical evolution of a free-fall collapsing cloud in the process of forming a low-mass star, then explores the chemical evolution of the remnant of the warm core located in the vicinity of the newly formed star. The core is represented by a uniform slab subdivided into 5 shells represented by 5 depth points of increasing visual extinction from the edge of the core to its centre. The results are obtained from a two-phase calculation: Phase I, the collapsing phase, and Phase II, the warming up phase after a new star was born. The initial elemental abundances relative to hydrogen that we have adopted from Viti *et al.* (2004) are listed in Table (2.1).

Gas-phase chemistry occurs during the collapsing phase and atoms and molecules are depleted on to grain surfaces and hydrogenate when possible. As previously stated in §(1.6), the depletion efficiency is determined by the fraction of the gas-phase material that is frozen on to the grains. This fraction is arranged by adjusting the grain surface area per unit volume, and assumes a sticking probability of unity for all species. In our model, apart from direct hydrogenation, the only other surface reactions we include are the formation of CH_3OH and H_2CO from CO and of CH_3CN from the reaction of methane, CH_4, with HCN, as it has been shown that gas phase reactions are not sufficient to form CH_3OH and CH_3CN (e.g. Tielens & Hagen 1982; Watanabe *et al.* 2003; Garrod *et al.* 2008). The advantage of this step is that the initial molecular fractional abundances used in the second stage of the model calculations are computed by a real time-dependence of the chemical evolution of gas-dust interaction process, i.e. they are self-consistent not assumed.

In Phase II, the warming-up phase, we follow the chemistry of the remnant core, after the star is born, for $\sim 10^7$ yrs, assuming a uniform density throughout the core. The choice of the time scale of tracing the chemistry is arbitrary. For cores around low-mass star forming

Table 2.1: Model initial physical parameters and elemental abundances relative to hydrogen.

Physical parameters	
Core density †	1.0×10^7 - 2.0×10^8 cm^{-3}
Core maximum temperature	100 K
Core radius	30 - 150 AU
Depletion percentage †	85 - 100%
Initial elemental abundances	
Carbon	1.79×10^{-4}
Oxygen	4.45×10^{-4}
Nitrogen	8.52×10^{-5}
Sulphur	1.43×10^{-6}
Helium	7.50×10^{-2}
Magnesium	5.12×10^{-6}

† This parameter varies only during the collapsing phase (Phase I).

regions, at 10^7 yrs, the physical structure, hence the density, will be different, therefore, we expect that our model results will be a poor approximation of reality at late times. In this phase, the central star heats up the surrounding gas and dust, causing sublimation of the icy mantles. In our modelling, the desorption of the species is based on the experimental results by Collings *et al.* (2003a) in which they showed that molecular ices can be divided into five categories: (i) CO-like, (ii) H_2O-like, (iii) intermediate, (iv) reactive, and (v) refractory. For each category one can estimate the fraction of a particular molecular species that is desorbed in various temperature bands. These bands are from 1) the pure species, 2) a monomolecular layer on H_2O ice, 3) desorption during the amorphous-to-crystalline H_2O ice conversion (the 'volcano' effect), 4) co-desorption when the H_2O ice desorbs, and 5) desorption of the bare grain surface (see Collings *et al.* 2004 for more details). Our treatment of the desorption of the species is pseudo-time-dependent in a sense that we allow a certain fraction of species to evaporate when the temperature reaches a specific value. This fraction of species is adopted to be the same estimated previously in Viti *et al.* (2004)) and given in Table (2.2).

Table 2.2: The fraction of species desorb at each desorption band as taken from Viti *et al.* (2004).

		desorbed fraction				
Category	**species**	solid†	Mono‡	Volcano	Co-des	Surface
CO-like	CO, N_2, O_2	0.35	0.7	0.667	1.0	0
	CS, NO, CH_4	0	0.7	0.667	1.0	0
Intermediate	HCN, HNC, H_2S, NS, HCS, C_2H_2	0	0.7	0.5	1.0	0
	OCS, CH_3CN, C_3H_4, CO_2, SO_2, HC_3N, C_2H_4	0	0.1	0.5	1.0	0
H_2O-like	H_2O, CH_3OH, SO, CH_2CO, C_2H_5OH, NH_3	0	0	0	1.0	0
	NO_2, H_2CO, $HCOOCH_3$, H_2CS					
Reactive	HS_2, C_2H, OCN, O_2H, C_2H_5, H_2CN, HNO, C_2, C_2H_3	0	0	0	1.0	0
Refractory	Mg, S_2	0	0	0	0	1.0

† Solid desorption occur around 20 K.

‡ Mono desorption depends on the binding energy of the species (E_b) and hence it does not occur at fixed temperature such as the cases of volcano and co-desorption.

The temperature at which species evaporate are calculated using a rate model (Collings *et al.* 2003b) to explain desorption processes in a phenomenological manner over relevant astronomical time scales. By running this chemical kinetic simulation of water-ice desorption, we calculated the different desorption temperatures using a power-law temperature profile fitted to a Sun-like star; see Eq. (2.1).

In the present work, we simulate the stellar heating effect in the same way as in Viti *et al.* (2004). We assume that the presence of an infrared source in the centre of the core or in its vicinity causes an increase in the gas and dust temperature. The temperature is a function of the luminosity (and therefore age) of the protostar as in Viti *et al.* (2004), but here we adjust the luminosity/mass power law to account for lower protostellar masses than in the hot core case. Viti *et al.* (2004) used the observed luminosity function of Molinari *et al.* (2000), and correlated the effective temperature of the gas with the age of the accreting protostar through a simple power law:

$$T_d(t) = 10 + A(t)^B \tag{2.1}$$

where $T_d(t)$ is the temperature profile of gas and dust in the core surrounding the stellar object, t is the evolutionary age of the collapsing core in yrs. A and B are two constants derived from the boundary conditions.

In their model, Viti *et al.* (2004) considered many assumptions. However, their major assumption is that the temperature of the gas and the dust surrounding the protostar increases according to the same power-law as the stellar temperature. For our study, we consider the same assumptions, but for a Sun-like star in which we assume that the collapse starts with a typical dark cloud of temperature 10 K and the maximum temperature of the gas, 100 K, is reached at the contraction time, $t_c = 38.9 \times 10^6$ yr (see Table 2, Bernasconi & Maeder 1996). Considering these boundary conditions, we derived an expression for the change of the temperature profile of the gas. The results of this expression underestimate the temperature of the core around the Class 0 source (100 K as observed by Ceccarelli (2004)) when it reaches its age $\sim 10^4$-10^5 yrs as estimated by André *et al.* (1993) (see panel (a) Fig. (2.1)). To solve this problem and match observations, we changed the boundary conditions and let the core reach 100 K at the age of Class 0 sources $\sim 10^5$ yr. We obtained good agreement with the expected temperature evolution, but the temperature is rapidly increasing during the early stages of the warming up phase then this rate declines (see panel (b) Fig. (2.1)). We recovered this problem by using the extrapolation method, in that we find the temperature expression for solar-type protostars based

on the previously estimated expressions for massive stars by Viti *et al.* (2004). Following this approach, the derived temperature profile shows good agreement with the expected temperature evolution (see; panel (c) in Fig. (2.1)). This temperature profile is in line with the previously estimated profiles by Viti *et al.* (2004) in which the heating rate slows down as the stellar mass decreases. The values of the constants A & B in expression (2.1) are 0.1927 and 0.5339,

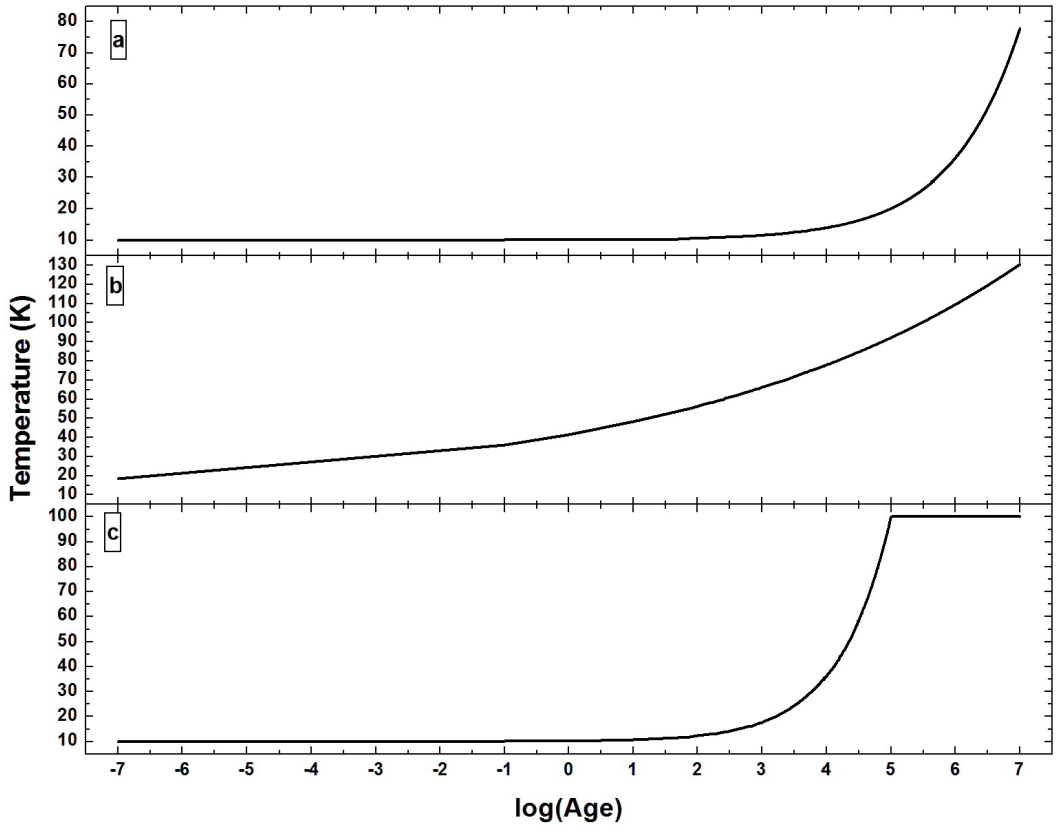

Figure 2.1: The temperature profiles as a function of time; derived for different boundary conditions (see text)

respectively.

In this work, UCL_CHEM is used in both time and space dependent mode and so the temperature profile needs to be a function of both time and space. Hence, we changed equation (2.1) by including another term describing the temperature evolution as a function of distance as derived by Nomura & Millar (2004). In their models, Nomura & Millar (2004) solved the radiative transfer equation for a clump warmed by a central star assuming that the radial profile of the temperature is defined as the inverse square law $T(r) \propto r^{-1/2}$, which is comparable to the profile obtained by Schöier *et al.* (2002) in which $T(r) \propto r^{-0.4}$. The temperature profile

in our model, shown in Eq. 2.2, is derived by combining the approach of Viti *et al.* (2004) (Eq. 2.1) with that of Nomura & Millar (2004):

$$T_d(t,d) = 10 + A(t)^B \times (d/R)^{-0.5} \quad \text{K} \tag{2.2}$$

where in this equation, $T_d(t,d)$ is the temperature profile of gas and dust in the core surrounding the stellar object, d is the distance from the core centre, and R is the core radius. A and B are the previously derived constants from the boundary conditions, in this case, the temperature at $\sim$ 150 AU from the star at t = 0 (T = 10 K) and $t = 10^5$ yrs (T = 100 K). The latter condition corresponds to the temperature obtained by Schöier *et al.* (2002). Thus, we find that the temperature profile of a typical warm core capable of reproducing the empirical assumptions we consider is given by

$$T_d(t,d) = 10 + 0.1927(t)^{0.5339} \times (d/R)^{-0.5} \quad \text{K} \tag{2.3}$$

Eq.(2.3), was then inserted in the chemical kinetic program (Collings *et al.* 2003b) to estimate the position of the different desorption bands. From this equation it can be seen that the temperature rises slower than in the case of high mass stars (Viti *et al.* 2004) affecting, as a consequence, the times at which the desorption of the different species occur. The desorption mechanisms, throughout the core, are time- as well as space-dependent processes. In general, the closer to the heating source the earlier the desorption occurs. Fig. (2.2) represents the temperature evolution through out the warm core at various radii (see figure key). The volcano and co-desorptions will occur at slightly different temperatures (and times) depending on the depth within the core but they are around 84 K (at $\sim 5\times10^4$ yrs, for the inner shell) and 95 K (at $\sim 7\times10^4$ yrs, for the inner shell) respectively. These results are in line with those previously calculated for hot cores where the desorption temperatures decrease as a function of slowing down of the heating rate so that the lower the stellar mass, the lower the volcano and co-desorption temperatures (see Table 2 in Viti *et al.* 2004).

Our chemical network is a modified version of the UMIST database (Le Teuff *et al.* 2000) with 127 gas phase species and 42 mantle species interacting in 1871 chemical reactions. Photo-reactions were included, taking into account both the external interstellar radiation field and the internal cosmic ray induced UV field. Both direct and indirect ionisation by cosmic rays were also included, using a cosmic ray ionisation rate, ζ, of $1.3 \times 10^{-17}\text{s}^{-1}$ (Lepp 1992). Observations of emission lines (e.g from H_2CO and H_2O) toward low-mass protostellar objects reveal that there is a gradient in both density and temperature. The dust temperature reaches

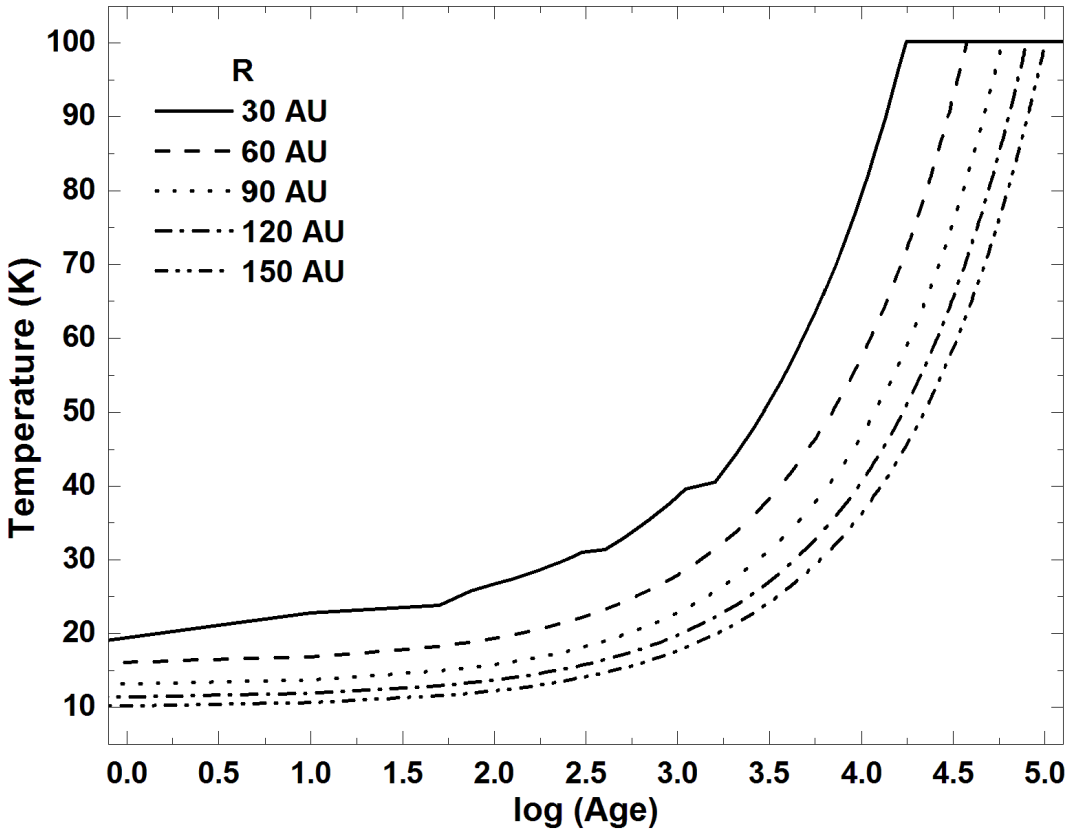

Figure 2.2: The time evolution of the temperature of a sun-like warm core at different core radii. Each radius corresponds to a certain value of A_v

100 K in cores where the densities vary between 1×10^7 cm^{-3}, such as the case of IRAS 16293-2422 (e.g Ceccarelli *et al.* 2000a,b; Ceccarelli 2004) and 2×10^8 cm^{-3} for NGC 1333-IRAS 4A, B (Maret *et al.* 2004), and their radii range from 200 AU down to 27 AU.

In order to investigate the sensitivity of the chemistry to the physical parameters of warm cores around low-mass stars, we ran a grid of chemical models where we varied (i) the final density of the collapsing core and (ii) the percentage of the accreted species on to grain surfaces. A characteristic of our chemical model is that we simultaneously follow the chemistry as a function of time and depth: the mantle evaporation is temperature-dependent and the temperature profile is dependent on both the distance from the core centre and time. Table 2.1 summarises the various physical parameters used in our model. The ice composition at the end of Phase I will depend both on the final density of the collapsing core and the percentage of accreted species on the dust.

2.3 Results

In this section we present our model calculations for the chemical evolution of a typical hot corino in the warming up phase, Phase II, where mantle species evaporate. It is important to remember that the ice composition at the end of Phase I will depend both on the final density of the collapsing core and the percentage of accreted species on the dust. In our model, typical abundances calculated (with respect to the total number of hydrogen nuclei) for high density and high depletion, for the most relevant species i.e H_2O, CO, H_2CO, CH_4, CH_3OH, are 4.0×10^{-4}, 3.7×10^{-5}, 3.6×10^{-9}, 1.4×10^{-4}, and 3.8×10^{-7}; respectively. Detection by ISO (van Dishoeck 2004) and recently Spitzer (Öberg *et al.* 2008) of CH_4 ice show lower values of $\sim 10^{-6}$, for the gas+ice components (e.g. Boogert *et al.* 1998). It is clear that our model predicts higher abundance (about two orders of magnitude more) of icy CH_4 than observations. We believe that our high abundance of mantle methane arises as a consequence of our assumption that hydrogenation (in this case, of carbon) is very efficient. However, our results are in agreement with those of Boogert *et al.* (1998) modelling results (10^{-4}) when they form icy CH_4 via the successive hydrogenation of accreted C atoms. The lower observed abundance of mantle CH_4 by ISO (Boogert *et al.* 1998; van Dishoeck 2004) could be attributed to its large beam size. The ISO beam encompasses material outside the core and the ISO observations are of young stellar objects in which sublimation may have already reduced the CH_4 component. Hence, the detection may be under-estimating the CH_4 ice abundance within the pre-stellar core.

2.3.1 Chemical trends

Fig. (2.3) shows how the computed fractional abundance, in Phase II, of selected species varies as a function of the radius of the core at around 4×10^4 yrs: not surprisingly the inner parts of the core show an increase of the molecular fractional abundances for most of the species while they are very low in the outer regions of the core. Such trends are also present as a function of time as shown in Figures (2.4) & (2.5), where fractional abundances of selected species as a function of (logarithmic) time at visual extinction of $\sim$ 140 mags for a warm core at two different densities, are presented (2.0×10^8 cm^{-3}, solid line, and 1.0×10^7 cm^{-3}, dashed line).

All the species in our sample show sudden increases in their abundances corresponding to their multi-step sublimation from grain mantles (see Collings *et al.* 2004). However, the fractional abundances of H_2CO and CH_3OH are interesting because they show extra 'jumps' which

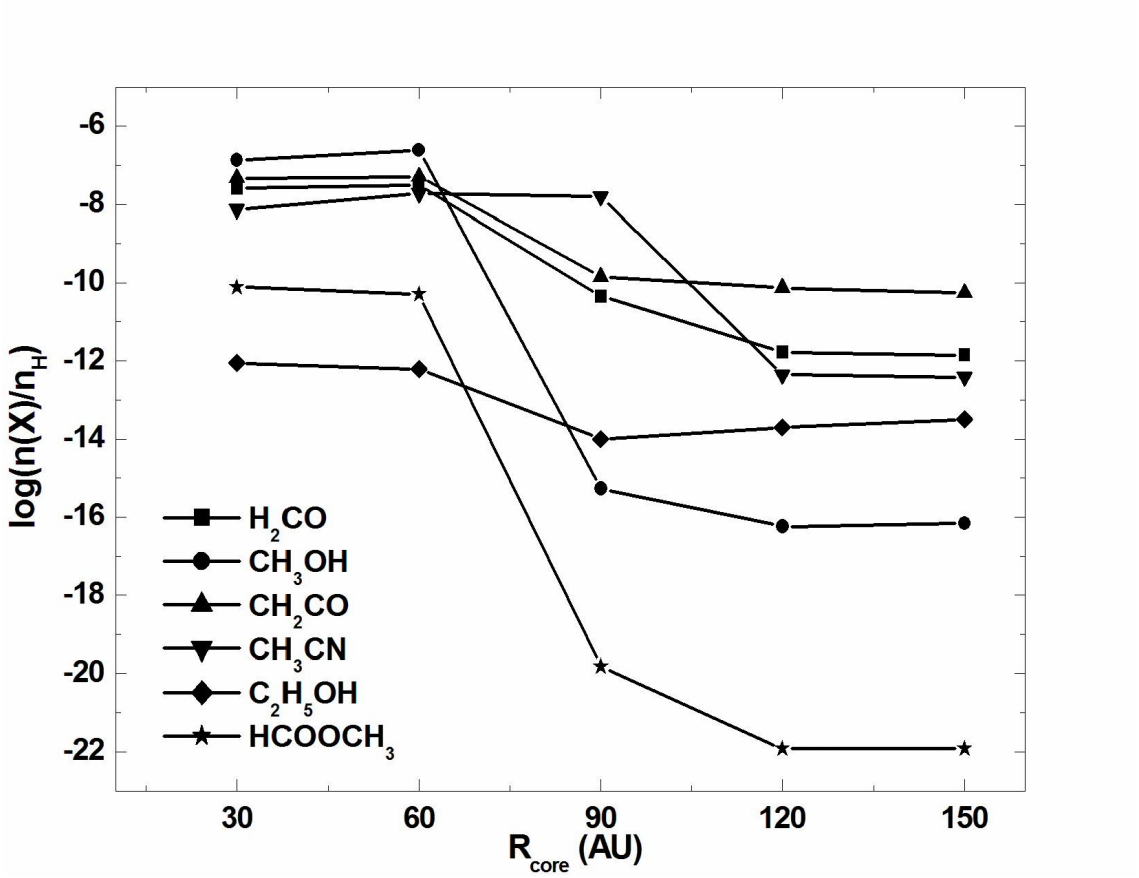

Figure 2.3: Fractional abundances with respect to the total hydrogen nuclei as a function of the core radius (R_{core}) for selected organic species at 4×10^4 years for a model with full depletion and density of 2×10^8 cm^{-3}.

cannot be explained by sublimation from grains. The increase in the abundances of H_2CO and CH_3OH around these jumps is associated with the 'volcano' desorption of CH_4 from grains. The increase in H_2CO and CH_3OH seen in conjunction with the CH_4 'volcano' desorption is due to a sequence of gas-phase reactions involving CH_4. Although, in our model, both H_2CO and CH_3OH are formed on grains, via the successive hydrogenation of CO (as confirmed experimentally and studied theoretically (e.g. Tielens & Hagen 1982; Watanabe *et al.* 2003) there is still a contribution from gas-phase chemistry, especially for H_2CO. Our detailed chemical analysis shows that at the time of the jump, the formation of H_2CO is dominated by the oxidisation of CH_3 which is in turn formed efficiently by the destruction of CH_4 by He^+ ions. Methanol is found to be a secondary product of CH_5^+ which is mainly formed (at that time) via two ion-molecule reactions involving CH_4; one with H_3^+ and the other with N_2H^+. Destruction of CH_5^+ leads to CH_3^+ which reacts with water to form $CH_3OH_2^+$ which recombines

to give methanol. These sequences of reactions which involve CH_4 contribute to the observed amount of both H_2CO and CH_3OH at the 'jump'. In fact, the 'jump' in abundance for methanol is rather small because the $CH_3OH_2^+$ recombination reaction is rather inefficient (see Geppert *et al.* 2006) For most species, the abundances are lower at lower density with the exceptions

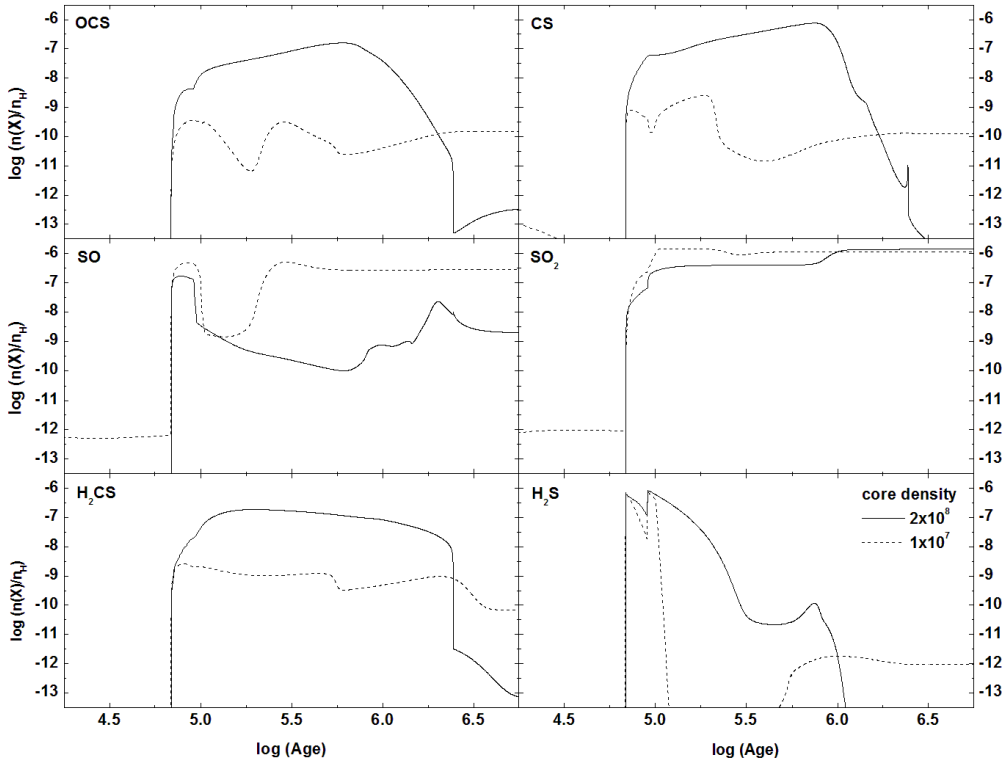

Figure 2.4: The time evolution of the fractional abundances of S-bearing molecules at $A_v = 142.7$ mag. The different curves compare the evolution of the species at two different final densities for the collapsing cloud (see key).

of SO and SO_2. SO is mainly produced by reactions involving atomic and molecular oxygen during early and late times respectively, while it is destroyed by HCO^+ via radical-molecule reactions which are more pronounced during late times. SO is also destroyed while forming SO_2 via oxidisation and radical-molecule reactions, during both early and late times. At high densities, SO is destroyed more efficiently than in less dense cores. For less dense cores, the chemistry reaches steady state earlier and the evaporation peaks are more pronounced.

In Figures (2.6) & (2.7) we show models with depletion efficiencies of 100% and 85%

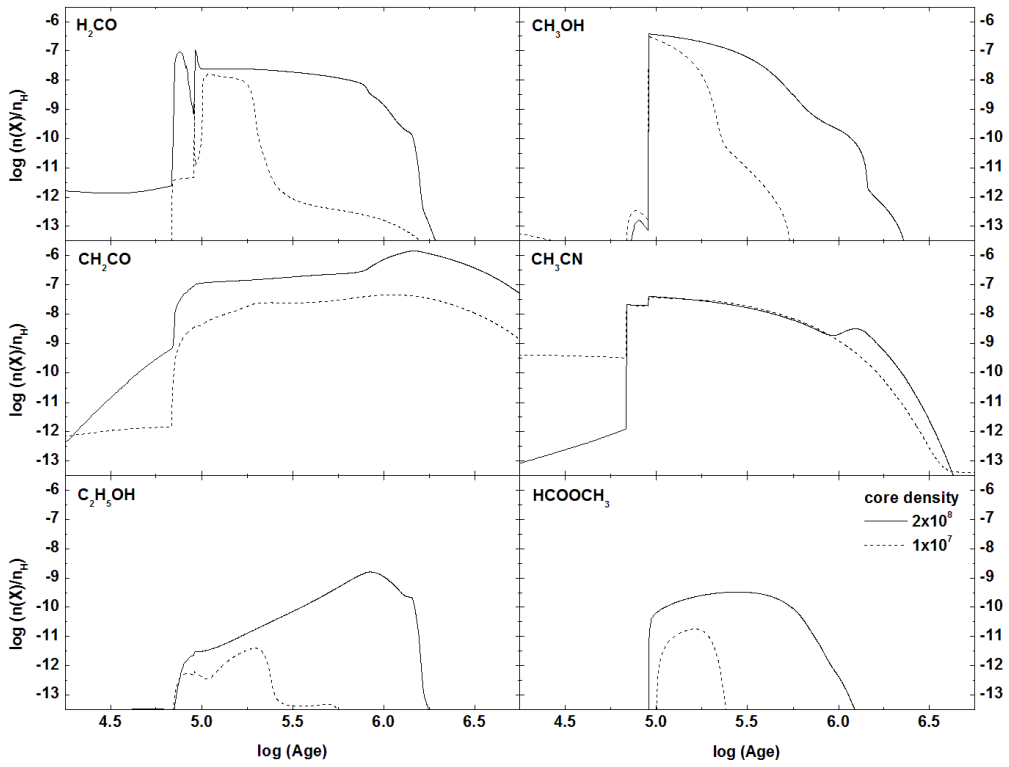

Figure 2.5: The same as in Fig. (2.4), but for large and organic molecules.

respectively. Lowering the depletion efficiency reduces the yield of most species. However, some species (Fig. (2.6); e.g. SO, SO_2) show higher abundances at lower depletion efficiencies: this is due to the higher abundance of atomic sulphur in the gas phase during Phase I which leads to an appreciable amount of SO and SO_2 even before the warm core forms. In general, models where all heavy elements are frozen out give abundances that are more in line with the observed abundances, see Table (2.3) and §(2.3.3). We have also run a model where sulphur does not hydrogenate as it freezes but remains in atomic form (Wakelam *et al.* 2004) and, as expected, we find that this affects the early stages of Phase II by lowering the abundance of H_2S by a factor of 30; however, by 10^5 yrs the bulk of the sulphur is locked in CS, SO and SO_2, regardless of its initial form.

From our results so far it is clear that, as in the case of hot cores, sulphur-bearing species show the most variation, whether with time, radius, density or depletion. Ratios of sulphur-

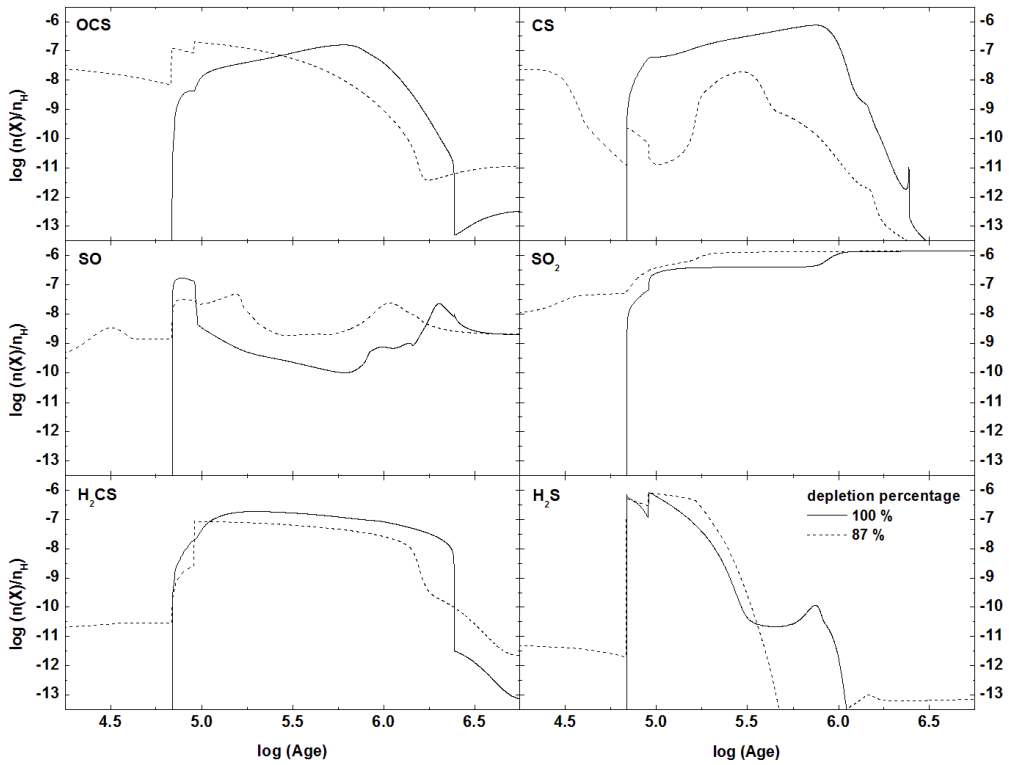

Figure 2.6: The time evolution of the fractional abundances of S-bearing molecules in a warm core region, of density $n_H = 2.0 \times 10^8$ cm^{-3}, at a point with $A_v = 142.7$ mag. The profiles compare the evolution of the fractional abundances at different depletion efficiencies on the grain surfaces (see key).

bearing molecules may therefore be used as tracers of the physical characteristics of warm cores. The SO/CS, SO/H_2CS, and SO/OCS ratios are less than 1 at early times ($\leqslant 1 \times 10^4$ yrs), while those of H_2S/SO_2 and H_2S/H_2CS are higher than 2 at later times ($\geqslant 6 \times 10^6$ yrs). The slowing down of the temperature increase allows more species to survive in the gas-phase, and hence show higher abundances at late times. This result is in line with the prediction of both Hatchell *et al.* (1998) and Viti *et al.* (2004) for the change of the abundances of sulphur-bearing species. The key difference between low and high mass cores is the abundance of H_2S as a function of time: this species decreases much more drastically with time for low-mass cores. Note that H_2S drives the sulphur bearing chemistry (see Hatchell *et al.* 1998; Viti *et al.* 2004). These ratios may therefore, in principle, be used as evolutionary indicators for

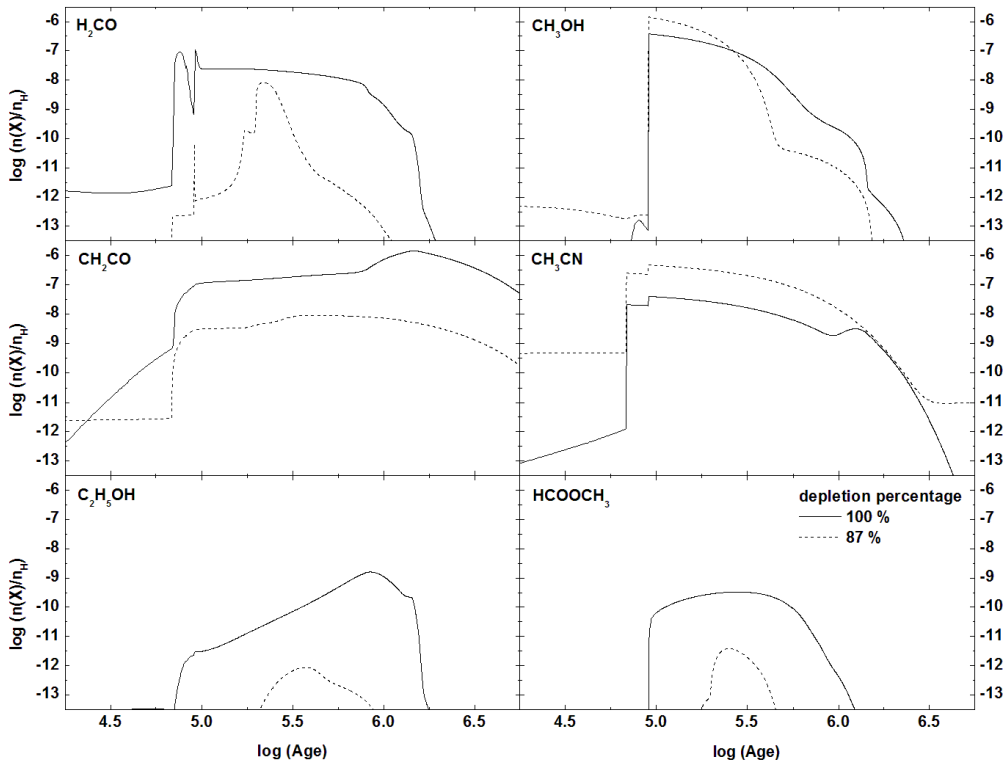

Figure 2.7: As in Figure (2.6), but for the large and organic molecules

warm cores, although, as Wakelam *et al.* (2004) pointed out, care needs to be taken because sulphur-bearing ratios at early times are strongly dependent on the nature of sulphur in the icy mantles.

We also compared the chemical evolution of the species in different shells. Figs. (2.8) & (2.9) show these results for two points at 30 AU (solid line) and 150 AU (dashed line) from the central star. We find that both the trends and the fractional abundances of the species are similar in both shells, but shifted towards earlier times for the inner shell. Amongst the studied species, SO and H_2S are the only molecules that show some differences in their trends and/or abundances when varying the core radius. The H_2S solid desorption peak is more pronounced in the outer shell and the SO peak is about 10 times more abundant in the outer shell than in the inner. These differences are due to the different warming rate in the shells. The fact that the inner shell reaches higher temperatures faster than the outer ones does not allow species to

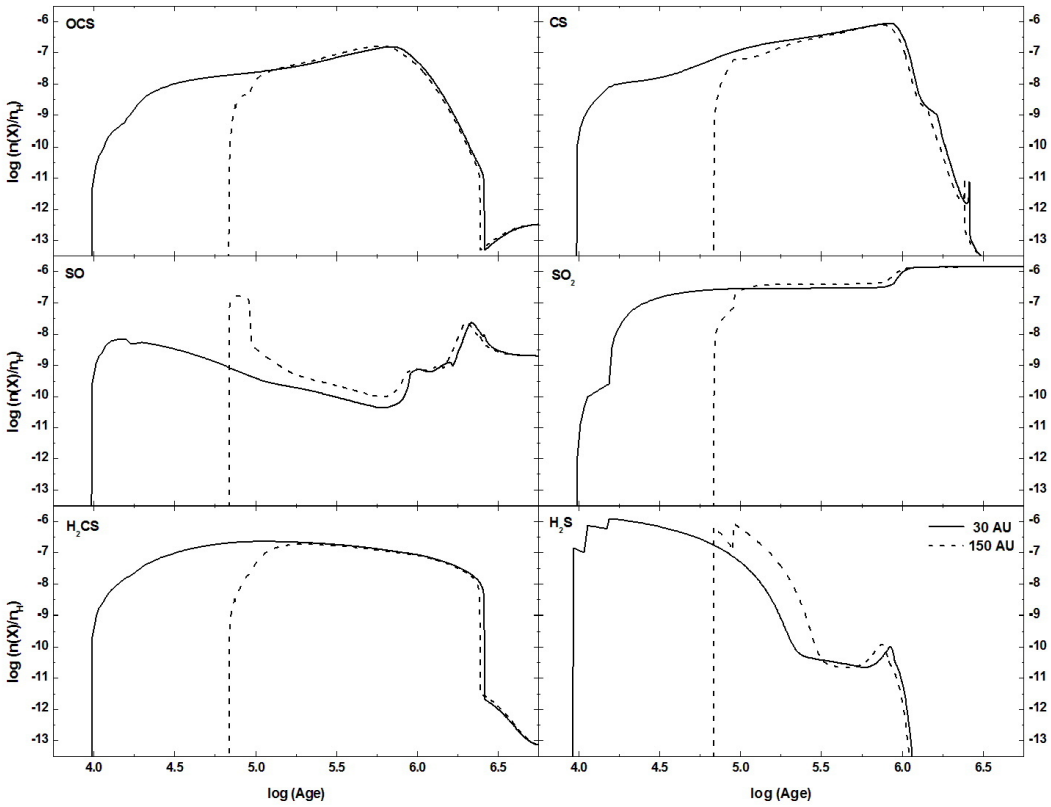

Figure 2.8: The time evolution of the fractional abundances of S-bearing molecules in a warm core region, of density $n_H = 2.0 \times 10^8$ cm^{-3}, at two points with different radii from the central star (see key).

be abundant for longer times, but they are quickly converted into other molecules.

2.3.2 Comparison with models of hot cores

The main aim of this study was to determine whether the predicted chemistry of warm cores differs substantially from that of hot cores and in particular whether we can identify molecules that would be enhanced in warm cores but not in hot cores. Viti *et al.* (2004) ran chemical models of hot cores for different stellar masses. In this work we compare our results for a one solar mass warm core with those of Viti *et al.* (2004) for a 5 M$\odot$ hot core. Typical hot cores (as modelled by Viti *et al.* 2004) have temperatures of 300 K, sizes of about 0.03 pc, and densities of the order of 10^7 cm^{-3}; in this chapter we concentrate on the inner part of a typical warm core (or 'hot corino') and thus employ much smaller sizes, higher densities and lower temperatures

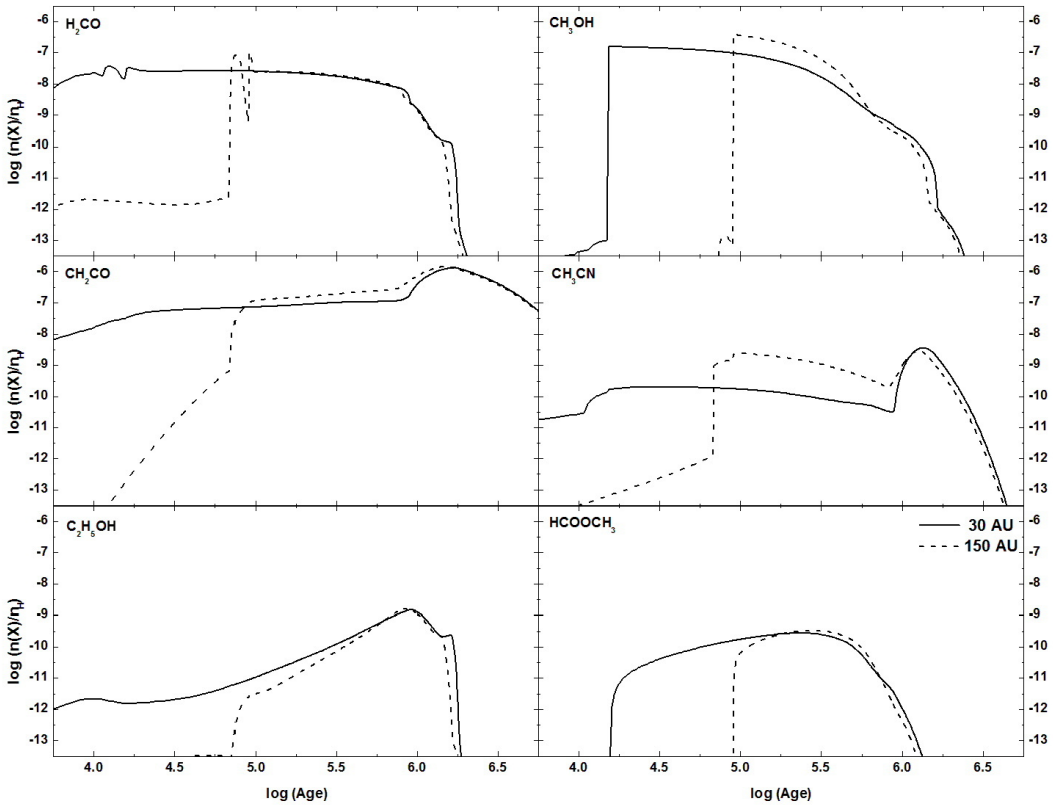

Figure 2.9: As in Figure (2.8), but for the large and organic molecules

(see Table 2.1). These differences in the physical initial conditions lead to two main differences in the chemistry: firstly we find that in general hot cores possess higher fractional abundances, at late times ($\geqslant 2 \times 10^5$ yrs), while those abundances are higher in warm cores at early stages. This is most likely due to the higher densities in warm cores (leading to a richer chemistry in both phases) and the different evaporation times (leading to different species being present in the gas phase at different times). Secondly, the evolutionary profiles of the species show almost the same trends shifted toward later times for hot cores. The observed jump in the abundances of species (such as H_2CO) in warm cores (e.g. Ceccarelli *et al.* 1996, 2000a,b) is not observed for the hot core case, which may indicate that these jumps are essential features in the warm core evolutionary profiles for those species. COMs show high abundances comparable to those found in hot cores, in particular for CH_3OH, CH_3CN, and C_2H_5OH. From the above discussion we conclude that the set of species used as evolutionary indicators for hot cores may be used

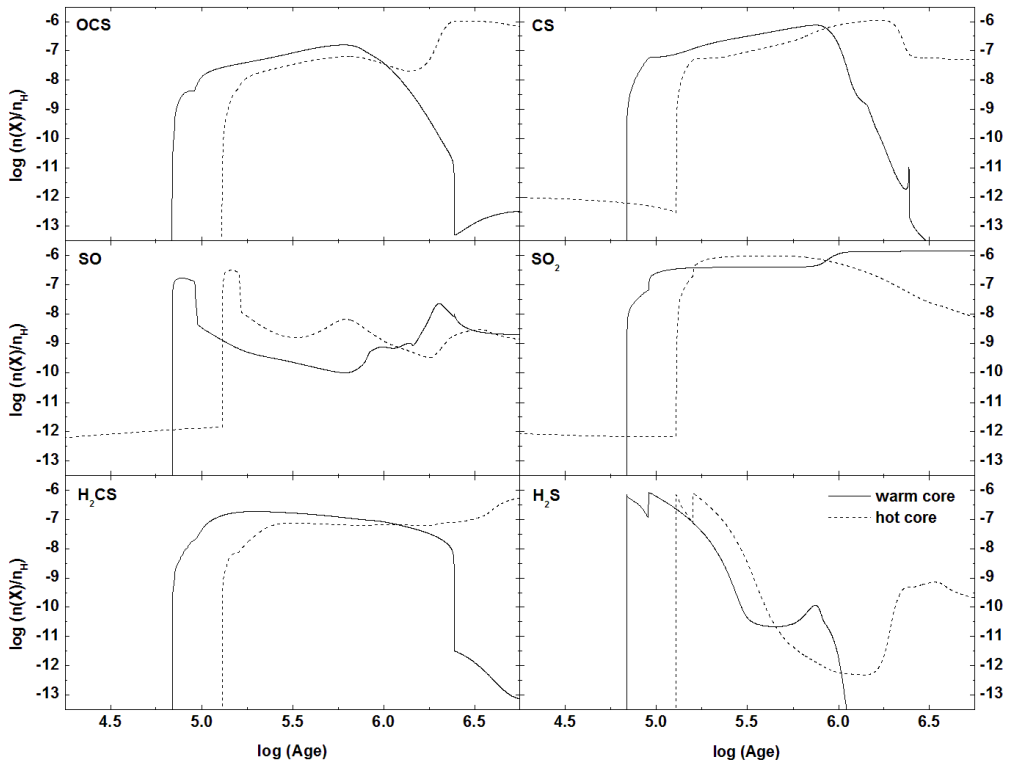

Figure 2.10: The time evolution of the fractional abundances of S-bearing molecules in a typical warm core compared to that in a $5M_{\odot}$ hot core (see key).

for the same purpose in warm cores.

2.3.3 Comparisons with observations of low-mass cores

While we do not attempt here to model any particular observed warm core, the physical parameters of one of our models with density of 2.0×10^8 cm^{-3} seem to be reasonably consistent with those observed toward the well-studied warm core around the solar type Class 0 source IRAS 16392-2422 (e.g Ceccarelli *et al.* 1999; Ceccarelli 2004, 2007). These authors find that at a radius of 150 AU and density 2.0×10^8 cm^{-3}, the dust temperature is $\sim$ 100 K. Hence we may qualitatively compare our results for our high density model to the observations of this core. Ceccarelli *et al.* (2000a,b) recorded sudden (spatially abrupt) increases in the abundances of a few observed species such as H_2O, SiO, and H_2CO. Schöier *et al.* (2002) found that in order to reproduce the physical properties of the dust and gas components constituting

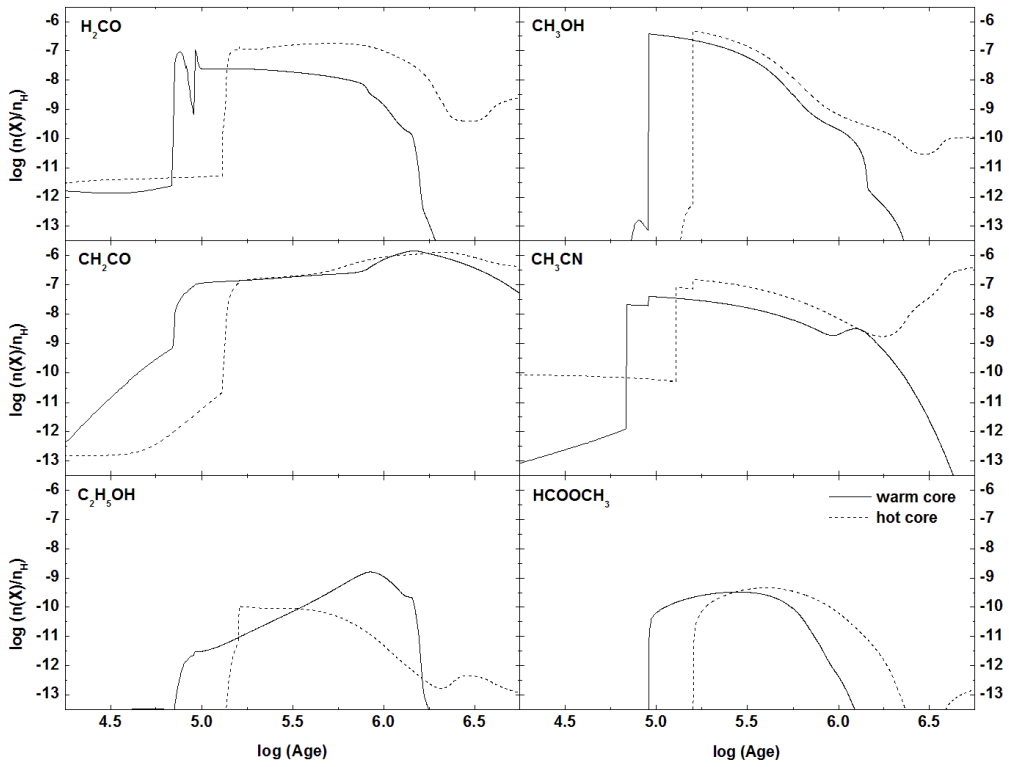

Figure 2.11: As in Figure (2.10), but for the large and organic molecules

the material in the circumstellar envelope of IRAS 16293-2422 a jump in the abundance of H_2CO and other species was indeed needed. Both of these papers proposed that these jumps, assumed around 80-90 K, result from the evaporation of mantle species in the hot-core like region around the protostar. Our model with density of 2.0×10^8 cm^{-3} does indeed reproduce the jumps in the profiles of H_2CO and CH_3OH, around 84 K, confirming their findings. A tentative comparison between our model calculations through the core and observational fractional abundances in IRAS 16293-2442 is shown in Table (2.3), at time around $8.5\times$ 10^4 yrs, when the dust temperature reaches $\sim$ 100 K. Because our model calculations are for a core of radius 150 AU, we compare our results with the observations of the inner core by Schöier *et al.* (2002), apart from the measurement of CH_3CN that was taken from Bisschop *et al.* (2008).

Sulphur-bearing species are, on average, in good agreement with observations during the early evolutionary stages ($t \leq 7 \times 10^4$ yrs) and hence they are good tracers of young cores with

Table 2.3: Our calculated fractional abundances in comparison with observations of IRAS 16293-2422. Observations are taken from Schöier *et al.* (2002), apart from CH_3CN was taken from Bisschop *et al.* (2008). Our results show an average range of the values calculated throughout the core at the five studied depth point between 30 and 150 AU.

Species	**This work**	**Observations**
OCS	$3 - 12 \times 10^{-9}$	2×10^{-7}
SO	$1 - 20 \times 10^{-8}$	2×10^{-7}
SO_2	$5 - 12 \times 10^{-8}$	1×10^{-7}
H_2CO	$9 - 25 \times 10^{-9}$	6×10^{-8}
CH_3OH‡	$2 - 3 \times 10^{-7}$	3×10^{-7}
CH_3CN	$6 - 13 \times 10^{-9}$	6×10^{-8}

‡ Our calculations for methanol are for core radius of ≤ 120 AU, after that the fractional abundance drops to $\sim 10^{-12}$

temperatures ≤ 84 K. On the other hand, we find that large complex molecules show good agreement with observations at later times ($t \geq 9 \times 10^4$ yrs) where the temperature exceeds 100 K. This result supports the view of grain mantles as factories of complex species and it underlines the importance of an accurate desorption treatment in the chemical modelling to provide abrupt changes in molecular abundances.

2.4 Conclusions

We report here results from a chemical model of a warm core (or hot corino) around a low-mass star. The core contains a protostellar object of solar mass whose radiation warms its inner part. This leads to sublimation of icy mantles deposited during the preceding collapse phase. We have introduced a detailed model of sublimation based on extensive laboratory results of Collings *et al.* (2004). These experiments imply that sublimation from mixed ices during the warming process occurs in several well-defined temperature bands. We have computed the positions of these bands for the solar-mass model and follow the resulting chemistry in a time- and space-dependent manner.

Although we have not attempted to model any specific astronomical source, the physical parameters we have used are sufficiently similar to those inferred from observations of a well-studied object, IRAS 16293-2422, for us to compare the model results with observations. The

predicted and inferred molecular abundances agree reasonably well.

The model that we have used is essentially a hot core model in which several physical parameters have been adjusted to be appropriate to warming by a solar-mass protostar. The generally satisfactory behaviour of the model results suggests that the chemical processes for both warm cores in low-mass star forming regions and hot cores in high mass star forming regions are similar.

Observations of warm cores show the existence at particular values of A_V of very substantial 'jumps' in abundance (by several orders of magnitude) in certain molecular abundances. We find that these jumps arise as a consequence of sublimation and subsequent rapid gas-phase chemistry. Such jumps do not occur in models that describe sublimation as an instantaneous process, rather than the staged process we have introduced.

We predict that ratios of certain sulphur species should be excellent tracers of physical conditions in warm cores, regardless of the (unknown) total sulphur abundance.

Finally, The comparison of the model results with observational results that show strong spatial dependence in molecular abundances within the core gives support to the treatment of sublimation. It appears to be important to take account of the laboratory results of Collings *et al.* (2003a, 2004) concerning sublimation of mixed ices.

CHAPTER 3

DEUTERIUM CHEMISTRY IN STAR FORMING REGIONS

3.1 Introduction

3.1.1 Observations of Deuterated species in ISM

Observations of interstellar deuterated molecules have long been used to probe the physical conditions within interstellar clouds. Although the interstellar ratio of deuterium to hydrogen (D/H) atoms is only $\sim 1.5 \times 10^{-5}$ (Linsky *et al.* 1995; Oliveira *et al.* 2003), it has been observed that the degree of deuterium fractionation, which is the abundance ratio of a molecule containing a deuterium atom (XD) to the equivalent molecule with a hydrogen atom (XH), is enhanced in many astrophysical regions such as cold, dark cores (e.g. Tiné *et al.* 2000), hot cores around massive star forming regions (e.g. Fontani *et al.* 2008), lukewarm cores (Sakai *et al.* 2009), and warm cores (or hot corinos) around low-mass star forming regions (e.g Ceccarelli *et al.* 1998c, 2001, 2007). Prior to the launch of the ISO satellite, attempts to detect the HD J = 1 - 0 line at 112 μm were unsuccessful although interstellar HD has been observed, like H_2, through ultraviolet absorption lines in diffuse clouds (van Dishoeck 2004). The launch of the Long Wavelength Spectrometer (LWS) and the Short Wavelength Spectrometer (SWS) onboard ISO, allowed the detection of the fundamental HD 112 μm line in emission and absorption, respectively. Wright *et al.* (1999) detected the first 112 μm emission line towards the Orion Bar, a nearby massive star forming region 400 pc away; four years later Polehampton *et al.* (2002) reported the detection of the same line in Sagittarius B2 (Sgr B2) a

giant molecular cloud near the Galactic centre. Almost simultaneous to the first detection of the HD 112 μm emission line, the 19.43 μm was seen with the SWS in the Orion molecular outflow (Bertoldi *et al.* 1999). ISO-LWS observations led to another detection of the fundamental HD absorption line at 112 μm towards a cold molecular cloud in the line of sight of the massive star forming region W49 (11 kpc from the Sun) (Caux *et al.* 2002).

Although the reported detections of the HD are just few, there is a growing body of observations for mono- as well as multiply deuterated species in the past decade. H_2D^+ had been detected towards two low-mass protostars, NGC1333 IRAS4 (Stark *et al.* 1999), IRAS16293-2444 (Stark *et al.* 2004), and several pre- and proto-stellar sources (Caselli *et al.* 2008). In addition, DCN and DCO^+ were detected towards Sgr B2 and Sgr A (for more details see review by Ceccarelli 2002). The first detection of doubly deuterated species (D_2CO) was towards Orion by Turner (1990). The same molecule was then detected towards the low-mass protostar IRAS16293-2444 (Ceccarelli *et al.* 1998c) with a D_2CO/H_2CO ratio 15 times higher than that obtained for Orion. IRAS16293-2444 is not the only case: observations reveal that the D_2CO/H_2CO ratio is high for all of the observed low-mass protostars (e.g. Ceccarelli 2002; Parise *et al.* 2006). D_2CO is not the only doubly deuterated species detected, NHD_2 was detected toward the dark cloud L134N (Roueff *et al.* 2000) and toward a low-luminosity prestellar core IRAS 16293E in the ρ Ophiucus molecular complex (Loinard *et al.* 2001). The detection of those species opened the field for more searches for other deuterated species, and now the detection of many deuterated species including ND_3, CHD_2OH, CD_3OH, D_2S, HD_2^+, CH_2DOH, and H_2D^+, has been reported in different regions in the sky; for references see Roberts *et al.* (2004) and Table (3.1). Sakai *et al.* (2009) detected carbon-chain deuterated species such as C_3D, C_4HD, DC_5N and others in the 'lukewarm' low-mass star forming region L1527 with an enhanced fractionation ratio. Most recently, Demyk *et al.* (2010) reported the detection of deuterated methyl formate $DCOOCH_3$ with a fractional abundance of about 10^{-7} towards IRAS16293-2444. To date, more than 151 species in space have been detected in interstellar clouds (Herbst & van Dishoeck 2009), of which 32 are deuterated species. A list of the observed deuterated species is given in Table (3.1).

Most of the observed species show an enhancement in their ratios with respect to their H-counterparts. Such high fractionation is found to be linked to the degree of depletion of heavy species on to grain surfaces, in particular CO, which destroys H_3^+. It is now well known that the key reaction for the formation of H_2D^+ is the deuteron exchange in the reaction between

HD and the molecular ion H_3^+, as given in reaction (3.1)

$$H_3^+ + HD \leftrightharpoons H_2D^+ + H_2 \tag{3.1}$$

H_2D^+ works as its analogue, H_3^+, and can initiate the same ion-molecule chain of reactions involving deuterium atoms as given in Eq. 3.2

$$H_2D^+ + X \longrightarrow XD^+ + HD \tag{3.2}$$

Further reactions of the molecular ion XD^+ with other neutral molecules spreads deuterium fractionation throughout the chemical network, leading to a wide range of abundant, deuterated molecules (e.g. Vastel *et al.* 2006).

Table 3.1: List of the observed deuterated species in cores around star forming regions. In this table, 'H' indicates high-mass star forming regions, 'L' refers to low-mass. Data with the symbol '†' is taken from Table 1 in Rodgers & Millar (1996).

	Species	**Region**	**Ref (e.g.)**
H_2D^+	H, L	Stark *et al.* (1999, 2004)
D_2H^+	H,L	Vastel *et al.* (2004); Caselli *et al.* (2008)
N_2D^+	H, L	Miettinen *et al.* (2009); Emprechtinger *et al.* (2009)
DCO^+	H, L	Penzias (1979); Stark *et al.* (2004)
DCN	H, L	Schilke *et al.* (1992); van Dishoeck *et al.* (1995)
DNC	†H, L	Rodgers & Millar (1996); van Dishoeck *et al.* (1995)
HDS	L	van Dishoeck *et al.* (1995)
D_2S	L	Vastel *et al.* (2003)
HDCS	L	Marcelino *et al.* (2005)
D_2CS	L	Marcelino *et al.* (2005)
HDCO	H, L	Loren & Wootten (1985); van Dishoeck *et al.* (1995)
D_2CO	H, L	Turner (1990); Ceccarelli *et al.* (1998c)
CH_3OD	H, L	Rodgers & Millar (1996); Parise *et al.* (2002)
CH_2DOH	H, L	Jacq *et al.* (1993); Parise *et al.* (2002)
CHD_2OH	L	Parise *et al.* (2002)
CD_3OH	L	Parise *et al.* (2004)

Continued on next page

Table 3.1 – continued from previous page

Species	Region	Ref (e.g.)
C_2D	H,L	Vrtilek *et al.* (1985); van Dishoeck *et al.* (1995)
C_3D	L	Sakai *et al.* (2009)
C_4D	L	Sakai *et al.* (2009)
C_3HD	L	Sakai *et al.* (2009)
DC_3N	L	Sakai *et al.* (2009)
DC_5N	L	Sakai *et al.* (2009)
NH_2D	H, L	Walmsley *et al.* (1987); Shah & Wootten (2001)
ND_3	L	van der Tak *et al.* (2002)
HDO	H, L	Jacq *et al.* (1990); van Dishoeck *et al.* (1995)
CH_2DCN	H	Gerin *et al.* (1992)
$DCOOCH_3$	L	Demyk *et al.* (2010)

3.1.2 Modelling Deuterated Species in the ISM

Interest in deuterium chemistry in the interstellar medium was aroused after the discovery of DNC in the Orion nebula. In the early attempts to study deuterium chemistry, gas-phase schemes were claimed to be efficient enough (Watson 1980) as they were able to reproduce the observed abundances within a reasonable factor. Tielens (1983), however, showed that grain surface reactions may indeed be needed. Because of the higher mass of D atoms compared to H atoms which produces a smaller zero-point energy and therefore higher binding energy, the residence time of D and HD on grains is larger than the collision time. This leads, in turn, to more reactions with other mantle species and hence more deuterium fractionation and more HD/H_2 on grains ($\sim 0.4\%$). From the above, grain mantles are good factories for deuterated species. In his time-independent model, Tielens (1983) studied the role of deuterium in surface chemistry. His results showed that the abundance of HDCO on grain mantles is higher than other deuterated species. He concluded that the reason for this is due to the fact that H abstraction from HDCO has a lower activation energy than D abstraction. In addition, his results showed that the ratio of concentrations of deuterated molecules to their hydrogenated counter parts in grain mantles depends strongly on the total hydrogen (H) density in the gas-phase and hence on the H_2D^+/H_3^+ ratio in the gas. Tielens also concluded that the abundances of mantle deuterated species are good indicators for the physical conditions in the gas-phase.

Brown & Rice (1986) developed gas-phase chemical models to include the fractionation of hydrogen isotopes assuming that deuterated and non-deuterated species have the same chemistry. In 1989, Brown & Millar (1989a) introduced the first chemical model involving deuterium chemistry, both in the gas-phase and on grain surfaces. They modelled a dense quiescent cloud and a hot molecular core in which they were concerned with the effect of including accretion and surface chemistry. For the dense cloud, they found that when the accretion dominates, the abundance of radicals (e.g. OD) or molecules (e.g. DCN) increase sharply before they decrease as they accrete onto grains. The reason for this is the removal of some species from the gas (due to their accretion) which are responsible for the destruction of them, and their accretion leads to increasing the deuterated species life time. In hot core models, including deuterium surface chemistry results in reproducing the large abundances of water and ammonia, and the degree of deuterium fractionation seen in the hot core. The same authors extended their network to include multiply deuterated species (Brown & Millar 1989b) and found that surface chemistry can produce small but significant amounts of multi-deuterated molecules. They obtained large degrees of fractionation for multiply deuterated species which implies that they could be observed in hot core regions. Millar *et al.* (1989) modelled the deuterium fractionation in dense interstellar clouds using a detailed numerical pseudo-time-dependent gas-phase chemistry for a temperature range 10 - 70 K. Their results showed that in cold clouds the major sources of fractionation are H_2D^+ and its daughter ions such as DCO^+ and H_2DO^+, while for warmer regions, up to 70 K, CH_2D^+, C_2HD^+, and associated species led to the high fractionation. More recently, Rodgers & Millar (1996) presented a model of the deuterium chemistry in hot cores. The importance of their work rests on the methodology they used in creating their deuterium network which is now used widely for generating deuterium chemical networks. They included all the deuterated analogues of all the species with less than nine atoms and extended all the important reactions involving H-bearing species to their D-bearing analogous assuming the same rate coefficient. The details of their methodology is not the focus of this thesis; the reader is referred to Rodgers & Millar (1996) for a detailed description. Their results showed that the fractionation of many evaporated species remains constant for about 10^5 yrs for a wide range of physical conditions and hence it is safe to assume that the deuterium fractionation of species observed in hot cores was present on grain surfaces. In addition, the authors found that their fractionation of HDO and NH_2D agrees well with those of Brown & Millar (1989b). They commented that the differences in the fractionation between the Orion hot core and compact ridge can be explained if the molecules in the ridge were formed at lower

temperatures. Therefore, they concluded that the fractionation of water and ammonia reflects the D/H ratio in the gas-phase when these molecules were formed. The high fractionation observed for H_2CO can be explained in terms of grain surface chemistry. The authors suggested the same scenario for methanol if it is formed on grains via hydrogenation of H_2CO.

Following the same methodology described in Rodgers & Millar (1996), Roberts & Millar (2000a) developed new chemical models including for the first time the deuterated sulphur-bearing species and gas-phase chemistry of some doubly-deuterated species to investigate the influence of varying a wide range of physical parameters, including density and freeze out on to grains, on the fractionation in interstellar clouds. They found that the fractionation ratios vary widely with temperature, depending on the fractionation process (i.e. due to H_2D^+, CH_2D^+ or C_2HD^+). In addition, they concluded that H_2S and HDS are good probes for regions where grain surface chemistry is important; however gas-phase chemistry is, in fact, sufficient to account for the high fractionation observed for mono- and doubly-deuterated species. Contrary to this result, Roberts & Millar (2000b) found that gas-phase chemistry is inefficient in reproducing doubly-deuterated species, and including surface chemistry enhances both the abundances of singly and doubly deuterated species. In their models, they used an extended version of the Roberts & Millar (2000a) model with a complete deuterium chemical network where for every reaction involving H-bearing molecule, its equivalent with a mono-deuterium counterpart was generated assuming statistical branching ratios for reactions containing more than one H-bearing product. They concluded that it is not necessary to have an active surface chemistry to enhance the fractionation of singly deuterated species while it is more important for doubly deuterated species. They commented that the high observed fractionation ratios (e.g. [HDCO]/[H_2CO] and [D_2CO]/[H_2CO]) seen in hot and warm cores might indicate that they had been set in the earlier, colder phase of the cloud's history and preserved on grain surfaces. If this were the case, such deuterated species are good probes of fractionation on grain surfaces. Following this work, Roberts *et al.* (2002) concluded that methanol could be used as another indicator for the grain chemistry because it is formed via routes involving H_2CO on grains.

Roberts *et al.* (2003) showed that deuterium fractionation via gas-phase chemistry can be more efficient if the role of multiply deuterated isotopomers of H_3^+ is taken into account. In their models, the authors, for the first time, included all the possible deuterated isotopomers of H_3^+. Their model results showed that in dense ($n(H_2) > 10^5$ cm^{-3}), highly depleted regions such as prestellar cores, the inclusion of HD_2^+ and D_3^+ enhances the fractionation of ionic and neutral species. That is because their inclusion allows more deuterium to transfer to

other species. In addition, the models predict that in dense depleted regions, the abundance of HD_2^+ will be similar to that of H_2D^+ and D_3^+ will be the dominant deuterated isotopomer of H_3^+. In addition, the authors concluded that according to their models, applicable to prestellar cores, a high atomic D/H ratio (≥ 0.3) is necessary for grain-surface chemistry to reproduce the high formaldehyde and methanol fractionation seen in star forming regions. These results and the discovery of multiply deuterated species in the interstellar medium motivated Roberts *et al.* (2004) to release a new version of their chemical model which includes multiply deuterated species. In this work the authors compared two different chemical reaction schemes: the UMIST 'rate99' (Le Teuff *et al.* 2000) and the so-called New Standard Model (NSM) from the Ohio State University (Terzieva & Herbst 1998). They found that the temperature dependence (as $\sqrt{300/T}$) of the ion-polar-molecule reactions in the NSM causes the destruction of polar neutrals (H_2O, CH_3OH, ... etc.) by molecular and atomic ions as (H_3^+, HCO^+, and C^+) to be $\sim$ 5 times higher than rate99 at 10K. This issue varied the time dependence of the species abundances significantly between the two models. By comparing the two reaction sets, the author commented that 'rate99' better reproduces the high observed fractionation of D_2CO, while NSM network is more successful at keeping ammonia in the gas after the depletion of CO on to grains. Roberts *et al.* (2004) also emphasised the importance of experimental as well as theoretical work for the improvement of key parameters for astrochemical modelling (e.g. binding energies, desorption rates). Astronomers are now keen to understand the origin and nature of the high deuterium fractionation ratio observed towards low-mass prestellar cores. In a follow up to their previous observations of HDCO/H_2CO and DCN/HCN ratios in a selection of low-mass protostellar cores (Roberts *et al.* 2002), Roberts & Millar (2007) observed and modelled the [D_2CO]/[H_2CO] and [N_2D^+]/ [N_2H^+] ratios towards a sample of low-mass protostellar cores to probe the physical conditions and chemical history of the gas, and to distinguish between gas-phase and grain-surface chemical processing in star forming regions. Their results show that for low-mass cores, there is no correlation between the enhancement of the formaldehyde fractionation and the N_2H^+ fractionation decrease while the fractionation of deuterated species observed towards hot molecular cores is most likely set during the early evolutionary stages.

The large number of observed species in both hot and warm cores and the very high degree of fractionation seen in warm cores motivated us to investigate whether the inclusion of deuterated molecules in our chemical network (described previously in Chapter 2) would have an influence upon the chemical evolution of hot and/or warm cores, and whether the two regions

show similarities in terms of deuterium chemistry as they present some common features for the non-deuterated case (see Chapter 2).

In this thesis, we present a new chemical model for both low and high mass cores. Although deuteration is set at the time of the prestellar phase, in our present study we are interested in exploring the deuterium chemistry in regions where a protostellar object exists. For this reason, we concentrate on modelling the chemical evolution of cores at the protostellar stage and not the prestellar phase as previously studied by (e.g. Roberts & Millar 2000a,b). A novelty of our model is the inclusion of the temperature dependent treatment of the desorption of the species, both deuterated and non-deuterated. In addition, we studied the evolution of deuterium chemistry for cores around massive stars ($M \geq 10\ M_{\odot}$).

3.2 Chemical Model and Network

The chemical model is the UCL_CHEM code described previously in §(1.6) and Chapter 2. We have extended the species set to include all the mono-deuterated counterparts for H-bearing species. D_2CO and HD_2CO^+ are the only doubly deuterated species in our network. The deuterated chemical network is based on the network described previously in Roberts & Millar (2000a) that is originally adapted from the UMIST database ratefile95 (Millar *et al.* 1997), but updated following Roberts *et al.* (2004).

In generating the deuterated reaction set, Roberts & Millar (2000a) adopted the approach described in Millar *et al.* (1989) and Rodgers & Millar (1996). They assume that both deuterium- and hydrogen-bearing species react with the same species at the same rate. Where there is uncertainty into which product the deuterium atom is incorporated they assume statistical branching ratios between the various possibilities. In addition to these assumptions, and according to the results of the experimental work carried out by Larsson *et al.* (1996), Roberts & Millar (2000a) replaced the recombination rate coefficient for H_2D^+ by a value two times slower than the corresponding reaction for H_3^+ (determined by Sundstrom *et al.* 1994), and for the branching ratios for each possible product channel; the products with 'HD+H' are three times more favoured than those with 'H_2+D'. In addition, they included theoretically determined rate coefficients for several radiative association reactions involving deuterated species, derived by Millar *et al.* (1989), and a number of direct fractionation reactions listed in Table 1 in Roberts & Millar (2000a). The rate coefficients for some radiative association reactions (Roberts *et al.* 2004) and binding energies for surface species were also updated (Roberts & Millar 2007).

Table 3.2: Rate coefficients for the updated radiative association reactions in our network. Data is taken from Table 3 in Roberts *et al.* (2004).

Reaction			α	β
			(cm^3 s^{-1})	
$CH_3^+ + H_2$	$\longrightarrow$	$CH_5^+ + h\nu$	$1.3(-14)$	-1.0
$CH_3^+ + HD$	$\longrightarrow$	$CH_4D^+ + h\nu$	0.0	....
$CH_2D^+ + H_2$	$\longrightarrow$	$CH_4D^+ + h\nu$	$2.0(-14)$	-1.0
$CH_3^+ + H_2O$	$\longrightarrow$	$CH_3OH_2^+ + h\nu$	$5.5(-12)$	-1.7
$CH_3^+ + HDO$	$\longrightarrow$	$CH_3OHD^+ + h\nu$	$1.1(-11)$	-1.7
$CH_2D^+ + H_2O$	$\longrightarrow$	$CH_2DOH_2^+ + h\nu$	$1.1(-11)$	-1.7

Note: $a(-b)$ stands for $a \times 10^b$.

According to our species file we updated our chemical network, where required. A list of the updated reaction coefficients is given in Table (3.2).

Besides these updates, we included all the freeze out reactions for hydrogen bearing species and their deuterium counterparts, assuming that the products would have the same branching ratios assumed for their hydrogen equivalents. The surface chemistry considered here is a very simple surface chemistry which includes, besides the H_2 and HD formation on grains, rapid hydrogenation of species, where energetically possible (see section 1.6).

The influence of adding the deuterated species to the chemical network on the chemical evolution of warm and hot cores is studied by running models with two different chemical networks: **network 1** includes reactions involving *only* H-bearing species (similar to those in Chapter 2) and **network 2** contains all the reactions in network 1 in addition to their mono-deuterated counterparts. In network 2, we include only mono-deuterated species as a first approximation and to keep the size of the chemical network and the computation time reasonable. Network 1 consists of 173 species linked in 1948 reactions while network 2 has 265 species, including 74 D-bearing species, involved in 4204 reactions, both in gas-phase and on grain surfaces.

In addition, we studied the effect of varying important physical parameters, namely the final density of the collapsing core and the depletion efficiency of gaseous species onto grain surfaces, on the chemical evolution of deuterated species in both hot and warm cores. A summary of the grid of models we used in this study is given in Table (3.3); see §(3.3) for more

details of this table.

In these models, the initial elemental abundances are those used by Viti *et al.* (2004), see Table (3.4), apart from HD which is taken from Roberts & Millar (2007), to reflect the cosmic D/H ratio calculated by Linsky *et al.* (1995); Oliveira *et al.* (2003). The radius of the hot core is assumed to be 0.03 pc while that of the warm core is 150 AU. For the warm core case, it is important to bear in mind that we are interested in the innermost part of the core where the sublimation of mantle species occur, and which is estimated to have a small radius of 150 AU and a temperature of around 100 K (e.g. Ceccarelli *et al.* 1999; Ceccarelli 2004).

Table 3.3: Summary of the grid of our models.

warm cores									
Models	**Mass**	**Size**	**Temperature**	**†Density**	**†Depletion**	**Chemical**	**Desorption temperature**		**Temperature profile**
	$M_\odot$	**AU**	**K**	**cm^{-3}**	**%**	**network**	**volcano**	**H_2O co-des**	**A**	**B**
M1W	1	150	100	2.0×10^8	100	1	83.6	95.5	0.1927	0.5339
M2W	1	150	100	2.0×10^8	100	2	83.6	95.5	0.1927	0.5339
M3W	1	150	100	1.0×10^7	100	2	83.6	95.5	0.1927	0.5339
M4W	1	150	100	2.0×10^8	85	2	83.6	95.5	0.1927	0.5339
hot cores									
Models	**Mass**	**Size**	**Temperature**	**†Density**	**†Depletion**	**Chemical**	**Desorption temperature[a]**		**Temperature profile[a]**	
	$M_\odot$	**pc**	**K**	**cm^{-3}**	**%**	**network**	**volcano**	**H_2O co-des**	**A**	**B**
M1H	5	0.03	300	1.0×10^7	100	1	86.3	97.5	4.856×10^{-2}	0.6255
M2H	5	0.03	300	1.0×10^7	100	2	86.3	97.5	4.856×10^{-2}	0.6255
M3H	5	0.03	300	1.0×10^6	100	2	86.3	97.5	4.856×10^{-2}	0.6255
M4H	5	0.03	300	1.0×10^7	85	2	86.3	97.5	4.856×10^{-2}	0.6255
M5H	10	0.03	300	1.0×10^7	100	2	88.2	99.4	7.847×10^{-3}	0.8395
M6H	15	0.03	300	1.0×10^7	100	2	89.5	100.8	9.697×10^{-4}	1.085
M7H	25	0.03	300	1.0×10^7	100	2	90.4	101.6	1.706×10^{-4}	1.289
M8H	60	0.03	300	1.0×10^7	100	2	92.2	103.4	4.700×10^{-7}	1.98

[a] The desorption temperatures and the values of the constants A and B for hot cores (M $\geq$5$M_\odot$) are taken from Viti *et al.* (2004). The constants A and B are described previously in §(2.2), Chapter 2.

† These parameters vary only during the collapsing phase (Phase I) of the chemical model.

Table 3.4: Model initial elemental abundances with respect to the total number of H nuclei.

Species	**Initial abundances**
Carbon	1.79×10^{-4}
Oxygen	4.45×10^{-4}
Nitrogen	8.52×10^{-5}
Sulphur	1.43×10^{-6}
Helium	7.50×10^{-2}
Magnesium	5.12×10^{-6}

As in Chapter 2, the model is a two-step calculation: the first is the collapsing phase which starts at low density, $\sim$ 400 cm^{-3}, undergoes a free-fall collapse (Rawlings *et al.* 1992) at a fixed temperature of 10 K until the core reaches its final density (as given in Table (3.4)). By the end of this phase, all the species, apart from light atoms such as H, H_2, He, and HD, are assumed to be depleted onto grain surfaces and hydrogenate when possible.

In the warming up phase (Phase II), we explore the chemical evolution of the remnant core, assuming a uniform density throughout the core. The new star heats up the surrounding gas and dust allowing the mantle species to evaporate. The effect of this heating is expressed as a function of both time and space. In this work, our temperature profile is similar to that described previously in detail in §(2.2) in Chapter 2.

The evaporation of surface species occurs at various temperature bands (e.g Collings *et al.* 2003a, 2004). Following Roberts & Millar (2000a), we assume that hydrogen and deuterium atoms react in the same way to other species, therefore, in our modelling we treat the evaporation of deuterated molecules from grain surfaces as we dealt with their hydrogen counterparts (McCoustra - private communication). The treatment of this behaviour in our models is pseudo-time-dependent in which we allow a fraction of mantle species to evaporate at certain temperatures corresponding to a specific desorption peak (see Table 1 in Viti *et al.* 2004, and §(1.6) in this thesis for more details).

3.3 Results and Discussion

In this work, we ran a grid of 12 models; 4 for hot corinos (or warm cores) and 8 for hot cores ($\geq$ 5M$\odot$). Table (3.3) summarises our grid of models with their physical conditions. Column 1

gives the names of the model; in that 'W' stands for 'warm' while 'H' refers to 'hot'. Columns 2 to 8 show the physical conditions of each model. In the next few lines we describe the abbreviations we use for the different models we run. For simplicity, while describing, we will omit the 'W' or 'H' specifications because the model numbers are the same for both warm and hot cores. Models M1 are the reference models of typical warm or hot cores without the inclusion of deuterated species; i.e. in network 1 as described in Chapter 2. M2 are those when deuterated species are included i.e. network2 as explained in §(3.2). All the models for M2 and latter models use network 2. M3 are models at lower densities than M2 while M4 show partial[1] depletion of gaseous species onto grain surfaces; see §(3.3.2 b). Models M5 to M8 are those of massive hot cores (M $>5M\odot$).

In the following sections we present our results for the comparisons of models M1 and M2 to investigate the effect of including deuterated species onto the chemistry of hot and warm cores; see §(3.3.1). We also compare the reference models M2 with M3 and M4 to explore the sensitivity of deuterium chemistry in star forming regions to the variations in both the density and the depletion efficiency, respectively; see §(3.3.2). Finally, we explore the chemistry in massive hot cores and compare models M5 to M8 with M2, in §(3.3.3)

3.3.1 Importance of Deuterium Chemistry

The effect of the inclusion of deuterated species on our chemical network has been studied for hot and warm cores. Figures (3.1) - (3.4) show the differences between the H-bearing network (network1: solid line) and the D-bearing network (network2: dashed lines), for both types of cores. In general for warm cores, Figures (3.1) and (3.2), we see clearly that the inclusion of deuterated species in the network has almost no impact on the chemistry of the main isotope (non-deuterated) species in the core, except for H_2CO and CH_3OH that show small variations in their abundances, while for the hot core case, Figures (3.3) and (3.4), the influence is significant. More specifically, for warm cores, including deuterium in the chemical network slightly increases the abundances of both H_2CO and CH_3OH, in particular at early times, prior to their sublimation from grain mantles. When H_2CO evaporates from the grains, its abundance in both networks converges while that of methanol remains about 7 times higher in the deuterium network compared to network 1. The desorption peaks and the 'jumps' discussed

[1]In this chapter and the next chapters, the term 'fully depleted' gas refers to interstellar gas which is 100% depleted on to grains by the end of the collapsing phase while 'partially depleted', in this thesis, means a depletion percentage of 85%

earlier (e.g. Schöier *et al.* 2002 and Chapter 2) are reproduced by network 2. The chemical analysis revealed that in models with network 1, without the inclusion of deuterated species, formaldehyde is formed efficiently via the oxidisation reactions of CH_3 and is destroyed by H^+ to form either HCO^+ or H_2CO^+. The same routes dominate the chemistry when including deuterated species, i.e. in network 2, with an additional route of formation via H_2DCO^+. The latter route vanishes after the desorption of the species from grains (at $\sim 10^5$ yrs) causing the obtained conversion of the abundance of H_2CO in the two networks; see Fig. (3.2). In network 1, methanol is produced via 'CH_3OH_2 + NH_3' while in network 2 it is formed via 'CH_3OHD + NH_3' with a minor contribution from the hydrogenated route. On the other hand, its decomposition in both networks is because of H^+ ions. The abundance of H^+ in network 1 is higher than that in network 2 leading to more destruction of the molecule. This is the main reason for methanol to possesses higher abundances in network 2 than in network 1. Neither of the two networks can produce a significant amount of complex species (larger than methanol).

In the case of hot cores, for most of the studied species, the evolutionary profiles look similar in the two networks, apart from that of CH_2CO. The evaporation peaks are less pronounced in network 2 for some species such as H_2CO, H_2O, and CH_2CO. The decay of the sulphur bearing species is 'shifted' towards later times in network 2 and its rate is slowed down. The fractional abundances of OCS, SO, and SO_2 species in model M2H are lower than those obtained in M1H for times $\leq 2.4\times10^6$ yrs. For large species, the fractional abundances of CH_3CN are not influenced at all by the addition of deuterium to the network (model M2H) while those of CH_2CO and $HCOOCH_3$ show a significant decrease in their abundances down to ~ 3 orders of magnitude for the latter.

The decrease in the abundance of $HCOOCH_3$ is mainly due to its reaction with H_2DO^+ to form water via the following pathway:

$$\mathrm{H_2DO^+ + HCOOCH_3 \longrightarrow H_4DC_2O_2 + H_2O} \tag{3.3}$$

Through the life time of the hot core, the destruction rate of CH_2CO is higher than its production rate which causes the large decrease in its abundance. Ion-molecule reactions with He^+, Eqs. (3.4), lead to the destruction of CH_2CO at times earlier than 3.64×10^4 yrs.

$$\begin{aligned} &\mathrm{He^+ + CH_2CO \longrightarrow CO + CH_2^+} \\ &\mathrm{He^+ + CH_2CO \longrightarrow CO^+ + CH_2} \end{aligned} \tag{3.4}$$

At later times, the cosmic ray induced photoionisation reaction dominates the chemistry to

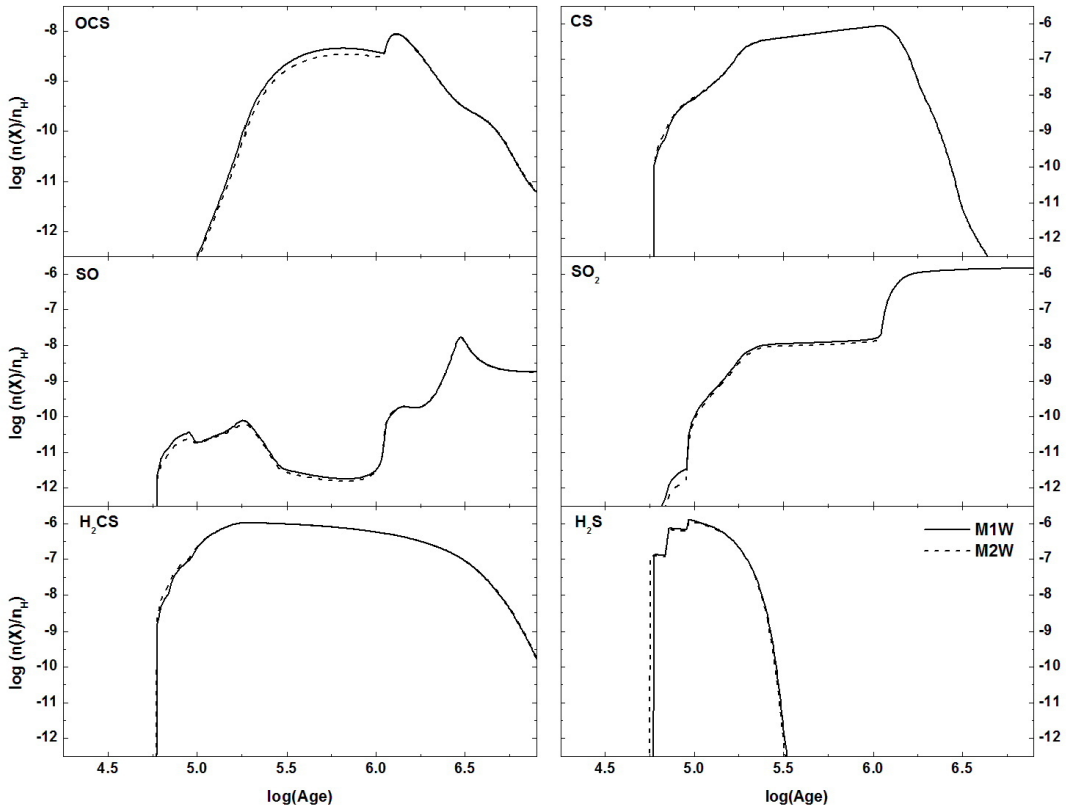

Figure 3.1: Chemical evolution of the S-bearing species as a function of time in a comparison between network 1 (M1W:solid line) and network 2 (M2W:dashed line) for a warm core

form CO and CH_2:

$$CH_2CO + CRPHOT \longrightarrow CO + CH_2 \tag{3.5}$$

On the other hand, the abundances of H_2CO and CH_3OH are enhanced by about an order of magnitude each. Water abundances decrease in network 2 at earlier times, however the two model calculations converge after the evaporation of mantle species.

From the above results, it is clear that the inclusion of deuterated species in the chemical network significantly affect the chemistry of hot cores while its influence on the chemistry of warm cores is minor.

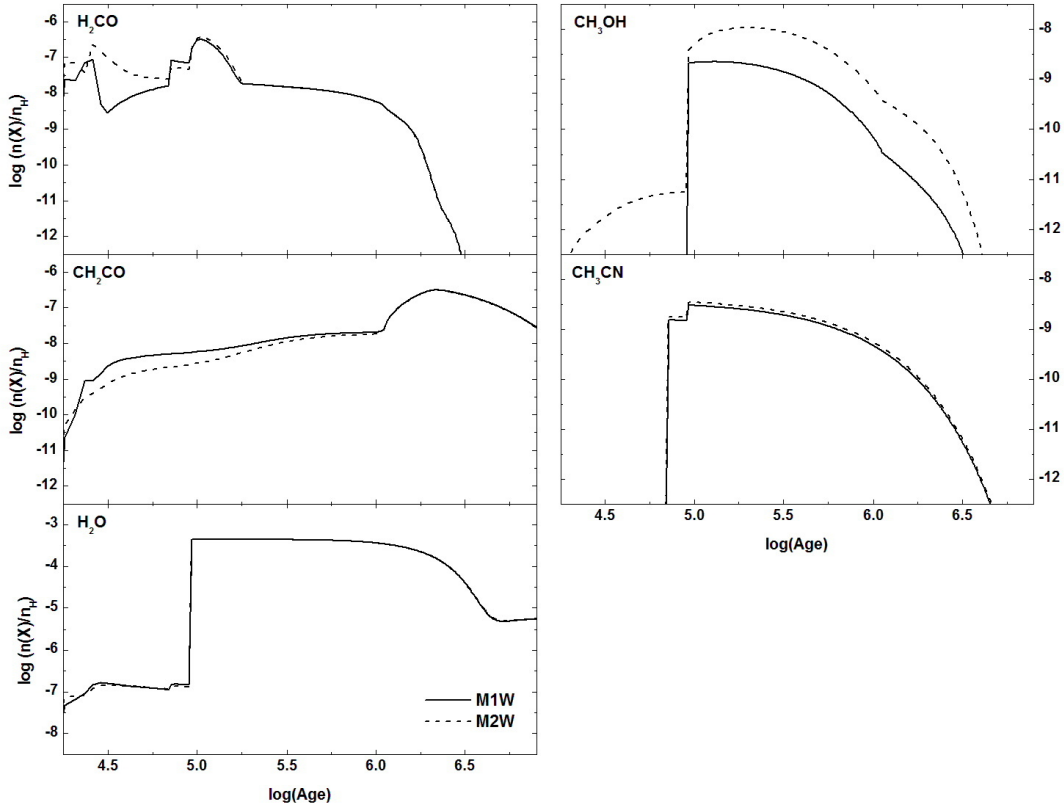

Figure 3.2: Same as in Fig. (3.1), but for other molecules (see key)

3.3.2 Sensitivity of Deuterium Chemistry to the Initial Conditions

In this section we study how sensitive the deuterium chemistry in warm and hot cores is to the changes in the environment, in particular density and the degree of depletion. We ran a total of 6 models, all using network 2, for both warm and hot cores in which we changed the final density of the collapsing core and the depletion percentage of heavy species onto grains; see the grid of model in Table (3.3).

(a) Influence of changing the final density:

For hot corinos, Figs. (3.5) and (3.6) show the chemical evolution of a set of deuterated species in the warming up phase for two models: model M2W for a typical warm core (solid line) and model M3W for a less dense core (dashed line) as a function of time. Species, as expected, are more abundant in denser cores; exceptions are HDO, CH_3OD and CH_2DOH that show higher

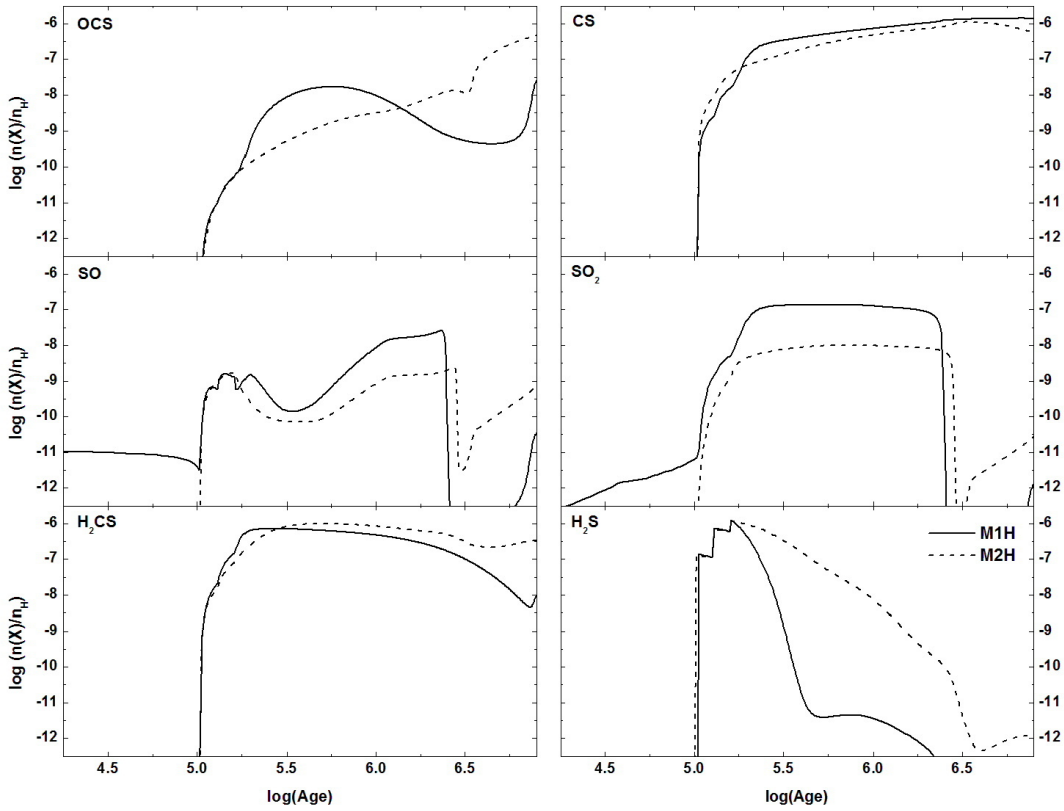

Figure 3.3: Chemical evolution of the S-bearing species as a function of time in a comparison between network 1 (M1H:solid line) and network 2 (M2H:dashed line) for a $5M_{\odot}$ hot core

abundances for less dense regions, in particular during early times ($t \leq 10^5$ yrs). The chemical analysis reveals that in dense regions for times $\leq 10^5$ yrs those species (HDO, CH_3OD and CH_2DOH) are destroyed via reactions with H^+ which are not efficient in less dense regions. Therefore, their abundances remain high for longer times in less dense regions. All the species experience a rapid and steeper decay in their abundances in less dense cores than in denser ones. The chemical trends in the two models remain the same except for HDCO which shows fluctuations in its abundance in particular after 10^5 yrs. The two deuterated methanol counterparts show the same evolutionary profile, but CH_3OD seems to survive longer than CH_2DOH.

Our results also show that changing the final density of the collapsing core influences the fractional abundances of non-deuterated species, Figures (3.7) and (3.8), even more than it does

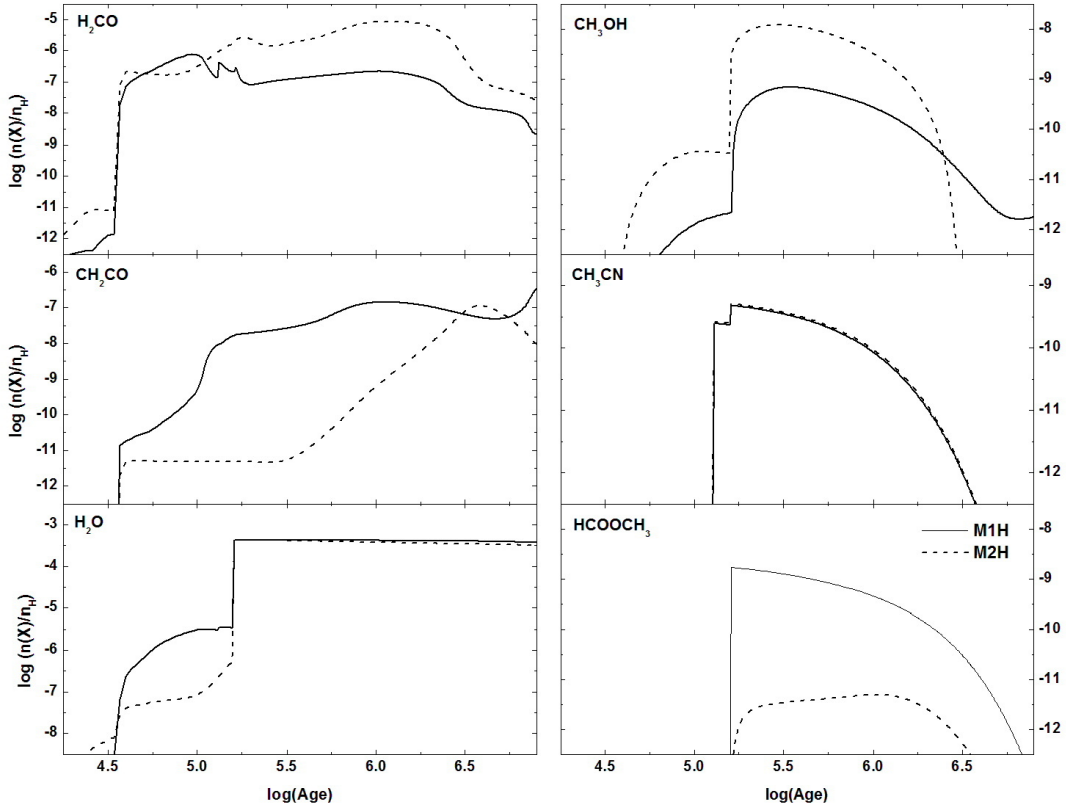

Figure 3.4: Same as in Fig. (3.3), but for water and large molecules (see key)

using network 1 (see Figures (2.4) and (2.5), in Chapter 2). Here, in the next part, we discuss these effects for the main isotopes, in network 2, in some detail. Most of the species show lower abundances for less dense cores, again as expected, exceptions are SO, SO_2, H_2CO, and CH_2CO. SO is mainly formed in gas-phase via reactions involving molecular and atomic oxygen during early and late times, respectively, while it is destroyed via ion-molecule reactions with DCO^+ to form DSO^+ and CO. At all times, SO is consumed to form SO_2 via oxidisation and radical molecule reactions, at low and high densities, respectively. At any time, the destruction rate, of both SO and SO_2, is higher in dense cores than that in less dense ones.

$$\begin{aligned} &DCO^+ + SO \longrightarrow DSO^+ + CO \\ &O_2 + S \longrightarrow SO + O \end{aligned} \tag{3.6}$$

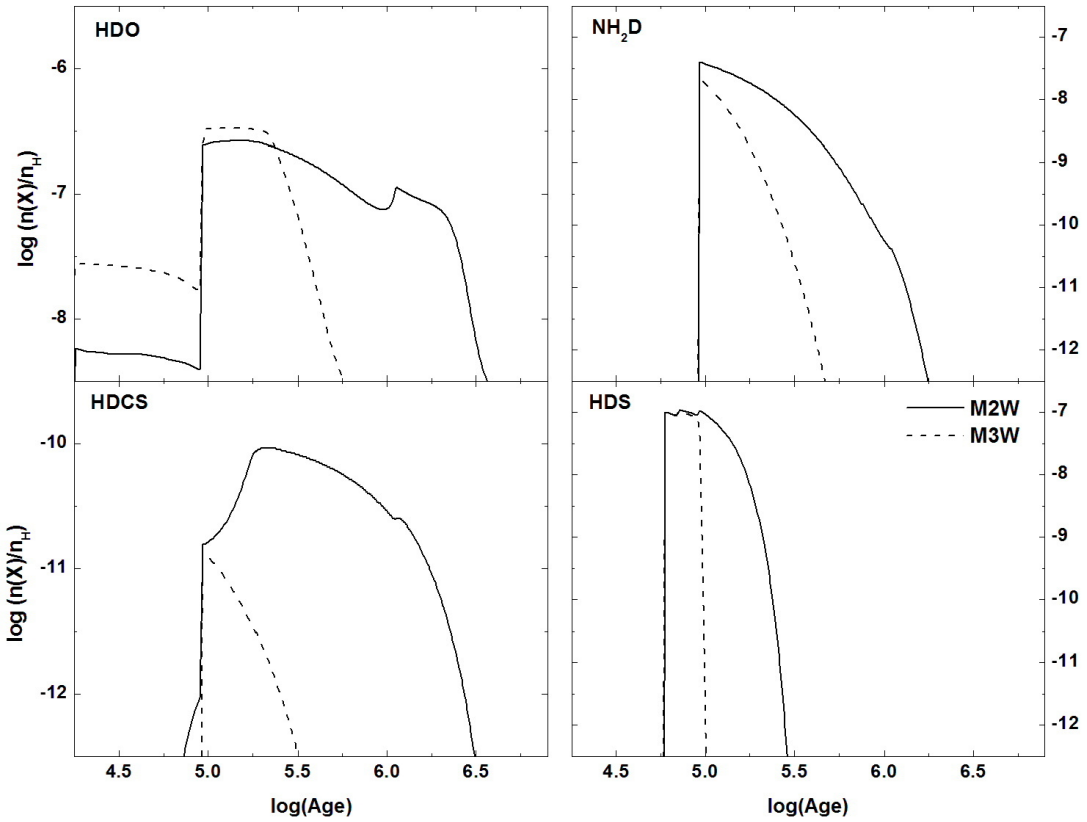

Figure 3.5: Chemical evolution of HDO, NH_2D, HDCS, & HDS as a function of time in network 2 at two different densities for a warm core (see key)

$$\begin{aligned} \mathrm{OH} + \mathrm{SO} &\longrightarrow \mathrm{SO_2} + \mathrm{H} \\ \mathrm{O} + \mathrm{HS} &\longrightarrow \mathrm{SO} + \mathrm{H} \end{aligned} \tag{3.7}$$

At times $\sim 5.6 \times 10^4$ yrs, OCS is more abundant in less dense cores because at those particular times its formation is more enhanced than in denser cores. In addition, the destruction of the molecule via CR photons is not efficient for low density cores. Thus, the molecule shows higher abundances in less dense cores. Sulphur bearing species are found to reach steady state earlier in less dense cores, and their evaporation peaks are more pronounced than in denser cores.

At high densities H_2CO is formed via the reaction of H_2DCO^+ with H_2O and destroyed via the reverse reaction which is very efficient. The destruction of H_2CO at lower densities via

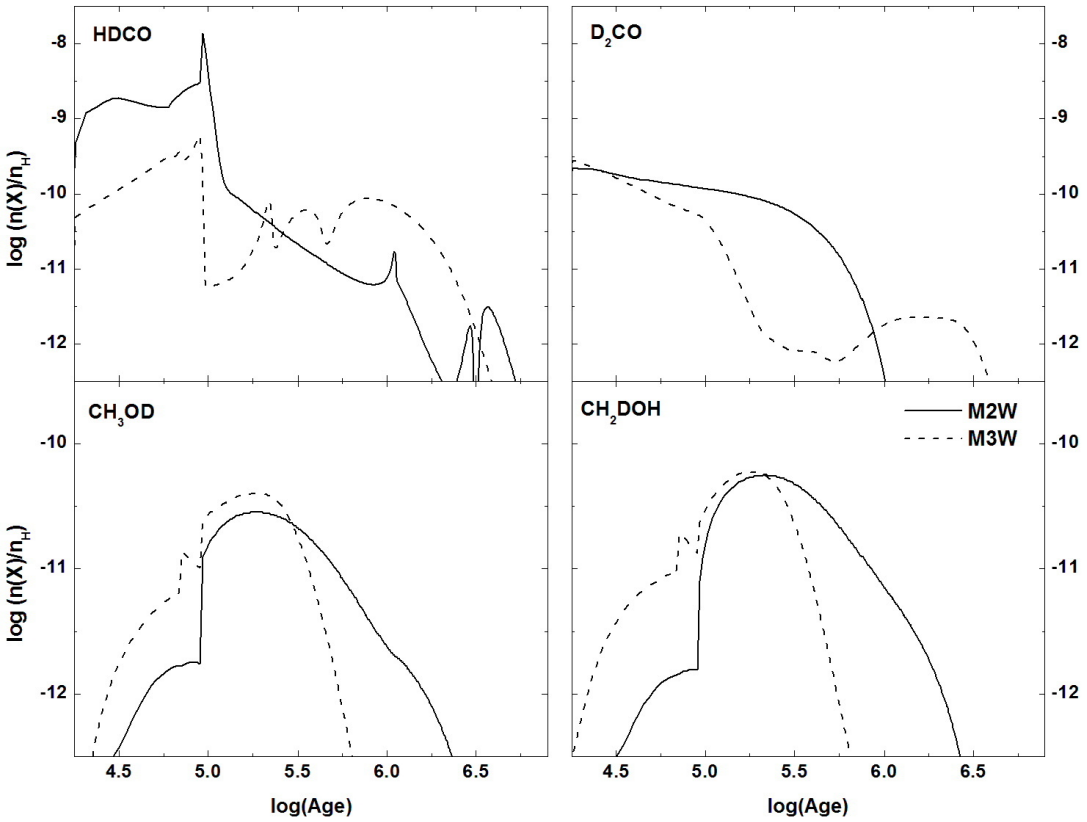

Figure 3.6: Same as in Fig. (3.5), but for deuterated H_2CO & CH_3OH (see key)

atomic oxygen is less efficient than its formation by CH_3 oxidisation reactions; see reactions (3.8). CH_2CO is more abundant at lower density due to the same reason: its formation is more efficient in the low density regime.

$$\begin{aligned} &H_2DCO^+ + H_2O \longleftrightarrow H_2CO + H_2DO^+ \\ &CH_3 + O \longrightarrow H_2CO + H \\ &O + H_2CO \longrightarrow CO + OH \end{aligned} \tag{3.8}$$

Complex molecules such as $HCOOCH_3$ are "unobservable" and deuterated species rapidly decay becoming less abundant when the core density decreases.

In general, we find our results in agreement with those previously obtained for warm cores (see §(2.3) in Chapter 2). In the current study, we found that for less dense cores, the abundances of SO, SO_2, OCS ($t \leq 2\times10^5$ yrs), and H_2CO increase while for the rest of the species the abundances decrease, including OCS at times larger than 2×10^5 yrs. These results, again,

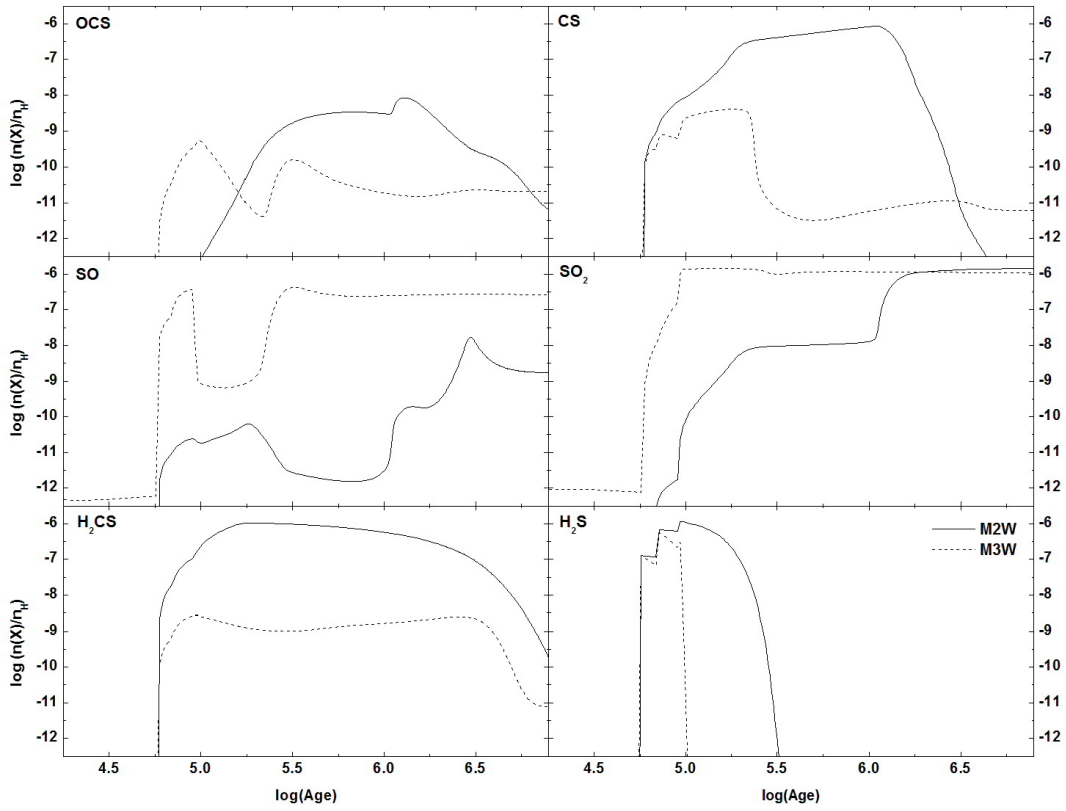

Figure 3.7: Chemical evolution of normal S-bearing species as a function of time in network 2 at two different densities for a warm core (see key)

show that sulphur-bearing species show the most variation with the change in density and hence they may be used as good tracers for the physical conditions of the region. The SO/CS, SO/OCS, and SO/H_2CS ratios are >1 for times later than 2×10^5 yrs while those of H_2S/H_2CS and H_2S/SO_2 <1 at times larger than $\sim2\times10^5$ yrs. The absence of complex molecules such as $HCOOCH_3$ in low density cores (models M3) may imply that the formation of these large molecules require denser environments ($> 10^7$ cm^{-3}).

For hot cores, the variation in the calculated fractional abundances as a function of time at different densities (model M2H, solid line, and model M3H, dashed line) is shown in Figures (3.9) and (3.10). Molecules in hot cores are less affected by the decrease in core density than they are in hot corinos. However, deuterated water shows a slightly higher abundance at times $\leq 2 \times 10^5$ yrs, and both forms of deuterated methanol are less abundant in lower density hot

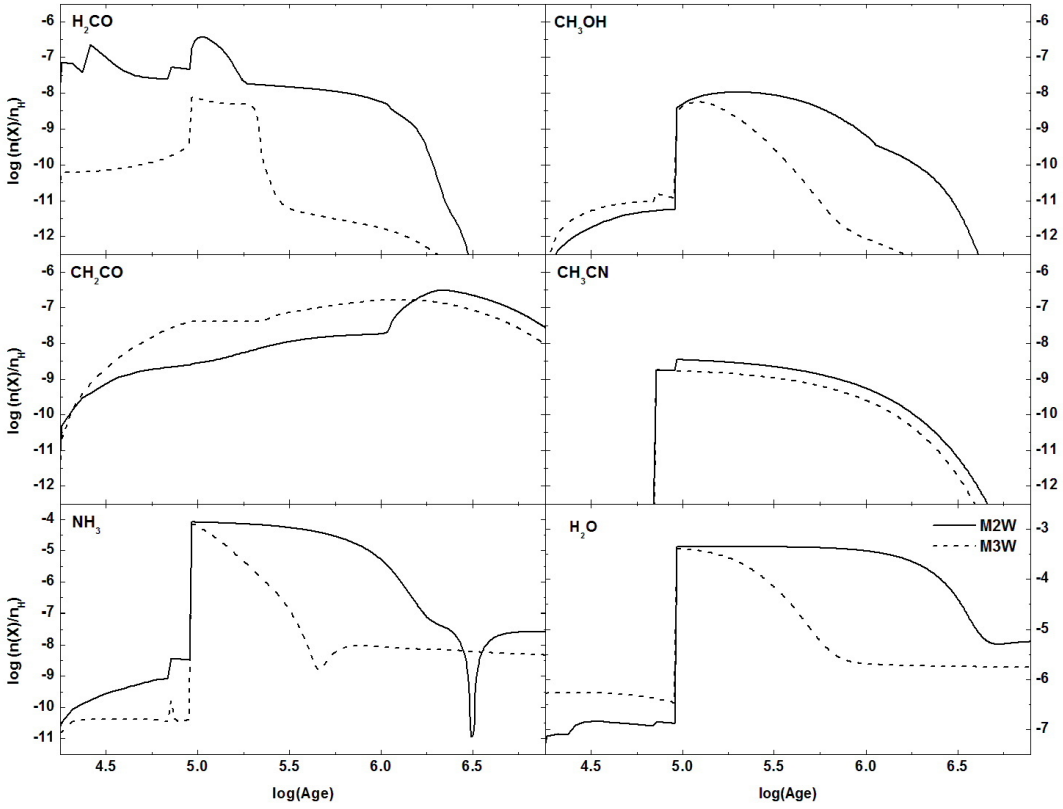

Figure 3.8: Same as in Fig. (3.7) but for organic species, ammonia and water (see key)

cores. One can also notice that the desorption peaks of the species in less dense cores are more pronounced than in denser cores. A plausible explanation for this is that the probability of collision between species in denser, warm cores, is higher than in less dense, hot cores. Thus, the destruction rate of less abundant species in warm cores increases as they are often destroyed to form other molecules, which is not the case for hot cores (less dense regions). There could also be other reasons if one considers the dynamical differences between hot and warm cores. Warm cores are closer to the radiating source and are influenced by the outflows of the young embedded source more than in the case of hot cores. This may result in destroying the species in gas-phase before they have time to accrete onto grains leading to a shortage in their mantle abundances. This shortage will, in turn, cause the desorption peaks of these species to be less pronounced than in the case of less dense hot cores.

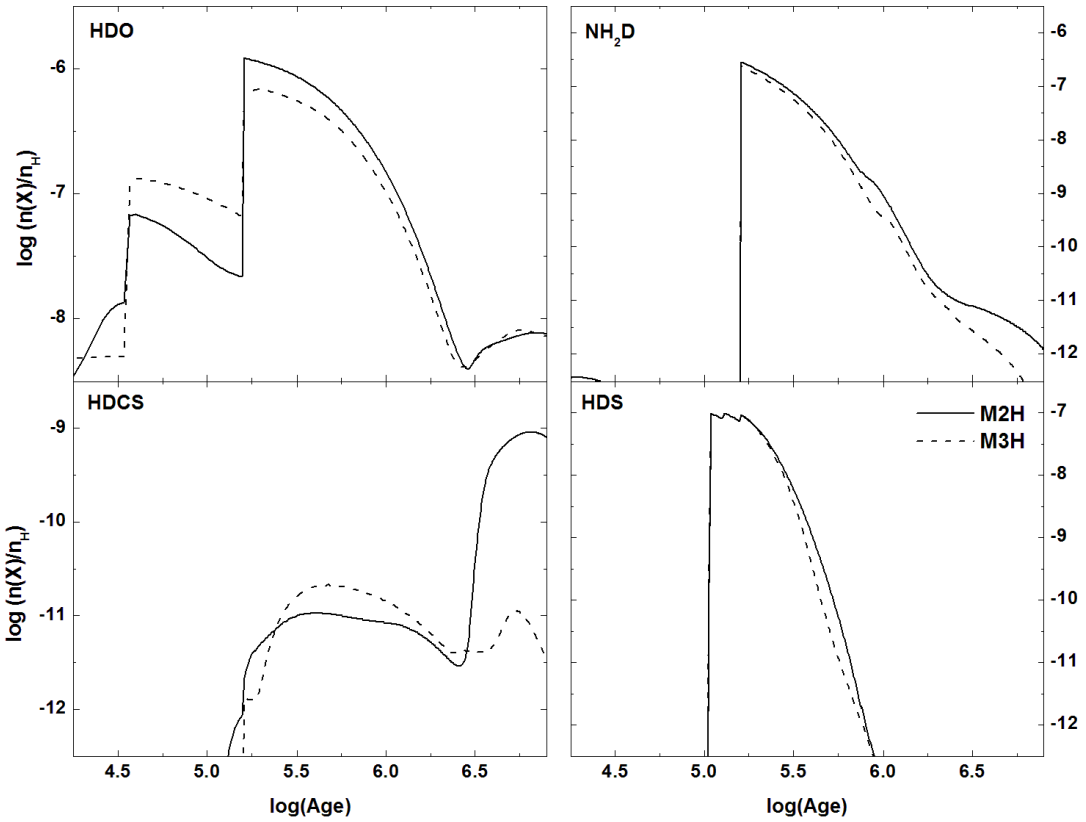

Figure 3.9: Chemical evolution of HDO, NH_2D, HDCS, & HDS as a function of time in network 2 at two different densities for a 5 $M_{\odot}$ hot core (see key)

(b) Impact of varying the depletion efficiency:

Observations reveal that the enhancement of the deuterated species to their fully hydrogenated forms arises in regions where the CO molecules are heavily depleted onto grains (e.g. Bacmann *et al.* 2003; Millar 2005). Hence we discuss the results of modelling warm and hot cores with fully and partially depleted gas (models M2W and M4W for warm cores, and M2H and M4H for hot cores), respectively.

In the case of warm cores, the chemical evolution of deuterated molecules in a fully depleted gas (solid line) is plotted in comparison with the case of partially depleted gas (dashed line), both as a function of time, in Figs (3.11) and (3.12). Models with partially depleted gas lead to lower abundances for all deuterated species, apart from HDCS, at late times ($t \geq 9\times10^4$ yrs) while during earlier times the abundances of those species are enhanced, with the excep-

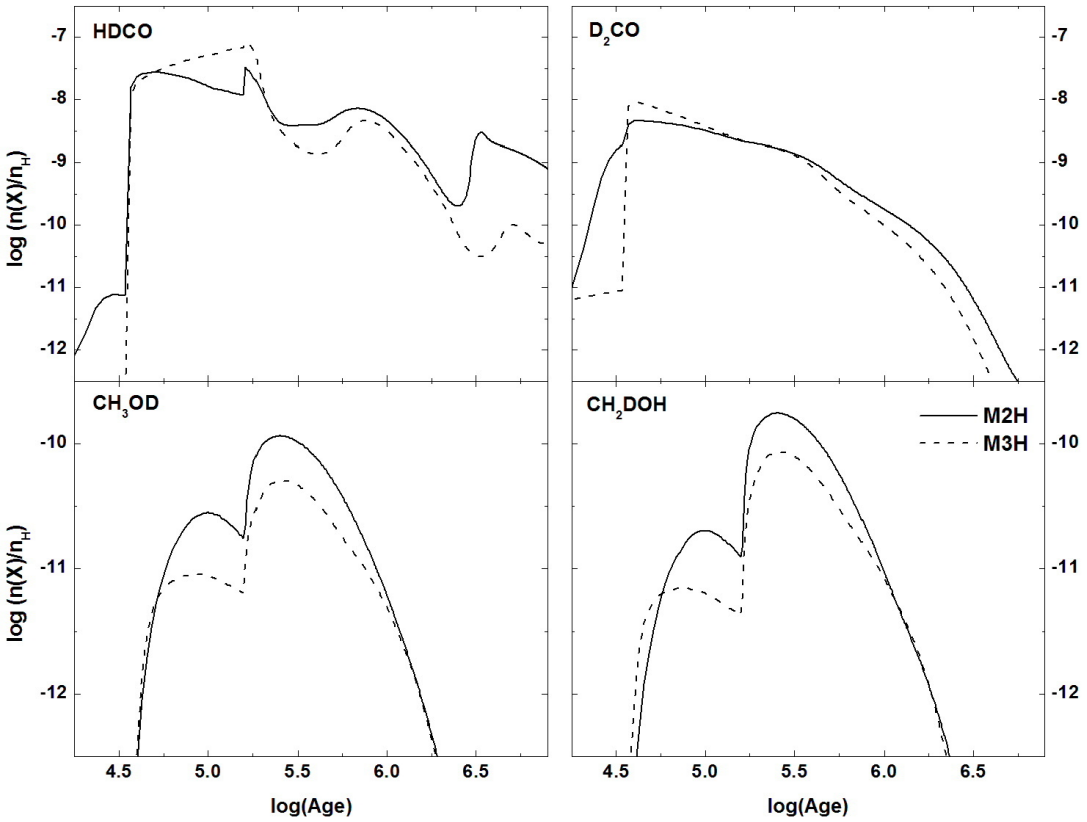

Figure 3.10: Same as in Fig. (3.9), but for deuterated H_2CO & CH_3OH (see key)

tion of NH_2D. Prior to 9×10^4 yrs, the formation rate of HDCS is similar in both models while after that time, and when mantle species sublimate, formation of HDCS increases.

On the contrary, when depletion is high D_2CO is enhanced. Bacmann *et al.* (2003) observed D_2CO in a sample of prestellar cores and correlated the deuterium fractionation ratio $[D_2CO]/[H_2CO]$ to the degree of CO depletion (see Fig 2 in Bacmann *et al.* 2003). They found that the higher the depletion factor the higher the fractionation ratio i.e. higher production of D_2CO. Our results are in line with these observations in that we found that the D_2CO/H_2CO ratio increases rapidly towards the end of the collapsing phase (e.g. see Fig. (3.20)) when most of the heavy species are believed to be depleted onto grain surfaces. D_2CO is believed to be formed on grain surfaces during the cold prestellar stages (Tielens 1983) and hence its fractionation ratio traces the grain surface chemistry (Roberts 2008) thus it is not surprising to see an increase in the D_2CO/H_2CO at the time of D_2CO sublimation.

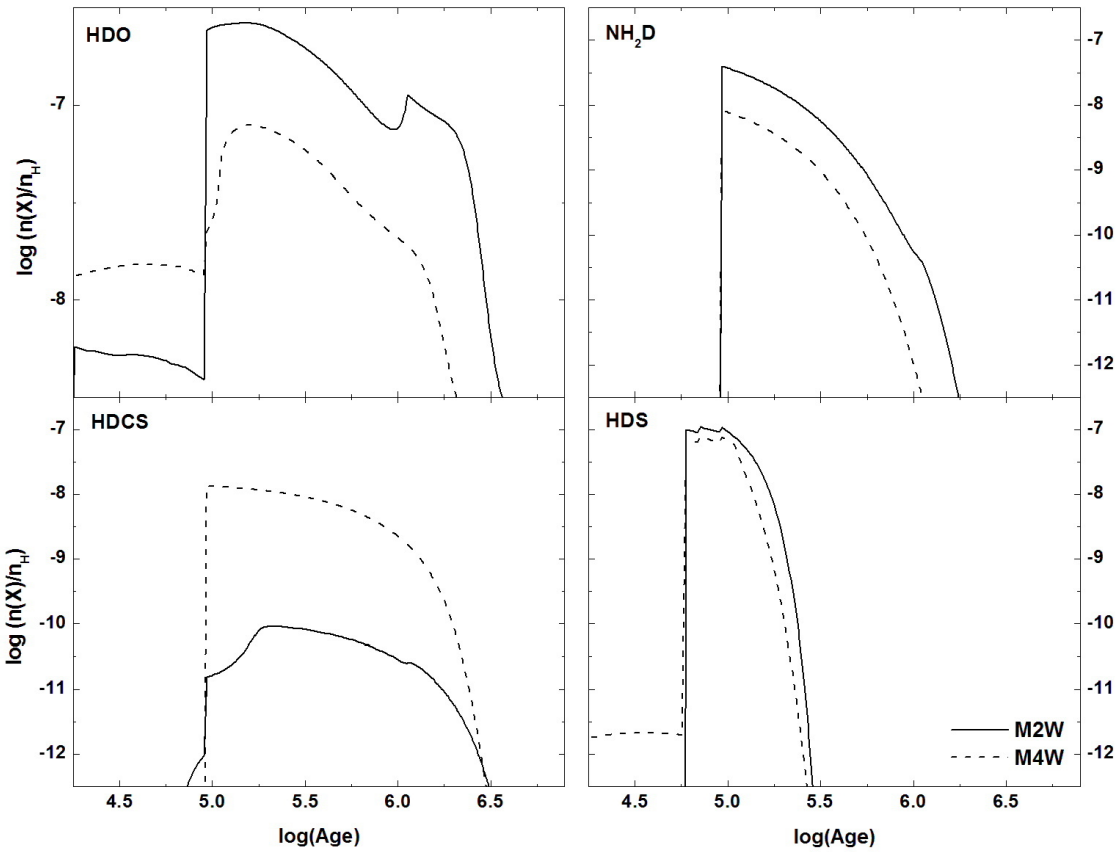

Figure 3.11: Chemical evolution of HDO, NH_2D, HDCS, & HDS as a function of time in network 2 at two different depletion efficiencies (see key)

On the other hand, N_2D^+/N_2H^+, see Fig. (3.20), is much higher for model M2W than M4W. This result is in line with observations by Roberts (2008) in which they argued that the N_2D^+/N_2H^+ ratio traces the gas in the extended envelope (lower density than the core) and it is found to increase as CO depletion increases in the cold prestellar phase (Bacmann *et al.* 2003). Rawlings *et al.* (1992); Bergin & Langer (1997) found that the increase in the depletion rate results in an increase of the N_2H^+ fractional abundance. Our results are in agreement with their models in that we also find that the formation of N_2H^+ increases when all species are depleted. N_2D^+ abundance is enhanced in models with less depletion on to grains (M4W). From the above discussion we conclude that D/H ratios of N_2H^+ trace the depletion degree in the gas-phase while those of H_2CO trace the grain surface chemistry.

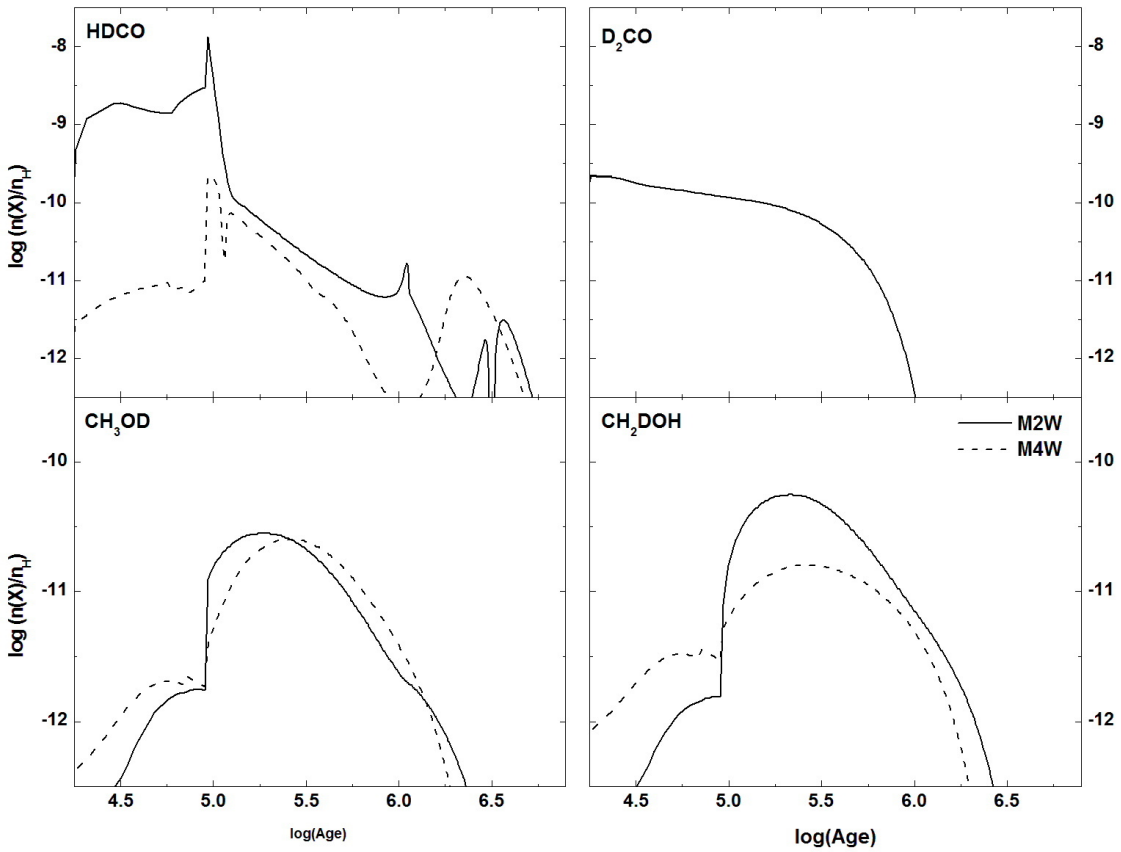

Figure 3.12: Same as in Fig. (3.11), but for deuterated H_2CO & CH_3OH (see key)

HDO in warm cores shows an increase in its abundance which cannot be explained in terms of mantle sublimation. The chemical analysis at the time around the 'jump' ($\sim 1.7 \times 10^4$ yrs) revealed that this jump is indirectly related to the formation of methane (CH_4) via gas-phase reactions (see Chapter 2). At the time of the 'jump', deuterated water is formed via reactions involving H_2CO and destroyed by CH_5^+ to form CH_4. At the same time, H_2CO is formed via the oxidisation reactions of C_2H_3, the latter being a secondary product of CH_4. Therefore, we argue that the jump in the HDO is related to the increase in the methane abundance at that time in gas-phase chemistry.

We discussed above how sensitive the fractional abundances of deuterated species are to the depletion percentage. In the following few lines we will discuss the sensitivity of non-deuterated species to the variation in the freeze-out degree of species on to grain surfaces in warm core environments where deuterated species are present, i.e. when we use network 2 for

our modelling; see Figures (3.13) and (3.14). The partially depleted gas model yields higher abundances for almost all the species during their early evolutionary stages; however, the two model calculations converge when the desorption from grain surfaces takes place. Variations in the depletion percentage of the species on to grain surfaces influence the fractional abundances of the species in our sample in particular during early times, but H_2S and HDS are the least affected. The H_2CO abundance decreases as the depletion percentage decreases. The chemical analysis for the molecule unveiled that the formation of the molecule is efficient in both models, with comparable values of formation rates, while the two models show differences in the efficiency of the destruction pathways. In models M4 the destruction is dominated by reactions involving OH to form water during early times $<2\times10^3$ yrs and atomic O to form CO at later times. Both of these routes are not efficient in models M2, with 100% depletion, causing the abundance of formaldehyde to decrease in models M4 compared to that in M2.

Surprisingly, methanol abundances, in partially depleted gas, are enhanced by about 3 orders of magnitude when compared to the fully depleted model. The chemical analysis unveiled that for less depleted gas the production rate of methanol, in Phase II, is larger or equal to its destruction rate up to 10^5 yrs, then the production rate decreases and hence the abundance starts to decrease. Not only that, but it also seems that the formation of CH_3OH is mainly via CH_3OHD^+, which seems to survive longer in less depleted gas. Deuterated species are less abundant as the depletion onto grains decreases with the exception of HDCS which is formed efficiently in gas phase and hence it is enhanced when the abundances in the gas phase increase due to the lowering in the depletion.

In the set of studied species, OCS, SO, CH_2CO, CH_3CN, and methanol are very good indicators of depletion in the warm core. In the case of hot cores, Fig.s (3.15) and (3.16), decreasing the depletion efficiency as in model M4H (dash line) leads, generally, to a decrease in the gas-phase abundances with the exception of HDCS. During early times, $t \leq 1.6 \times 10^5$ yrs, the HDO and deuterated H_2CO and CH_3OH, Fig. (3.16), show a slight enhancement in their abundances while they all show lower abundances, in particular, at later evolutionary times. NH_2D and HDS are the least affected; however, their decay is slightly faster than in models M2H. Unlike warm cores, D_2CO is observable in hot cores even when depletion is low and hence it is a good indicator for hot cores, similarly is deuterated methanol.

HDCO is a good tracer for hot cores, Fig. (3.16) because it is abundant during most of the lifetime of the core. The species shows an increase in its abundance which cannot be explained by its sublimation from grain mantles (as in warm cores but shifted towards later times $\sim$ 3.7

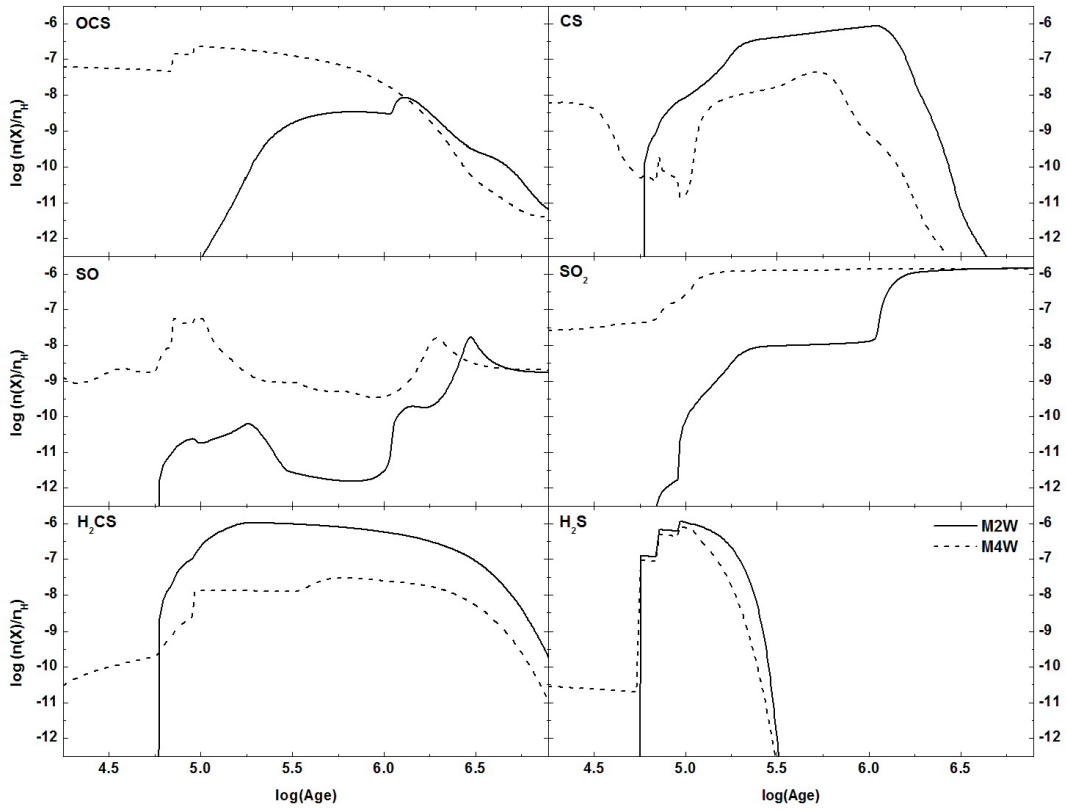

Figure 3.13: Chemical evolution of the S-bearing species as a function of time in network 2 at two different depletion efficiencies (100%: solid line) and (85%: dashed line)

$\times 10^4$ yrs). The chemical analysis showed that this 'jump' is related to the formation of CH_4 as described above for warm cores, but in hot cores H_2CO is mainly formed via oxidisation reactions of CH_3 which could be formed via CH_4. From the above we conclude that deuterated species are more useful indicators of hot cores than of warm cores. This result might indicate that deuterium chemistry is more active at higher temperatures.

3.3.3 Deuterium chemistry in massive hot cores

Viti *et al.* (2004) studied the chemical evolution of hot cores around stars with various masses from 5 to 60 solar masses. They found that ratios of sulphur bearing species (e.g. H_2S/SO_2, H_2S/CS, SO/CS) are good indicators of the early stages of massive star formation while large organic molecules such as CH_3OH, $HCOOCH_3$, and C_2H_5OH indicate late evolutionary stages.

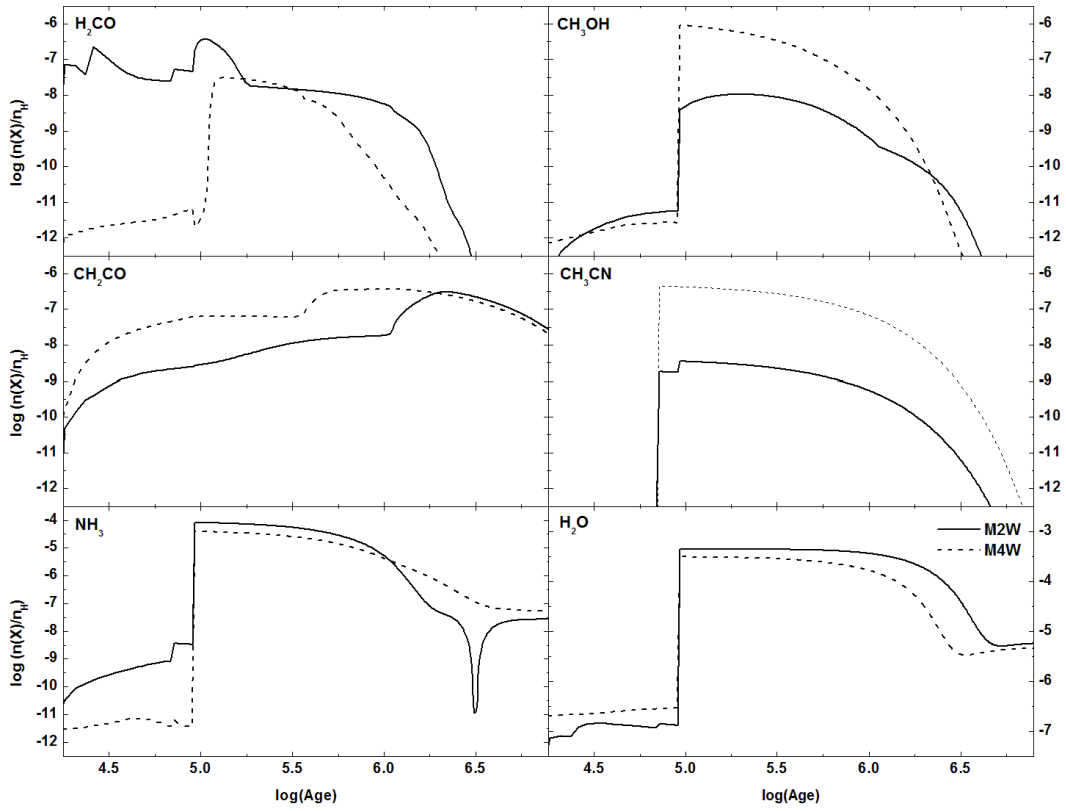

Figure 3.14: Same as in Fig. (3.13), but for large molecules (see key)

In this work, we aim to investigate whether the deuterated counterparts of these evolutionary indicators could be used for the same purpose. In order to achieve this aim, we ran a grid of 4 models, M5H - M8H, see Table (3.3), to cover the range of masses between 10 and 60 solar masses. Figures (3.17) and (3.18) illustrate the chemical evolution of sulphur bearing species and the large organic molecules and their counterparts, respectively. The evolutionary profiles of the molecules in our sample are, generally, the same, in that as the stellar mass increases there is a reduction in their evaporation peaks (in particular those of H_2S) and a shift towards earlier times. The shift in time is related to the heating rate of the star; massive stars approach a certain temperature faster than less massive ones. Our results are in line with those obtained by Viti *et al.* (2004). In addition, ratios of deuterated sulphur bearing species can also indicate the chemical evolutionary stage of a hot core. Generally, the H_2S/HDCS>1 ratio traces later evolutionary stages up to $4 - 5 \times 10^6$ yrs while HDS/H_2CS>1 is a good indicator for earlier

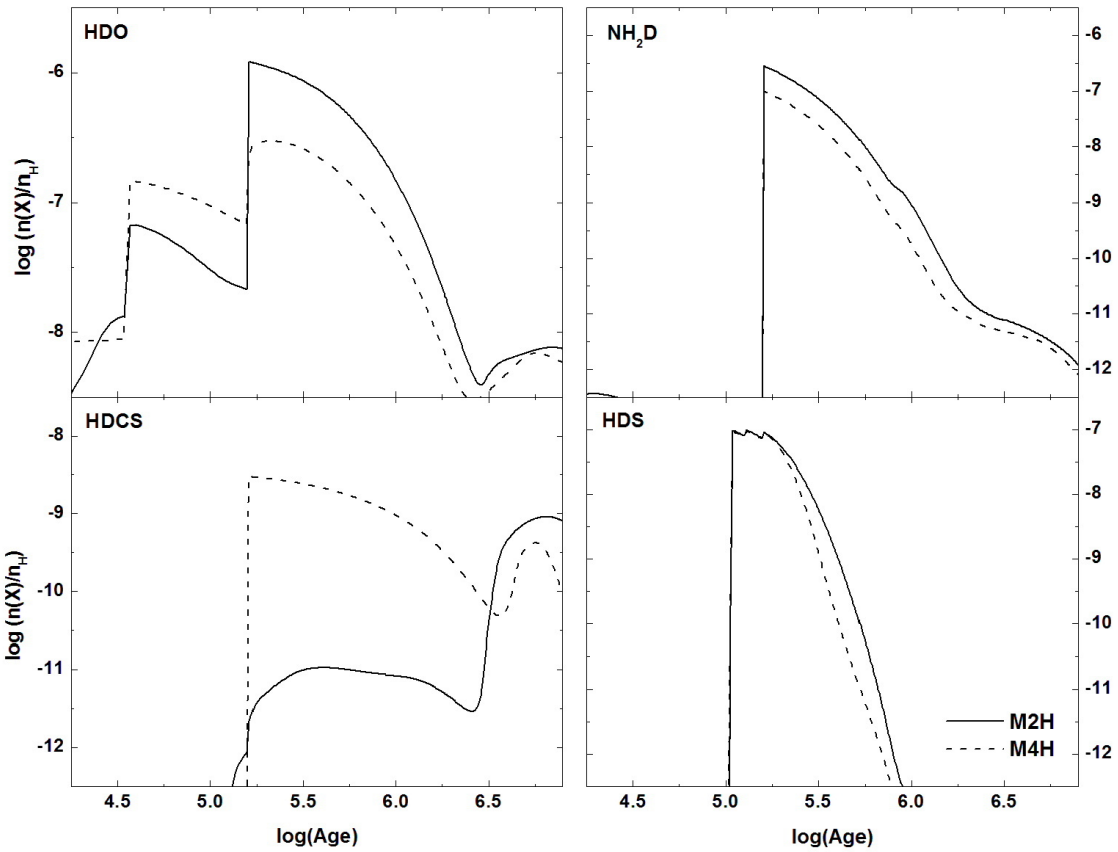

Figure 3.15: Chemical evolution of the S-bearing species as a function of time in network 2 at two different depletion efficiencies (see key)

stages around 5×10^4 yrs. HDS/SO_2 >1 indicates cores younger than 2×10^5 yrs. SO/CS<1 represents cores older than 5×10^4 yrs. The ratio HDS/HDCS is not a good chemical clock of hot cores because it declines always at the same time around 5×10^5 yrs regardless of the mass of the core. Ammonia, organic molecules and their deuterated counterparts, Fig. (3.18), show insignificant variations in their abundances as a function of stellar mass, which exclude them from being good tracers of the core mass. However, they all are abundant during evolutionary stages later than 5×10^5 yrs. Hence, we conclude that the ratios of deuterated sulphur bearing species can also be used as chemical clocks for the hot cores around massive stars. Our results are in agreement with the model results by Wakelam *et al.* (2004) in that the fractional abundances of S-bearing species are sensitive to variations in the physical conditions of the environment such as temperature and density. However, those authors concluded that ratios

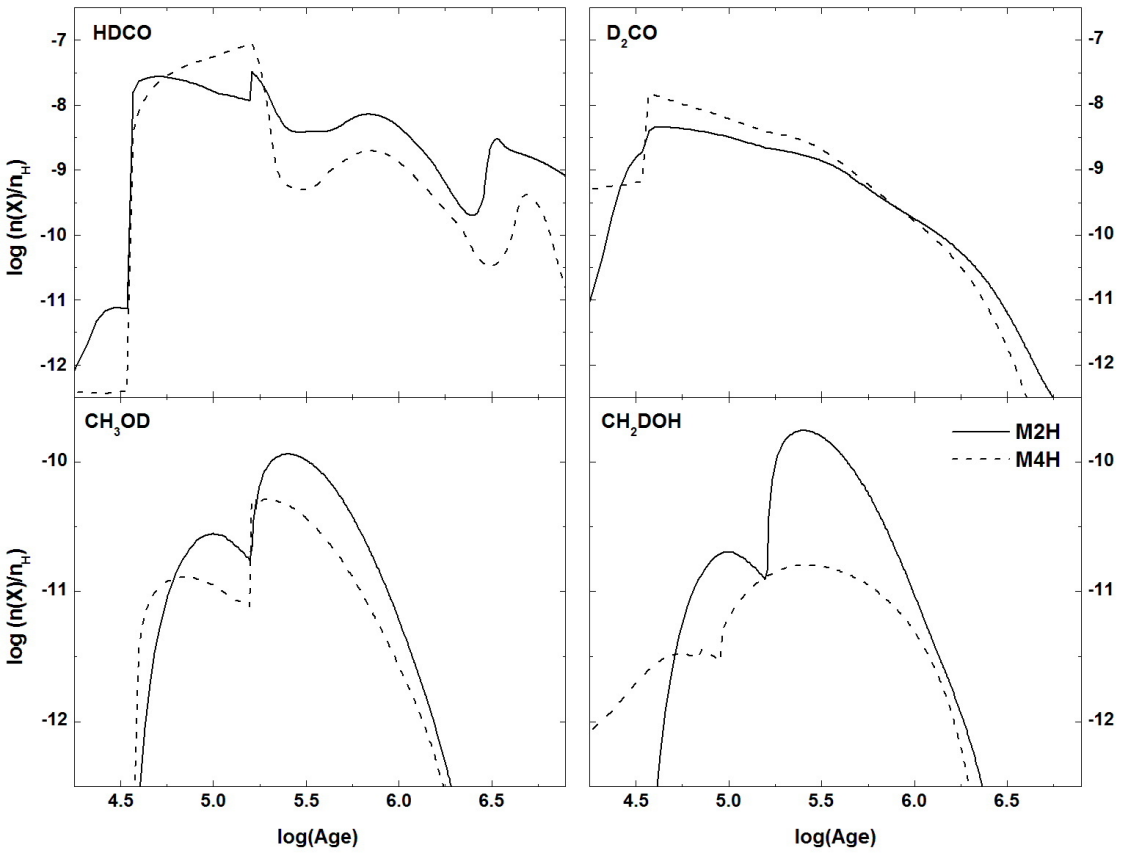

Figure 3.16: Same as in Fig. (3.10), but for large molecules (see key)

of S-bearing species (main isotopes i.e. non-deuterated counterparts) cannot be easily used as chemical clocks.

3.4 Comparison with observations of deuterated species in warm cores

In this work we do not attempt to model any particular source. However, our physical conditions for warm cores, given in Table (3.3), are close to those of some Class 0 sources such as IRAS 16392-2422 and NGC 1333 IRAS 4A, B (e.g. Ceccarelli *et al.* 2007; Maret *et al.* 2004). A qualitative comparison between the fractional abundances of various observed species in warm cores around low-mass stars with our calculated abundances for a typical warm core (model M2W) is given in Table (3.5). Observations of some species such as NH_2D and D_2CO

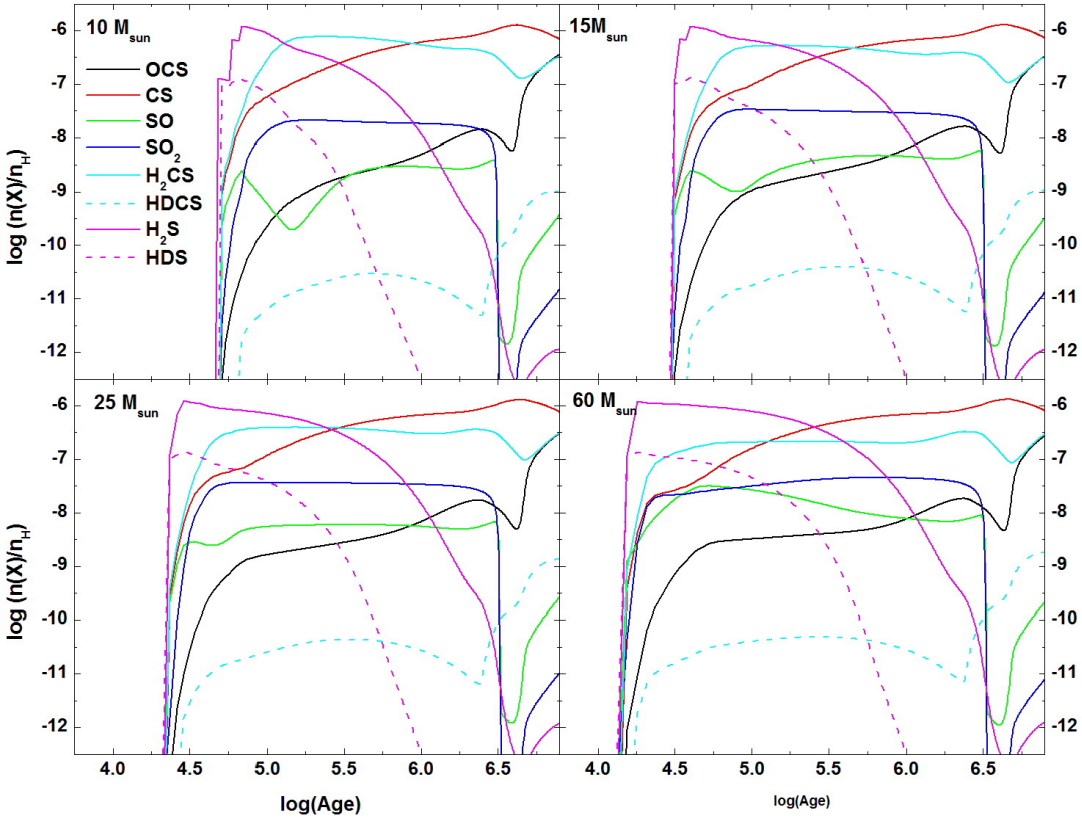

Figure 3.17: Chemical evolution of sulphur bearing species and their deuterated counterparts as a function of time for massive hot cores (see key)

are given in terms of column densities. Because hydrogen nuclei are the most abundant, the total amount of material along a line of sight can be approximated in terms of N_H, the hydrogen column density. The total visual extinction is commonly used as a stand-in for N_H in dense regions. Therefore, the total column density of hydrogen at a particular point of visual extinction A_v (in mag) can be described as '1.6×10^{21} * A_v' where 1.6×10^{21} cm^{-2} is the hydrogen column density at one magnitude (see Snow & McCall 2006 for more details and references). For any species, the fraction of it along line of sight can be calculated knowing the species number density (fractional abundance) and the visual extinction of the region. In our model, we used the same relation to calculate the column density of a species Y, N(Y), at a point of visual extinction A_v given its fractional abundance, X(Y); see Eq. (3.9).

$$N(Y) = X(Y) * 1.6 \times 10^{21} * A_v \tag{3.9}$$

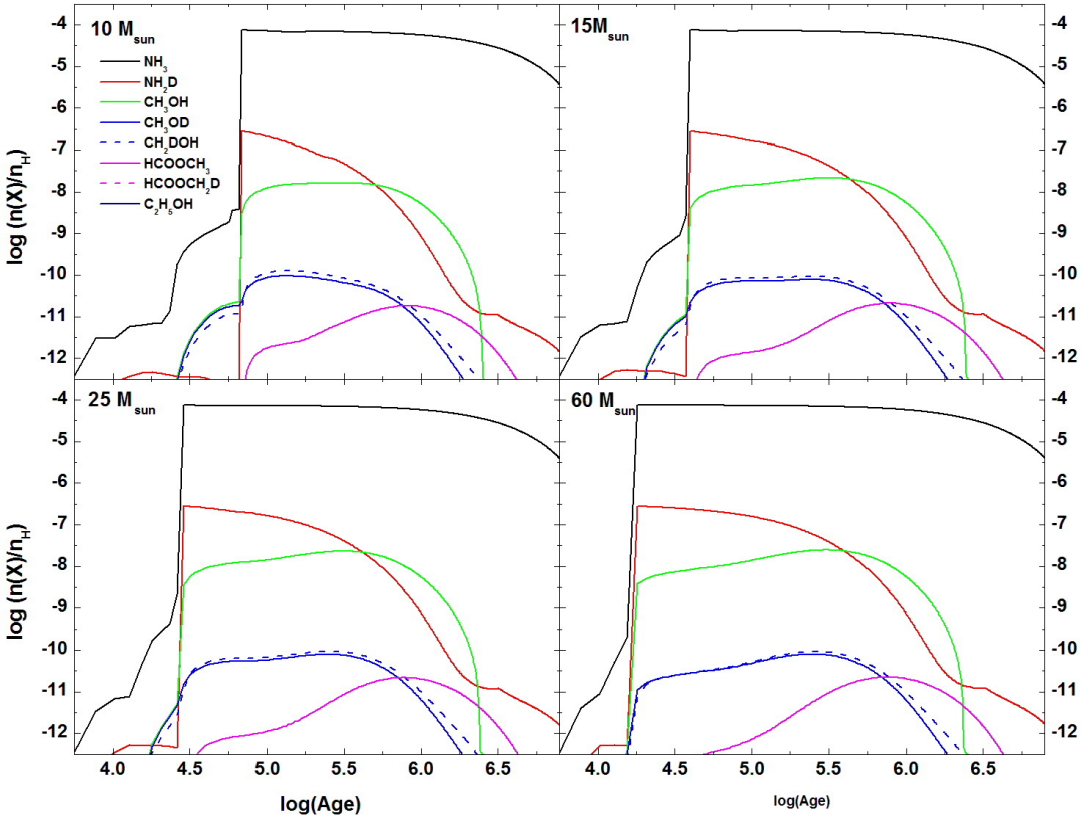

Figure 3.18: Same as in Fig. (3.17), but for large organic species and Ammonia (see key)

Times where our model results best fit observations are also given in Table (3.5).

Most of the species in our sample match observations during times between 10^4 and 10^5 yrs which is the assumed age for a typical Class 0 source (André *et al.* 1993). Exceptions are the ions that fit observations during times earlier than 10^4 yrs and show a rapid decrease after that and deuterated ammonia that matches observations at times later than 2×10^5 yrs. Currently, our model is underestimating the abundances of some deuterated species by a few orders of magnitude, such as CH_3OD, CH_2DOH, N_2D^+, and cannot reproduce the recently observed deuterated methyl formate $DCOOCH_3$. The main reason for this is the fact that our chemistry does not include any multiply deuterated species that play a role in enhancing the deuterium fractionation via gas-phase chemistry as shown by Roberts *et al.* (2003): the inclusion of multiply deuterated isotopomers of H_3^+ in chemical models, with accretion onto grains, at high densities ($\sim 10^6$ cm^{-3}) significantly increases the molecular D/H ratio for several species in

particular the ions N_2D^+ and DCO^+ (see Table 1 in Roberts *et al.* 2003). Roberts *et al.* (2003) found that for models with high densities, the inclusion of HD_2^+ and D_3^+ allows more deuterium to be transferred to other species, thus increasing the efficiency of the fractionation. The latter causes D_3^+ to be the most abundant form of deuterated H_3^+, and forms more N_2D^+ and DCO^+ than their hydrogen forms that dominate in models without multiply deuterated species. The authors concluded that their models are neither reproducing the observed D_2CO/H_2CO nor methanol abundances in protostellar cores, and they emphasise that surface chemistry followed by desorption of the species should affect the abundances. From the above, we also conclude that chemical models with a complete set of multiply deuterated isotopomers, when available, and grain chemistry followed by more realistic treatment of the molecular evaporation from grain mantles are essential for better understanding of deuterium chemistry and more accurate calculations of deuterium fractionation in different interstellar regions.

From the above discussion, we conclude that a complete set of reactions both in gas-phase and on grain surfaces is important to fully understand the chemistry of the region under study. In addition, it is now clearer to us the vital role grain surfaces play as factories of large organic molecules and their deuterated counterparts.

In the next few lines we compare model calculations of molecular D/H ratios for a typical warm core (model M2W) to those observed in Class 0 sources, specifically observed in IRAS 16293-2422, see Table (3.6) and Fig. (3.19). Calculated ratios match observations during times around few$\times 10^4$ yrs, which is roughly the age estimated for a Class 0 source (André *et al.* 1993). The jumps observed in some ratios such as D_2CO/H_2CO and $D_2CO/HDCO$ occur around the time of the sublimation of H_2CO and HDCO molecules from grain surfaces. These jumps can probe the formation of species on grain mantles; D_2CO is one of the key species that is believed to be formed on grain surfaces, the jump in the ratio around the time of the H_2CO evaporation indicates that the former is efficiently formed on grains relative to the latter. This view is in line with Roberts (2008) results in which the author concluded that D_2CO/H_2CO ratio can be used as a probe for grain surface chemistry. At the moment, our model is not reproducing the observed quantity of ammonia thus the NH_2D/NH_3 ratio is always underestimated. The N_2D^+/N_2H^+ ratio matches observations only during early times $\sim 4\times 10^3$ yrs, and it is much lower than observations for times later than that. Roberts & Millar (2007) surveyed the N_2D^+/N_2H^+ ratio around a sample of Class 0 sources. They concluded that the high ratio they observe represents the cooler gas in the extended envelope around the source and not the hot gas in the core. This view supports our results in that we are modelling

Table 3.5: Comparison between observations of deuterated species in a selection of warm cores around low-mass stars and our model calculation. Some observations are given in terms of column densities (cm^{-2}), and those are indicated by the '†' symbol in the table.

Species	**Observations**	**This Work**	**Time of best fit yrs**	**Ref**
DCO^+	1-5(-11)	$\sim$ 1-5(-11)	$\leq$ 9.00(3)	van Dishoeck *et al.* (1995)
				Stark *et al.* (2004)
H_2D^+	6-9(-12)	$\geq$ 1(-13)	$\geq$ 3.12(3)	Caselli *et al.* (2008)
† **N_2D^+**	0.1-8.1(12)	0.1-1.6(12)	0.26-1.3(4)	Emprechtinger *et al.* (2009)
DCN	2.5(-11)	1.3-5.7(-10)	1.7-9(4)	van Dishoeck *et al.* (1995)
DNC	5(-12)	$\leq$ 1(-13)	all times	van Dishoeck *et al.* (1995)
HDS	1.5(-10)	1(-7)-1(-10)	6(4)-2.5(5)	van Dishoeck *et al.* (1995)
†**HDCS**	4.5-7(12)	1-9(12)	2.14(5)-1.3(6)	Marcelino *et al.* (2005)
HDO	1(-8),	$\geq$1(-9)	$\geq$1.7(4)	van Dishoeck *et al.* (1995)
	2-3(-10)			Shah & Wootten (2001)
	1(-7)			Parise *et al.* (2005)
NH_2D	1(-9),	4(-8) - 1(-10),	9(4)-9(5),	van Dishoeck *et al.* (1995)
	2.3(-11)	1(-11)	$\geq$9(5)	Shah & Wootten (2001)
HDCO	1.1(-10)	1-2.7(-10)	0.18-1.4(5)	van Dishoeck *et al.* (1995)
†**D_2CO**	1(14)	0.1 - 0.9(14)	0.16-3.6(5)	Ceccarelli *et al.* (1998c)
†**CH_3OD**	1.5(14)	1-7(12)	0.9-7.53(5)	Parise *et al.* (2002)
†**CH_2DOH**	3(15)	1-2(13)	1.4-3.5(5)	Parise *et al.* (2002)
C_2D	4.5(-11)	1-4.5(-11)	3.8-5.5(4)	van Dishoeck *et al.* (1995)
†**$DCOOCH_3$**	6(14)	$\leq$1(9)	all times	Demyk *et al.* (2010)

† The method we used to convert our abundances in to column densities is described in the text. Here, a(b) means a$\times 10^b$

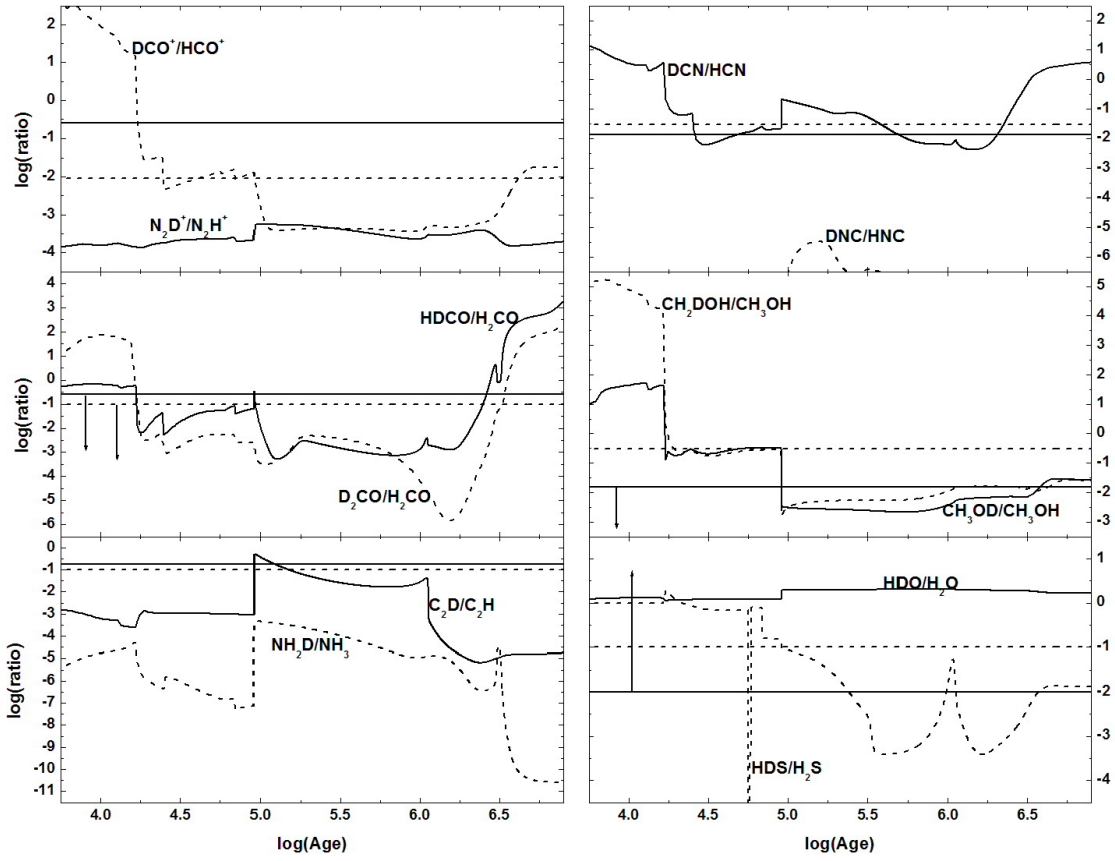

Figure 3.19: Some key molecular D/H ratios for a typical warm core model (M2W) with full depletion and high density during the warming up phase, at 150 AU from the core centre, in comparison with observations, straight lines (see key)

the inner part of the core which is warm and compact.

In Figures (3.20) and (3.21), we compare the calculated ratios for a typical warm core model M2W with those at lower densities M3W and partial depletion M4W during the warming up phase as a function of time. Observations are represented with the dark grey straight line; see Table (3.3). From these figures it is clear that models with higher density and fully depleted gas are, in general, closer to observations. Less dense cores, model M3W in Fig (3.20), show lower fractionation except for the N_2D^+/N_2H^+ ratio that becomes closer to the observed value but not in good agreement with it. This is again further evidence that this ratio is mainly produced in less dense regions not in the compact core. Models with partially depleted gas, i.e.

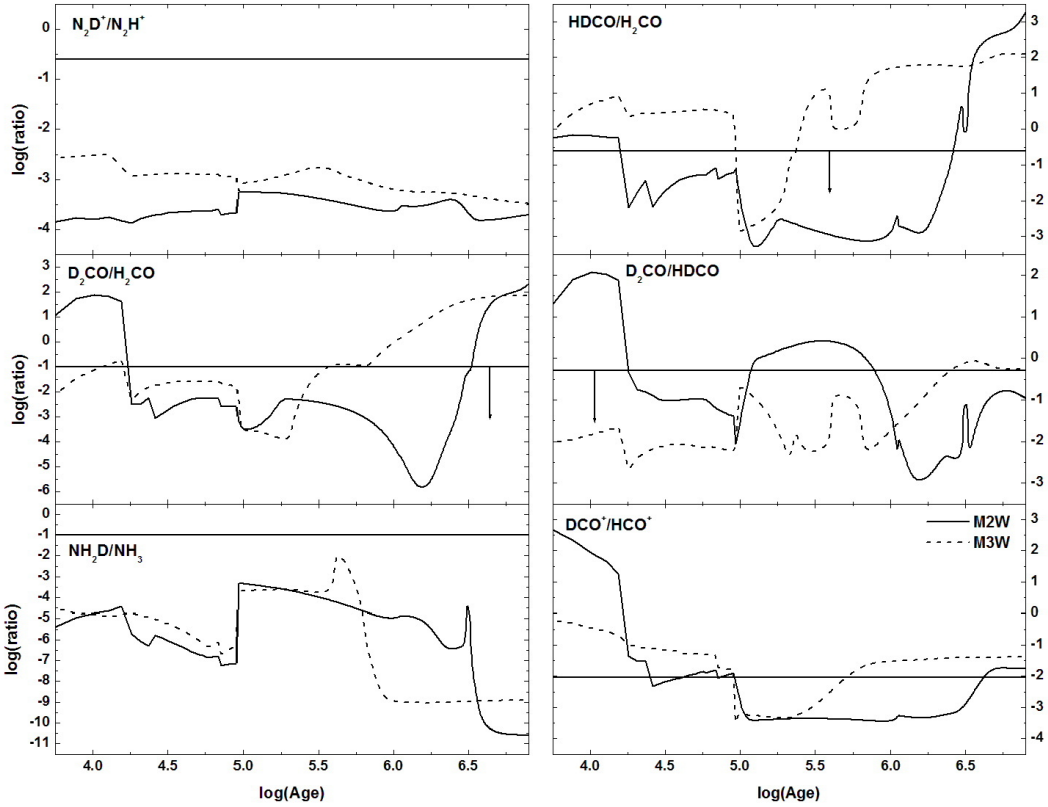

Figure 3.20: Sample of molecular D/H ratios in protostellar warm core as calculated from models M2W and M3W (see Table (3.3) and figure key)

model M4W in Fig. (3.21), show higher ratios of deuterated H_2CO species which indicate that the amount of H_2CO formed on grains is less. This means that these ratios are good tracers for surface chemistry status (Roberts 2008).

From Table (3.6) and the figures we conclude that models with higher densities and fully depleted gas are closer to observations at times 10^4-10^5 yrs, which is a reasonable age for cores around low-mass stars (André *et al.* 1993; Ceccarelli *et al.* 2000a).

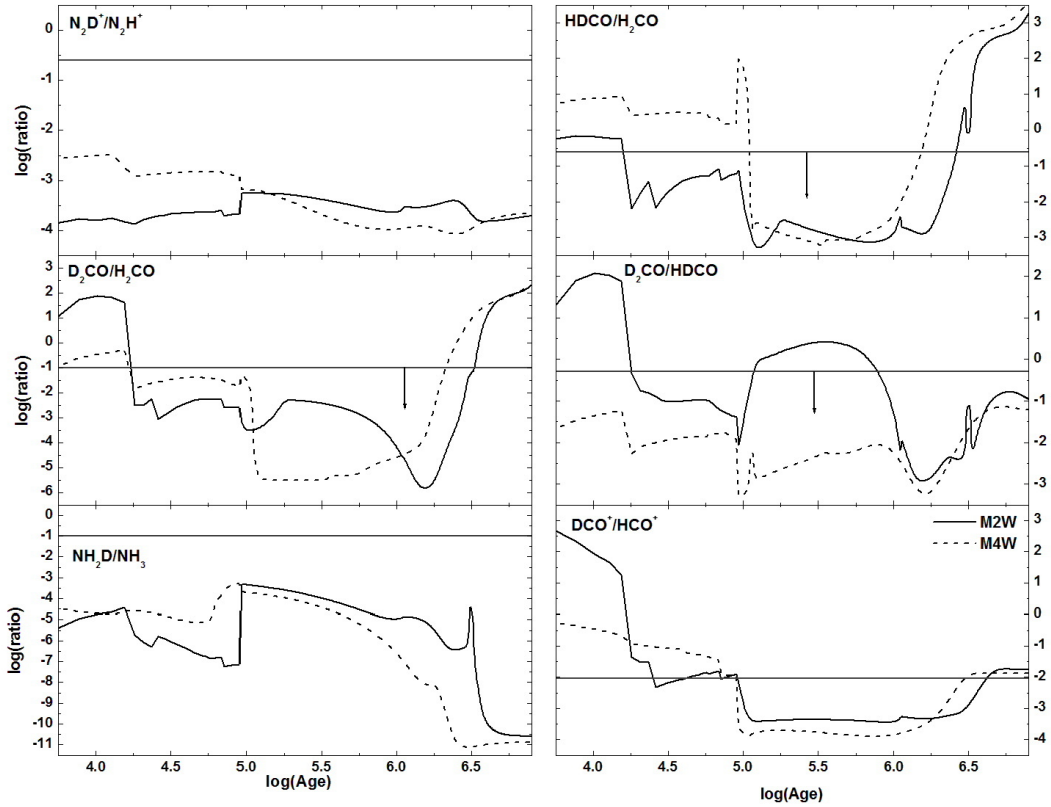

Figure 3.21: Same as in Fig. (3.20), but for models M2W and M4W (see key)

Table 3.6: The calculated fractionation ratio for species in a typical warm core compared to those observed in IRAS 16293-2422

Ratio	**Observations**	**This Work**	**Time (yr)**	**Ref**
DCO^+/HCO^+	0.009	0.009	$\sim$ 4.03(4)	van Dishoeck *et al.* (1995)
DCN/HCN	0.013	0.012	2.6(4)	van Dishoeck *et al.* (1995)
DNC/HNC	0.03	$\leq$ 1(-7)	all times	van Dishoeck *et al.* (1995)
C_2D/C_2H	0.18	0.18	4.7(4)	van Dishoeck *et al.* (1995)
$HDCO/H_2CO$	$\leq$0.25	few(-1)	2(3)-1.6(4)	van Dishoeck *et al.* (1995)
				Ceccarelli *et al.* (1998c)
D_2CO/H_2CO	$\leq$0.1	$\leq$0.1	$\geq$1.7(4)	Ceccarelli *et al.* (1998c)
$D_2CO/HDCO$	$\leq$0.5	$\leq$0.5	1.8(4)-1.32(5)	Ceccarelli *et al.* (1998c)
NH_2D/NH_3	0.1	$\leq$1(-4)	all times	van Dishoeck *et al.* (1995)
HDO/H_2O	$\geq$ 0.01	1-2	all times	van Dishoeck *et al.* (1995)
CH_3OD/CH_3OH	$\leq$0.1, 0.015	$\leq$0.1	$\geq$ 1.74(4)	van Dishoeck *et al.* (1995)
				Parise *et al.* (2004)
CH_2DOH/CH_3OH	0.306	1-9(-1)	$\geq$ 1.74(4)	Parise *et al.* (2004)
HDS/H_2S	0.1	0.15$\pm$0.01	6.9-9.1(4)	van Dishoeck *et al.* (1995)
^{a}**N_2D^+/N_2H^+**	0.25	$\ll$0.25	all times	Roberts & Millar (2007)

a(b) means a$\times 10^b$

[a] Ratio observed in NGC 1333 IRAS4 by Roberts & Millar (2007)

3.5 Conclusions

We modelled deuterium chemistry in warm and hot cores using the UCL_CHEM chemical model. Unlike previous studies, our study focuses on the protostellar phase where the evaporation of mantle species occurs and influences the chemistry of the core. The novelty of our model is the treatment of the evaporation following the results of the recent experiments by Collings *et al.* (2003a, 2004); see Chapter 2 for more details. In this piece of work we modelled deuterium chemistry by investigating the influence of including deuterium chemistry into our chemical models and the sensitivity of deuterium chemistry to the variations in the physical parameters of the environment for both warm and hot cores. We found that fractional abundances of species in hot cores are more affected by the inclusion of deuterium chemistry into chemical models than those in warm cores. We also found that deuterium chemistry is sensitive to variations of the model physical parameters, in particular the depletion percentage onto grain surfaces. For both warm and hot core environments, we found that lowering the depletion percentage decreases the abundance of most of the studied deuterated species with the exception of HDCS in both cores and D_2CO in hot cores. In hot cores, D_2CO is slightly enhanced before it decays. This result is in line with observations of low-mass cores with highly depleted CO (Bacmann *et al.* 2002, 2003). Species in hot core environments are more sensitive to the changes in the cores density than in warm cores. In Table (3.7) we classified species into categories according to how strongly they are affected by the inclusion of deuterated species into the chemical network in hot and warm cores. We also classified species according to their sensitivity to the changes in the physical conditions of the region where they exist. If the species is classified as strongly affected it means that its abundance changes more than one order of magnitude while if the abundance of the species varies within a factor of five (whether an enhancement or reduction) we consider it as a slightly affected species. If the abundances are affected by less than a factor of five, then the species is not affected by the changes in the environment where it is formed. Ratios of deuterated sulphur species were also used as chemical clocks for massive hot cores as their H counterparts were found to be (Viti *et al.* 2004), although care must be taken due to the uncertainties related to the sulphur initial abundances as well as its form on the mantle.

Although our model was successful, in general, in investigating the deuterium chemistry in hot and warm cores, the model failed in reproducing large organic species such as methyl formate, $HCOOCH_3$, its deuterated counterpart, and D_2CO. The reason for this, we believe,

is the simple surface chemistry we have adopted. The fact we have not included the multiply deuterated species might also affect the abundances of some species (e.g. N_2D^+) and hence the molecular D/H ratios because multiply deuterated species are claimed to be important in enhancing the deuterium fractionation (e.g. Roberts *et al.* 2003).

Table 3.7: Classifying the species in hot and warm core according to their influence by adding deuterium to the chemical network and their sensitivity to variations in the physical parameters in the deuterium chemistry

Adding Deuterated Species

Category	**hot core**	**warm core**
Not affected	H_2S, CS, H_2CS, CH_3CN	OCS, CS, SO, SO_2, H_2CS H_2S, CH_3CN, H_2O
Slightly affected		CH_3OH, H_2CO, CH_2CO
Extremely affected	OCS, SO, SO_2, H_2O $HCOOCH_3$, H_2CO, CH_3OH	

Changing the final density of the collapsing cloud

Category	**hot core**	**warm core**
Not affected	HDS, H_2S, CS NH_2DS, ^1D_2CO	H_2S, HDS CH_3CN,HDO
Slightly affected	^2H_2CS, ^{3}HDCO CH_3OD, CH_2DOH	NH_3, H_2O CH_3OD, CH_2DOH
Extremely affected		HDCO, ^4D_2CO, NH_3 H_2CO, CH_3OH, CH_2CO

Varying the depletion efficiency of species on to grains

Category	**hot core**	**warm core**
Not affected	HDS, HDO, D_2CO, NH_2D	HDS, HDO, H_2S, NH_3
Slightly affected	CH_3OD, CH_2DOH	NH_3, NH_2D, CH_2CO
Extremely affected	HDCS	OCS, CS, SO, SO_2 HDCS, D_2CO, HDCO H_2CS, H_2CO, CH_3OH, CH_3CN

[1] for times $\geq 6\times10^4$ yrs, [2] for times $\leq 4\times10^6$ yrs

[3] for times $\leq 5\times10^6$ yrs, [4] for times $\geq 10^5$ yrs

CHAPTER 4

DEUTERATED SPECIES IN EXTRAGALACTIC ENVIRONMENTS

Deuterated species such as DCO^+, DCN, DNC, N_2D^+ have been observed in extragalactic environments (Martín *et al.* 2006). Such observations motivated us to extend our theoretical study to extragalactic environments. In this chapter I will summarise a study (led by Dr. Estelle Bayet; see Bayet *et al.* 2010) on the detectability of deuterated species in various extragalactic star forming regions. The chemical evolution of the species in external galaxies was studied using an adapted version of the chemical model I introduced previously in Chapter 3, and described in details in §(3.2), to extragalactic environments.

4.1 An Overview

The past few years have seen an enormous development in studies of molecular deuteration in galactic star forming regions, triggered by the discovery of a large fraction of deuterated molecules with D/H ratio higher than the canonical ratio, 1.5×10^{-5} (Oliveira *et al.* 2003). High molecular deuteration can occur by two different mechanisms. One involves gas-phase chemistry and ion-molecule deuterium exchange reactions taking place at low temperatures (Watson 1980). The second mechanism is based on grain chemistry (Tielens 1983).

In this work, we investigate theoretically deuteration in extragalactic star-forming environments, where the physical conditions can be drastically different from what we see in our own Galaxy. To date, very few detections of deuterated species such as DCN, DNC, and N_2D^+ have been attempted in extragalactic environments (e.g. Mauersberger *et al.* 1995; Martín *et al.*

2006). In a previous paper, Bayet *et al.* (2008) investigated, theoretically, the non-deuterated chemistry in a variety of extragalactic environments and identified a set of species to trace the warm and dense gas. In the current study, we extend our chemical network to include all mono-deuterated species (hereafter called D-species) to investigate the differences in the D-fractionation and the D/H ratios in star forming regions (i.e. gas with n(H_2) $\geq 10^5$ cm^{-3}) in various types of galaxies (i.e Starburst, Active Galactic Nucleus, low metallicity). We also aim at providing a set of potentially detectable deuterated species to trace the dense star-forming molecular gas in external galaxies for observers using the Herschel or the forthcoming Atacama Large Millimetre/submillimetre Array 'ALMA' facilities. In addition, one of the aims is to study the sensitivity of deuterium chemistry in extragalactic environments to the changes in the physical parameters such as; the density (ρ), the temperature (T), the far UV radiation field (FUV-RF), the CR ionisation rate (ζ), and the metallicity (met).

4.2 The Model

The chemical model used in this study is the deuterated version of the UCL_CHEM used in Chapter 3; see §(3.2). So far, only mono-deuterated species have been observed in external galaxies and therefore the chemical network with only mono-deuterated species is suitable and sufficient for such study. However, we believe that for more accurate modelling the inclusion of doubly and triply deuterated species is important (Roberts *et al.* 2003).

In this piece of work, we have run a grid of 15 models for various types of galaxies including: normal spiral (NS), Starburst (SB), active galactic nucleus (AGN), low metallicity (low-met), and high redshift galaxies (high-z). For all the models, we investigated the chemistry at three different densities; 10^5, 10^6, and 10^7 cm^{-3}, labelled in figures by the indices 1 to 3 for each model. This approach has allowed us to distinguish where deuterated species are most likely to form and which gas density is better matching observations of the studied extragalactic regions. In modelling the various types of galaxies, we have assumed the following:

Normal spiral, NS : this model represents the standard case which we define to be our reference model. In this model, we use the standard physical parameters and initial elemental abundances used in Bayet *et al.* (2008).

Starburst, SB: here we have used a FUV radiation field of 1000 times the standard value, and a temperature of 500 K.

The Active galactic Nucleus, AGN: we modelled this case by enhancing the cosmic ray ionisation rate to be 100 times the standard value.

The Low metallicity, low-met: we are mimicking this type of galaxy by decreasing the metallicity to be one fifth of the solar value coupled with an increase of the gas-to-dust mass ratio by a factor of 5. We have also assumed an increase of FUV radiation field of 1000 times the standard value, and a temperature of 500 K.

The High redshift, high-z: this case is represented by a metallicity as low as one fifth of the solar values, an increase of FUV radiation field by 1000 times the standard value, a temperature of 500 K and an increase of the cosmic ray ionisation rate by a factor of 100 times the standard value.

The standard values of the physical parameters (of the reference model) is given in Table (4.1) together with the initial elemental abundances used throughout the whole grid of models.

4.3 Results

Our model results show that extragalactic deuterium chemistry is sensitive to the changes in the physical conditions of the region under study. When the gas density increases from n(H_2) = 10^5 cm^{-3} to n(H_2) = 10^7 cm^{-3}, regardless of the galaxy type, we can divide deuterated species into three categories: the first includes those which are insensitive to density changes (e.g. HDO, NH_2D and HDCS), the second has those that increase with density (e.g. HDS, C_2D and CH_3OD) and the last category includes the species which show a decrease in their fractional abundances (e.g. DCN, DNC and CH_2DOH). The species in the first category are good tracers of dense gas (10^5 cm^{-3} or higher) despite the differences in environment type.

Variation in FUV-RF or temperature does not lead to significant changes in abundances for species such as HDO, NH_2D, DCN, D_2CO, HDCS, CH_2DOH and CH_3OD. However, HDCO and HDS abundances decrease between a factor of 5 and 15 when the FUV radiation field increases. This is due to the UV photodissociation reactions. At early times ($< 10^5$ yrs), and at relatively low density (n(H_2) = 10^5 cm^{-3}) the abundance of C_2D increases by three orders of magnitude with the increase of both FUV radiation field and temperature. Hence, C_2D is likely to be a good indicator of excitation in galaxies. Fig. (4.1) shows our results for NS and SB cases.

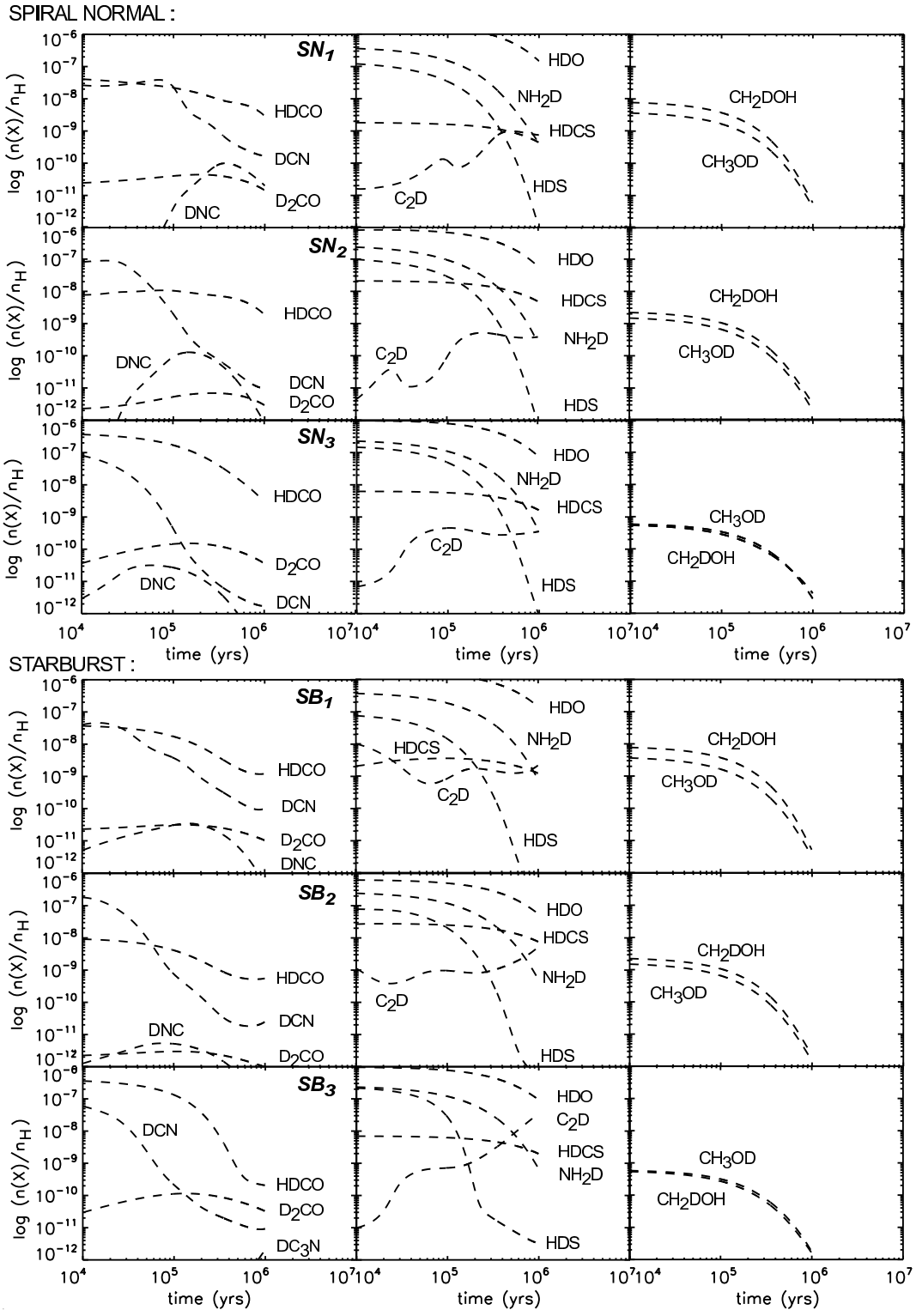

Figure 4.1: Fractional abundances as a function of time of various D-species for the NS case (top set of plots) and the SB case (bottom set) for the three gas densities as indicated by the indices. 1 for the lowest density 10^5 cm^{-3} and 3 for the highest density 10^7 cm^{-3}. Figure is taken from Bayet *et al.* (2010).

Table 4.1: The initial physical conditions of our reference model and the initial elemental abundances used for running our grid of models.

Physical Parameter

Parameter	**Standard value**
$\rho^{\dagger}$	400 cm^{-3} (Phase I), 10^7 cm^{-3} (Phase II)
T	10 K (Phase I), 300 K (Phase II)
UV-RF	1 Habing
ζ	1.3 $\times 10^{-17}$ s^{-1}
$\mathbf{A}_v$	580.6 mag
Met	Solar values
Gas-to-dust ratio	100
H_2 formation rate coefficient	$1.0\times10^{-17} \times \sqrt{T}$ cm^{3}s^{-1}

Initial elemental abundances

Carbon	1.4×10^{-4}
Oxygen	3.2×10^{-4}
Nitrogen	6.5×10^{-5}
Sulphur	1.43×10^{-6}
Helium	7.50×10^{-2}
Magnesium	5.1×10^{-6}

† The final density of the collapsing core is treated as a free parameter in Phase I of the model calculations. It ranges between 10^5 to 10^7 cm^{-3}, but it is constant through out the core in Phase II.

Increasing the cosmic ray ionisation rate (ζ) by a factor of 100 leads to a significant reduction, by several orders of magnitude, of the fractional abundance of the most abundant species in our models (e.g. HDCS, NH_2D, D_2CO, HDCO, CH_2DOH, HDO, DNC). Chemical analysis suggests that the general decrease of abundances is probably due to the release of reactive ions such as ionised carbon, reacting quickly with many oxygen-bearing species such as HDCO, D_2CO, etc. However, some species such as DCO^+, N_2D^+ (both at low density only), DC_3N and DCN (whatever the gas component) show abundances increased by several orders of magnitude with ζ. In the case of nitrogen-bearing species, we suspect that the main reservoir of nitrogen, N_2, becomes ionised and gives rise to N^+, a reactive species that promotes the forma-

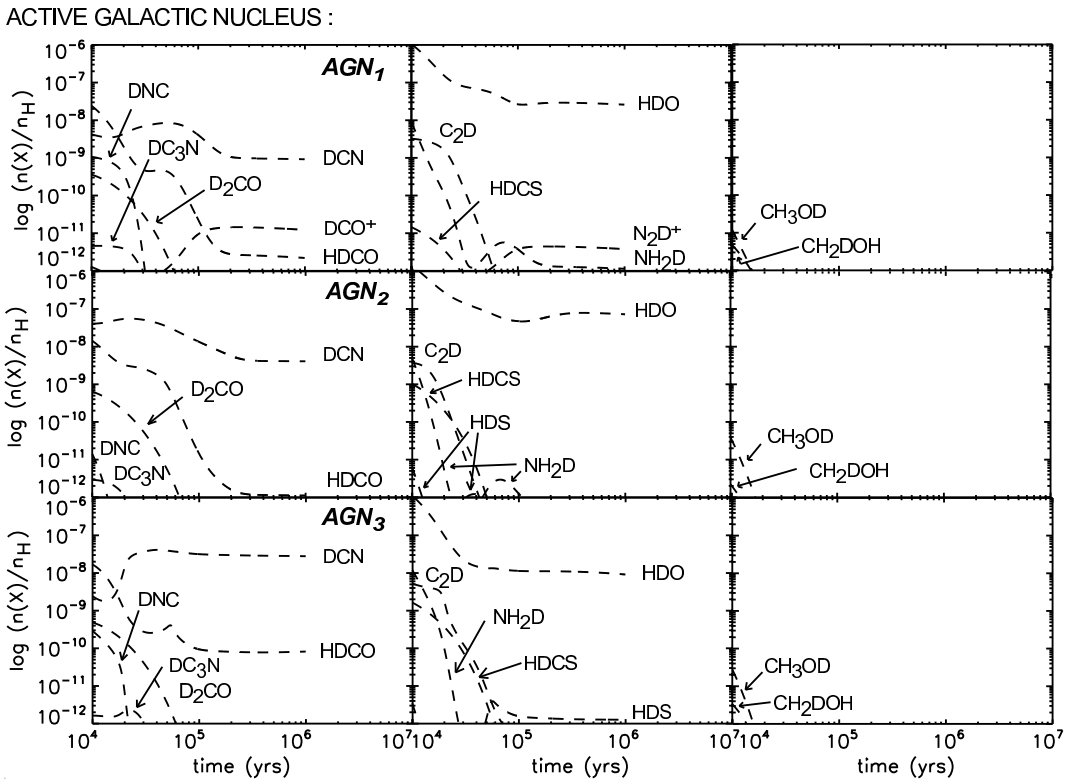

Figure 4.2: Same as Fig. (4.1) but for AGN models. Figure is taken from Bayet *et al.* (2010).

tion of nitrogen-bearing species. Species such as N_2D^+ and DCN are likely to be good tracers for regions with an enhanced CR ionisation rates. Fig. (4.2) shows the chemical evolution of the species in the three categories for AGN models.

Decreasing the metallicity tends to reduce the abundances of HDCO, D_2CO, DNC, NH_2D and HDS, and to enhance those of C_2D and DCN. Species such as HDCS, CH_2DOH, CH_3OD are insensitive to changes in the metallicity. Therefore, these species are good tracers of dense gas (10^5 cm^{-3}) despite the metallicity of the source. This result is interesting in particular for high redshift galaxies. This result is supported by Bayet *et al.* (2008) in which those authors noted similar results for the species' hydrogen counterparts (such as CH_3OH). Fig. (4.3) shows our results for the low-metallicity and high redshift cases.

The D-fractionation calculated from the chemical abundances of all species do not show similar D/H ratio values, regardless of the environment. In protostellar galactic cores around low-mass star forming regions, such as IRAS 16293-2422, this behaviour was reported by (e.g. van Dishoeck *et al.* 1995; Ceccarelli *et al.* 1998c; Parise *et al.* 2004). Authors suggested that the origin of the high observed D/H ratios is the cool extended envelope around the source

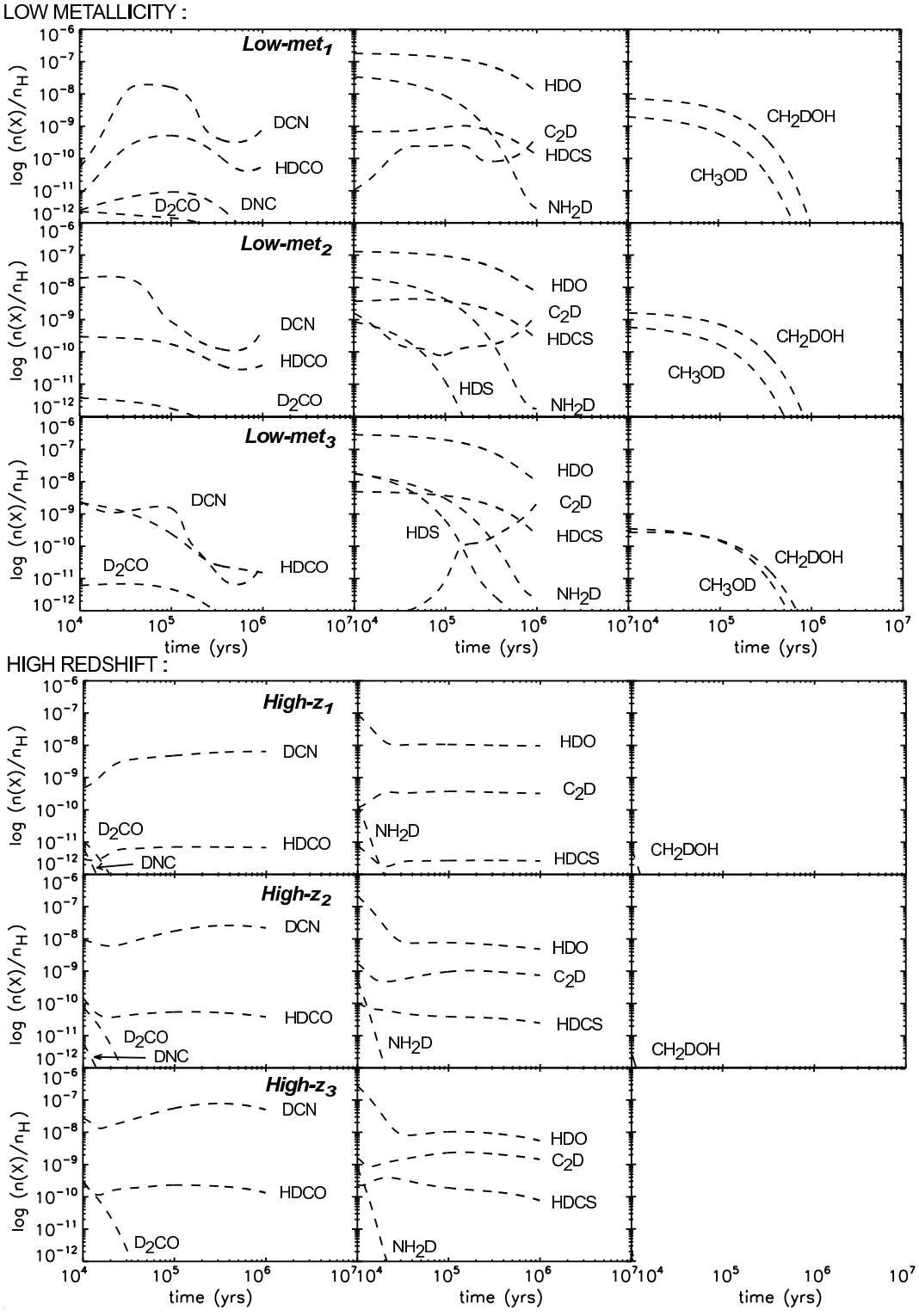

Figure 4.3: Same as Fig. (4.1) and (4.2), but for low metallicity and high redshift models. Figure is taken from Bayet *et al.* (2010).

rather than the hot dense gas of the hot corino. In our model calculations we obtain high values of D/H ratios for models with the lowest densities (10^5 cm^{-3}). Fig. (4.4) shows an example of the evolution of the molecular D/H ratio in models of NS and SB.

The predicted fractional abundances of HDO, DCN and HDCO, regardless of the simulated environment, are always high ($> 10^{-10}$). Hence, we expect these species to be detectable in all the investigated environments. DCO^+, DC_3N, DNC and N_2D^+ are also interesting as they seem to trace particular regions; DCO^+ and N_2D^+ for the densest gas component in AGNs, DNC for the densest gas component in NS, and DC_3N traces the low-density component of the gas in SB galaxies. C_2D and HDCS are predicted to be excessively reactive to the presence of cosmic ray ionisation whereas they survive easily in FUV-enhanced environments. HDS is more sensitive to FUV changes than C_2D and HDCS and it survives both FUV and cosmic ray ionisation as long as the gas is dense. Then HDS can be used to distinguish between the different gas components in SB and AGN environments. In low metallicity regions, HDS is undetectable, but HDCS and C_2D remains abundant. The set of tracers is summarised in Table (4.2).

Table 4.2: List of the D-species we identify as tracers for the different external galactic environments.

D-tracer	**Environment**[†]
DNC	NS at high density of 10^7 cm^{-3}
DC_3N	SB at low density of 10^5 cm^{-3}
DCO^+, N_2D^+	AGN with density of 10^7 cm^{-3}
C_2D, HDCS	enhanced ζ regions
HDS	enhanced FUV-RF regions
D_2CO, CH_2DOH, CH_3OD	NS and SB, density $\geq 10^5$ cm^{-3}

[†] See the text for abbreviations

4.4 Conclusions

In this study we modelled different types of extragalactic environments using the deuterated version of the UCL_CHEM model described in Chapter 3. Although we are not aiming at modelling a particular extragalactic source, our results show, a general good agreement (up to a factor of 3) with the limited set of deuterated species observed so far in external galaxies.

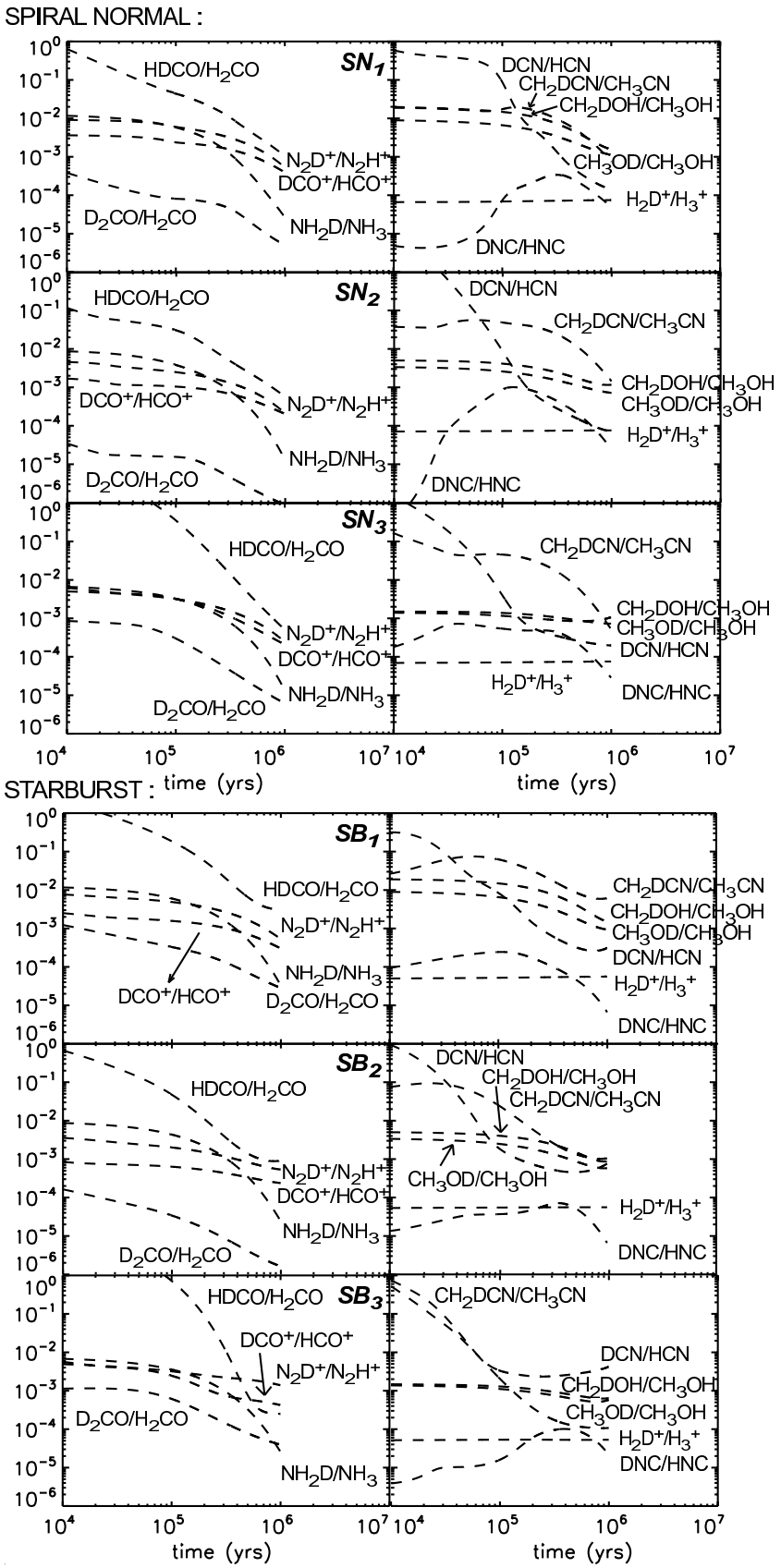

Figure 4.4: D/H abundance ratios as a function of time for various D-species in the spiral normal case (top set of plots) and in the starburst case (bottom set). Figure is taken from Bayet *et al.* (2010).

It is doubtful whether we can compare the predicted column densities with the observed one for N_2D^+ because we expect that omitting the inclusion of multiply-deuterated species, in this study, might affect the fractional abundances of this molecule as investigated by Roberts *et al.* (2003). With such restriction in mind, it appears however that all the models except that of AGN at low density can reproduce the observed upper limit of the column density of N_2D^+, $N(N_2D^+) \leq 9.4 \times 10^{10}$ cm^{-2} observed by Martín *et al.* (2006). Normal spiral models with the highest density can reproduce the DCN observed value within a factor of 11.

From this study, we predicted HDO, DCN and HDCO to be detectable in all extragalactic environments with fractional abundances as high as 10^{-10}. In addition, we identified a set of species to trace different environments; see Table (4.2).

CHAPTER 5

GRAIN SURFACES: KEYS FOR DEUTERIUM CHEMISTRY

The study presented in this chapter has been performed toward the end of my PhD studies (i.e. after the work presented in Chapter 6). However, it can be regarded as a continuation of the work performed in Chapter 3.

5.1 Introduction

The existence of dust grains was first confirmed by the detection of the first interstellar extinction by Trumpler (1930), and since then the composition of grains has been a key question. In dark clouds, temperatures are as low as 10 K allowing the removal of a fraction of gas-phase species to freeze onto grain surfaces in a process known as 'depletion' or 'freeze out' process (e.g. Hasegawa *et al.* 1992; Gibb *et al.* 2000; Bisschop *et al.* 2006) forming the so-called icy mantles. The formation, construction, and compositions of these mantles has been a subject of active research (e.g. Tielens & Hagen 1982; Cuppen & Herbst 2007). Tielens & Hagen (1982) used numerical simulations to estimate the mantle compositions of dust grains. Their results predicted that the key mantle species are H_2O, CO, H_2CO, NH_3, N_2, O_2, CO_2, H_2O_2 and their concentrations depends strongly on the physical conditions of the gas from which they accrete onto grains. These predictions were confirmed by direct detection of mantle composition by IRAS and ISO (e.g. Ehrenfreund & Schutte 2000) which showed that the main molecular component in ice mantles in molecular clouds have approximate abundances of H_2O, 100%; CO_2, 12-16%; and CO,45%.

Dust grains provide sites for the formation of species that cannot be produced easily in the gas phase such as H_2 and CO_2 and enhances the production of species that are slowly formed in gas-phase such as H_2CO and CH_3OH (Biham *et al.* 2003 and references therein). Whereas the deuterium enrichment was explained to take place in gas-phase in cold environments (Roberts *et al.* 2003), it is certainly driven by surface reactions in hot regions (Tielens 1983; Ceccarelli *et al.* 2001). The latter is confirmed via the recent observations of deuterated methanol (e.g. Parise *et al.* 2002, 2004) which is not efficiently formed in the gas-phase (Turner 1998).

Methanol is a key molecule in driving the complexity of the chemistry in interstellar regions. When methanol and other species evaporate from grain surfaces, they undergo a warm gas-phase chemistry at 100 K (in hot corinos) or greater ($\geq$ 300 K in hot cores) to produce more complex species such as methyl formate, $HCOOCH_3$ (Garrod & Herbst 2006). The latter is observed towards hot cores (e.g. Gibb *et al.* 2000), and hot corinos (e.g. Bottinelli *et al.* 2004; Remijan & Hollis 2006). The formation of $HCOOCH_3$ has long been thought to be a gas-phase process, via reactions involving protonated methanol, $CH_3OH_2^+$, that reacts with formaldehyde, H_2CO, to produce protonated methyl formate, $HCOOCH_3^+$. Subsequent dissociative recombination with electrons would then complete the process. In this way, large amounts of methyl formate could be produced in hot cores on timescales of 10^4-10^5 year after the evaporation of mantle methanol. This gas-phase procedure was considered in many hot core chemical models (e.g. Millar *et al.* 1991; Caselli *et al.* 1993; Charnley *et al.* 1995). Recently, in their quantum chemical calculations Horn *et al.* (2004) showed that the reaction between H_2CO and $CH_3OH_2^+$ is highly inefficient in producing protonated $HCOOCH_3$ because the reaction possesses a high activation energy ($\sim$ 15000 K). Although the authors suggested other routes to form protonated $HCOOCH_3$, their models at 100K were not able to reproduce the observed abundance of $HCOOCH_3$. Recent chemical models of hot cores by Garrod & Herbst (2006) and experimental work by Watanabe & Kouchi (2008) showed that methyl formate can be formed on grain surfaces via 'CH_3O + HCO', where both reactant species are formed on grains. Experimental work by Bennett & Kaiser (2007b) showed that CH_3O and HCO are formed via the UV photodissociation of methanol, which produces CH_3O and an H atom that reacts with CO to produce HCO.

The high abundances of deuterated methanol observed in hot corinos (Parise *et al.* 2002, 2004) motivated Demyk *et al.* (2010) to look for deuterated methyl formate in IRAS 16293-2422. Their observations revealed a tentative detection of $DCOOCH_3$ with equal column densities of $\sim 6\times10^{14}$ cm^{-2} in the two cores A and B which give a deuterium fractionation of 15%.

It is likely that $DCOOCH_3$ is formed on grain surfaces in a way similiar to that of $HCOOCH_3$ (Demyk *et al.* 2010). As described above for methyl formate, similar routes are proposed to form its deuterated form. The first route is directly via

$$DCO + CH_3O \longrightarrow DCOOCH_3 \tag{5.1}$$

on grains. In reaction (5.1), DCO is formed via the deuteration of icy CO via D species accreted from the gas phase. This reaction (D + CO) is confirmed to be ten times less efficient than the hydrogenation route (H + CO); and therefore could not be the first step of producing deuterated methanol, $CH_3OH_2^+$, or formaldehyde. This may be the same case for $DCOOCH_3$ (Hidaka *et al.* 2009). Energetic processes on ices such as UV photodissociation or CR bombardment may be more efficient in forming $DCOOCH_3$ via reaction (5.1) as proposed by Bennett & Kaiser (2007b). In their scenario, DCO may be formed from the reaction of CO with a deuterium atom produced by the UV photodissociation of deuterated methanol. CH_3OD is the best candidate to produce a D-atom via UV photodissociation, since if the UV photons break the O−D bond of CH_3OD, CH_3O and a D atom are easily produced. This is not the case for any other deuterated methanol species, for which the simultaneous production of CH_3O and D would require intermediate reactions. Alternatively, $DCOOCH_3$ can be produced by the H/D substitution in solid $HCOOCH_3$ during the warm-up of the ice mantles similar to the formation of deuterated formaldehyde and participates in the formation of deuterated methanol species (Hidaka *et al.* 2009; Ratajczak *et al.* 2009).

Our motivation for the following study is to improve our calculated column densities of $HCOOCH_3$ and its deuterated counterpart in Chapter 3 by including their formation on grain surfaces. In addition, we aim at enhancing the production of D_2CO by including its formation on grains via H/D substitution of HDCO. The aim of this study is to test whether the inclusion of the formation of $HCOOCH_3$, $DCOOCH_3$, and D_2CO on grain surfaces via the routes proposed above influences their calculated fractional abundances in chemical models, in particular during the warming up phase. If they affect the calculations of their abundances, we should expect an enhancement in their abundances.

5.2 Chemical model

In this study we use the same chemical model described in Chapter 3 with the addition of grain surface pathways to form methyl formate and its deuterated form following the proposed routes

described in §(5.1). As described in Chapter 2 §(2.2), the surface chemistry considered in our network is simple: we include direct hydrogenation of all species including the formation of both formaldehyde and methanol from CO and that of CH_3CN from 'CH_4 + HCN'. The new network now will include also the formation of methyl formate

$$\mathrm{mCH_3OH} \; + \; \mathrm{mCO} \longrightarrow \; \mathrm{HCOOCH_3} \tag{5.2}$$

and $DCOOCH_3$

$$\mathrm{mCH_3OD} \; + \; \mathrm{mCO} \longrightarrow \; \mathrm{DCOOCH_3} \tag{5.3}$$

where 'm' refers to 'mantle' species. It is important to bear in mind that in our modelling we do not distinguish between the different isomers of a mono-deuterated species, i.e. $DCOOCH_3$ and $HCOOCH_2D$ are equivalent.

Recent experimental results (Hidaka *et al.* 2009) showed that the formation of D_2CO proceeds on grain surfaces efficiently via H-D substitution reactions in which the formation of D_2CO takes place via

$$\mathrm{DCO} \; + \; \mathrm{D} \longrightarrow \; \mathrm{D_2CO} \tag{5.4}$$

Following the same recipe, we included the formation of D_2CO in our surface chemistry network in which mantle DCO is deuterated by gaseous D-atoms landed on the surface to form D_2CO.

In the context, WC-O is the 'old' chemical model for warm cores without the inclusion of the formation of methyl formate or D_2CO on grains as described in Chapter 3 while WC-N is the 'new' version of the model with the inclusion of the three reactions (5.2), (5.3), and (5.4) above.

5.3 Results and Discussion

We ran a model of typical warm core in which the material collapses in a free-fall mode into a final density of 10^8 cm^{-3} then we follow the chemistry of the remnant core after star formation occurs using the new version of the code described in §(5.2). Fig. (5.1) represents the chemical evolution of the H_2CO and CH_3OH and their deuterated forms as a function of time in both the old , WC-O:solid line, and the new, WC-N:dash line, models. In this figure, the observed jump (indicated by an arrow in the figure) in the abundance of H_2CO (Schöier *et al.* 2002) is

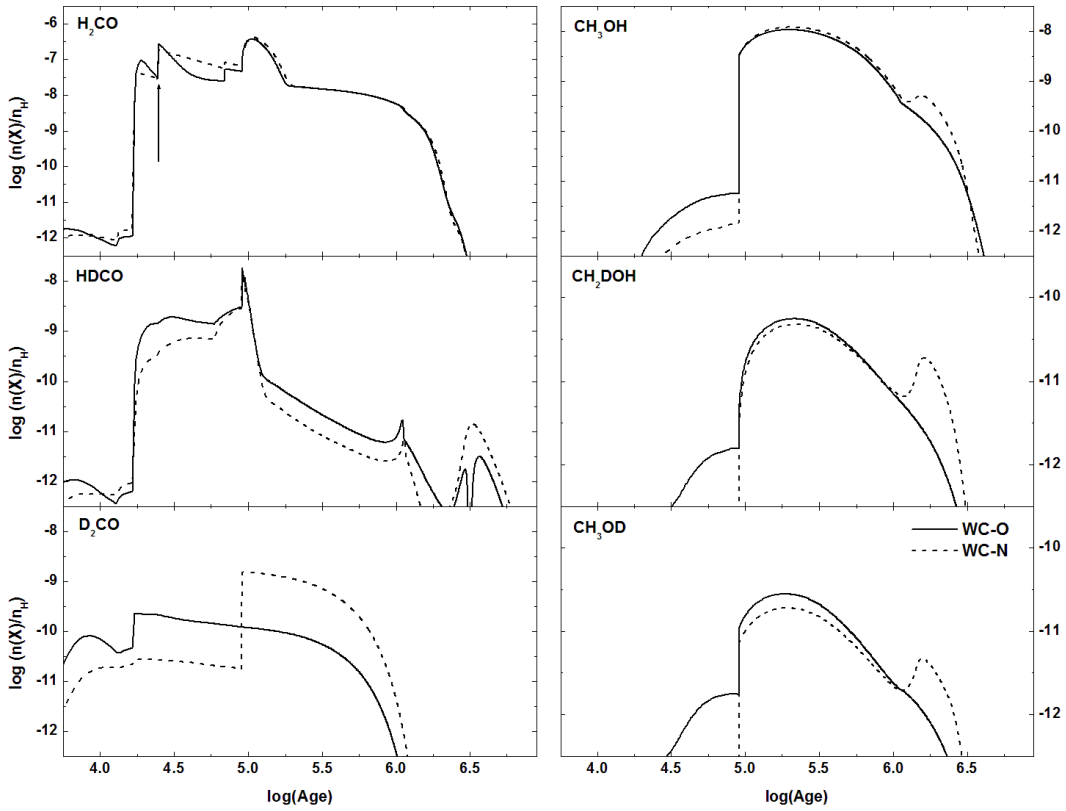

Figure 5.1: The time evolution of key mantle species, H_2CO and CH_3OH, and their deuterated forms in a typical hot corino in the warming up phase after the inclusion of the formation of D_2CO on grain surfaces (see key). The arrow indicates the observed jump by Schöier *et al.* (2002).

reproducible. HDCO is two times less abundant than in WC-O because a fraction of its parent molecule, DCO, is used to form D_2CO which shows an enhanced abundance up to a factor of fifteen with respect to models WC-O. This result is in line with those obtained experimentally by Hidaka *et al.* (2009) in which they observed an increase in the D_2CO abundance with a decrease in HDCO. Their results confirmed the formation of D_2CO on grains by the D addition to DCO as follows

$$H_2CO \xrightarrow{D} HCO + HD \xrightarrow{D} HDCO \xrightarrow{D} DCO + D_2 \xrightarrow{D} D_2CO \qquad (5.5)$$

Our calculated abundance and column density of D_2CO ($\sim 3.5\times10^{14}$ cm^{-2}) is comparable to that observed in the warm core around the Class 0 source IRAS 16293-2422 ($\sim 1.0\times10^{14}$

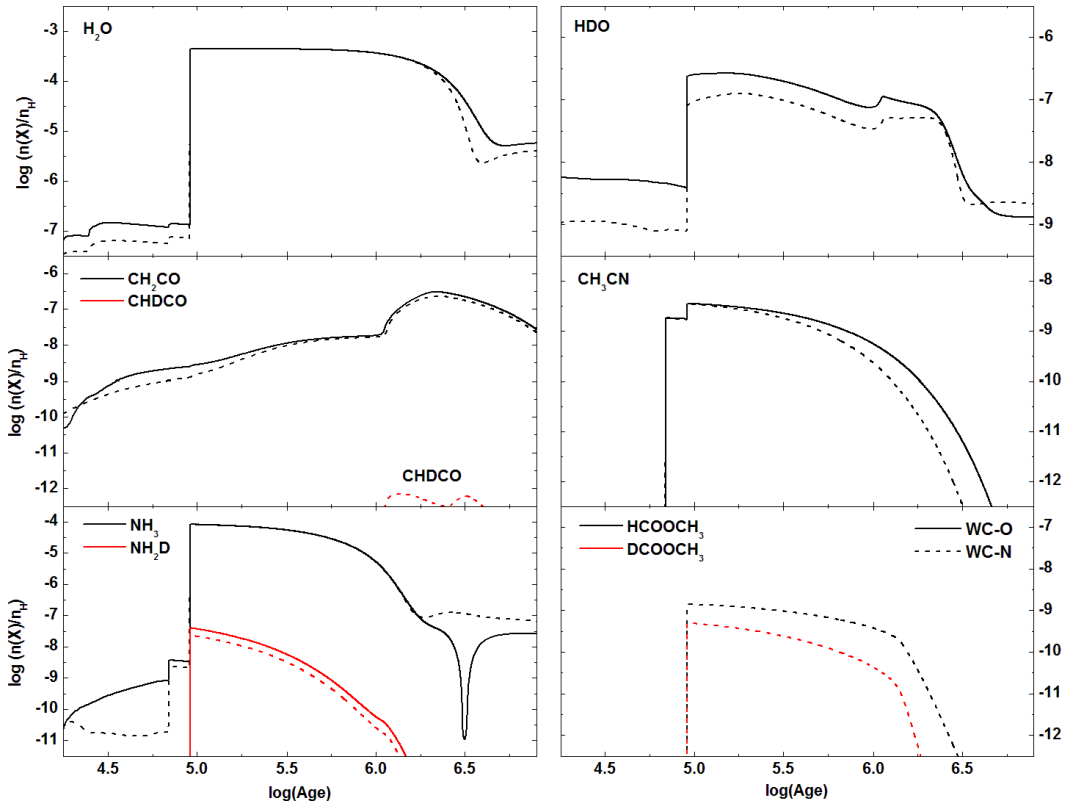

Figure 5.2: The time evolution of water, ammonia and large molecules including methyl-foramte and its mono-deuterated form in a typical hot corino in the warming up phase after the inclusion of the grain surface formation route of the latter (see key).

cm^{-2}, Ceccarelli *et al.* 1998c) within a factor of three.

The abundance of water, Fig. (5.2), does not change with the inclusion of the deuteration reaction of DCO to form D_2CO on grains while that of HDO shows a little decrease by a factor of two to three. This is because HDO is formed via routes involving both DCO and DCO^+ which are now used to form D_2CO and hence reducing the available fraction that forms HDO. CH_2CO and CH_3CN are not affected by the changes in the surface reactions, and CHDCO is now weakly observable. CHDCO is formed via the oxidisation of C_2H_2D which is more abundant in the WC-N model than in the WC-O one, in particular at late times ($\sim 10^6$ yrs) allowing more CHDCO to form and then become detectable.

No significant changes appear in the fractional abundance of the deuterated ammonia at any time while the abundance of NH_3 is not affected at times earlier than 1.6×10^6 yrs. After

that time, the decrease in the abundance of NH_3, which occurs at late times, in models WC-O disappears in WC-N. Around these times (3.14×10^6 yrs) a chemical analysis reveals that NH_3 is mainly formed via 'NH_3^+ + NO' and destroyed by $DCNH^+$. The abundance of $DCNH^+$ shows an enhancement through out the warming up phase particularly after the species evaporate from grain surfaces and it becomes very abundant in models WC-O around 3.14×10^6 yrs; after this time its abundance declines. This behaviour enhances the destruction of NH_3 at that time. On the other hand, the destruction of NH_3 via this route in models WC-N is minor and hence the evolutionary trend of NH_3 is smoother.

Methyl formate and $DCOOCH_3$ are predicted in model WC-N to be potentially observable with abundances (column densities) comparable to that recently obtained by Demyk *et al.* (2010). Our calculated column density, around the time of evaporation, for $HCOOCH_3$ is $\sim 3.0\times10^{14}$ cm^{-2} and $\sim 1.0\times10^{14}$ cm^{-2} for $DCOOCH_3$. The calculated value for $HCOOCH_3$ is two orders of magnitude less than the observed $\sim$ 0.9-1.0 $\times10^{16}$ cm^{-2} (Bottinelli *et al.* 2004) while that for $DCOOCH_3$ is comparable to the recently observed value $\sim 6.0\times10^{14}$ cm^{-2} by Demyk *et al.* (2010).

5.4 Conclusions

We ran a chemical model for a typical warm core with the inclusion of surface reactions to form $HCOOCH_3$, $DCOOCH_3$, and D_2CO. Our results show an enhancement in the abundance of the three species with $HCOOCH_3$ and $DCOOCH_3$ becoming observable; however, $HCOOCH_3$ is two orders of magnitude lower than the observed value. The shortage of the production of $HCOOCH_3$ is possibly linked to the formation of methanol on grain via the successive hydrogenation of CO. We expect to form more methyl formate if we enhance the hydrogenation of CO on grain surfaces. This project can be extended, in future, to estimate the necessary and sufficient CH_3OH/CO ratio on grains to reproduce the observed column density of $HCOOCH_3$ within a reasonable factor. In addition, CHDCO is now predicted to be detectable with low abundances. Other key mantle species show insignificant variations in their abundances such as HDO and HDCO. The observed jump in the evolutionary trend of H_2CO is still reproducible.

From this short study, our main conclusions support the view that the chemistry of hot corinos is driven by surface chemistry which plays a vital role in the formation of many large species such as CH_3OH and more complex molecules as methyl formate. In addition, grain surfaces are factories of deuterated species which can form in a similar way to their H-bearing

counterpart as in the cases of $DCOOCH_3$ and D_2CO.

CHAPTER 6

ON THE ORIGIN OF INTERSTELLAR CLOUDS

6.1 Introduction

The interstellar medium (ISM) is formed of gas and dust particles structured in large scale structures (a few parsecs in size) called interstellar clouds where condensed clumps of gas may collapse to form new stars. Interstellar molecules are detected everywhere in the ISM and they range in size from simple diatomics to more complex species with more than 6 atoms (e.g. Herbst & van Dishoeck 2009). The chemistry of the first generation of stars was totally controlled by reactions involving hydrogen, H, and helium, He, because the gas at that time was almost pure H and He. Heavier elements than He such as carbon, C, oxygen, O, and nitrogen, N, are important in the chemistry that controls the formation of the second generations of stars. This chemistry leads, in turn, to the formation of the present observed species (Hartquist *et al.* 1998). Interstellar molecules are formed in the interstellar clouds themselves from atoms and dust particles ejected from older stars, either explosively, as in the case of supernovae, or less violently, as in the case of low-mass stars (Williams 2003a). The densest clouds that are most protected from UV radiation from stars are known as dense, dark, or molecular clouds. The most tenuous clouds, almost fully exposed to the interstellar radiation field are diffuse clouds. Clouds that fall between these two types are referred to as translucent clouds (Snow & McCall 2006). An overview on the interstellar medium is given in Chapter 1.

Hollenbach *et al.* (1976) considered diffuse clouds as accumulations of gas swept up from even a more tenuous intercloud atomic gas by wind-blown around massive stars. Alternatively, Price *et al.* (2003) considered them as a transient phase of a dynamical cycle of matter into

and out of star forming regions. In their view, the authors considered Hollenbach et al. diffuse cloud to be then accumulated to a denser gas as in molecular clouds and star forming regions. When a star forming event takes place, the material expands (because of the stellar winds and outflows) and becomes less dense i.e. diffuse. In this view the material is recycled and the diffuse cloud can be considered part of an expansion as well as a contraction phases. The authors were able to identify a set of species to be indicators for both phases, simple hydrides and hydrocarbons for the expansion phase and atomic ions for the collapse, and another set to trace the stage of the evolution of the material in a recycling process.

However, whether the initial chemical conditions of the gas affect the chemical evolution of the star forming cores remain a strongly debated issue when validating chemical models. This debate motivated us to perform this study which aims to investigate the sensitivity of the chemistry of these dense star forming cores to the initial chemical composition of the collapsing gas and to the collapse mode itself; free-fall or retarded. In order to achieve our goal, we modelled the chemistry of dense star forming cores formed via different scenarios by running a large grid of chemical models where the key difference between them is the initial chemical compositions of the collapsing gas, see §(6.2).

6.2 The Model

In this study we use the extended version of the UCL_CHEM chemical model, including deuterium chemistry, described in detail in Chapter 3. In our models, we assume that the cloud collapse follows the so-called modified collapse introduced by Rawlings *et al.* (1992) as given by Eq. (1.7); see §(1.6) in Chapter 1. In this equation, the collapsing mode is determined by the factor B; free-fall if B = 1, retarded if B $<$ 1. In all the previous models (e.g. those in Chapters 2 and 3) we considered only the free-fall mode of collapse, but in this study we also look into the case of retarded collapse in order to study the influence of changing the collapse mode on the final molecular contents of the collapsing gas. The value of B = 0.1 is used throughout this study to mimic the retarded collapse mode.

In this chapter, the term 'raw gas' refers to interstellar gas that mainly consists of atomic species while 'processed gas' is gas that remains after a previous star formation event. Here we use the terms 'diffuse', 'translucent', and 'dense' to reflect the physical conditions of the collapsing gas and not its chemical compositions. Table (6.1) summarises the initial physical properties of the three types of processed interstellar gas we use in our grid of models which is

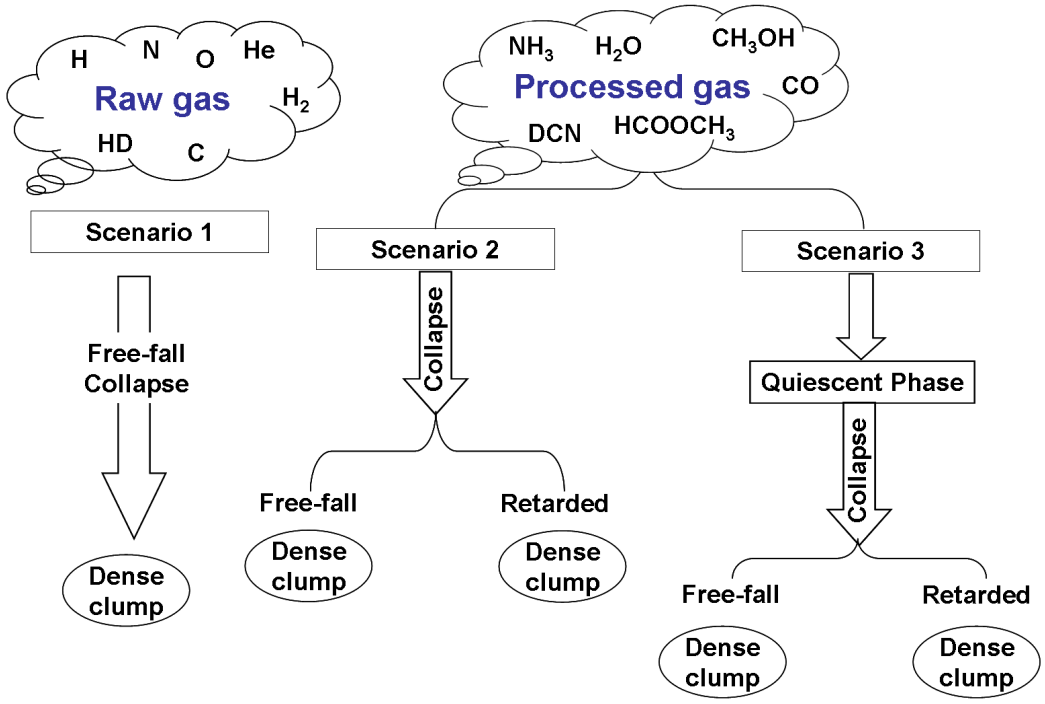

Figure 6.1: sketch of the different scenarios we use to model the dense clump.

listed in Table (6.2). The key aim of this study is to investigate whether the initial composition of the collapsing gas influences the chemical compositions of the newly formed dense clump. In order to achieve this goal, we modelled the formation of a dense clump via three different scenarios illustrated in Fig. (6.1).

In Scenario 1, the dense clump is formed from a raw gas at low density of 400 cm^{-3} undergoes a free-fall collapse at 10 K to form a dense clump of final density 10^8 cm^{-3}. This scenario is actually Phase I of the warm core models described in Chapters 2 and 3. We run the same model considering Scenario 2, i.e. we start with processed gas to form the dense clump, Model X in Table (6.2). In Scenarios 2 and 3, we model the chemistry of a dense clump formed from a processed gas remnant from a previous formation of stars. In these scenarios, we run a grid of models where the processed gas undergoes collapse (either in a free-fall or retarded mode) either directly from the processed gas or after a quiescent phase, and forms a denser clump of a final density of 10^5 or 10^6 cm^{-3}. More specifically, in order to investigate whether the abundances of the species in the star forming core are influenced by the initial conditions of the cloud we follow two approaches: in the first we collapse the processed gas immediately to form a dense clump, scenario 2, while in the second approach the cloud collapses after an

Table 6.1: Summary of the physical parameters used in our models to represent the different types of initial gas used to form the dense clumps

Parameter	**Gas Type**		
	Diffuse	**Translucent**	**Molecular**
Density (cm^{-3})	10^2	10^3	10^4
Temperature (K)	100	10	10
$^*A_v$ (mag)	1	2	3

* A_v is the visual extinction.

interval of 10^6 yrs (1Myr) of quiescent chemistry, scenario 3; see Fig. (6.1).

Table 6.2: Summary of our grid of models starting from processed gas. † Model 1 was calculated for two different sizes (see text).

Models	**density range** cm^{-3}	**Temperature** K	**Size** pc	**Collapse type**
		Diffuse Gas		
1	10^2 - constant	100	5.2	—
	10^2 - $10^{5\dagger}$	10	0.052/0.1	free-fall
	10^2 - 10^5	10	0.052	retarded
2	10^2 - constant	100	5.2	—
	10^2 - 10^6	10	0.052	free-fall
	10^2 - 10^6	10	0.052	retarded
3	10^2 - 10^5	10	0.052	free-fall
	10^2 - 10^5	10	0.052	retarded
4	10^2 - 10^6	10	0.052	free-fall
	10^2 - 10^6	10	0.052	retarded
X	400 - 10^8	10	150 AU	free-fall
		Translucent Gas		
5	10^3 - constant	10	1.04	—
	10^3 - 10^5	10	0.052	free-fall
	10^3 - 10^5	10	0.052	retarded

Continued on next page

Table 6.2 – continued from previous page

Models	density range	Temperature	Size	Collapse
	cm^{-3}	K	pc	type
6	10^3 - constant	10	1.04	—
	10^3 - 10^6	10	0.052	free-fall
	10^3 - 10^6	10	0.052	retarded
7	10^3 - 10^5	10	0.052	free-fall
	10^3 - 10^5	10	0.052	retarded
8	10^3 - 10^6	10	0.052	free-fall
	10^3 - 10^6	10	0.052	retarded
	Molecular Gas			
10	10^4 - constant	10	0.16	—
	10^4 - 10^5	10	0.052	free-fall
	10^4 - 10^5	10	0.052	retarded
11	10^4 - constant	10	0.16	—
	10^4 - 10^6	10	0.052	free-fall
	10^4 - 10^6	10	0.052	retarded
12	10^4 - 10^5	10	0.052	free-fall
	10^4 - 10^5	10	0.052	retarded
13	10^4 - 10^6	10	0.052	free-fall
	10^4 - 10^6	10	0.052	retarded

In Scenario 3, we are mimicking the quiescent phase by running a static time-dependent chemistry , i.e. no collapse occurs. At relatively low densities $\leq 10^4$ cm^{-3}, the collision between species and grains is rare and thus the accretion is not really efficient. In addition, due to lower concentrations of dust in these regions the visual extinction A_v is < 5 mag thus interstellar photons are easily penetrating the cloud and destroying grain mantles efficiently. For these reasons we assume that grains are almost bare and the freeze out is not efficient in such quiescent regions.

Chemical models of star forming regions show that all molecules except for H_2 are removed from the gas phase within $\sim 10^9/n_H$ yrs, where n_H (cm^{-3}) is the total number density of H in the region (Willacy & Millar 1998). When a cloud collapses to a final density of 10^5 or 10^6

cm^{-3}, the accretion time scales to remove all the species from the gas phase (10^4 and 10^3 yrs) are much shorter than the life time of the interstellar cloud ($\sim 10^7$ yrs) (Wooden *et al.* 2004). Therefore, the depletion percentages (amount of species removed from the gas) is not 100%. In our models, we assume that the depletion percentage of species in a collapsing cloud (regardless of its initial density) to a clump of final density 10^5 cm^{-3} is 70%, and 80% for a clump of final density 10^6 cm^{-3}.

For models in scenario 3, the initial abundances for the collapsing phase are those obtained from the last time step of the quiescent phase.

6.3 Results and Discussion

In this section, we discuss our model results for dense clumps that are formed by three different scenarios, see §(6.2), from a collapsing interstellar gas; Fig. (6.2) for Scenario 1, Figures (6.3) to (6.5) for Scenario 2, and Figures (6.8) to (6.17) for Scenario 3. These figures represent the time evolution of the fractional abundances of a wide range of species including sulphur-, nitrogen-, and carbon- bearing species in addition to larger ones. These species are divided into three sets, given in Table (6.3). Notice that these sets have no common physical or chemical properties. In all figures, we focus on the late stages of the collapse where the fractional abundances of the species show some variations. The two sets of figures (6.3) to (6.5) and (6.8) to (6.17) represent our results for diffuse, translucent and molecular interstellar gas, undergoing free-fall (left column) or retarded (right column) collapse into a clump of final density 10^5 cm^{-3} (top panel) or 10^6 cm^{-3} (bottom panel), in Scenarios 2 and 3 respectively. In Scenario 3, the collapse is preceded by a million years of a quiescent chemistry of a processed gas rich in its molecular contents (leftover from a previous star formation event). The quiescent phase is shown in a separate plot at the top of the collapse plots.

6.3.1 Scenario 1 versus Scenario 2

In this part we discuss the effect of varying the initial chemical conditions of the interstellar collapse on the final chemical composition of the final dense clump. We run two chemical models where the physical conditions of the initial gas are similar to those of Phase I in models described in Chapters 2 and 3 (density of 400 cm^{-3} and temperature of 10 K) but different in their gas chemical conditions; one is raw and the other is processed. The gas in both models undergoes a free-fall collapse to form a dense clump of density 10^8 cm^{-3}. Fig. (6.2) represents

Table 6.3: The three sets of species in our plots.

Set	Species
S1	S, S^+, OCS, CS, SO, SO_2, H_2CS, HDCS, H_2S, HDS, OH
	OD, H_3^+, H_2D^+
S2	C, O, N, CO, H_2CO, HDCO, D_2CO, CH_3OH, CH_3OD
	CH_2DOH, CH_2CO, CH_3CN, $HCOOCH_3$, NH_3, NH_2D
S3	H_2O, HDO, C_2H, C_2D, CH_3, CH_2D, CN, NH, ND,C_3
	C_2H_2, C_2HD

the comparison between the time evolution of the chemical compositions of the dense clump formed in Scenario 1 (solid line) and Scenario 2, Model X (dashed line). In the top plot of the figure we show an example of the chemical evolution of the species during the collapsing phase. In this plot, as expected, the fractional abundances of the species in the processed gas are higher than those in the raw gas. Due to photoreactions, the abundances of the species in Scenario 2 decreases to converge with those in Scenario 1 at times few $\times$ 10^{3-4} yrs. After that the chemistry in the two scenarios reaches steady state and the calculated abundances of the species in the two models are almost identical. The bottom panel in the figure focuses on the late stages of the collapse.

Surprisingly, the differences between the fractional abundances of the species in the two scenarios are insignificant ($<$ 3 times) except for H_2O and HDO which are $\sim$ 10 times more abundant in Scenario 1, see the bottom set of figures in Fig. (6.2). In both scenarios, the water formation proceeds via 'OH + H' reaction. The chemical analysis revealed that throughout the collapse, the abundance of OH is higher than that in Scenario 2 and hence more H_2O is produced in models start with raw gas. On the other hand, deuterated water is formed by the reaction '$CH + H_2DO^+$' in both models. The abundance of CH in the two clumps is comparable throughout the collapse time, but it becomes more abundant in the raw gas by the end of the collapsing phase enhancing the abundance of HDO in Scenario 1. Here, we conclude that water and deuterated water are the most influenced species by changing the initial chemical composition of the interstellar gas.

6.3.2 Scenario 2 versus Scenario 3

In this section we compare the results of scenario 2 where the interstellar gas collapses immediately to form a denser prestellar core to those of scenario 3 in which the gas collapses after an interval of quiescent chemistry of million years. Figures (6.3) to (6.5) illustrate the time evolution of the fractional abundances of the three sets of species at late stages of the collapse. Fig. (6.6) is an example to show these differences for a set of key mantle species, in models M1 and M3 with the free-fall collapse. Generally, the differences between the abundances in the two approaches, for all gas types, are insignificant (less than 3 times) for both modes of collapse. These differences vanish as the density of the clump increases, see the bottom panel of all figures. The chemical trends of the species are similar despite the initial density and molecular contents of the gas in the collapsing cloud. Here we are going to discuss in details the results of the two scenarios for the case of dense clumps formed from diffuse gas (models M1 to M4). The same discussion is applicable for the other types of interstellar gas.

The bottom set of plots in Fig. (6.3), represents the late stages of the chemical evolution of species in a diffuse gas collapses via either free-fall (left column) or retarded mode (right collapse) to a clump of final density of 10^5 cm^{-3} (top panel) and 10^6 cm^{-3} (bottom panel), and the top plot is an example to show the early stages of the collapse. During the early stages of the collapse, molecules in scenario 2 (models M3 and M4) possess higher abundances than those in scenario 3 (models M1 and M2). The two abundances converge at times around few$\times 10^3$ yrs. The chemical analysis unveiled that during early stages, the chemistry is dominated by photoreactions that lead to the dissociation of molecules in scenario 2 and reduce their abundances to values close to those in Scenario 3, on time scales of $\sim 10^4$ yrs. After that time, the chemistry reaches a quasi steady-state and the photoreactions become less efficient (as the density of the clump increases) while other reaction types start to drive the chemistry of the clump such as ion-molecule reactions.

When the interstellar gas collapses, the free-fall mode shows more differences than the retarded one especially for less dense clumps (10^5 cm^{-3}), however these differences are still insignificant. The evolutionary trends of the species in both modes are alike which might imply that the mode of collapse does not strongly influence the chemistry of the gas. Increasing the initial density of the collapsing gas, Fig. (6.4) and Fig. (6.5), the differences in the abundances of the species in the free-fall collapse decreases while they become identical in the retarded mode, particularly for denser clumps (10^6 cm^{-3}).

During the collapse, the fraction of molecular hydrogen continues to fall off throughout the collapse with a rise in the abundance of atomic hydrogen until both abundances reach the same value at 2.7×10^6 yrs after which the fraction of H_2 starts to increase on the expense of atomic H. By the end of the collapsing phase, all H is converted into H_2 - see Fig. (6.7). The time after which the H_2 formation starts is in agreement with that obtained by Price *et al.* (2003), if one considers that those authors modelled a more dense diffuse gas, 10 cm^{-3}. In models M3, all the molecules follow the same trend in which they are dissociated until they reach certain abundance (almost that in models M1) then they reach a steady state. These results imply that in order to suppress photodissociation and enhance other chemical processes, a critical fraction of species, in particular H_2, needs to be achieved regardless of their initial fraction in the cloud. This critical fraction is reached on time scales of 10^3 - 10^4 yrs, see top illustration in Fig. (6.3) which is in line with the typical time scale of photodissociation (Price *et al.* 2003).

Retarding the collapse leads to a reduction in the fractional abundances of all the species. However, water and SO_2 possess higher abundances in the retarded mode than they do in free-fall. Detailed analysis of the trends of the species during the collapse for all the studied gas types is given in §(6.3.3).

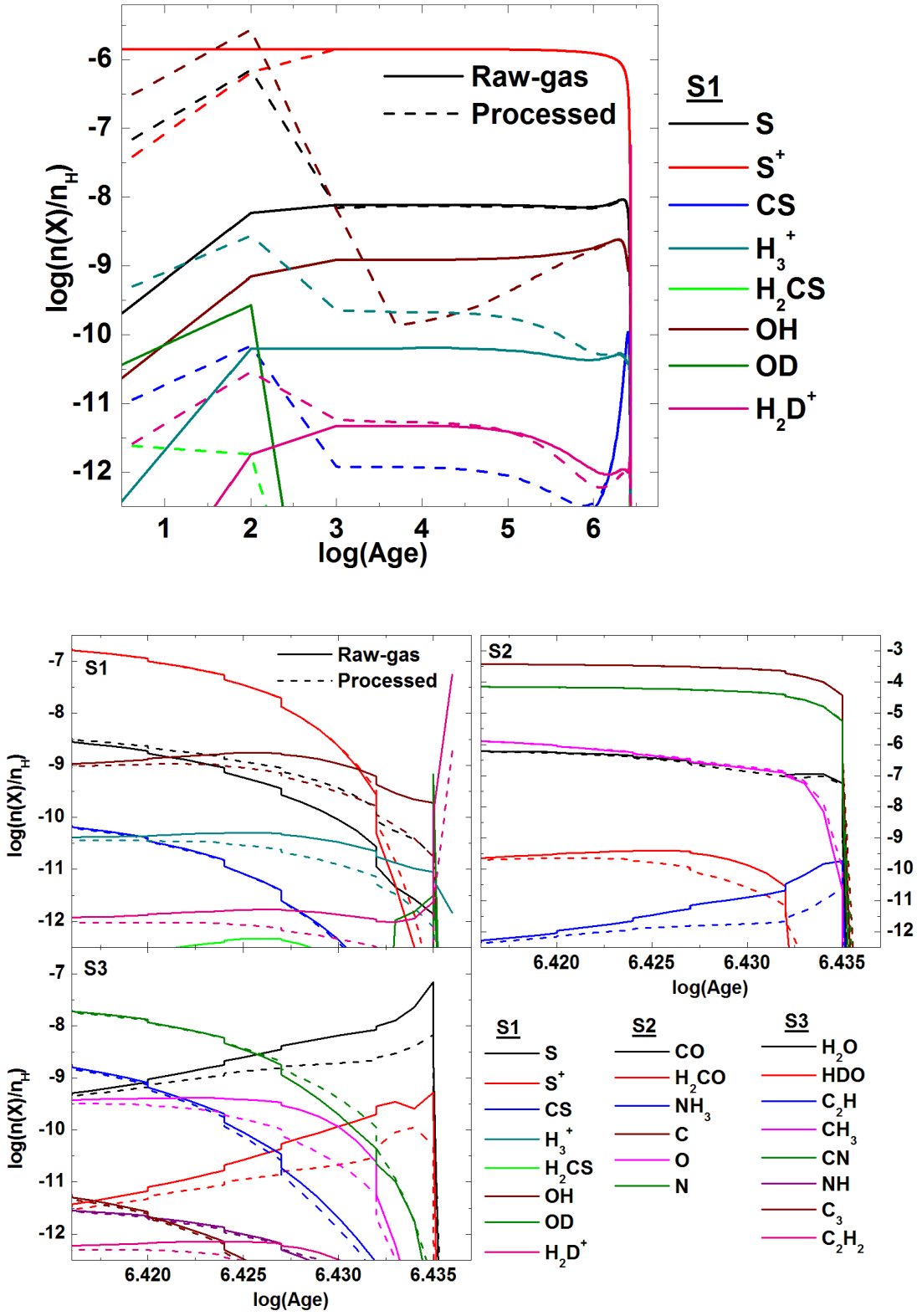

Figure 6.2: Effect of varying the initial contents of the input gas in chemical models, i.e. atomic (Scenario 1) or processed (Model X, Scenario 2) on the ultimate chemical content of the cloud under study (see key). The chemical evolution of the three sets of species (see key) as a function of time is presented for the whole time interval (top plot) with a zoomed-in version showing the latest stages of the collapse (bottom set of plots).

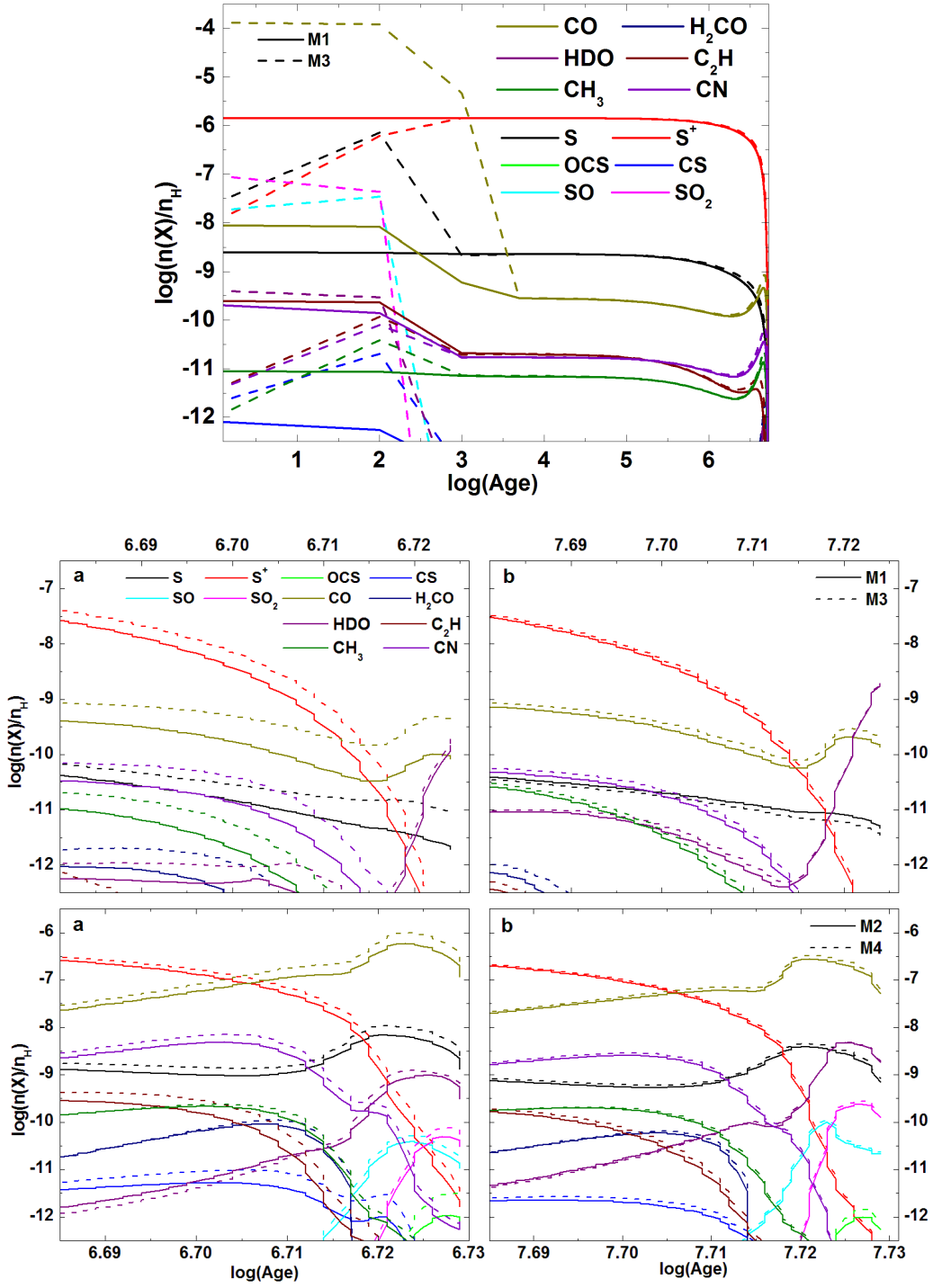

Figure 6.3: A comparison between the fractional abundances of a set of selected species (see key) in a diffuse processed gas at 10^2 cm^{-3} which collapses either following Scenario 2 (dashed line) or Scenario 3 (solid line) to a final density of 10^5 cm^{-3} (top panel) or 10^6 cm^{-3} (bottom panel). These plots show the latest stage of the collapse, a) free-fall and b) retarded, where almost all the heavy species are on grains because the earlier stages show flat chemistry; see top plot for an example of the early stages of the collapse.

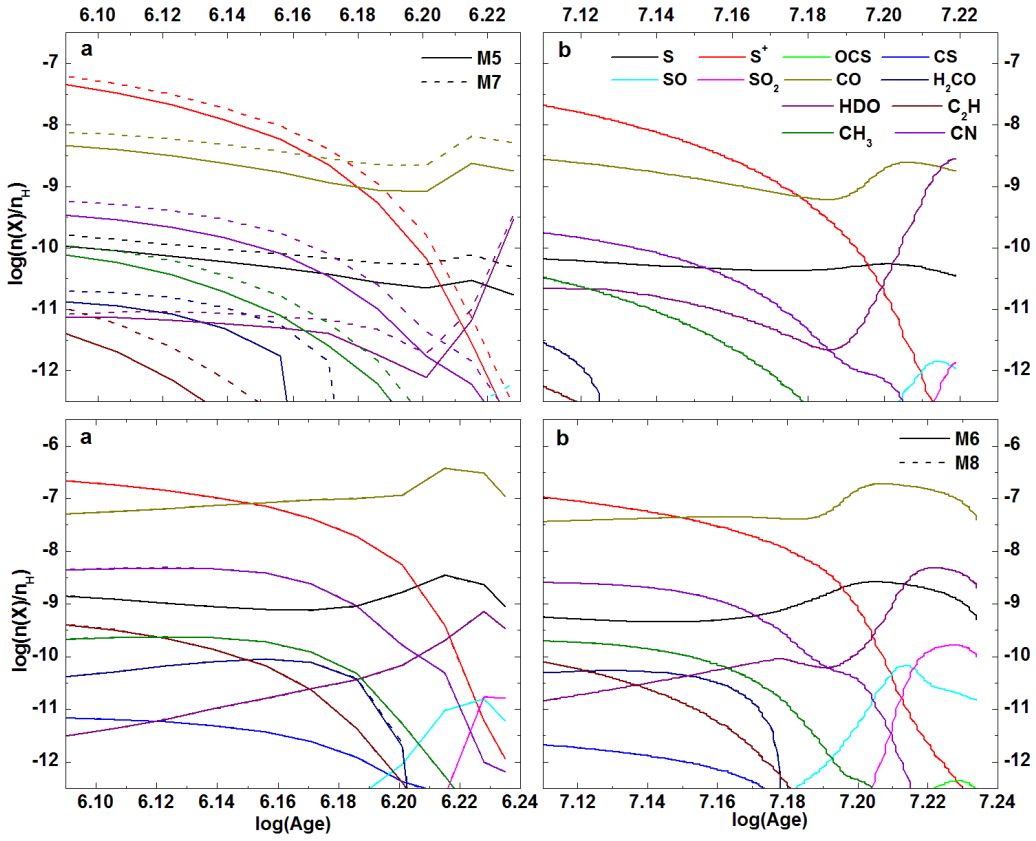

Figure 6.4: Same as in Fig. (6.3), but for a dense clump formed from a translucent interstellar gas of density 10^3 cm^{-3}.

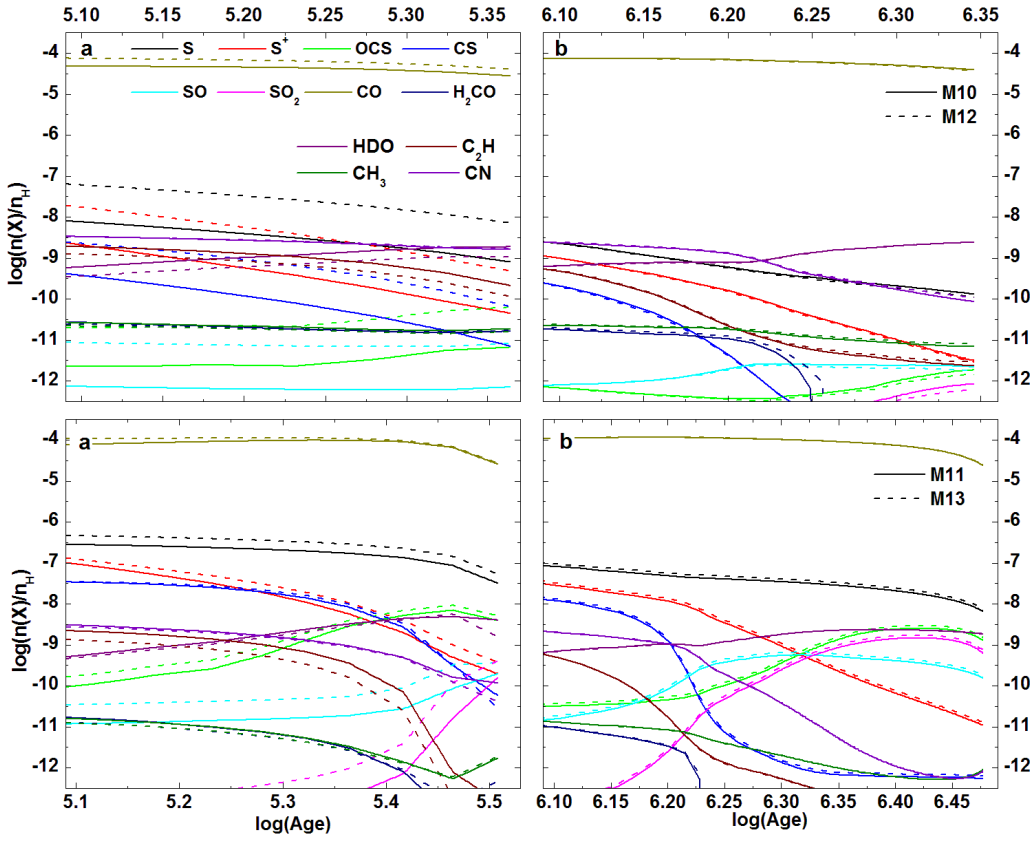

Figure 6.5: Same as Figs. (6.3) & (6.4), but for a dense clump formed from a molecular gas of initial density of 10^4 cm^{-3} (see key).

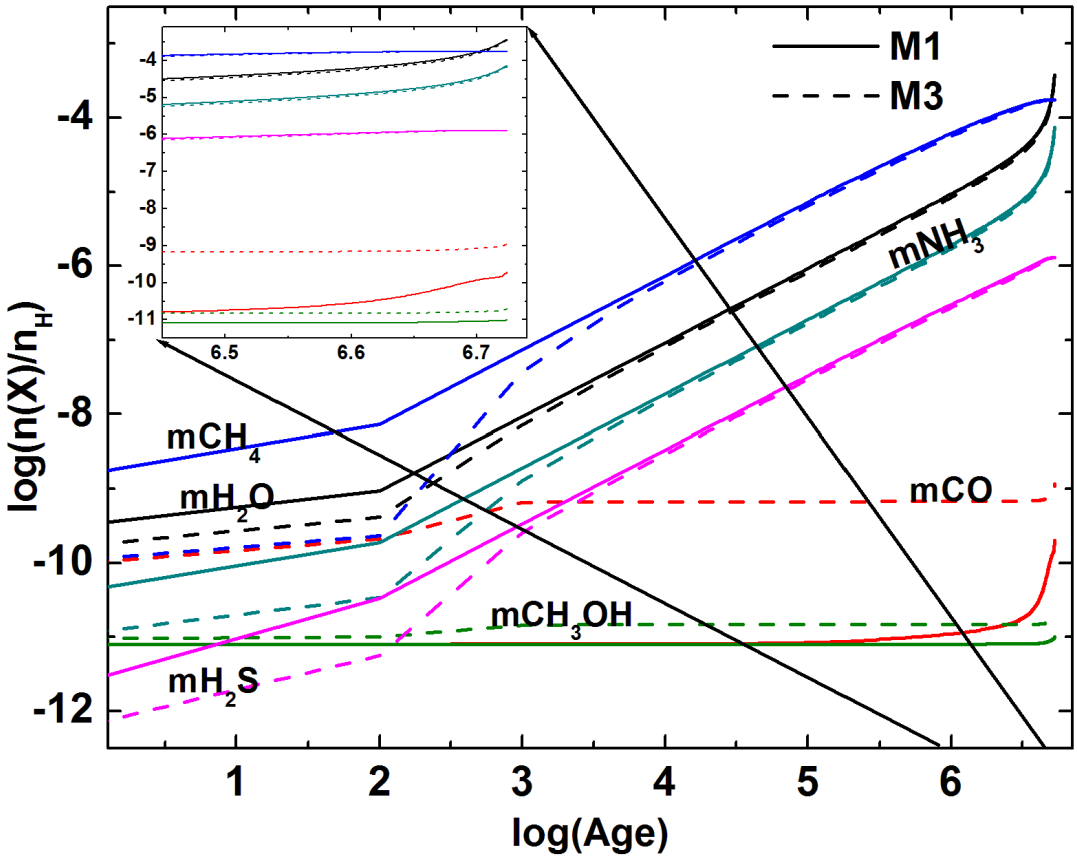

Figure 6.6: Same as in Fig. (6.3), but for key mantle species in diffuse processed gas undergoes a free-fall collapse to a prestellar core of final density 10^5 cm^{-3} (see key).

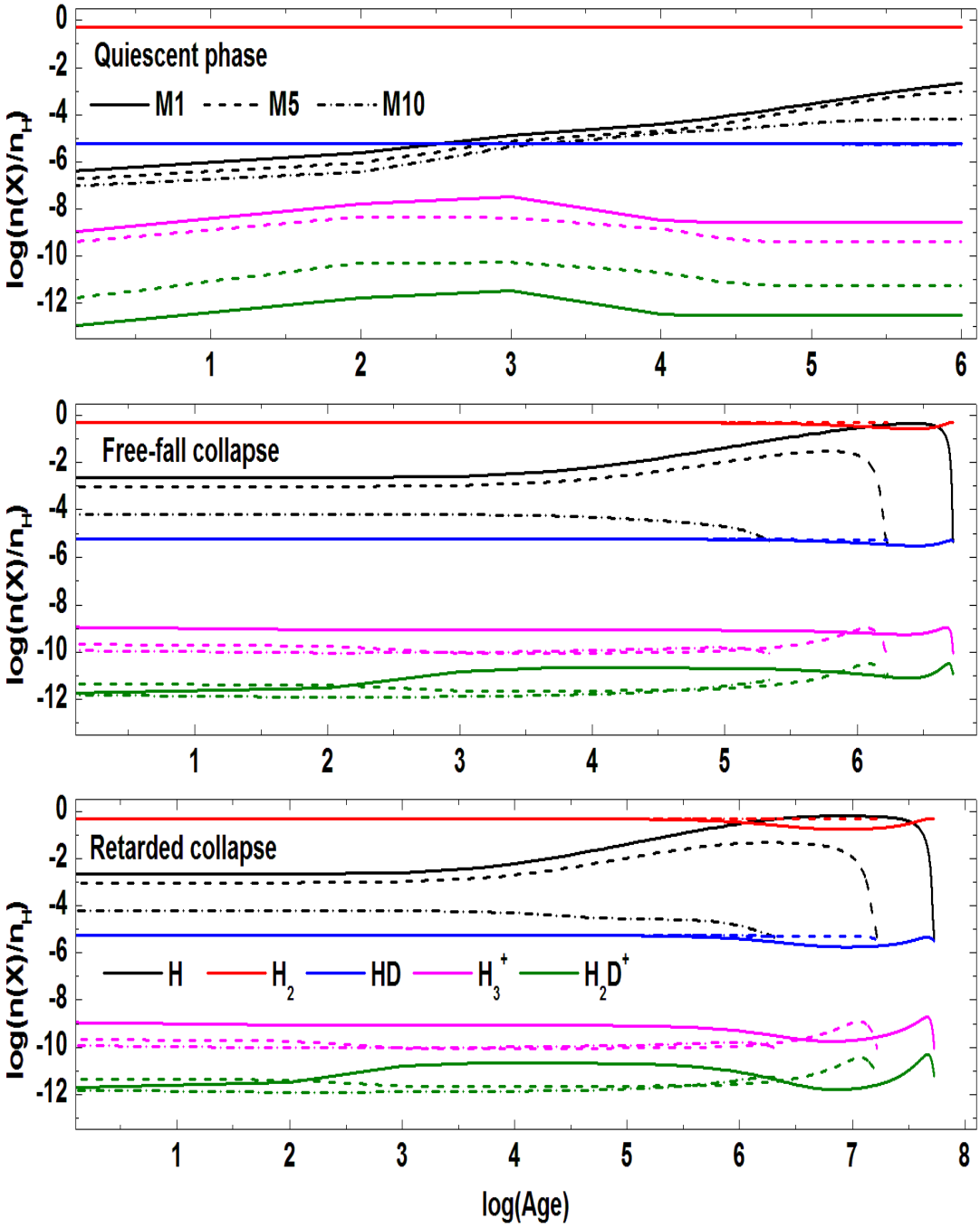

Figure 6.7: The time evolution of the fractional abundances of the essential forms of hydrogen in three different types of gas (see key) in Scenario 3; quiescent phase (top panel) followed by a free-fall collapse (middle panel) or a retarded collapse (bottom panel).

6.3.3 Detailed analysis of the chemistry in Scenario 3

From the previous sections it is shown that neither the initial chemical conditions of the collapsing cloud nor the collapsing mode influences the chemical compositions of the final dense clump. Therefore, regardless of how a dense prestellar core is formed, its chemical composition remain well defined, despite few negligible differences. In this section we discuss in detail the chemistry of these dense clumps in Scenario 3 where the collapse is preceded by a quiescent phase. The results are given in Figures (6.8) to (6.17) for the different initial interstellar gases used in this modelling. In all figures, the top panel is the quiescent phase which is then collapsed either free-fall (left column) or retarded (right column) to form a dense core of final density 10^5 cm^{-3} (top set) or 10^6 cm^{-3} (bottom plots).

(a) Quiescent phase:

It is clear that during this phase all the species suffer a dramatic decrease in their abundances during the early stages of evolution (up to 10^4 yrs). This decrease decelerated as the initial density of the gas increases. For dense gas (10^4 cm^{-3}), as expected, more species are predicted to be detectable. In the context below, we discuss in detail the chemistry of the quiescent phase for both diffuse and translucent 'processed gas' which show some similarities in their evolutionary trends; see Figs. (6.8) to (6.14). Generally, for both diffuse and translucent clouds, all the species in the quiescent phase suffer a steep decrease in their abundances due to photoreactions, as discussed in §(6.3.1). During this quiescent phase and for the times later than 10^4 yrs, species such as SO_2, H_2D^+, OD, SO, NH_3, CH_2CO, and HDO become undetectable while others decrease in fractional abundances then remain constant at either $\geq 5 \times 10^{-9}$ (e.g. S, H_3^+, OH, CO, O, H_2O, CN, C_2H) or $\leq 10^{-10}$ (e.g. CS, NH, CH_3).

Chemical analysis for the species in set S1, Figs (6.8) and (6.11), shows that the decrease in the abundances of S-bearing species is mainly due to photodissociation reactions. This leads to an increase of the abundances of S and S^+. On the other hand, SO recombines with C to form CS efficiently up to 10^4 yrs. At that time, CS is in a steady state which is represented by the the plateau in Figs. (6.8) and (6.11) after 10,000 yrs.

For set S2, Figs (6.9) and (6.12), the decrease in the abundance of CO is associated with a slight increase in the abundance of both atomic C and O. In diffuse clouds, the increase in the abundance of atomic oxygen occur up to 10^4 yrs then its abundance starts to decrease as that of CO does. On the other hand, in translucent gas, the destruction of CO increases the abundance of atomic O. The formation of CO is not as efficient as it is in diffuse clouds because atomic O

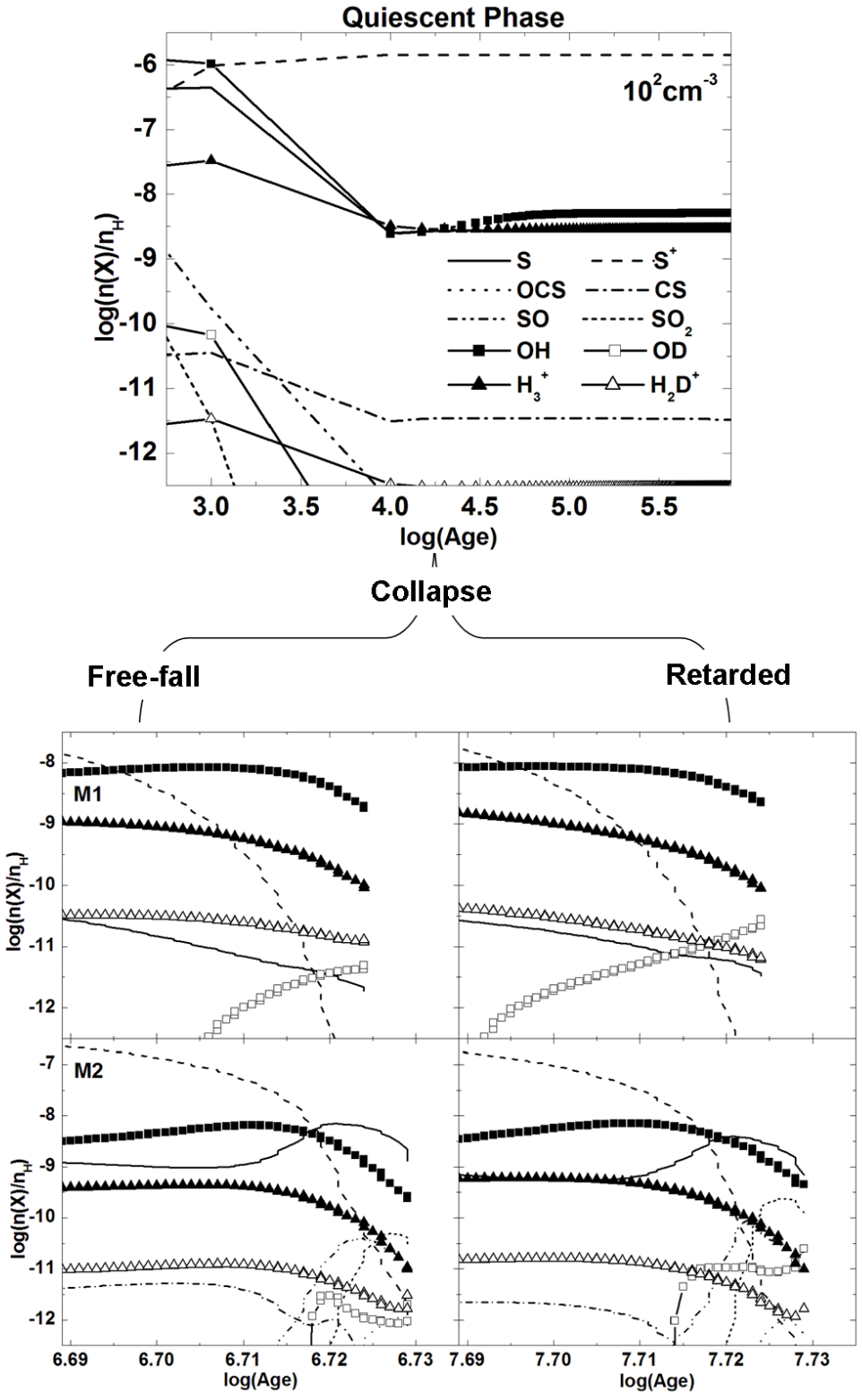

Figure 6.8: The time evolution of the fractional abundances of a the species in set S1 in Scenario 3 (see key). The quiescent phase (for 1Myr) is represented in the top plot while the set of bottom figures show the evolution during the collapsing phase, either free-fall (left column) or retarded (right column), to a denser clump of a final density of 10^5 cm^{-3} (M1: top panel) or 10^6 cm^{-3} (M2: bottom panel). The clump is formed from a diffuse gas of initial density 10^2 cm^{-3}.

is consumed more in forming radicals and water as unveiled by the chemical analysis. These results indicate that large amount of the cloud's atomic O is trapped into CO. Ammonia is not observable in quiescent clouds for times later than 3000 yrs, because it is all converted to other N-bearing species such as NH and NH_2. The same behaviour is obtained for translucent gas but ammonia is detectable throughout the time of evolution of the cloud. Photodissociation reactions do not destroy all of the ammonia produced in the medium allowing some of it to be observable in the medium. This in turns affects the abundance of atomic nitrogen which is less abundant in translucent clouds than in the case of diffuse clouds. Thus we conclude that the decrease in the abundance of NH_3 indirectly enhances that of atomic N abundance due to the photodissociation of NH and NH_2. Large organic species are not observable in diffuse clouds while a little amount of H_2CO can be detected in translucent clouds.

For set S3, Figs (6.10) and (6.13), molecules such as C_3 and C_2H_2 are observable in translucent clouds with fractional abundances 5 $\times 10^{-10}$ and 10^{-11} respectively, but they are undetectable in diffuse clouds. Water is more abundant in translucent clouds during early $<10^4$ yrs than in diffuse clouds, then the two fractional abundances converge to the same value ($\sim 10^{-9}$) after 3×10^4 yrs. Prior that time, the formation of H_2O in both clouds is via the reaction of H_2DO^+ and CH, but because CH is more abundant in translucent clouds than in diffuse one, water is more abundant in translucent clouds. After that, the formation and destruction routes of H_2O are in balance which leads to the observed constant evolutionary trend of the species. Deuterated water, HDO, is undetectable in diffuse clouds while in translucent clouds it starts at high fractional abundance that decays until around 10^4 yrs it becomes barely detectable, $\leq 10^{-12}$. In the two clouds, the abundances of C_2H during early times ($<10^4$ yrs) are similar then it decreases in diffuse clouds until the difference becomes an order of magnitude by the end of the quiescent phase. The same trend is obtained for CH_3, NH, and CN with higher abundances in translucent clouds up to 2 orders of magnitude. The fractional abundance of CH_2D is undetectable in diffuse clouds while it shows a weak peak around 10,000 yrs in translucent clouds then disappears. That is because its parent molecule (CH_3D) is more abundant in translucent clouds than it is in diffuse medium.

We may conclude that the dominant photodissociation during the quiescent phase implies that, regardless the initial composition of the gas, by the time the collapse starts, most of the gas is in atomic form.

Photoreactions in dense gas are not as efficient as less dense gas, so that the decline in the abundances of the species is less than that discussed for diffuse and translucent gas. Our

models predict that all deuterated species are undetectable apart from H_2D^+ and CH_2D. The absence of larger deuterated species may be either because they appear in denser regions than 10^4 cm^{-3} or because our models produce little amounts of both H_2D^+ and CH_2D that initiate the deuterium chemistry in interstellar clouds.

(b) The collapse phase:

When clouds collapse, the occurrence of the species depends very much on the initial density of the collapsing gas, see the collapse panel of all figures. However, some species are always detectable with fractional abundances $\gtrsim 10^{-9}$ regardless of the initial density of the collapsing cloud and the collapse mode. These species include atoms (e.g. S, S^+, C, N, and O) as well as simple molecules and ions such as OH, H_3^+, CO, H_2O. Here we discuss the chemistry during the collapse. We discuss the case of diffuse and translucent gas followed by the case of dense gas.

For the low-density gas, by the end of the collapse regardless of the mode, all species in set S1 are not observable in models M1, Fig. (6.8) top panel, except S, S^+, OH, OD, H_3^+, H_2D^+ while in models M2 (bottom panel) those species remain detectable beside OCS, CS, SO, and SO_2 that become above the adopted detection limit ($\sim 10^{-12}$). In models M2, both SO and SO_2 are more abundant in the retarded collapse mode (right column of all plots). The same species in set S1 are observed in models M5 and M6, Fig. (6.11), with slightly higher abundances toward the end of the collapse and with SO and SO_2 more abundant in the retarded mode. The decrease in the abundance of S^+ occurs because of its conversion into other species rather than freezing out onto grain surfaces.

For species in set S2, Figures (6.9) and (6.12), in both modes all deuterated species are undetectable even for models with higher final density, M2 and M6, with the exception of CH_2DOH which is very faint in models M2 at the end of the collapsing phase. Chemical analysis revealed that, in both clouds, CH_2DOH is totally formed via the reaction '$CH_2DOH_2^+$ + NH_3' and decomposed by C^+ to form H_2DCO^+. Our results show that at late stages of the collapse, NH_3 is more abundant in models M2 than in models M6, for both modes, allowing more CH_2DOH production in models M2. In addition, the abundance of C^+ in models M1, M5, and M6 is higher than in M2 and hence CH_2DOH destruction is more efficient in these models. The oxidisation of CH_3 is the main route to form H_2CO which is barely seen in models M1, the free-fall collapse, but detectable in the rest of our grid. That is because the abundance of CH_3 is very low in models M1 in comparison to the others. This result may indicate that

large molecules require higher densities and/or longer time scales to be formed.

The differences in the abundances of the species in set S3 in diffuse and translucent cases, Figures (6.10) and (6.13), are generally less than 10 times for models M1 and M5 whereas these differences vanishes in models M2 and M6 apart from C_2H which is 2.5 times more abundant in the free-fall collapse of M6 than M2. In models M5, the abundances of both H_2O and HDO are similar to those of models M1 for the free-fall mode while they are twice their abundance for the same model in the retarded mode. C_2H is undetectable in models M1 while it is observable in models M5 within the assumed detection limit (5×10^{-11}) for both types of collapse. CH_3 and CN abundances are 7 times higher in models M5 than that in models M1 for both collapsing modes. NH is almost the same in both models.

From the above discussion, it is clear that the chemistry in diffuse and translucent clouds is mainly affected by the UV radiation penetrating them, and is dominated by photodissociation and photoionisation of molecules and atoms. These processes remain effective until most photons have been absorbed by the dust and the photo-rates have fallen below those of other chemical reactions (van Dishoeck *et al.* 2006). Photoprocesses are hindered in denser regions where the concentration of dust particles is high and the regions are opaque (i.e. higher A_v). Our results are in agreement with this view and we find that the decay of the species due to photodissociation slows down as the cloud is denser. Among the selective species in our study, CO is a good example to present this agreement because its abundance increases as the cloud density does and hence the visual extinction. In order to confirm this agreement, we run a test model (M9) similar to model M1 (but with a different size 0.1 pc, see Table (6.2)) of a quiescent cloud collapses to a clump of final density of 10^5 cm^{-3} but more opaque than the clump of model M1, with A_v = 20 mag. The results are given in Fig. (6.14) which presents the fractional abundances of CO as a function of both time (top panel) and A_v (bottom panel) in models M1 (solid line) and M9 (dashed line). The abundance of CO as a function of either time or A_v is enhanced in models M9 by $\sim$ 2 to 3 times in comparison to that in models M1. Although these differences are relatively insignificant, observationally and theoretically, this result highlights the role of photo-processes and confirms its importance in star forming regions.

In the case of **dense gas**, Figures (6.15) to (6.17), some species become detectable while others disappear. In set S1, Fig. (6.16), almost all the abundances of sulphur bearing species are enhanced and for denser clumps (model M11) HDS become detectable with low abundance in the free-fall collapsing mode. The chemical analysis revealed as the final density of the clump increases, the formation rate of S-bearing species is enhanced in the free-fall mode comparing

to that in retarded collapse. That is because the sulphur content in the free-fall collapsing cloud is higher than that in the retarded. The exception is SO_2 which is more abundant in clouds which undergo retarded collapse. OCS is formed via 'CO + S' and destroyed by C^+ to CS^+ and CO. When the collapse is retarded C^+ is more abundant leading to an enhancement in the destruction rate of OCS and hence lower abundance. Therefore, OCS is always more abundant in the free-fall collapse than in the retarded one. On the other hand, SO_2 shows higher abundances in retarded collapse. It is mainly formed via the radiative recombination of SO and O and destroyed by C atoms to form CO and SO. throughout the collapsing phase, the abundance of C atoms in retarded mode is less than that in the free-fall allowing more SO_2 to form in the former case.

In Set S2, the abundances of ammonia and CH_2CO are enhanced with respect to theirs in diffuse and translucent clouds. The production of CH_2CO is via the oxidisation of C_2H_3 while its destruction is mainly via photodissociation reactions. Dense clouds possess high abundances of C_2H_3 and are less influenced by UV photons, leading to an enhancement in the formation of CH_2CO in dense clouds over that in diffuse and translucent clouds. H_2DO^+ is found to be abundant in clouds undergoing a retarded collapse. When it reacts with NH_3, H_2DO^+ forms water and deuterated water. This leads to the enhancement of NH_3 in free-fall collapsing mode. Methanol and its deuterated forms, CH_2DOH and CH_3OD, are now detectable in dense clumps in models M11 in the free-fall collapse. The main route to form these species is via the reaction 'NH_3 + CH_3OHD^+' and they are destroyed by either photoreactions or C^+. In retarded collapse, the abundance of C^+ is higher than that in free-fall collapse and it is even higher for denser clumps (i.e. M11). This leads to less methanol forms in retarded collapse. The absence of methanol in diffuse and translucent clouds is mainly due to the photoreactions which are more efficient at low densities than in higher densities where photons are attenuated by dust particles.

The enhancement in the abundances obtained for the species in sets S1 and S2 is also observed for species in set S3. H_2O is more abundant in retarded mode collapse than in the free fall. In the latter, water is formed via reactions involving H_2DO^+ and HNC while in the former mode H_2DO^+ reacts with either CH or NH_3. The production rate of water in the retarded collapse is twice as high as it is in the free-fall mode.

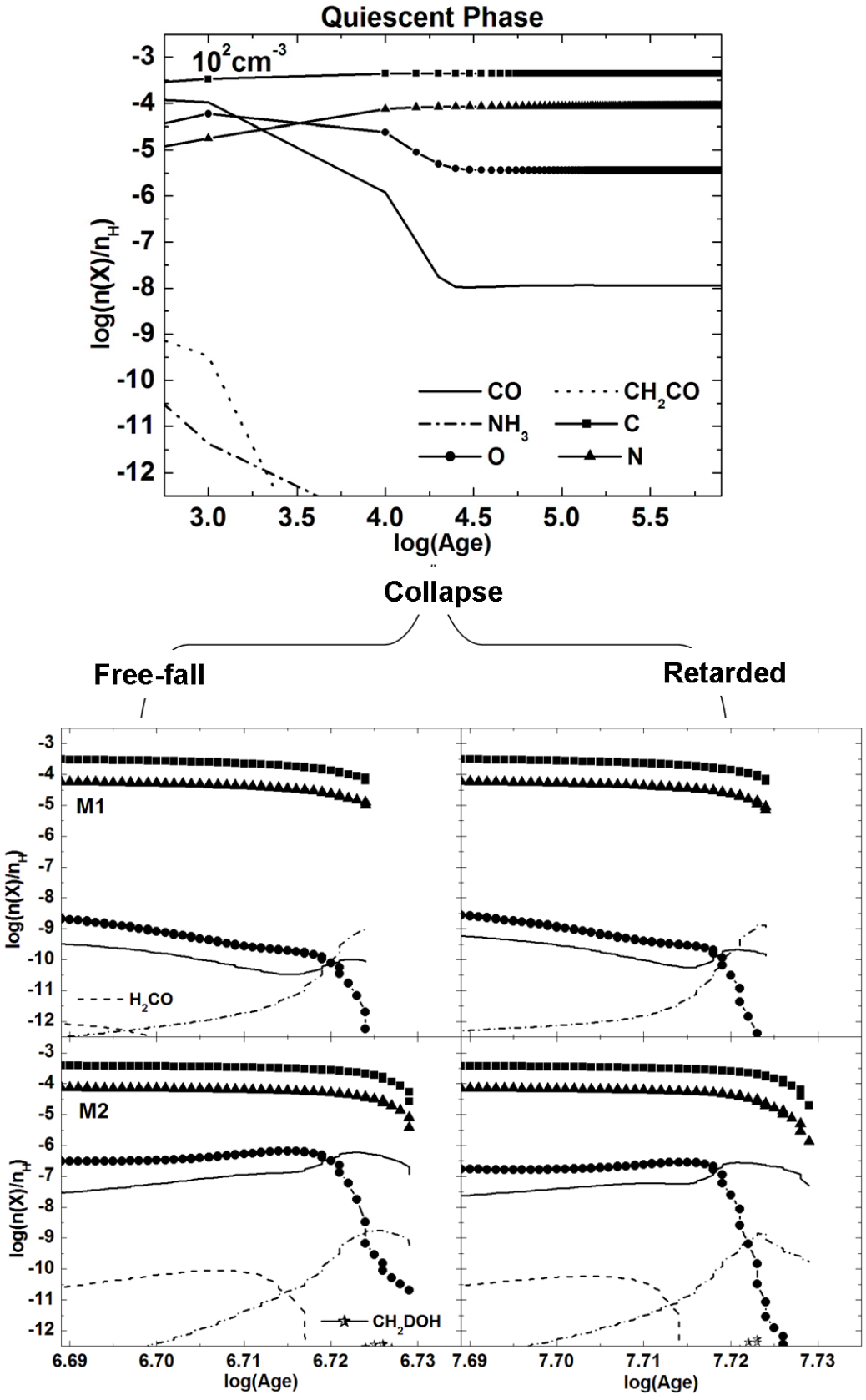

Figure 6.9: Same as in Fig. (6.8), but for the species in set S2 (see key).

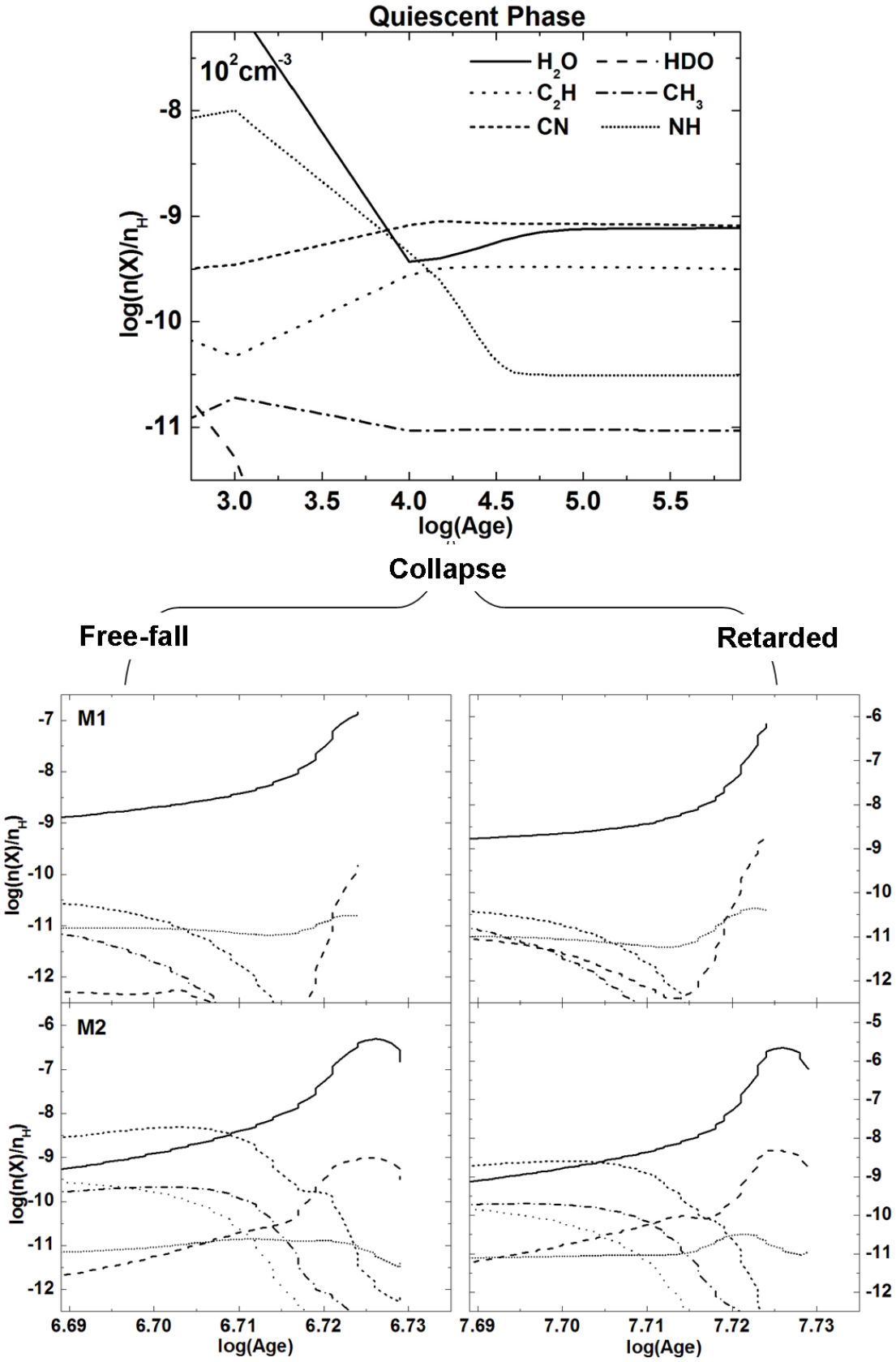

Figure 6.10: Same as in Figs. (6.8) & (6.9), but for the species in set S3 (see key).

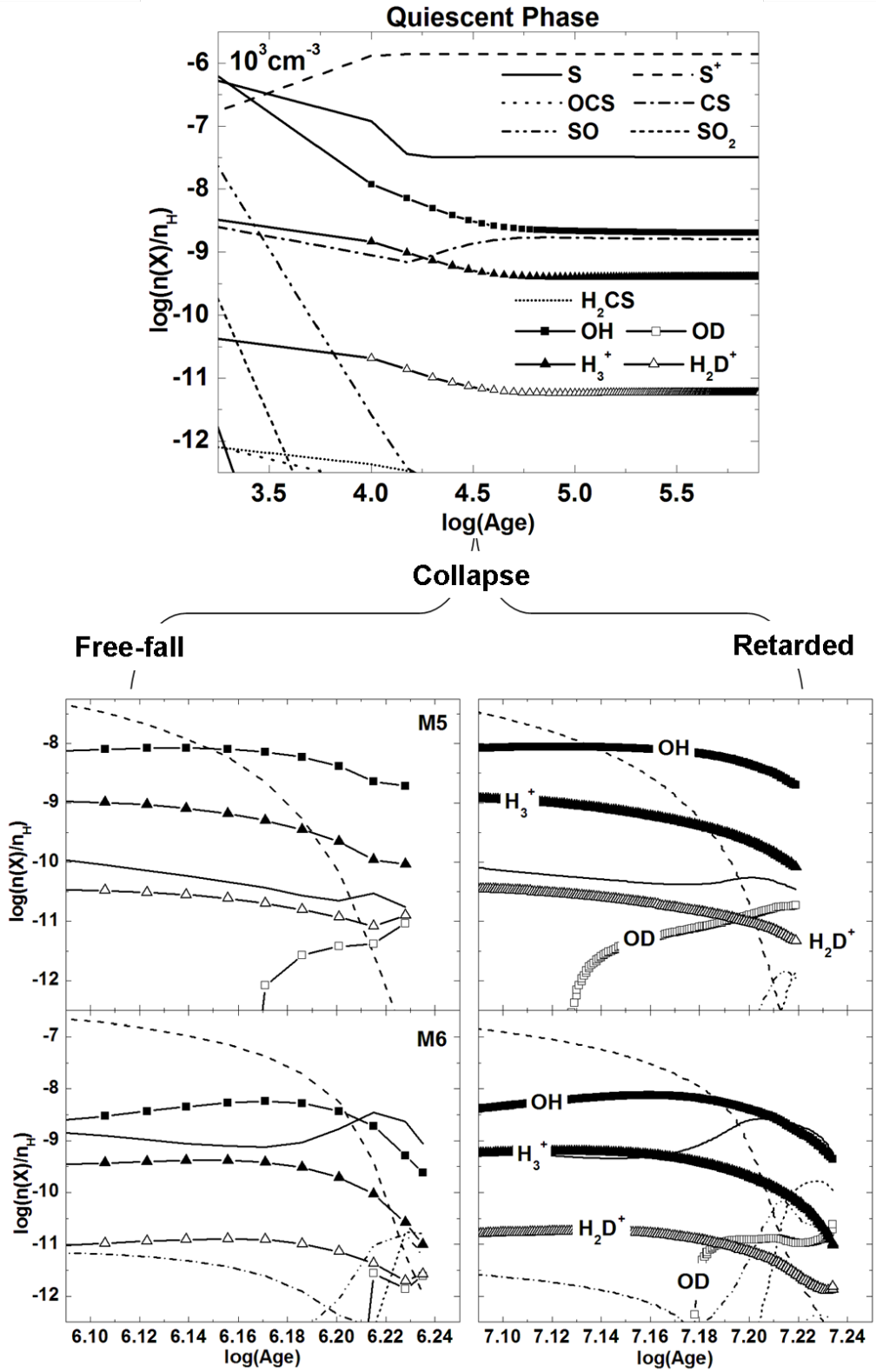

Figure 6.11: The time evolution of the fractional abundances of the species in set S1 (see key) for a clump formed from translucent gas of density 10^3 cm^{-3}, in Scenario 3. The top plot shows the quiescent phase for 1Myr. The chemistry during the collapsing phase, given in the collapse panel, either free-fall (left column) or retarded (right column), to a denser clump of a final density of 10^5 cm^{-3} (M5: top panel) or 10^6 cm^{-3} (M6: bottom panel).

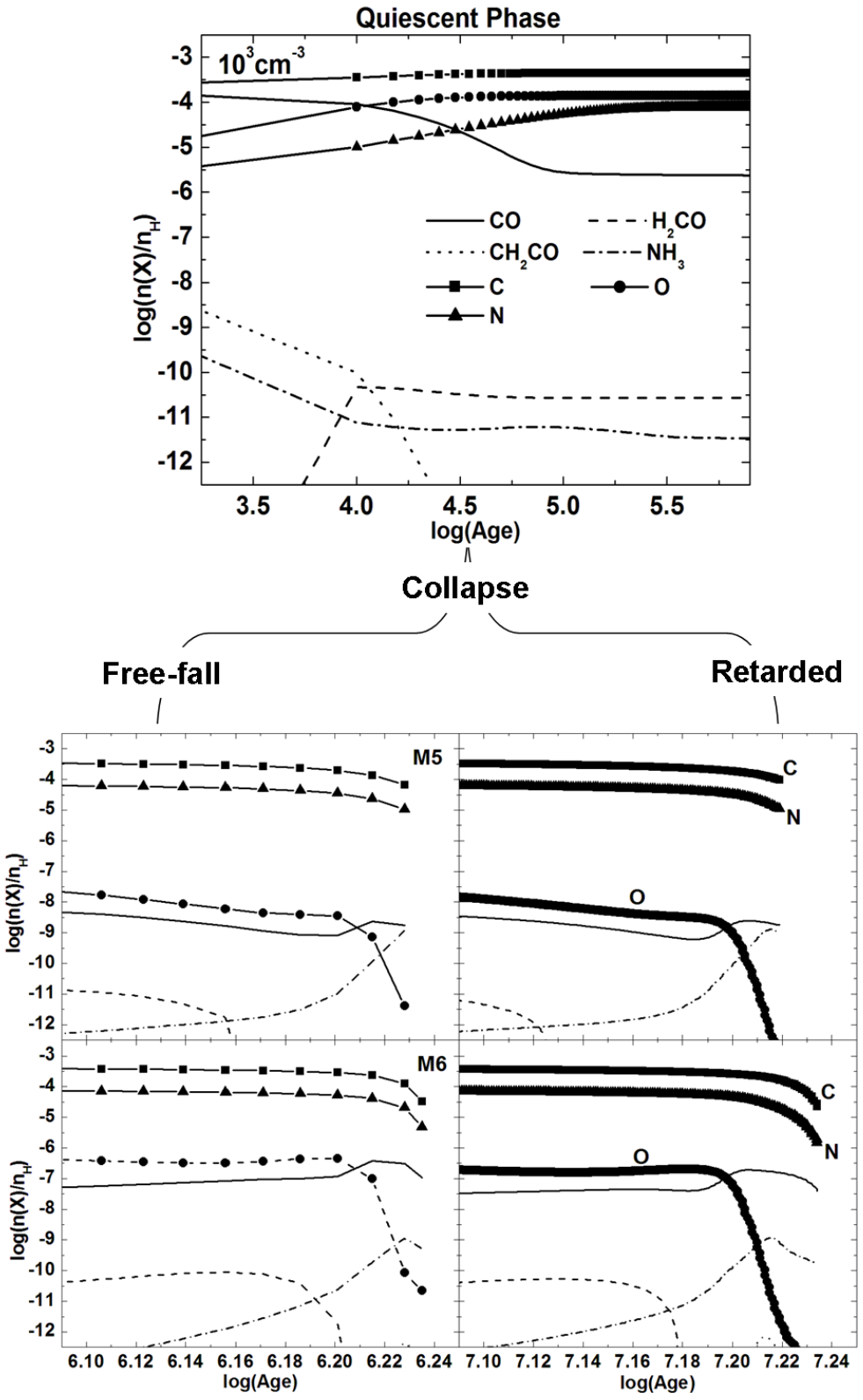

Figure 6.12: Same as in Fig. (6.11), but for the species in set S2 (see key).

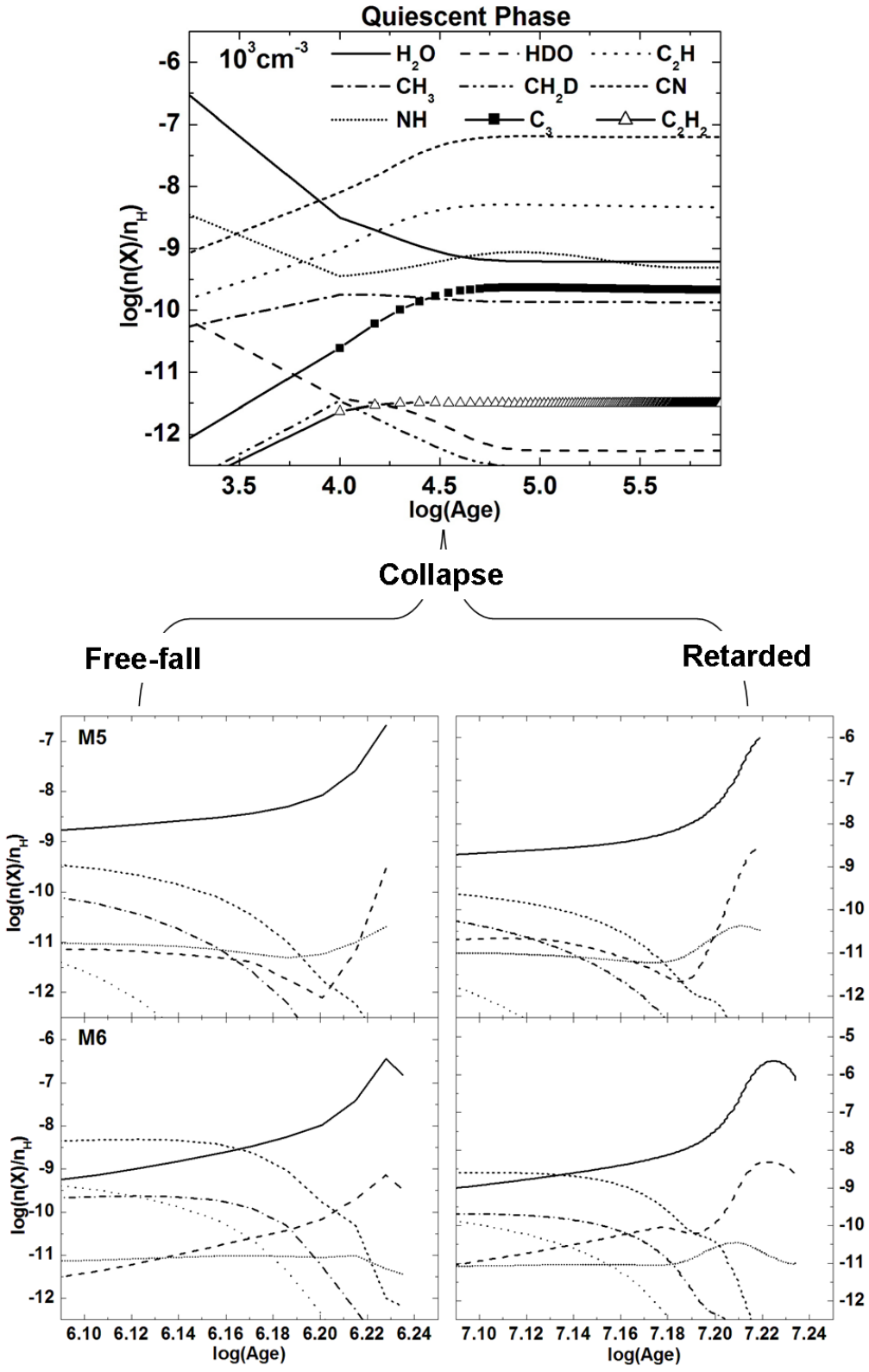

Figure 6.13: Same as in Figs. (6.11) & (6.12), but for the species in set S3 (see key).

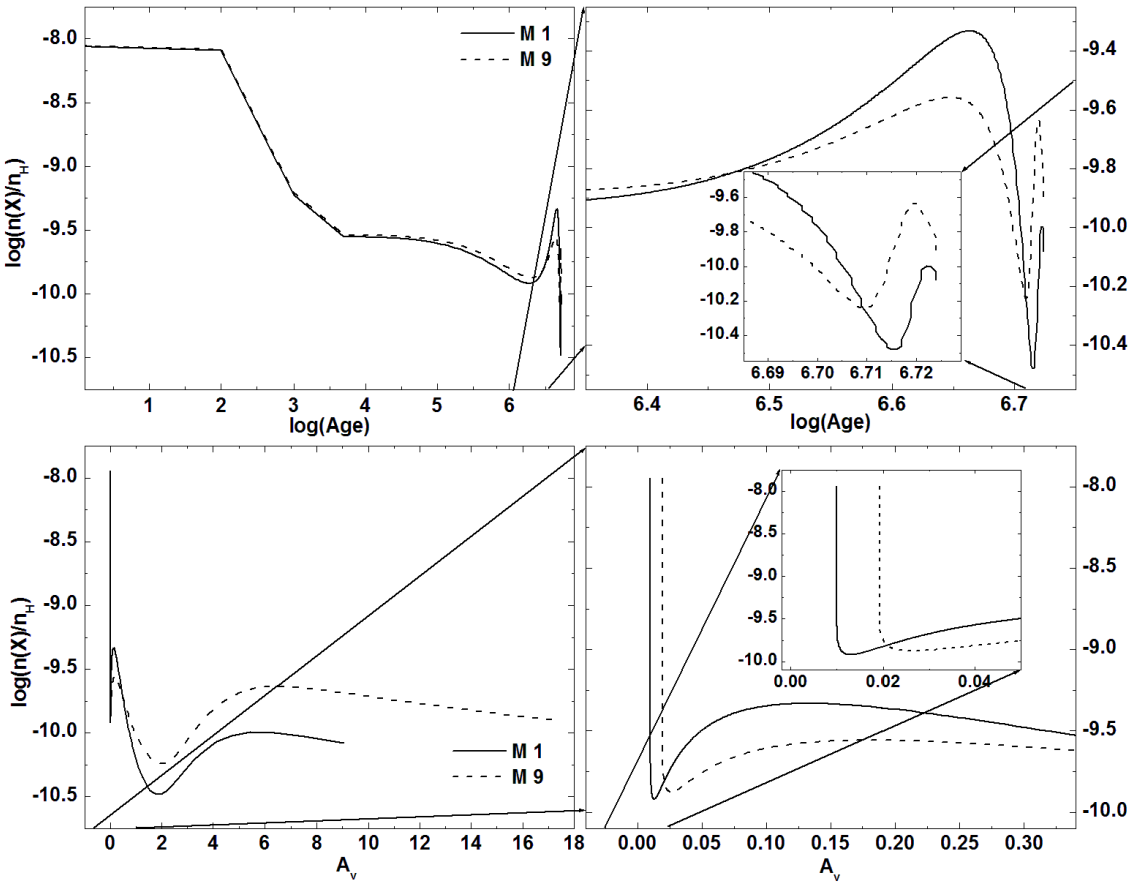

Figure 6.14: The influence of varying the opacity of the cloud (model M9) on the fractional abundances of CO in a clump of density of 10^5 cm^{-3}. The results are plotted as a function of time (top panel) and visual extinction , A_v (bottom panel) in comparison with those of models M1 (see key). Plots in the right column are a zoomed-in version of those in the left column towards late stages of the collapse.

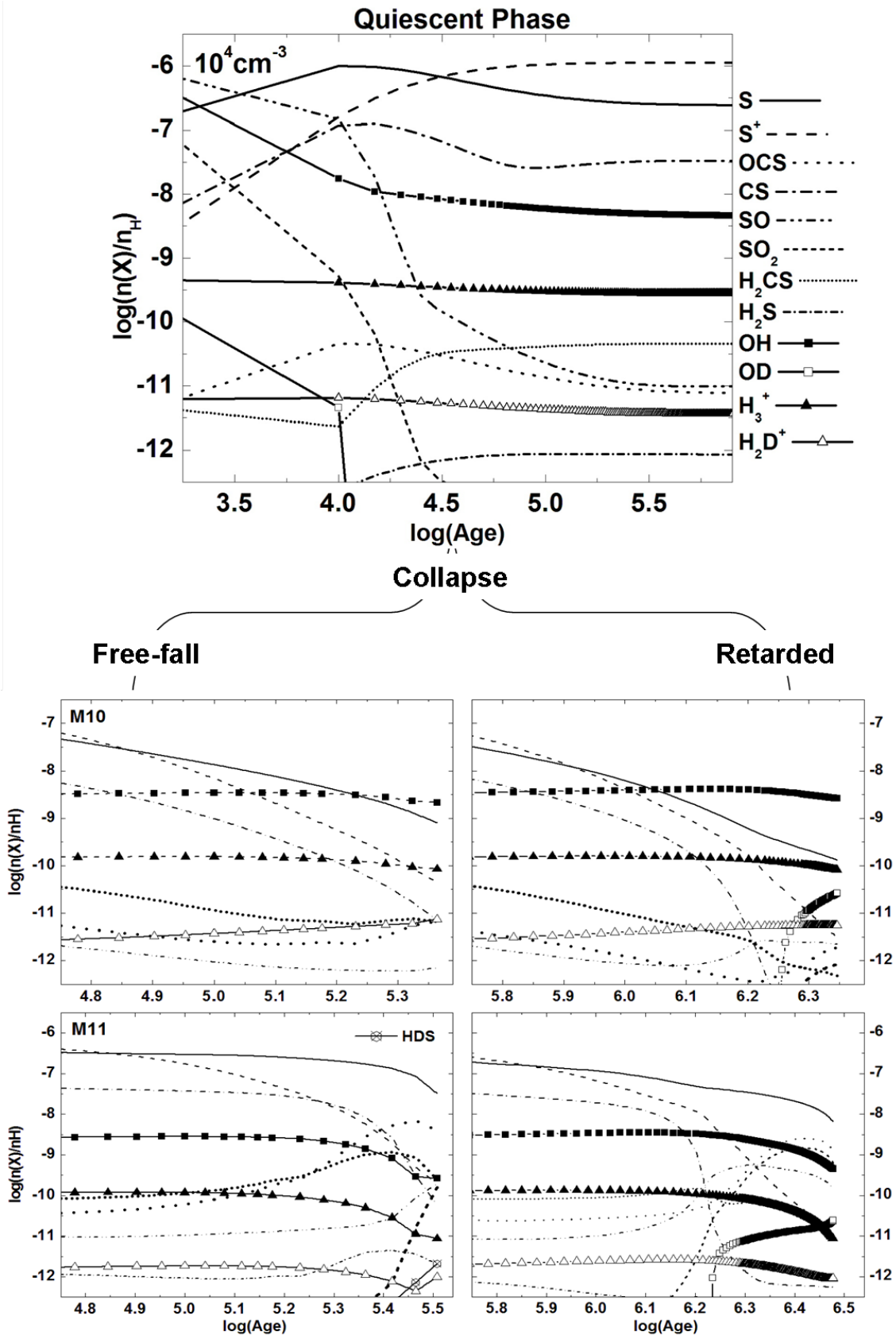

Figure 6.15: The time evolution of the fractional abundances of the species in set S1 in dense clumps (see key) formed from an interstellar dense gas (10^4 cm^{-3}) collapses either free-fall (left column) or retarded (right column), bottom set of plots, after a quiescent phase, top plot, of 1Myr, to a final density of 10^5 cm^{-3} (M10: top panel) or 10^6 cm^{-3} (M11: bottom panel).

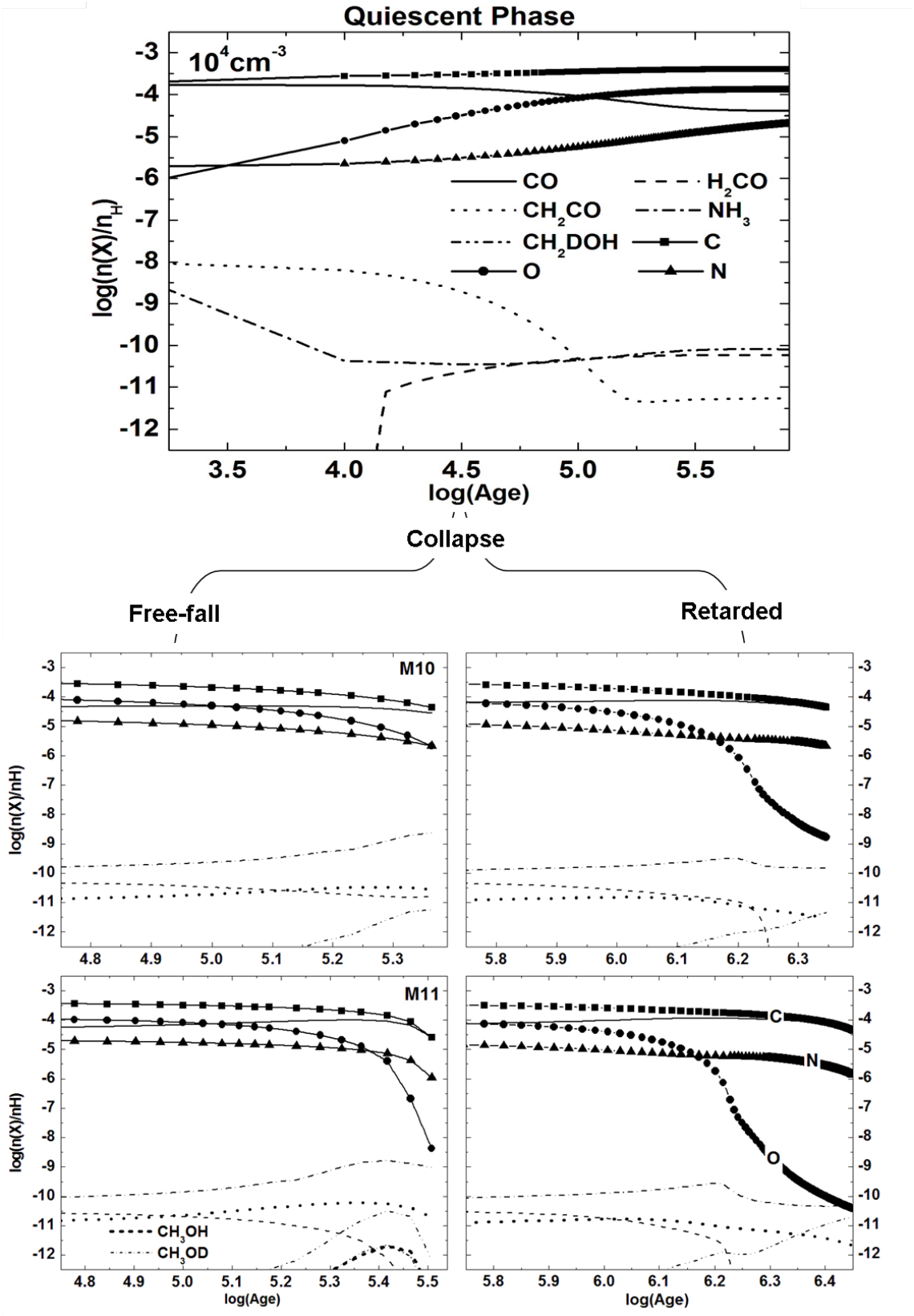

Figure 6.16: Same as in Fig. (6.15), but for the species in set S2 (see key).

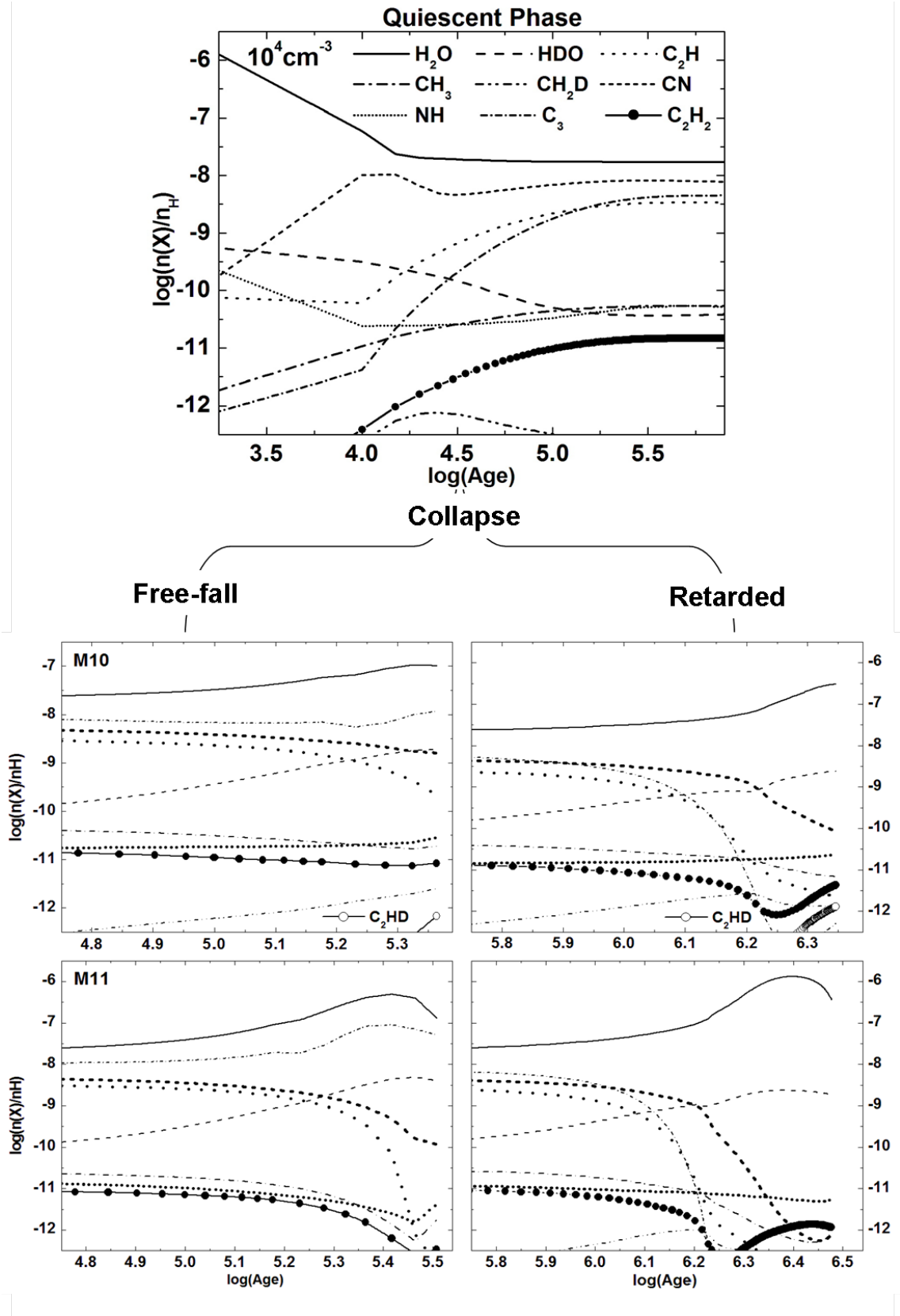

Figure 6.17: Same as in Figs. (6.15) & (6.16), but for the species in set S3 (see key).

Table 6.4: Comparison between the column density observed in the line-of-sight to ζ Per and our results of a quiescent diffuse cloud simulation. Our results are the average through the period of the simulation 1Myr.

Species	**Observations**	**Our model**
H_2	3.2-7.1(20)	8.01(20)
S	1.8(13)	0.43(13)
S^+	1.6(16)	0.3(15)
CO	6.1(14)	1.8-16(13)
NH	1.0(12)	5.0-7.0(10)
CN	3.0(12)	1.3(12)
OH	4.0(13)	3.0-8.0(12)
H_3^+	8.0(14)	5.0(12)

All observational results are taken from Table 2 in Price *et al.* (2003) and references therein. The notation a(b) represents a$\times 10^b$.

6.4 Comparison with observations

In this study we are not aiming at modelling a particular source. However, we are comparing our calculated fractional abundances of the quiescent diffuse cloud simulation to those observed in line of sight of ζ Per. Observations are taken from Table 2 in Price *et al.* (2003) and references therein. From Table (6.4), our results are in agreement with the observed column densities within a factor of $\sim$10 with exception for S^+ and H_3^+. The latter are not in agreement with observations with differences up to 2 orders of magnitude less for H_3^+.

We also compare our results for Scenarios 2 and 3 with observations of the dark prestellar core L1498 in the Taurus complex. The core has density of 10^5 cm^{-3} and temperature of 10 K (Tafalla *et al.* 2006). We found that our results best fit the observations for models in which the dense clump is formed from a dense processed gas. Scenario 2 can reproduce the observed abundance of SO which is not reproducible in Scenario 3. The abundance of NH_3 best fits observations during late times ($\geq 10^5$ yrs) of the collapse. CO fits observations throughout the collapse period. Table (6.5) summarises our best fit calculations in comparison with observations of L1498.

Table 6.5: Comparison between the abundances of some observed species towards the dense dark core L1498 and our results of a dense clump of density 10^5 cm^{-3} formed from a processed gas.

Species	**Observations**	**Our model**	
		M10	**M12**
CO	2.5(-5)	$\sim$ 1.0(-5)	$\sim$ 1.0(-5)
CS	3.0(-9)	0.15 - 4(-8)	1.0 - 5.0(-9)
NH_3	2.8(-8)	$\sim$ 2.0(-9)	$\sim$ 5.0(-9)
SO	4.0(-10)	—	0.1 - 1.0(-9)

All observational results are taken from Tafalla *et al.* (2006).

The notation a(b) represents a$\times 10^b$.

6.5 Conclusions

In this chapter we studied, theoretically, whether we can trace back the initial chemical conditions of a dense clump, where stars are formed, via studying its present chemical contents and whether these contents are affected by the nature (raw or processed gas) of the initial composition of the cloud and/or the mode of the collapse; free-fall or retarded. In order to achieve our aim, we ran a large grid of chemical models (described elsewhere Chapters 2 and 3) for diffuse, translucent, and molecular gas; see Table (6.2).

We found that the chemical composition of an interstellar cloud is independent of its initial chemical content or its nature, but it is strongly dependent on the physical conditions, in particular the density. Therefore, studying the present chemical composition of an interstellar cloud is not a useful tool to know its initial content. This result seems to disagree with the results of Price *et al.* (2003). This is because in their models they investigated the effect of changing initial chemical compositions on the abundances in diffuse clouds in two cycles. The first is the collapsing phase in which they start from low density gas (10 cm^{-3} and 10 K) which then undergoes a free-fall collapse to a denser clump. In this phase, the chemistry is dominated by UV radiation, which destroy the species, for longer time. On the other hand, in their expansion phase, they start their modelling from a dense region where the penetration of the UV radiation is inefficient due to the high opacity allowing the species to retain their high fractional abundances for longer time. In this view, our grid of models always corresponds to their collapsing phase and hence the chemistry does not show very significant differences when varying the

initial chemical conditions.

In addition, we found that there is a possibility to identify the collapsing mode of the interstellar cloud via few species which can be identified as collapse mode indicators. These species are H_2O and SO_2 for the retarded collapse and H_2CS, NH_3, and OCS for the free-fall mode.

Photoprocesses are the key in regulating the chemistry in interstellar clouds. We found that photochemistry is hindered as the density increases and thus photons are more readily absorbed by dust particles. In this case, other chemical pathways become active such as ion-molecule reactions. We find that the time a cloud needs to reach a steady state chemistry is in the range of 10^3 - 10^4 yrs which is similar to the photodissociation time-scale of diffuse clouds (Price *et al.* 2003).

Finally, we found that an interstellar cloud needs to have a certain amount of molecular hydrogen in order to attain a steady state and at which photoprocesses become less efficient. From our model calculations, this fractional abundance, with respect to the total amount of hydrogen nuclei, is $\sim$ 0.5, regardless the scenario of the formation of the dense clump. In other words, photoprocesses are suppressed when almost all the hydrogen atoms become in the molecular form. The critical density for deuterated species to present in an interstellar cloud with detectable abundances is $\geq 10^4$ cm^{-3}.

In summary, we can conclude that the chemical compositions of prestellar cores are not very sensitive to changes in the initial chemical conditions of the interstellar gas from which they form.

CHAPTER 7

CONCLUSIONS

The work presented in this thesis mainly deals with theoretical studies of the chemistry of hot corinos (or 'warm cores') around low-mass star forming regions. In order to mimic the chemistry of these cores, several chemical models were run and analysed through out this thesis, all of them based on the UCL_CHEM code described in **Chapter 1**. The thesis *does not* focus on modelling a particular source but it gives a general insight on the chemistry of such cores. It has been shown that very likely all low-mass protostars have inner regions warm enough that the grain mantles evaporate. These regions are known as 'hot corinos' because their chemistry is as rich as that in 'hot cores'; which are cores around massive stars. Hot corinos are warm (100 K), dense (10^8 cm^{-3}) cores surrounding low-mass star forming regions. The first corino was discovered towards IRAS 16293-2422, a young solar-type Class 0 protostar embedded in the ρ Per cloud. Observations revealed warm cores to be rich in their molecular contents and to show high percentage of deuterium fractionation, even higher than observed toward hot cores. Understanding the chemistry of these regions is essential in order to unveil their physical conditions.

Chapter 2 discusses the chemical modelling of hot corinos using UCL_CHEM . This study focuses on mimicking the chemistry of warm cores to investigate whether it is similar to that of hot cores, and hence whether hot corinos are a scaled-down version of the hot cores. The study also attempts to identify a set of species able to trace warm cores. We introduced a detailed model of sublimation based on experimental results by Collings *et al.* (2004) and adapted from a published one for hot cores by Viti *et al.* (2004). We adjusted several physical parameters to appropriately model a solar- mass protostar. The generally satisfactory behaviour of the model

results suggested that the chemical processes for both warm cores in low-mass star forming regions and hot cores in high mass star forming regions are similar. The model was capable at reproducing the observed 'jumps' in abundances of certain molecular abundances. We found that these jumps arise as a consequence of sublimation and subsequent rapid gas-phase chemistry. Such jumps do not occur in models that describe sublimation as an instantaneous process. We predicted that ratios of certain sulphur species should be excellent tracers of physical conditions in warm cores, regardless of the "unknown" total sulphur abundance. The comparison of the model results with observational results that show strong spatial dependence in molecular abundances within the core gave support to the view that detailed consideration must be given to the treatment of sublimation.

Observations show that hot corinos possess high levels of deuteration. Several deuterated species were observed towards low-mass warm cores such as HDCO, D_2CO, NH_2D, ND_3, CH_3OD, CH_2DOH, and $DCOOCH_3$. These observations motivated us to extend our modelling of star forming regions to include the deuterium chemistry in **Chapter 3**. In this study, we applied the chemical model used previously in Chapter 2 with a new chemical network. The reaction file was extended to include all the mono-deuterated counterparts of the species in addition to D_2CO which is the sole doubly deuterated molecule in our network. We investigated the influence of including deuterium chemistry into our chemical models and the sensitivity of deuterium chemistry to the variations in the environmental physical characteristics for both hot corinos and hot cores. The work also aimed at identifying a set of deuterated species to be evolutionary indicators for the hot cores and/or corinos. Our results showed that fractional abundances of species in hot cores are more affected by the inclusion of deuterium chemistry into chemical models than those in warm cores. We also found that deuterium chemistry is sensitive to variations of the model physical parameters, in particular the depletion percentage on to grain surfaces. For both warm and hot core environments, we found that lowering the depletion percentage decreases the abundance of most of the studied deuterated species with the exception of HDCS in both cores and D_2CO in hot cores. In addition, we found that the chemical trends of massive hot cores ($\geq$ 10M$\odot$) are similar to those of a 5M$\odot$ hot core but shifted toward earlier times. That is due to the different rates of warming up in which massive cores reaches certain temperature faster, thus earlier, than less mass cores. Ratios of deuterated sulphur species can also be used as chemical clocks for massive hot cores as their H counterparts were found to be in Chapter 2.

Observations revealed the existence of deuterated molecules in extragalactic environments.

These observations motivated us to extend our modelling to study the deuterium chemistry in extragalactic environments. This study was led by Dr. Estelle Bayet (Bayet *et al.* 2010) and is summarised in **Chapter 4**. The study aimed at investigating the detectability of deuterated species in various extragalactic star forming regions such as normal spirals, starbursts, active galactic nucleus, low metallicity, and high redshift galaxies. In this work we studied the sensitivity of deuterium chemistry to changes in the environments' physical parameters such as FUV radiation, temperature, CR ionisation rate, and gas density. We found that deuteration in extragalactic environments is sensitive to the variations in the physical conditions of the region. We also found that regardless of the galaxy type and the gas density, deuterated species can be divided into three categories: the first includes those which are insensitive to density changes (e.g. HDO, NH_2D and HDCS), the second has those that increase with density (e.g. HDS, C_2D and CH_3OD) and the last category includes the species which show a decrease in their fractional abundances (e.g. DCN, DNC and CH_2DOH). The first category contains tracers of dense gas ($\geq 10^5$ cm^{-3}). Our calculation predicted HDO, DCN and HDCO to be detectable in all extragalactic environments with fractional abundances as high as 10^{-10}.

Our models in Chapter 3 were not capable of reproducing the observed column densities of methyl formate, $HCOOCH_3$ and its deuterated counterpart. The most recent observations of the warm core towards IRAS 16293-2422 confirmed the existence of $DCOOCH_3$ (Demyk *et al.* 2010). These observations were published towards the end of my PhD, however they motivated me to carry on a short study, presented in **Chapter 5**. In this project, our aim was to improve the calculated column densities of $HCOOCH_3$ and its deuterated counterpart and also to enhance the production of D_2CO by including their formation on grain surfaces via routes proposed by recent experiments. The key aim of this study was to test whether the inclusion of the formation of $HCOOCH_3$, $DCOOCH_3$, and D_2CO on grain surfaces influences their calculated fractional abundances in chemical models, in particular during the warming up phase. Our results indeed show an enhancement in the abundance of the three species with $HCOOCH_3$ and $DCOOCH_3$ becoming observable; however, $HCOOCH_3$ is still two orders of magnitude lower than the observed value. The shortage of the production of $HCOOCH_3$ is possibly linked to the formation of methanol on grain via the successive hydrogenation of CO. We expect to form more methyl formate if we enhance the hydrogenation of CO on grain surfaces. This project can be extended, in future, to estimate the necessary and sufficient CH_3OH/CO ratio on grains to reproduce the observed column density of $HCOOCH_3$ within a reasonable factor. In addition, our calculations predicted CHDCO to be detectable in warm cores with low abundances. We

found that other key mantle species show insignificant variations in their abundances such as HDO and HDCO. The observed 'jump' in the evolutionary trend of H_2CO is still reproducible. Our main conclusions supported the view that the chemistry of hot corinos is primarily driven by surface chemistry which plays a vital role in the formation of many large species such as CH_3OH and more complex molecules such as methyl formate. In addition, grain surfaces are factories of deuterated species which can form in a similar way to their H-bearing counterpart as in the cases of $DCOOCH_3$ and D_2CO.

In **Chapter 6**, we turned our attention to the study of the ISM focusing on the origin of the interstellar clouds. We utilise the chemical models described in Chapter 3 to investigate the sensitivity of the chemistry of dense star forming cores to the initial chemical composition of the collapsing gas and to the collapse mode itself; free-fall or retarded. In this work, we ran a large grid of chemical models in which we form a dense prestellar core starting from different types of interstellar gas: diffuse, translucent and dense. We proposed three scenarios to form the final dense clump, the main difference between them is the chemical conditions of the gas; i.e. its molecular content. We found that the ultimate chemical composition of an interstellar cloud is independent of its initial molecular contents or their nature, but it is strongly dependent on the physical conditions, in particular the density. In addition, we found that there is a possibility to identify the collapsing mode of the interstellar cloud via few species which can be identified as collapse mode indicators; H_2O and SO_2 for the retarded collapse and H_2CS, NH_3, and OCS for the free-fall mode. As expected, photoprocesses are the key regulator for the chemistry in interstellar clouds. Our results showed that interstellar clouds need 10^3 - 10^4 years to attain a steady state chemistry and an amount of molecular hydrogen of ~ 0.5 cm^{-3} regardless its initial chemical and physical conditions. This time-scale is comparable to Price *et al.* (2003) results. Finally, we predicted deuterated species to be detectable in regions with densities $\geq 10^4$ cm^{-3}.

Bibliography

Aikawa, Y., 2008, *ApSS*, **313**, 35

Aikawa, Y., Herbst, E., Roberts, H. & Caselli, P., 2005, *ApJ*, **620**, 330

Ali, A., Shalabiea, O. M., El-Nawawy, M. S. & Millar, T. J., 2001, *MNRAS*, **325**, 881

André, P., Basu, S. & Inutsuka, S., 2009, in Chabrier, G. (ed.), *Structure Formation in Astrophysics* (Cambridge University Press), p. 254

André, P., Ward-Thompson, D. & Barsony, M., 1993, *ApJ*, **406**, 122

André, P., Ward-Thompson, D. & Barsony, M., 2000, *Protostars and Planets IV*, 59

Awad, Z., Viti, S., Collings, M. P. & Williams, D. A., 2010, *MNRAS*, 1006

Bachiller, R., 1996, in P. A. Shaver (ed.), *Science with Large Millimetre Arrays*, p. 243

Bacmann, A., André, P., Puget, J., Abergel, A., Bontemps, S. & Ward-Thompson, D., 2000, *A&A*, **361**, 555

Bacmann, A., Lefloch, B., Ceccarelli, C., Castets, A., Steinacker, J. & Loinard, L., 2002, *A&A*, **389**, L6

Bacmann, A., Lefloch, B., Ceccarelli, C., Steinacker, J., Castets, A. & Loinard, L., 2003, *ApJL*, **585**, L55

Bayet, E., Awad, Z. & Viti, S., 2010, *ApJ*, submitted

Bayet, E., Viti, S., Williams, D. A. & Rawlings, J. M. C., 2008, *ApJ*, **676**, 978

Bennett, C. J. & Kaiser, R. I., 2007a, *ApJ*, **660**, 1289

Bennett, C. J. & Kaiser, R. I., 2007b, *ApJ*, **661**, 899

Bergin, E. A., Alves, J., Huard, T. & Lada, C. J., 2002, *ApJL*, **570**, L101

Bergin, E. A. & Langer, W. D., 1997, *ApJ*, **486**, 316

Bergin, E. A. & Tafalla, M., 2007, *ArA&A*, **45**, 339

Bernasconi, P. A. & Maeder, A., 1996, *A&A*, **307**, 829

Bertoldi, F., Timmermann, R., Rosenthal, D., Drapatz, S. & Wright, C. M., 1999, *A&A*, **346**, 267

Biham, O., Pirronello, V. & Vidali, G., 2003, in V. Pirronello, J. Krelowski, & G. Manicò (ed.), *Solid State Astrochemistry*, pp. 211–250

Bisschop, S. E., Fraser, H. J., Öberg, K. I., van Dishoeck, E. F. & Schlemmer, S., 2006, *A&A*, **449**, 1297

Bisschop, S. E., Jørgensen, J. K., Bourke, T. L., Bottinelli, S. & van Dishoeck, E. F., 2008, *A&A*, **488**, 959

Boogert, A. C. A., Helmich, F. P., van Dishoeck, E. F., Schutte, W. A., Tielens, A. G. G. M. & Whittet, D. C. B., 1998, *A&A*, **336**, 352

Bottinelli, S., Ceccarelli, C., Neri, R., Williams, J. P., Caux, E., Cazaux, S., Lefloch, B., Maret, S. & Tielens, A. G. G. M., 2004, *ApJL*, **617**, L69

Brown, P. D. & Millar, T. J., 1989a, *MNRAS*, **237**, 661

Brown, P. D. & Millar, T. J., 1989b, *MNRAS*, **240**, 25

Brown, R. D. & Rice, E., 1981, *Royal Society of London Philosophical Transactions Series A*, **303**, 523

Brown, R. D. & Rice, E. H. N., 1986, *MNRAS*, **223**, 429

Brown, W. A., Viti, S., Wolff, A. J. & Bolina, A. S., 2006, *Chemical Evolution of the Universe, Faraday Discussions, volume 133, 2006, p.113*, **133**, 113

Butner, H. M., Charnley, S. B., Ceccarelli, C., Rodgers, S. D., Pardo, J. R., Parise, B., Cernicharo, J. & Davis, G. R., 2007, *ApJL*, **659**, L137

Caselli, P., Benson, P. J., Myers, P. C. & Tafalla, M., 2002b, *ApJ*, **572**, 238

Caselli, P., Hasegawa, T. I. & Herbst, E., 1993, *ApJ*, **408**, 548

Caselli, P., van der Tak, F. F. S., Ceccarelli, C. & Bacmann, A., 2003, *A&A*, **403**, L37

Caselli, P., Vastel, C., Ceccarelli, C., van der Tak, F. F. S., Crapsi, A. & Bacmann, A., 2008, *A&A*, **492**, 703

Caselli, P., Walmsley, C. M., Tafalla, M., Dore, L. & Myers, P. C., 1999, *ApJL*, **523**, L165

Caselli, P., Walmsley, C. M., Zucconi, A., Tafalla, M., Dore, L. & Myers, P. C., 2002a, *ApJ*, **565**, 331

Caux, E., Ceccarelli, C., Pagani, L., Maret, S., Castets, A. & Pardo, J. R., 2002, *A&A*, **383**, L9

Caux, E., Parise, B., Castets, A., Ceccarelli, C. & Tielens, A., 2005, in C. Lidman & D. Alloin (eds.), *The Cool Universe: Observing Cosmic Dawn*, volume 344 of *Astronomical Society of the Pacific Conference Series*, p. 206

Cazaux, S., Tielens, A. G. G. M., Ceccarelli, C., Castets, A., Wakelam, V., Caux, E., Parise, B. & Teyssier, D., 2003, *ApJL*, **593**, L51

Ceccarelli, C., 2002, *Planet Space Sci.*, **50**, 1267

Ceccarelli, C., 2004, in D. Johnstone, F. C. Adams, D. N. C. Lin, D. A. Neufeeld & E. C. Ostriker (eds.), *Star Formation in the Interstellar Medium: In Honor of David Hollenbach*, volume 323 of *Astronomical Society of the Pacific Conference Series*, p. 195

Ceccarelli, C., 2005, in D. C. Lis, G. A. Blake & E. Herbst (eds.), *Astrochemistry: Recent Successes and Current Challenges*, volume 231 of *IAU Symposium*, pp. 1–16

Ceccarelli, C., 2007, in J. Lemaire & F. Combes (eds.), *Molecules in Space and Laboratory*, pp. 1–7

Ceccarelli, C., Caselli, P., Herbst, E., Tielens, A. G. G. M. & Caux, E., 2007, in B. Reipurth, D. Jewitt & K. Keil (eds.), *Protostars and Planets V*, pp. 47–62

Ceccarelli, C., Castets, A., Caux, E., Hollenbach, D., Loinard, L., Molinari, S. & Tielens, A. G. G. M., 2000a, *A&A*, **355**, 1129

Ceccarelli, C., Castets, A., Loinard, L., Caux, E. & Tielens, A. G. G. M., 1998c, *A&A*, **338**, L43

Ceccarelli, C., Caux, E., Loinard, L., Castets, A., Tielens, A. G. G. M., Molinari, S., Liseau, R., Saraceno, P., Smith, H. & White, G., 1999, *A&A*, **342**, L21

Ceccarelli, C., Caux, E., White, G. J., Molinari, S., Furniss, I., Liseau, R., Nisini, B., Saraceno, P., Spinoglio, L. & Wolfire, M., 1998a, *A&A*, **331**, 372

Ceccarelli, C., Caux, E., Wolfire, M., Rudolph, A., Nisini, B., Saraceno, P. & White, G. J., 1998b, *A&A*, **331**, L17

Ceccarelli, C., Hollenbach, D. J. & Tielens, A. G. G. M., 1996, *ApJ*, **471**, 400

Ceccarelli, C., Loinard, L., Castets, A., Tielens, A. G. G. M. & Caux, E., 2000b, *A&A*, **357**, L9

Ceccarelli, C., Loinard, L., Castets, A., Tielens, A. G. G. M., Caux, E., Lefloch, B. & Vastel, C., 2001, *A&A*, **372**, 998

Charnley, S. B., Kress, M. E., Tielens, A. G. G. M. & Millar, T. J., 1995, *ApJ*, **448**, 232

Collings, M. P., Anderson, M. A., Chen, R., Dever, J. W., Viti, S., Williams, D. A. & McCoustra, M. R. S., 2004, *MNRAS*, **354**, 1133

Collings, M. P., Dever, J. W., Fraser, H. J. & McCoustra, M. R. S., 2003b, *ApSS*, **285**, 633

Collings, M. P., Dever, J. W., Fraser, H. J., McCoustra, M. R. S. & Williams, D. A., 2003a, *ApJ*, **583**, 1058

Cuppen, H. M. & Herbst, E., 2007, *ApJ*, **668**, 294

Cuppen, H. M., van Dishoeck, E. F., Herbst, E. & Tielens, A. G. G. M., 2009, *A&A*, **508**, 275

Dalgarno, A., 2006, *Chemical Evolution of the Universe, Faraday Discussions, volume 133, 2006, p.9*, **133**, 9

Demyk, K., Bottinelli, S., Caux, E., Vastel, C., Ceccarelli, C., Kahane, C. & Castets, A., 2010, *A&A*, **517**, A17

di Francesco, J., Evans, II, N. J., Caselli, P., Myers, P. C., Shirley, Y., Aikawa, Y. & Tafalla, M., 2007, *Protostars and Planets V*, 17

Duley, W. W., 1996, *MNRAS*, **279**, 591

Duley, W. W. & Williams, D. A., 1984, *Interstellar chemistry*

Duley, W. W. & Williams, D. A., 1986, *MNRAS*, **223**, 177

Duley, W. W. & Williams, D. A., 1993, *MNRAS*, **260**, 37

Dyson, J. E. & Williams, D. A., 1997, *The physics of the interstellar medium*

Ehrenfreund, P. & Schutte, W. A., 2000, *Advances in Space Research*, **25**, 2177

Emprechtinger, M., Caselli, P., Volgenau, N. H., Stutzki, J. & Wiedner, M. C., 2009, *A&A*, **493**, 89

Field, G. B., Goldsmith, D. W. & Habing, H. J., 1969, *ApJL*, **155**, L149

Flower, D., 2007, *Molecular collisions in the interstellar medium*

Flower, D. R., Pineau des Forêts, G. & Walmsley, C. M., 2004, *A&A*, **427**, 887

Fontani, F., Caselli, P., Bourke, T. L., Cesaroni, R. & Brand, J., 2008, *A&A*, **477**, L45

Garrod, R. T. & Herbst, E., 2006, *A&A*, **457**, 927

Garrod, R. T., Wakelam, V. & Herbst, E., 2007*a*, *A&A*, **467**, 1103

Garrod, R. T., Weaver, S. L. W. & Herbst, E., 2008, *ApJ*, **682**, 283

Garrod, R. T., Widicus Weaver, S. L. & Herbst, E., 2007*b*, in *Molecules in Space and Laboratory*

Geppert, W. D., Hamberg, M., Thomas, R. D., Österdahl, F., Hellberg, F., Zhaunerchyk, V., Ehlerding, A., Millar, T. J., Roberts, H., Semaniak, J., Ugglas, M. A., Källberg, A., Simonsson, A., Kaminska, M. & Larsson, M., 2006, *Chemical Evolution of the Universe, Faraday Discussions, volume 133, 2006, p.177*, **133**, 177

Gerin, M., Combes, F., Wlodarczak, G., Encrenaz, P. & Laurent, C., 1992, *A&A*, **253**, L29

Gibb, E., Nummelin, A., Irvine, W. M., Whittet, D. C. B. & Bergman, P., 2000, *ApJ*, **545**, 309

Gould, R. J. & Salpeter, E. E., 1963, *ApJ*, **138**, 393

Hartquist, T. W., Caselli, P., Rawlings, J. M. C., Ruffle, D. P. & Williams, D. A., 1998, *The Molecular Astrophysics of Stars and Galaxies, edited by Thomas W. Hartquist and David A. Williams. Clarendon Press, Oxford, 1998., p.101*, **4**, 101

Hartquist, T. W. & Williams, D. A., 1990, *MNRAS*, **247**, 343

Hasegawa, T. I. & Herbst, E., 1993, *MNRAS*, **261**, 83

Hasegawa, T. I., Herbst, E. & Leung, C. M., 1992, *ApJS*, **82**, 167

Hatchell, J., Thompson, M. A., Millar, T. J. & MacDonald, G. H., 1998, *A&A*, **338**, 713

Herbst, E., 1995, *Annual Review of Physical Chemistry*, **46**, 27

Herbst, E. & Klemperer, W., 1973, *ApJ*, **185**, 505

Herbst, E. & van Dishoeck, E. F., 2009, *ArA&A*, **47**, 427

Hidaka, H., Watanabe, M., Kouchi, A. & Watanabe, N., 2009, *ApJ*, **702**, 291

Hollenbach, D., Chu, S. & McCray, R., 1976, *ApJ*, **208**, 458

Hollenbach, D. J. & Tielens, A. G. G. M., 1997, *ArA&A*, **35**, 179

Hollis, J. M., Jewell, P. R., Lovas, F. J. & Remijan, A., 2004, *ApJL*, **613**, L45

Horn, A., Møllendal, H., Sekiguchi, O., Uggerud, E., Roberts, H., Herbst, E., Viggiano, A. A. & Fridgen, T. D., 2004, *ApJ*, **611**, 605

Jacq, T., Walmsley, C. M., Henkel, C., Baudry, A., Mauersberger, R. & Jewell, P. R., 1990, *A&A*, **228**, 447

Jacq, T., Walmsley, C. M., Mauersberger, R., Anderson, T., Herbst, E. & De Lucia, F. C., 1993, *A&A*, **271**, 276

Konigl, A. & Pudritz, R. E., 2000, *Protostars and Planets IV*, 759

Lada, C. J., 1985, *ArA&A*, **23**, 267

Lada, C. J., 1987, in M. Peimbert & J. Jugaku (eds.), *Star Forming Regions*, volume 115 of *IAU Symposium*, pp. 1–17

Lada, C. J. & Harvey, P. M., 1981, *ApJ*, **245**, 58

Lada, C. J. & Wilking, B. A., 1984, *ApJ*, **287**, 610

Larsson, M., Lepp, S., Dalgarno, A., Stroemholm, C., Sundstroem, G., Zengin, V., Danared, H., Kaellberg, A., Af Ugglas, M. & Datz, S., 1996, *A&A*, **309**, L1

Le Teuff, Y. H., Millar, T. J. & Markwick, A. J., 2000, *A&AS*, **146**, 157

Leger, A., Jura, M. & Omont, A., 1985, *A&A*, **144**, 147

Lepp, S., 1992, in P. D. Singh (ed.), *Astrochemistry of Cosmic Phenomena*, volume 150 of *IAU Symposium*, p. 471

Li, A. & Greenberg, J. M., 2003, in V. Pirronello, J. Krelowski, & G. Manicò (ed.), *Solid State Astrochemistry*, pp. 37–84

Linsky, J. L., Diplas, A., Wood, B. E., Brown, A., Ayres, T. R. & Savage, B. D., 1995, *ApJ*, **451**, 335

Lis, D. C., Roueff, E., Gerin, M., Phillips, T. G., Coudert, L. H., van der Tak, F. F. S. & Schilke, P., 2002, *ApJL*, **571**, L55

Loinard, L., Castets, A., Ceccarelli, C., Caux, E. & Tielens, A. G. G. M., 2001, *ApJL*, **552**, L163

Loren, R. B. & Wootten, A., 1985, *ApJ*, **299**, 947

Marcelino, N., Cernicharo, J., Roueff, E., Gerin, M. & Mauersberger, R., 2005, *ApJ*, **620**, 308

Maret, S., Bergin, E. A. & Lada, C. J., 2006, *Nature*, **442**, 425

Maret, S., Ceccarelli, C., Caux, E., Tielens, A. G. G. M., Jørgensen, J. K., van Dishoeck, E., Bacmann, A., Castets, A., Lefloch, B., Loinard, L., Parise, B. & Schöier, F. L., 2004, *A&A*, **416**, 577

Martín, S., Mauersberger, R., Martín-Pintado, J., Henkel, C. & García-Burillo, S., 2006, *ApJS*, **164**, 450

Mauersberger, R., Henkel, C. & Chin, Y., 1995, *A&A*, **294**, 23

McKee, C. F. & Ostriker, J. P., 1977, *ApJ*, **218**, 148

Miettinen, O., Harju, J., Haikala, L. K., Kainulainen, J. & Johansson, L. E. B., 2009, *A&A*, **500**, 845

Millar, T. J., 2005, *Astronomy and Geophysics*, **46**(2), 020000

Millar, T. J., Bennett, A. & Herbst, E., 1989, *ApJ*, **340**, 906

Millar, T. J., Farquhar, P. R. A. & Willacy, K., 1997, *A&AS*, **121**, 139

Millar, T. J., Herbst, E. & Charnley, S. B., 1991, *ApJ*, **369**, 147

Molinari, S., Brand, J., Cesaroni, R. & Palla, F., 2000, *A&A*, **355**, 617

Morrison, D., Wolff, S. & Fraknoi, A., 1996, *The Observatory*, **116**, 40

Nejad, L. A. M. & Wagenblast, R., 1999, *A&A*, **350**, 204

Nejad, L. A. M., Williams, D. A. & Charnley, S. B., 1990, *MNRAS*, **246**, 183

Nomura, H. & Millar, T. J., 2004, *A&A*, **414**, 409

Öberg, K. I., Boogert, A. C. A., Pontoppidan, K. M., Blake, G. A., Evans, N. J., Lahuis, F. & van Dishoeck, E. F., 2008, *ApJ*, **678**, 1032

Öberg, K. I., Linnartz, H., Visser, R. & van Dishoeck, E. F., 2009b, *ApJ*, **693**, 1209

Öberg, K. I., van Dishoeck, E. F. & Linnartz, H., 2009a, *A&A*, **496**, 281

Oliveira, C. M., Hébrard, G., Howk, J. C., Kruk, J. W., Chayer, P. & Moos, H. W., 2003, *ApJ*, **587**, 235

Pagani, L., Pardo, J., Apponi, A. J., Bacmann, A. & Cabrit, S., 2005, *A&A*, **429**, 181

Parise, B., Castets, A., Herbst, E., Caux, E., Ceccarelli, C., Mukhopadhyay, I. & Tielens, A. G. G. M., 2004, *A&A*, **416**, 159

Parise, B., Caux, E., Castets, A., Ceccarelli, C., Loinard, L., Tielens, A. G. G. M., Bacmann, A., Cazaux, S., Comito, C., Helmich, F., Kahane, C., Schilke, P., van Dishoeck, E., Wakelam, V. & Walters, A., 2005, *A&A*, **431**, 547

Parise, B., Ceccarelli, C., Tielens, A. G. G. M., Castets, A., Caux, E., Lefloch, B. & Maret, S., 2006, *A&A*, **453**, 949

Parise, B., Ceccarelli, C., Tielens, A. G. G. M., Herbst, E., Lefloch, B., Caux, E., Castets, A., Mukhopadhyay, I., Pagani, L. & Loinard, L., 2002, *A&A*, **393**, L49

Penzias, A. A., 1979, *ApJ*, **228**, 430

Pickles, J. B. & Williams, D. A., 1977, *ApSS*, **52**, 443

Pirronello, V., Accolla, M., Congiu, E. & Manico, G., 2007, in *Molecules in Space and Laboratory*

Polehampton, E. T., Baluteau, J., Ceccarelli, C., Swinyard, B. M. & Caux, E., 2002, *A&A*, **388**, L44

Prasad, S. S. & Tarafdar, S. P., 1983, *ApJ*, **267**, 603

Price, R. J., Viti, S. & Williams, D. A., 2003, *MNRAS*, **343**, 1257

Ratajczak, A., Quirico, E., Faure, A., Schmitt, B. & Ceccarelli, C., 2009, *A&A*, **496**, L21

Rawlings, J. M. C., Hartquist, T. W., Menten, K. M. & Williams, D. A., 1992, *MNRAS*, **255**, 471

Redman, M. P., Viti, S., Cau, P. & Williams, D. A., 2003, *MNRAS*, **345**, 1291

Remijan, A. J. & Hollis, J. M., 2006, *ApJ*, **640**, 842

Roberts, H., 2008, in S. Kwok & S. Sandford (ed.), *IAU Symposium*, volume 251 of *IAU Symposium*, pp. 99–104

Roberts, H., Fuller, G. A., Millar, T. J., Hatchell, J. & Buckle, J. V., 2002, *A&A*, **381**, 1026

Roberts, H., Herbst, E. & Millar, T. J., 2003, *ApJL*, **591**, L41

Roberts, H., Herbst, E. & Millar, T. J., 2004, *A&A*, **424**, 905

Roberts, H. & Millar, T. J., 2000a, *A&A*, **361**, 388

Roberts, H. & Millar, T. J., 2000b, *A&A*, **364**, 780

Roberts, H. & Millar, T. J., 2007, *A&A*, **471**, 849

Roberts, J. F., Rawlings, J. M. C., Viti, S. & Williams, D. A., 2007, *MNRAS*, **382**, 733

Rodgers, S. D. & Millar, T. J., 1996, *MNRAS*, **280**, 1046

Roueff, E., Tiné, S., Coudert, L. H., Pineau des Forêts, G., Falgarone, E. & Gerin, M., 2000, *A&A*, **354**, L63

Ruffle, D. P. & Herbst, E., 2001, *MNRAS*, **322**, 770

Sakai, N., Sakai, T., Hirota, T. & Yamamoto, S., 2009, *ApJ*, **702**, 1025

Salpeter, E. E., 1977, *ArA&A*, **15**, 267

Schilke, P., Walmsley, C. M., Pineau Des Forets, G., Roueff, E., Flower, D. R. & Guilloteau, S., 1992, *A&A*, **256**, 595

Schöier, F. L., Jørgensen, J. K., van Dishoeck, E. F. & Blake, G. A., 2002, *A&A*, **390**, 1001

Schutte, W. A. & Greenberg, J. M., 1991, *A&A*, **244**, 190

Shah, R. Y. & Wootten, A., 2001, *ApJ*, **554**, 933

Shalabiea, O. M. & Greenberg, J. M., 1994, *A&A*, **290**, 266

Shalabiea, O. M. & Greenberg, J. M., 1995a, *A&A*, **296**, 779

Shalabiea, O. M. & Greenberg, J. M., 1995b, *A&A*, **303**, 233

Shu, F. H. & Adams, F. C., 1987, in I. Appenzeller & C. Jordan (ed.), *Circumstellar Matter*, volume 122 of *IAU Symposium*, pp. 7–22

Snell, R. L., 1987, in M. Peimbert & J. Jugaku (ed.), *Star Forming Regions*, volume 115 of *IAU Symposium*, pp. 213–236

Snell, R. L., Loren, R. B. & Plambeck, R. L., 1980, *ApJL*, **239**, L17

Snow, T. P. & McCall, B. J., 2006, *ArA&A*, **44**, 367

Spitzer, L., 1978, *Physical processes in the interstellar medium*

Stahler, S. W., Shu, F. H. & Taam, R. E., 1980a, *ApJ*, **241**, 637

Stahler, S. W., Shu, F. H. & Taam, R. E., 1980b, *ApJ*, **242**, 226

Stark, R., Sandell, G., Beck, S. C., Hogerheijde, M. R., van Dishoeck, E. F., van der Wal, P., van der Tak, F. F. S., Schäfer, F., Melnick, G. J., Ashby, M. L. N. & de Lange, G., 2004, *ApJ*, **608**, 341

Stark, R., van der Tak, F. F. S. & van Dishoeck, E. F., 1999, *ApJL*, **521**, L67

Stecher, T. P. & Williams, D. A., 1967, *ApJL*, **149**, L29

Sundstrom, G., Mowat, J. R., Danared, H., Datz, S., Brostrom, L., Filevich, A., Kallberg, A., Mannervik, S., Rensfelt, K. G., Sigray, P., Ugglas, M. A. & Larsson, M., 1994, *Science*, **263**, 785

Tafalla, M., Myers, P. C., Caselli, P., Walmsley, C. M. & Comito, C., 2002, *ApJ*, **569**, 815

Tafalla, M., Santiago-García, J., Myers, P. C., Caselli, P., Walmsley, C. M. & Crapsi, A., 2006, *A&A*, **455**, 577

Terzieva, R. & Herbst, E., 1998, *ApJ*, **501**, 207

Tielens, A. G. G. M., 1983, *A&A*, **119**, 177

Tielens, A. G. G. M. & Charnley, S. B., 1997, *Origins of Life and Evolution of the Biosphere*, **27**, 23

Tielens, A. G. G. M. & Hagen, W., 1982, *A&A*, **114**, 245

Tiné, S., Roueff, E., Falgarone, E., Gerin, M. & Pineau des Forêts, G., 2000, *A&A*, **356**, 1039

Trumpler, R. J., 1930, *PASP*, **42**, 214

Turner, B. E., 1990, *ApJL*, **362**, L29

Turner, B. E., 1998, *ApJ*, **501**, 731

van de Hulst, H. C., 1948, *Harvard Observatory Monographs*, **7**, 73

van der Tak, F. F. S., Schilke, P., Müller, H. S. P., Lis, D. C., Phillips, T. G., Gerin, M. & Roueff, E., 2002, *A&A*, **388**, L53

van Dishoeck, E. F., 1998, *The Molecular Astrophysics of Stars and Galaxies, edited by Thomas W. Hartquist and David A. Williams. Clarendon Press, Oxford, 1998., p.53*, **4**, 53

van Dishoeck, E. F., 2004, *ArA&A*, **42**, 119

van Dishoeck, E. F. & Blake, G. A., 1998, *ArA&A*, **36**, 317

van Dishoeck, E. F., Blake, G. A., Jansen, D. J. & Groesbeck, T. D., 1995, *ApJ*, **447**, 760

van Dishoeck, E. F., Jonkheid, B. & van Hemert, M. C., 2006, *Chemical Evolution of the Universe, Faraday Discussions, volume 133, 2006, p.231*, **133**, 231

Vastel, C., Caselli, P., Ceccarelli, C., Phillips, T., Wiedner, M. C., Peng, R., Houde, M. & Dominik, C., 2006, *ApJ*, **645**, 1198

Vastel, C., Phillips, T. G., Ceccarelli, C. & Pearson, J., 2003, *ApJL*, **593**, L97

Vastel, C., Phillips, T. G. & Yoshida, H., 2004, *ApJL*, **606**, L127

Viti, S., Collings, M. P., Dever, J. W., McCoustra, M. R. S. & Williams, D. A., 2004, *MNRAS*, **354**, 1141

Viti, S., Natarajan, S. & Williams, D. A., 2002, *MNRAS*, **336**, 797

Viti, S. & Williams, D. A., 1999, *MNRAS*, **305**, 755

Vrtilek, J. M., Gottlieb, C. A., Langer, W. D., Thaddeus, P. & Wilson, R. W., 1985, *ApJL*, **296**, L35

Wakelam, V., 2009, in *American Astronomical Society Meeting Abstracts*, volume 214 of *American Astronomical Society Meeting Abstracts*, p. 15

Wakelam, V., Caselli, P., Ceccarelli, C., Herbst, E. & Castets, A., 2004, *A&A*, **422**, 159

Wakelam, V., Herbst, E. & Selsis, F., 2006, *A&A*, **451**, 551

Walmsley, C. M., Hermsen, W., Henkel, C., Mauersberger, R. & Wilson, T. L., 1987, *A&A*, **172**, 311

Ward-Thompson, D., 1996, *ApSS*, **239**, 151

Ward-Thompson, D., Scott, P. F., Hills, R. E. & Andre, P., 1994, *MNRAS*, **268**, 276

Watanabe, N. & Kouchi, A., 2008, *Progress In Surface Science*, **83**, 439

Watanabe, N., Shiraki, T. & Kouchi, A., 2003, *ApJL*, **588**, L121

Watson, W. D., 1980, in *Les Spectres des Molécules Simples au Laboratoire et en Astrophysique*, pp. 526–544

Willacy, K. & Millar, T. J., 1998, *MNRAS*, **298**, 562

Williams, D. A., 2003a, in V. Pirronello, J. Krelowski, & G. Manicò (ed.), *Solid State Astrochemistry*, pp. 1–20

Williams, D. A., 2003b, in V. Pirronello, J. Krelowski, & G. Manicò (ed.), *Solid State Astrochemistry*, pp. 21–35

Wooden, D. H., Charnley, S. B. & Ehrenfreund, P., 2004, in Festou, M. C., Keller, H. U., & Weaver, H. A. (ed.), *Comets II*, pp. 33–66

Wright, C. M., van Dishoeck, E. F., Cox, P., Sidher, S. D. & Kessler, M. F., 1999, *ApJL*, **515**, L29